STUDIES TOWARDS THE DEVELOPMENT OF NOVEL ANTIMALARIAL AGENTS

A thesis submitted in fulfilment of the requirement for the degree of

MASTER OF SCIENCE

of

RHODES UNIVERSITY

by

CHRISTIANA MODUPE ADEYEMI

B.Sc. Hons (Obafemi Awolowo University)

December, 2014

ABSTRACT

Considerable efforts have been made in the modification of existing antimalarial drugs, and the support of incentive programmes have led to a drastic decrease in malaria cases reported by WHO during the past 6 years. However, the development of drug resistance threatens the eradication of this deadly disease and has prompted research on the synthesis of novel antimalarial drugs.

Our research has involved the design and synthesis of novel benzylated phosphonate esters as potential 1-deoxy-D-xylose-5-phosphate reductoisomerase (DXR) inhibitors. A series of amidoalkylphosphonate esters were obtained by reacting various 3-subsituted anilines and heterocyclic amines with chloroalkanoyl chlorides and reacting the resulting chloroalkanamides with triethyl phosphite using *Michaelis-Arbuzov* methodology. Benzylation of the phosphonate esters afforded a series of novel *N*-benzylated derivatives in good yields and these compounds were fully characterised by NMR and HRMS methods. Several approaches to the introduction of a benzyl group at the C-2 position of the phosphonate ester derivatives have been explored, leading unexpectedly to the isolation of unprecedented tetrahydrofuranyl derivatives. Studies towards the preparation of potential bi-functional *Pf*DXR / HIV-1 RT inhibitors have also been initiated.

Preliminary *in silico* docking studies of selected non-benzylated and benzylated phosphonated derivatives into the *Pf*-DXR active-site has provided useful insight into the binding potential of these ligands. Bioassays have revealed a very low toxicity for all the synthesised phosphonated compounds and a number of these ligands also exhibit a promising inhibitory activity against the *Plasmodium* parasite.

ACKNOWLEDGMENTS

First and foremost I would like to thank the Unfailing God, for His pledge of changeless ominipotence and faithfulness. I would never have done this without you God. *Thanks being my strength, personal bravery and my invicible army; for you have made my feet like hinds' feet and have made me not to stand still in terror, but to walk and make progress upon my high places.* All thanks to you the Prince of Peace that always calms all raging storms and for other reasons too numerous to mention.

I take immense pleasure to express a deep sense of gratutide to my supervisor, Prof. Perry Kaye, for his creative suggestions, ever-listening ears, motivation and great enthusiasm which has inspired me to thrive for nothing less than excellence. Apart from my research, I have learnt a lot from him, admist all is humility and great mentorship style. I feel privileged to be associated with a person like him during my life.

My special words of thanks also go to my co-supervisor, Prof. Rui Krause, for being so helpful and motivating throughout this research. My sincere thanks to Dr. Rosa Klein for her willingliness to help at all times, and to Dr Lobb, for his kind assistance with the NMR instrument. My appreciation goes to Ms. Michelle Isaacs for my bioassay analysis and the entire Chemistry Department staff.

I would to like to acknowledge Prof. Remi Ogunfowokan, for his kind suggestions and encouragement that are always valuable to me. Special thanks to Dr. Tope Olomola for his moral support and motivation. I express my heart-felt gratutide to Oladapo Alabede, for always been there, I value your significant ideas to this work wholeheatedly. Thanks dear for being so kind to me; sincerely, I could not have asked for more... Thanks to Dayo Fashina for giving me his spare time to discuss and for his good advice. I would like to thank some of my friends; Charmaine Awolaja, Iviwe, Bola Jesumoroti and my colleagues in F22 laboratory who have extended their helping hands in some form or other. I am grateful to the Medical Research Council and Rhodes University for the financial support of this research.

My acknowledgement will never be complete without the special mention of the people who mean the world to me, my parents and siblings. Thank you Dad and Mum for believing in me, and giving me the liberty to choose my career which is what I desire. I can barely find words to express the love and support you all have given me. Your prayers, concern, good wishes and great support have been evident throughout my life. I value the love you all show me at all times which I can hardly repay.

CONTENTS

1. INTRODUCTION

1.1 MALARIA

1.1.1. History of malaria

Many years ago, Hippocrates related fevers to the presence of swamps and decaying matter, hence the Italian name "*mal'aria*" meaning "bad air" or "spoiled air". This theory was later discredited when scientists showed more interest in the discovery of malaria and the causative agent. In 1880, Alphonse Laveran was the first to describe malaria parasites in the red blood cells of humans by observing the discolouration of the skin of a French soldier in Algeria having fever. The discolouration was due to the presence of malaria pigment, haemozin, in his blood and this discovery won Laveran a Nobel Prize in 1907.[1,2] However, Sir Ronald Ross (1857-1932)[1] went further in his research to study how malaria can be transmitted through the sporogonic cycle of the parasite by identifying the *Plasmodium* parasite within the female anopheles mosquito. He concluded that malaria can be transmitted to a human host through a bite by an already infected mosquito. He won the Nobel Prize in Medicine in 1902 for his pioneering work on solving the problem of transmission of malaria which paved the way for further research on this disease by several scientists.

In 1948, Shortt and Garnham discovered the malaria parasite in the tissues of monkeys and humans, thereby confirming the theory of transmission postulated by Ross. They also established the tissue stages in the blood of the human host.[1,2] However, the evidence of relapse each time a human is infected with the disease was discovered by Krotoski in 1962 by understanding the liver stage of the mosquito.[1,2]

Over the years, understanding the complex life-cycle of the mosquito by various scientists has paved the way for several efforts to combat this deadly disease. Considerable efforts have also been made in the modification of existing drugs and in the synthesis of novel drugs, which can lead to the eradication of malaria.

1.1.2. The statistics and economic burden of malaria

In 2006, estimates point to 247 million people being infected with malaria, with 881 thousand death cases.[2] Out of 243 million people around the world living with malaria in 2008, approximately 863 thousand died.[2] In 2012, there was a huge improvement, with approximately 207 million newly infected malaria cases with 627 thousand deaths reported. Mostly children younger than 5 years and pregnant women have lost their lives from the disease each year due to their weak immune system against the deadly disease.[3] Sub-Saharan Africa has the most intense transmission of this deadly disease, followed by part of Latin America; Asia also has this endemic problem (Figure 1). However, Africa has 43 countries having 80% of the cases of malaria infection, but effective eradication programmes have helped to reduce malaria cases in 8 of these countries, including South Africa. Europe has the lowest burden of malaria transmission with 0.02% cases and no records of death (Figure 1).[3]

The statistical data obtained since 2006, reveals a great decrease in malaria transmission, with 8 African countries experiencing 75% reduction in attempts to meet the Millennium Development Goals (MDG) that were adopted by 189 nations and signed by 147 Heads-of-State and governments during the United Nations (UN) Millennium Summit in September, 2000.[2] The 8 outlined goals included a commitment to combat HIV/AIDS, malaria, and other diseases, but with the main intention being to drastically reduce malaria infection and child mortality.

The transmission of malaria can be influenced by temperature changes. Climatic changes in equatorial and tropical regions contribute to the transmission of the disease in these regions. It has been reported that the transmission rate is highest when temperatures exceed 18 ^{o}C, most especially during rainy season; this is attributed to the presence of swamplands and stagnant water which facilitates the breeding of mosquito vectors.[4] However, transmission decreases greatly when the temperature falls below 16 ^{o}C, and the colder winter season leads to a drastic decrease in malaria transmission in temperate regions.[4]

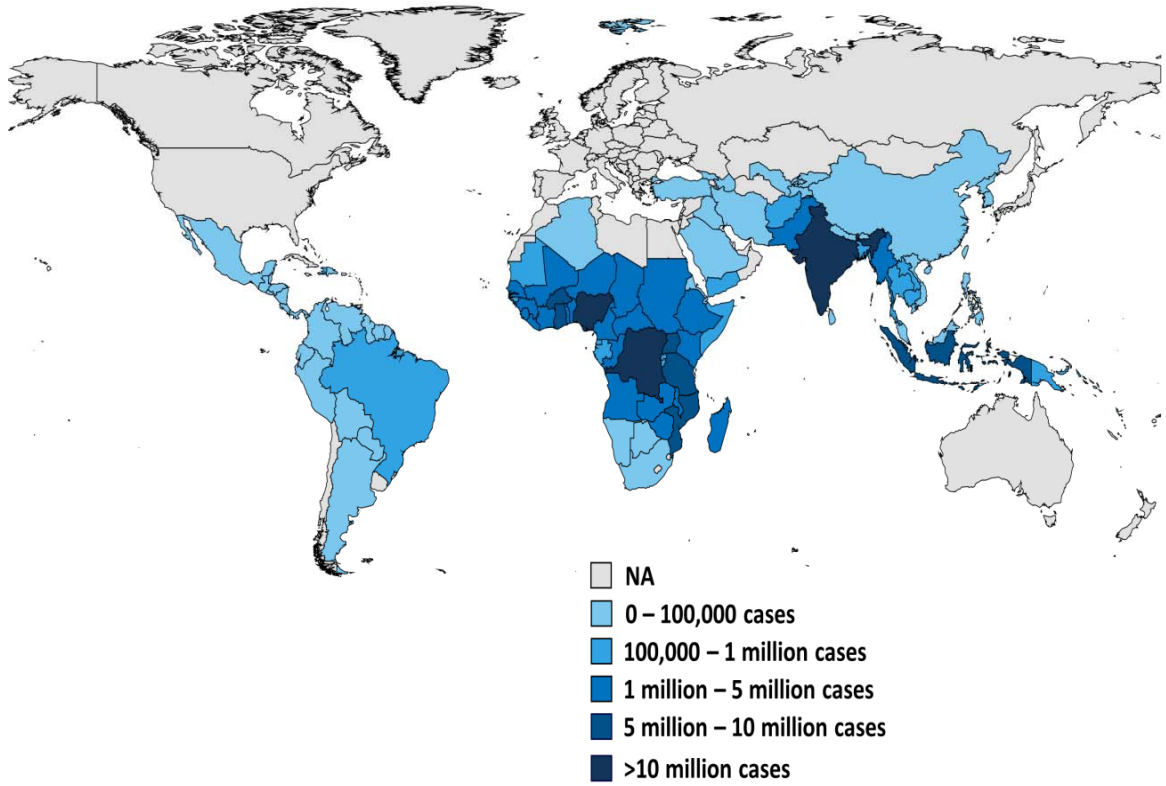

Figure 1. Estimated worldwide deaths (in millions) caused by malaria in 2012, reproduced by permission from WHO (www.who.int).[3]

1.1.3. The life cycle of the malaria parasite

The parasite is carried by over 120 species of the parasite genus *Plasmodium*, but only four of these infect humans to cause malaria; these are *Plasmodium falciparum*, *Plasmodium vivax, Plasmodium ovale* and *Plasmodium malariae*. Of all these, the most dangerous is *Plasmodium falciparum.*[5,6] The female anopheles mosquito is a carrier of the disease, and it acquires the parasite from the blood of the human host that already has the infection.[5] The parasite then passes through various mosquito stages in its life cycle before it can infect another host. Six critical stages can be identified in the life-cycle of the malaria parasite as illustrated in Figure 2 and detailed below.

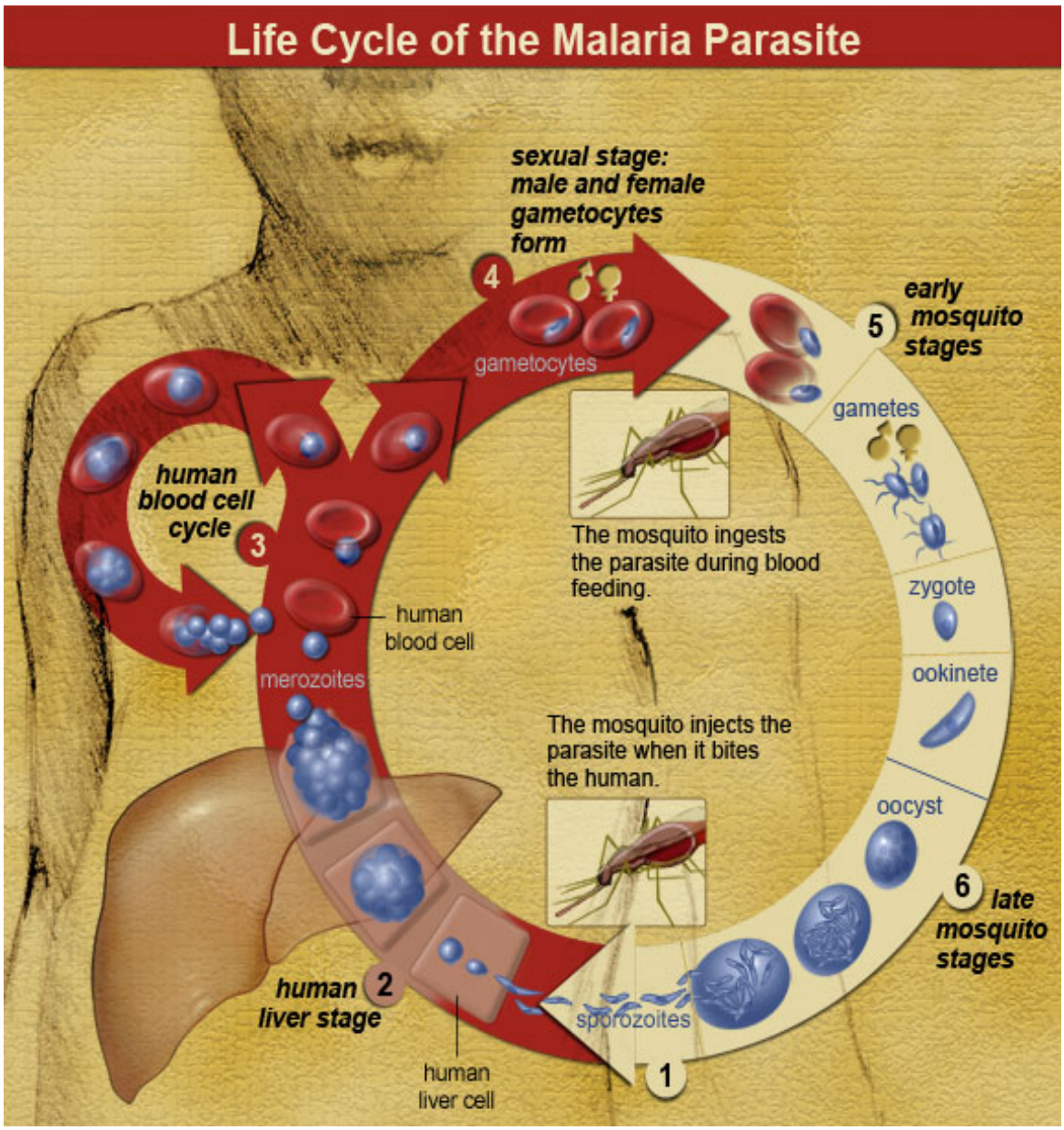

Figure 2. The plasmodia cycle, reproduced by permission from NIH.[5]

a. An infected female anopheles mosquito bites a human and, as a result, malarial sporozoites are inoculated into the human host from its salivary glands and these infect the liver.[5,7]

b. After 6-15 days, the sporozoites produce thousands of merozoites in each liver cell.[8] These result in extensive modification of the host cell, causing deformability, illness and complications that can last for months if not treated.

c. Still at the human blood stage, the merozoites migrate from the liver cells into the bloodstream,[5,9] beginning an asexual lifecycle of invasion of red blood cells, and releasing newly formed merozoites into the red blood cells repeatedly over 1-3 days.[9,10]

d. During the asexual cycle in the blood stage, a small percentage of merozoite-infected blood cells that have not replicated develop into sexually committed cells, the female and male gametocytes.[5,11]

e. Gametocytes are ingested by a female anopheles mosquito during a blood-meal from an infected host and develop in the mid-gut of the mosquito into male and female gametes.[11] Sexual reproduction occurs to form a zygote that develops into an ookinete. The ookinete migrates through the mid-gut epithelium and matures into an oocyst under the basal membrane.[5,11,12]

f. After 8-15 days, the oocysts burst and mature to form sporozoites, which upon rupture migrate to the salivary glands from where they are injected and infect humans during the next blood-meal taken by the mosquito.[5,6,9,12] Further transmission thus take place when the mosquito injects the infectious sporozoites through its salivary glands into a new host.[13]

1.1.4. Pathogenesis

The pathology of malaria is due to the replication of the infected parasite in the erythrocytes. The rupture of the erythrocytes leads to the release of cell debris into the blood stream of the human host, causing some of the clinical symptoms of malaria.[3,4] The primary symptoms of malaria include headache, fever, muscular and abdominal pain, weakness, vomiting, watery diarrhoea, chills and profuse sweating.[3,4] Depending on the *Plasmodium* species, the symptoms tend to assume a characteristic periodicity. In *P.vivax*, *P.ovale* and *P. falciparum* the periodicity is 48 hours and for *P.malariae* the periodicity is 72 hours. *P.falciparum* infections are more severe and when untreated can result in a death rate of 25% in adults.[4] Anaemia is the most immediate consequence of parasite replication and the destruction of erythrocytes. There can also be suppression of red cell production in the bone marrow, resulting in swelling of the spleen due to the accumulation of parasitized red cells and the proliferation of white cells.[13,14] If the infection is treated the spleen returns to normal size but, in chronic infections, the spleen continues to enlarge, and discolouration occurs due to the accumulation of the malaria pigment, hemozoin.[13,14]

In the pregnant female, *falciparum* infection may result in still-born foetuses, lower than normal birth weight, or abortion, while children born from infected mothers may develop cerebral malaria, as a consequence of the mechanical blockage of micro vessels in the brain, or organ damage.[4,15,16] The effects of malaria infection are summarised in Figure 3.

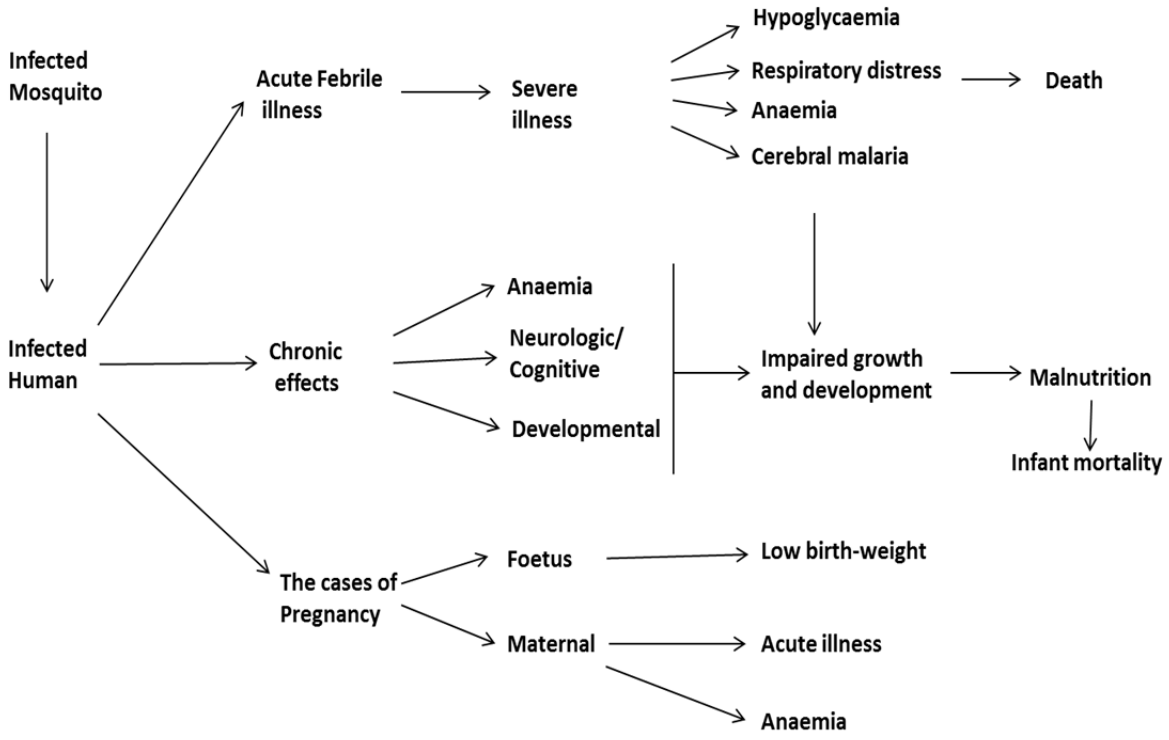

Figure 3. Manifestation of malaria parasite pathogenesis. Created from, Jeffrey Sachs *et al.* 2002, Clark *et al.* 2003, World malaria report, 2008.

1.1.5. Eradication efforts against malaria

The goal of any Malaria Control Programme is to reduce the number of malaria-related cases and deaths.[1,5] However, the permanent eradication of malaria in humans has proven to be complex and challenging. Despite serious efforts to control this disease, the results have been disappointing, with the parasite developing resistance to available drugs and also evading control measures and developing insecticide resistance. Combination drug therapy has been used to prevent the emergence of drug resistance,[1,15,16] and indoor spraying or the use of insecticide-impregnated bed nets have been effective in reducing transmission. Transmission-blocking vaccines have been developed, but an effective vaccine for the total eradication of malaria has not yet been produced.[1,17] The increasing drug resistance prompted WHO to establish the ABCD programme / approach for malaria.[17]

- **A**wareness of malaria.
- **B**ite prevention using bed-nets.
- **C**hemoprophylaxis (taking antimalarial medication as prescribed by the doctor).
- **D**iagnosis and the treatment of malaria.

Today, malaria eradication efforts include the "Roll Back Malaria" partnership initiated by the WHO, The United Nations Development Programme (UNDP), and the United Nations Children's Fund (UNICEF).[18] These organizations are collaborating with private companies to reduce the human and socio-economic burden of malaria, by providing bed nets and the necessary malaria drugs in rural areas, especially where access to treatment is limited.[18,19] To eradicate malaria altogether, however, long lasting insecticidal nets (LLIN), indoor residual spraying of insecticides (IRS) and intermittent preventive treatment (IPT) during pregnancy are needed.[17,19]

1.1.6. Currently used drugs and the development of drug resistance

Antimalarial drug resistance can be defined as the ability of a parasite to undergo continuous replication, when there is intake of a drug prescribed or recommended by the doctor to destroy the parasite.[20] The cause of resistance to currently used drugs may be due to several factors that include:- the overuse of antimalarial drugs; parasite adaptability at metabolic and genomic levels; inadequate therapeutic treatment of infections; and rapid proliferation of the parasite leading to the mutation of cells in the drug target thus reducing their sensitivity to the medication.[21] The currently used drugs (Figure 4), are grouped into five main classes:- quinolines; anti-folates; artemisinins; hydroxynapthoquinones; and antibiotics.[22]

1.1.6.1. Quinoline antimalarials

Quinoline itself is a heterocyclic aromatic organic compound that was first extracted from coal tar.[23,24] The quinoline derivatives which have served as a mainstay in chemotherapy against malaria include the natural product quinine **1**, and the synthetic drugs, chloroquine **2** and mefloquine **3** (Figure 4). Quinine **1** was the first antimalarial drug; it is extracted from bark of cinchona trees and has been used for centuries. The mode of action of quinine **1** and the development of resistance are similar to those observed with chloroquine **2**.[24] Chloroquine **2**, a synthetic drug, has significant therapeutic value, acting rapidly against the blood stages; it has low toxicity, good bioavailability, is reasonably inexpensive,[25] and is

widely used for the prophylactic treatment of malaria.[22] Its frequent use through the decades has eventually led to resistance in *Plasmodium falciparum*. Chloroquine's efficacy is thought to lie in its ability to interrupt haematin detoxification in malaria parasites as they grow within their host's red blood cells.[26-28] Toxic haematin is released in large amounts in the digestive food vacuole, and the parasite removes the toxic haematin by polymerization into innocuous crystals of haemozoin pigment and, possibly, by a glutathione-mediated process of destruction.[26-28] Chloroquine is thought to disrupt this detoxification by binding with haematin in a μ-oxodimer form, causing the accumulation of toxic haematin in the mid-gut of the parasite and thereby poisoning it. Resistance to this drug is caused mainly by mutations in the *Pf*crt gene.[26-28]

Mefloquine **3**, a piperidino derivative of quinine **1**,[29] is also blood-stage specific and acts on haemoglobin digestion.[29] In 1984, mefloquine **3** was introduced as a treatment for uncomplicated *falciparum* malaria, but substantial resistance developed within 6 years.[26-28] Like chloroquine **2**, mefloquine **3** induces the formation of toxic haeme complexes within the parasite food vacuole,[26-28] making it effective for both prophylaxis and acute therapy. It is now strictly used for resistant strains (usually combined with artesunate). Serious side-effects of mefloquine **3** include: psychological disturbances, such as anxiety, depression, restlessness, and confusion.[29] This medication should therefore not be used for people who have disorders such as schizophrenia or depression.

1.1.6.2. Antifolates

The antifolate drugs, pyrimethamine **4**, proguanil **5**, cycloguanil and sulfadoxine **6,**[22,26] act against malaria by interfering with folate metabolism, a pathway essential to malaria parasite survival. These drugs can be used both as prophylactic and therapeutic agents,[26] but unfortunately, the antifolates have proven susceptible to resistance in the malaria parasite.[27-28] Resistance is caused by mutations in the dihydropteroate synthase (*dhps*) gene and dihydrofolate reductase (*dhfr*) gene, two essential enzymes in the folate biosynthesis pathway.[26] Proguanil **5** mostly targets the *dhfr* enzyme, whereas the sulfa drugs affect the *dhps* enzyme. The antifolates, act by inhibiting these enzymes preventing the formation of tetrahydrofolate co-factors, which are important for the biosynthesis of pyrimidine and amino acids, such as methionine and serine.[26,30,31] The absence of pyrimidine inhibits DNA synthesis, while the deficiency in amino acids prevents parasite growth. Combining these

antifolates with other drugs that act on different targets in the parasite should greatly enhance efficacy and help prevent the development of resistance. Sulfadoxine-pyrimethamine combinations, for example, have shown long-term utility and are cheaper alternatives to combating the chloroquine-resistant parasites. They also prevent DNA synthesis in the plasmodia and act on schizonts during the erythrocyte stage.[26,27]

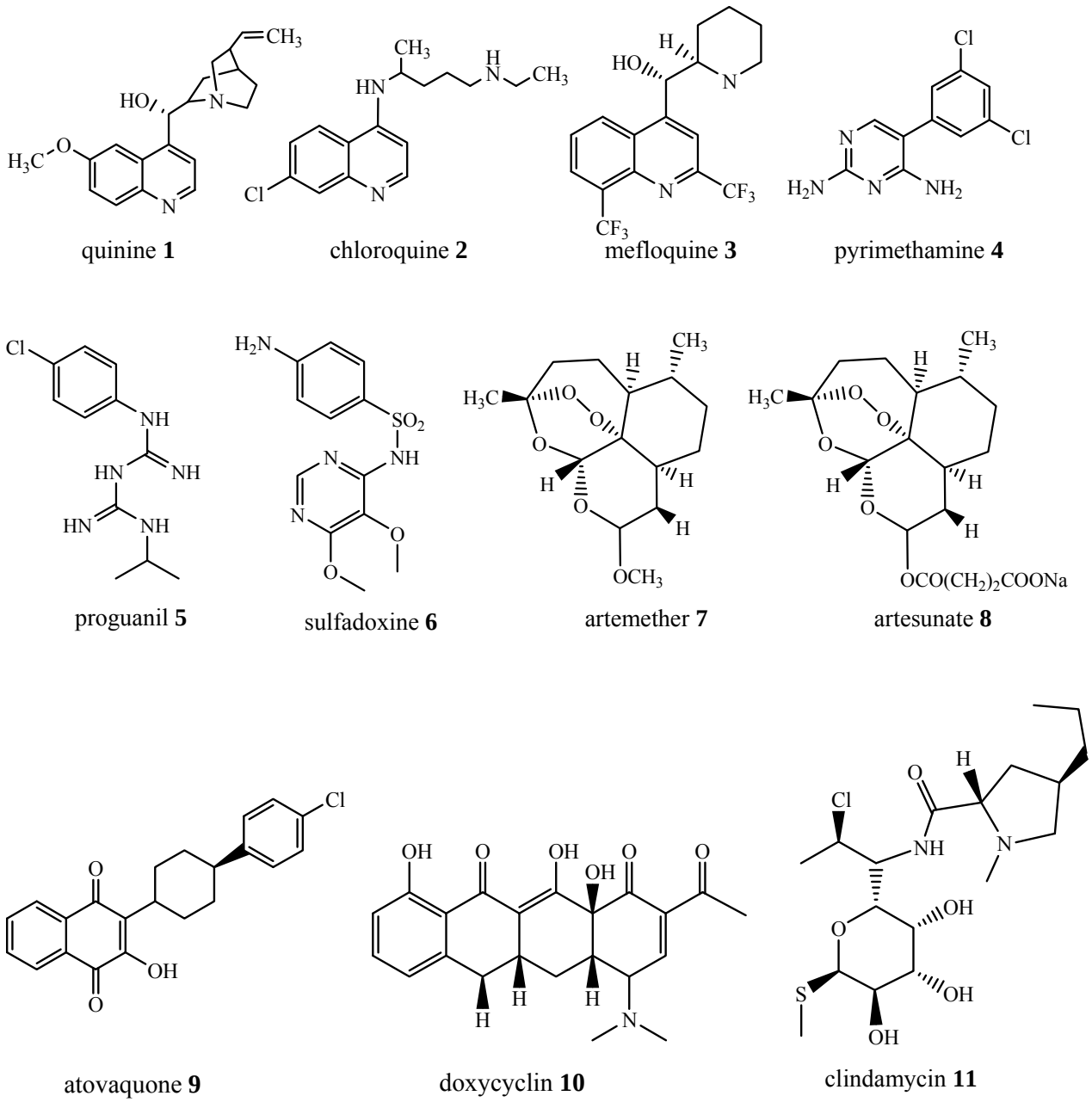

Figure 4. Structures of current antimalarial drugs.

1.1.6.3. Artemisinins

In 1979, artemisinin, an extract from the herbal plant *Artemisia annua*, was first reported to cure malaria in China.[24] Its derivatives include artemether **7**, artesunate **8** and arteether,[26,30] which act rapidly against the erythrocyte stage in the mosquito life-cycle. Artemether **7** and arteether are lipid-soluble drugs and both can be administered *via* intramuscular injection, while artesunate is water-soluble and it is administered orally or intravenously.[26]

Artemisinins bind to *pf*ATP6 (ATPase transporter) by hydrophobic interaction, allowing reductive cleavage of the *endo*-peroxide bridge and formation of carbon-centred radicals or free radicals. Although this mechanism is not fully understood, synthetic chemists have demonstrated that the *endo*-peroxide bridge is necessary for antimalarial activity.[24,26] Since peroxides are a known source of reactive oxygen species, such as hydroxyl radicals and superoxide,[25] this observation suggested that free radicals might be involved in the mechanism of action. Resistance to these drugs may be due to mutations in the *pf*ATP6 gene.[3,26,33] Combination therapies have been used to address the problem of resistance; examples include lumefantrine in combination with artemether **7**, amodiaquine in combination with artesunate **8** and piperaquine combined with dihydroartemisinin.[32,33]

1.1.6.4. Hydroxynaphthoquinones

The hydroxynaphthoquinone derivative, atovaquone **9** {2-[*trans*-4-(4′-chlorophenyl) cyclohexyl]-3-hydroxy-1,4-naphthaquinone} can be used for chemo-prophylaxis.[29] This antimalarial drug binds to the *cytochrome bc1* complex, interrupting mitochondrial electron transport leading to the collapse of the parasite membrane.[22,29] The mechanism of resistance in *Plasmodium* parasites towards atovaquone **9** is attributed to point mutations within the *cytochrome b* gene, thus reducing the binding affinity of the drug.[35]

1.1.6.5. Antibiotics

Several antibiotics display an antimalarial effect through their action on the prokaryote-like protein biosynthesis of the mitochondrion and/or the apicoplast.[35] Doxycyclin **10**, is the most widely used antibiotic of the tetracycline class against malaria. In combination therapy, it can be used with quinine or artesunate.[17,35] However, doxycyclin **10** cannot be used in children under the age of eight or in pregnant women due to its incorporation into developing bones and teeth; Clindamycin **11**, on the other hand, is considered safe in pregnancy and in young children.[22,26] The anti-malarial activities of these compounds involve the inhibition of DNA

replication (DNA gyrase, RNA polymerase) and the inhibition of protein synthesis by interacting with the RNA unit in *plasmodium* species.

Details covering the half-life, cellular target, advantages and adverse effect(s) of currently used drugs are summarised in Table 1.1.[22-35]

Drug	Half-life	Cellular target	Advantages	Adverse effect(s)
Quinolines				
Quinine	18 h	Haeme metabolism	Good inihibitory agent at the erythrocytic stage, good bio-availability	Neurotoxicity, hyploglycemia.
Chloroquine	1-2 months	Haeme metabolism	Fast action in the erythrocytic stage, hydrophilic, cheap.	Widespread resistance and itching.
Mefloquine	2-4 wks	Haeme metabolism	Potent in RBC stage	Depression
Amodiaquine	6 h	N-methyl transferase inhibitor	Effective against CQ resistant strains.	Hepatoxic effect
Anti-folates				
Sulfadoxine	3.5 h	Structural analog of PABA inhibits DHPS	Oral use, prophylaxis and treatment.	
Pyrimethamine	1.5 h	Folate synthesis inhibition of DHFR	Oral use, prophylaxis and treatment.	May affect folic acid in human.
Arterminins				
Artemether Artesunate	30 mins	Inhibits pfATP6	Fast acting	Short half-life and poor solubility.
Antibiotics				
Doxycyclin	18-22 h	Impairment of apicoplast genes resulting in abnormal cell division	Used for syphilis, and for malaria prophylaxis treatment.	Slow-acting.

1.2. IDENTIFYING NOVEL ANTIMALARIAL TARGETS AND DRUG DESIGN

For decades, malaria chemotherapy has relied on a limited number of drugs, each of which has led to resistance, thus prompting the synthesis of novel antimalarial agents and the identification of new drug targets. Various factors must be considered in the development of an antimalarial drug; the new drug needs to have low toxicity, readily inexpensive for purchase and efficacious.[20,31]

Some distinct organelles, such as the food vacuole, apicoplast and mitochondrion, provide useful targets for anti-malarial drugs.[37] The food vacuole is where the erythrocyte haemoglobin is hydrolysed into haeme which is then polymerized into insoluble haemozoin pigment. The antimalarial acts by preventing haemozoin formation, thus resulting in an accumulation of haeme which is toxic to the parasite in the parasite food vacuole, causing the parasite's death.[37] The mitochondrion which is involved in electron transport, genome replication, repair, recombination, transcription, and translation, is a valid drug target organelle due to the presence of cytochrome *C*-oxidoreductase (complex III) - an enzyme in the mitochondrion that can be easily mutated.[28,36,38]

The apicoplast, which is involved in the synthesis of DNA and Type II fatty acid synthesis, also helps in the synthesis of isoprenoid precursors,[39] generally involving the 1-deoxy-D-xylulose-5-phosphate reductoisomerase (DXR) enzyme. The DXR pathway is absent in humans, and is therefore is a good target for inhibition without causing harm to the human host.[40,41]

1.2.1. The isoprenoid pathway

Isoprenoids are biologically active molecules which constitute the largest single class of natural products.[43] They have diverse biological roles in pigments, plant hormones, vitamins (A, D, E and K), sterols, carotenoids and chlorophyll.[43,44] The biosynthesis of the phosphorylated five-carbon precursors, isopentyl pyrophosphate (IPP) and dimethylallyl pyrophosphate (DMAPP) occurs *via* two distinct routes: the mevalonate pathway (MVA pathway) and the methylerythritol phosphate pathway (MEP pathway) as shown in Figure 5.[43-45]

The mevalonate (MVA) pathway involves the condensation of two molecules of acetyl-CoA **12** to form acetoacetyl-CoA **13** catalysed by acetyl-CoA synthase (AAS); further condensation with another acetyl-CoA yields 3-hydroxy-3-methylglutaryl-CoA (HMG-CoA)

14 - a step catalysed by HMG-CoA synthase (HMGS) (Figure 5). [44-45] The enzyme, HMG-CoA reductase (HMGR), catalyses the irreversible reduction of HMG-CoA to form mevalonate (MVA) **15**,[44-46] which undergoes two successive phosphorylation steps to give mevalonic-5-monophosphate (MVA-P) **16** and mevalonic-5-diphosphate (MVA-PP) **17**. Subsequent decarboxylation in an ATP-dependent step yields IPP **18**, which is then transformed to DMAPP **19** by isopentenyl diphosphate isomerase also known as IPP isomerase.[44-47]

It has been reported, however, that the isoprenoid precursor **19** can be formed through a new metabolic route, namely, the non-mevalonate (NMVA) pathway.[44,45] This pathway is also known as the 1-deoxy-D-xylulose-5-phosphate (DXP) pathway, or 2-*C*-methyl-D-erythritol-4-phosphate (MEP) pathway.[45] The MEP pathway is comprised of seven enzymatic steps (Figure 5), the first being the condensation of glyceraldehyde-3-phosphate **20** and pyruvate **21** to produce 1-deoxy-D-xylulose-5-phosphate DOXP **22**,[45] in a transketolase-type reaction catalysed by 1-deoxy-D-xylulose-5-phosphate synthase (DXS). The DOXP is then converted into 2-*C*-methyl-D-erythritol-4-phosphate (MEP) **23**,[44,45] in a reaction mediated by the DOXP-reductoisomerase (DXR) enzyme. This step involves intramolecular rearrangement and reduction, which requires nicotinamide adenine dinucleotide phosphate (NADPH) and a co-factor in the form of a divalent cation (Mn^{2+}, Mg^{2+} or Co^{2+}).[44,45]

MEP **23** is converted to 4-diphosphocytidyl-2-*C*-methyl-D-erythritol (CDP-ME) **24**, in a reaction catalysed by CDP-ME synthase (Figure 5).[44,45] The adenosine triphosphate (ATP)-dependent CDP-ME kinase then phosphorylates the CDP-ME C-2 hydroxyl group, forming 4-diphosphocytidyl-2-*C*-methyl-D-erythritol-2-phosphate (CDP-ME-2P) **25** and adenosine diphosphate (ADP).[44] In the next step, the CDP-ME-2P is converted into 2-*C*-methyl-D-erythritol-2,4-cyclodiphosphate (MECP) **26** and cytidine monophosphate (CMP) in a reaction catalysed by MECP synthase.[44,45] 1-Hydroxy-2-methyl-2-(*E*)-butenyl-4-diphosphate synthase (HMBPP synthase) then converts MECP into 1-hydroxy-2-methyl-2-(*E*)-butenyl-4-diphosphate HMBPP **27**.[45] Finally, HMBPP forms IPP and DMAPP, the reaction being catalysed by HMBPP reductase (also called IPP / DMAPP synthase).[44-45]

This pathway, which is not present in humans, occurs in plastids.[45] Absence of the non-mevalonate pathway in higher organisms has opened a new platform for the development of novel antibiotics and antimalarials.

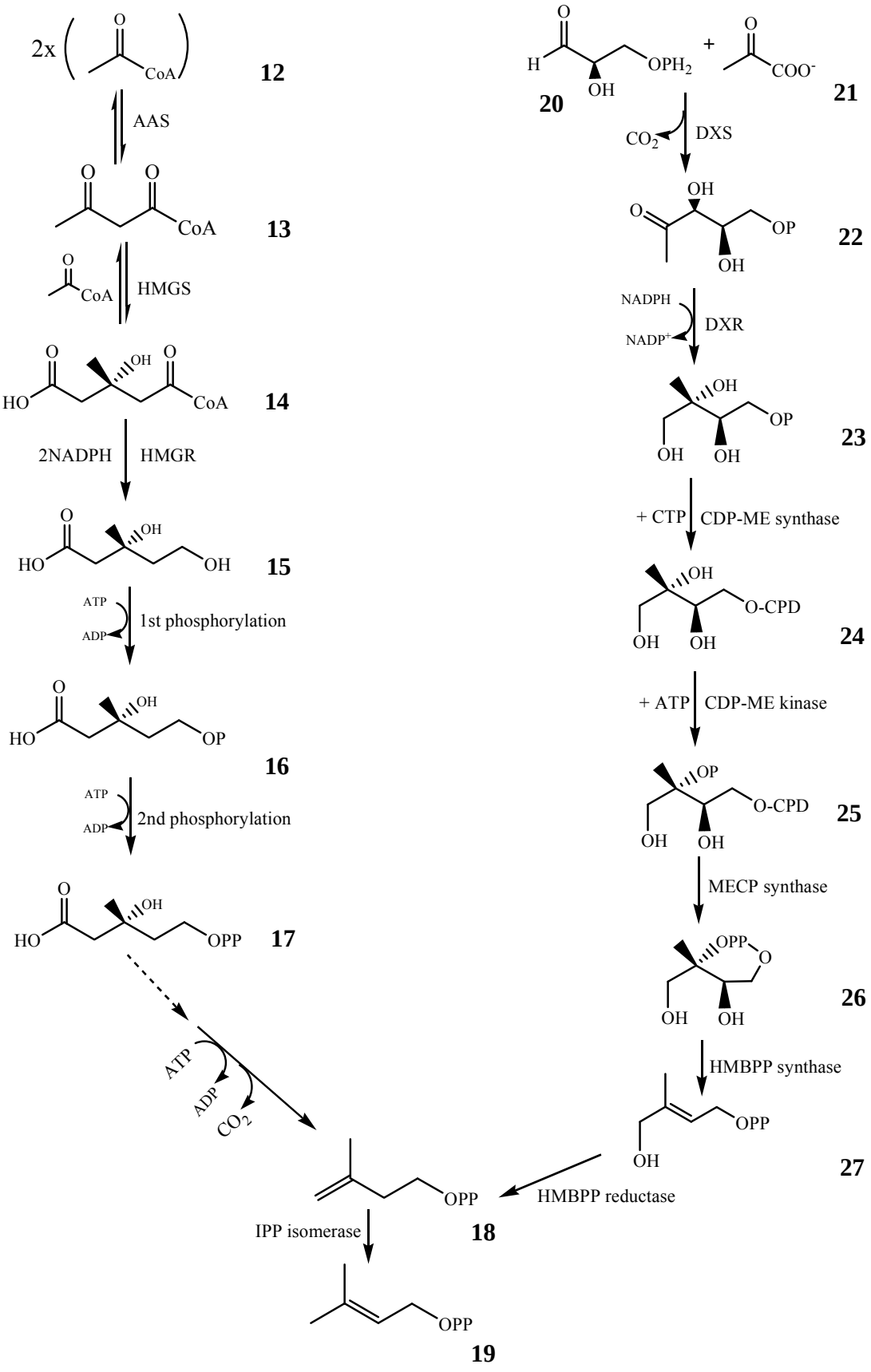

Figure 5. The two isoprenoid pathways showing the enzymes involved.[45]

1.2.2. Mechanism for the conversion of 1-deoxy-D-xylose-5-phosphate (DOXP) to 2-*C*-methyl-D-erythriol-4-phosphate (MEP)

The formation of MEP **23** from DOXP **22** in the non-mevalonate pathway requires the enzyme 1-deoxy-D-xylulose-5-phosphate reductase (DXR) and a divalent metal ion (Co^{2+}, Mn^{2+} or Mg^{2+}) co-factor which is involved in electrostatic interactions with DOXP.[48,49] Three different mechanisms have been suggested (Figure 6). In the first mechanism, a retroaldol / aldol reaction involves deprotonation of the C-4 hydroxyl group of 1-deoxy-D-xylulose-5-phosphate and cleavage of the C-3 and C-4 bond of the DOXP.[49] The cleavage produces the enolate of hydroxyacetone **28** and glycoaldehyde phosphate **29**, which then combine with the formation of a new bond between C-2 and C-4 to give 2-*C*-methyl-D-erythrose-4-phosphate **30** as an aldehyde intermediate (Figure 6).[47,49]

The second mechanism, involving an α-ketol rearrangement, occurs when the C-3 hydroxyl group of DOXP **22** is deprotonated to form a ketone, followed by migration of the phosphate bearing C-2 sub-unit to afford the intermediate 2-*C*-methyl-D-erythrose-4-phosphate. Hydrogens are later donated from NADPH to reduce the aldehyde into an alcohol (Figure 6).[49] The last proposed mechanism involves a 1,2-hydride shift in which hydride migrates from C-3 of DOXP **22** to C-2, after which rearrangement leads to the common intermediate 2-*C*-methylerythrose-4-phosphate **30**, NADPH reduction of which affords MEP **23** (Figure 6).[49]

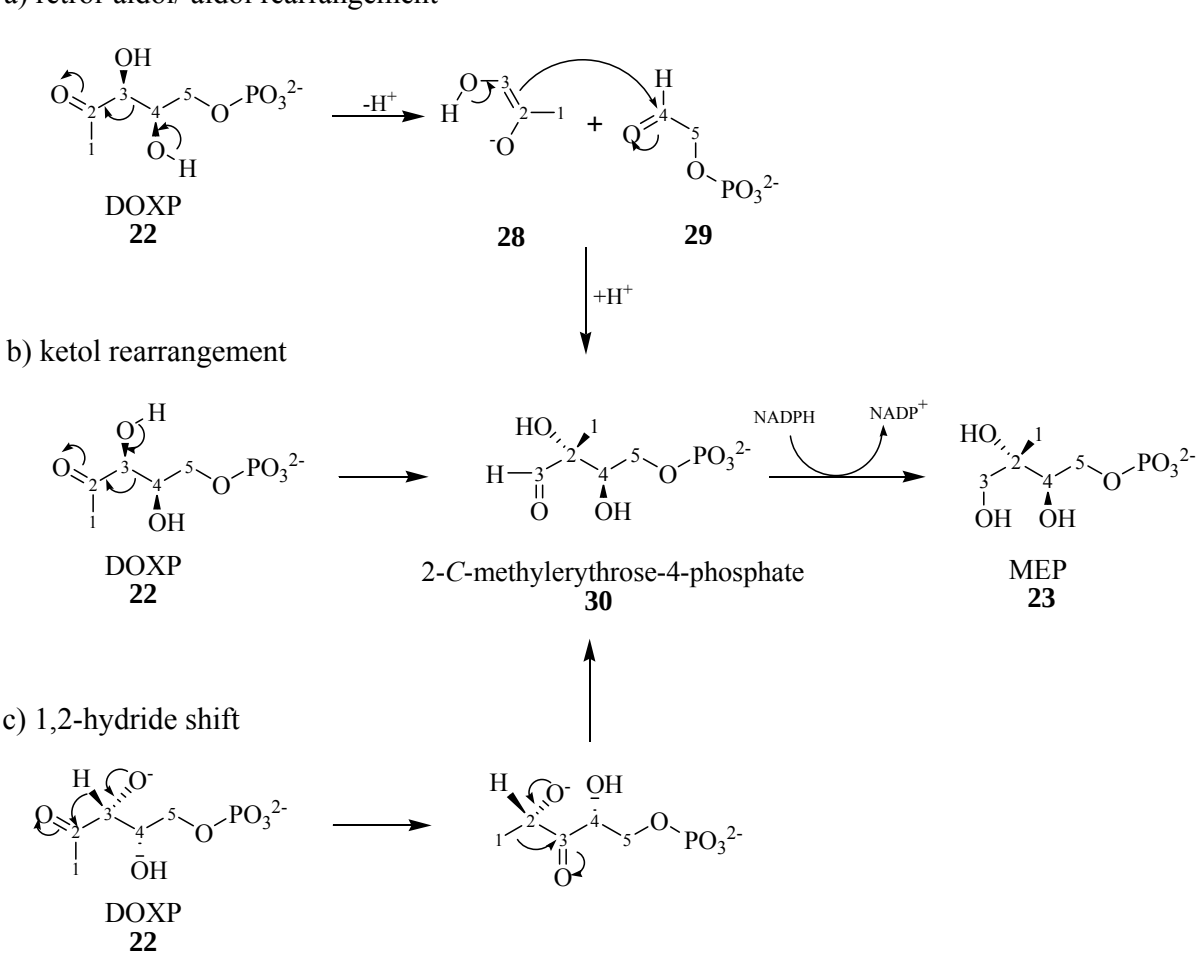

Figure 6. The three mechanisms proposed for the conversion of 1-deoxy-D-xylose-5-phosphate (DOXP) **22** to 2-*C*-methyl-D-erythriol-4-phosphate (MEP) **23**.[49]

The stereochemical aspects of the NADPH-mediated DXR-catalysed reaction in each of the proposed mechanisms,[49] are shown in Figure 7. The *re*-face attack of C-4 on the C-2 carbonyl carbon of DOXP precedes attack of the C-4 pro-*S* hydride from NADPH at the C-1 carbonyl of DOXP **22**, with the result that the pro-*R*-hydrogen at C-l of MEP can only be formed from the 4-*S*-hydrogen of NADPH.[50,51]

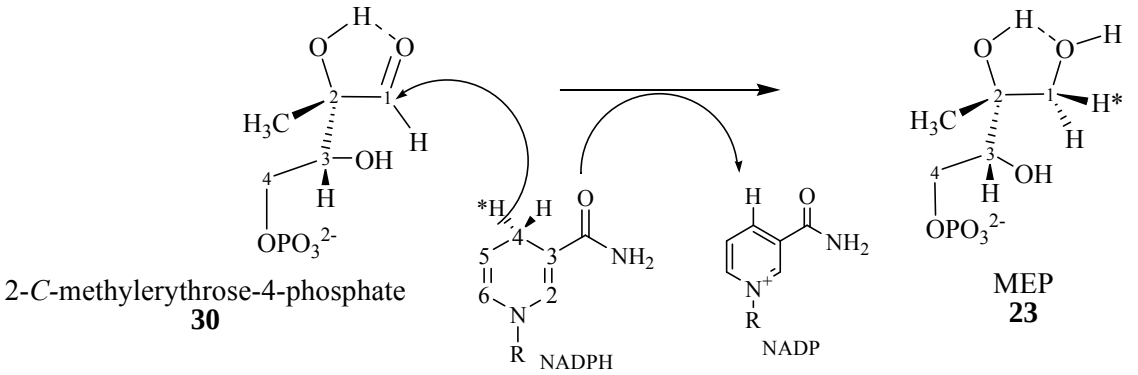

Figure 7. Stereochemical effects in the DXR-catalysed conversion of the common intermediate **30** to MEP **23**; H* is the pro-*S*-hydrogen of NADPH involved in the rearrangement.[50,51]

1.2.3. Structural Characterization of DXR

X-ray crystallography revealed that *Ec*DXR exists as an 86 kDa homodimer in its quaternary form, and each of its 43.5 kDa monomeric units comprises a V-shaped structure.[52,53] In 2010, the crystallization and preliminary X-ray analysis of *P.falciparum* DXR was reported by Tomonobu Umeda *et al*.[45] (Figure 8), showing similarities between the overall structure of *Pf*DXR with those of the DXR enzyme in *E.coli* and other species.

1.2.3.1. The crystal structure of Pf*DXR*

The *Pf*DXR monomer comprises two large domains as shown in Figure 8, namely the NADPH-binding domain responsible for the NADPH binding and the catalytic domain which supports the substrate binding.[45,51] The NADPH domain is larger than the catalytic domain and comprises 150 residues containing several parallel-stranded β-sheets and α-helices that bind with NADPH at the crevices of the domain. The catalytic domain has 135 residues and accommodates the divalent metal ion.[51] These two domains are separated by a linker region, which helps to give structural support to the *Pf*DXR active-site.[45,52,53]

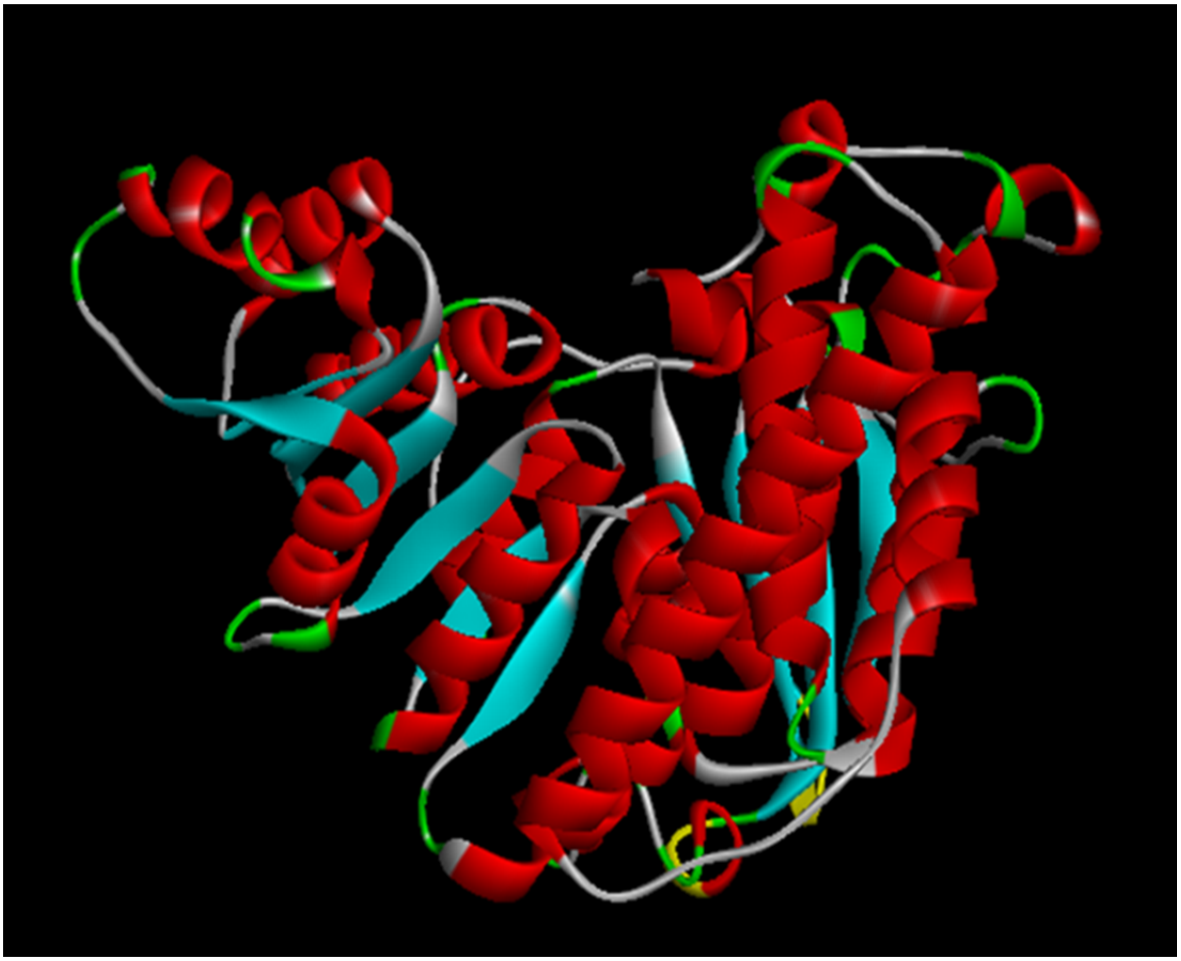

Figure 8. Ribbon representation of the *Pf*DXR crystal structure showing the three domains: the *N*-terminal domain (red); the connective domain (cyan); and the catalytic loop (green). (Generated using Discovery Studio Visualizer 4.0).[51]

1.2.3.2. The active-site; the substrate and metal binding properties

According to the reports made on the active-site of the DXR molecule by Umeda *et al*.,[45] DXR has a flexible structure. In Figure 9, the binding of fosmidomycin (an inhibitor) to the *Ec*DXR active-site appears to involve hydrogen-bonding interactions with several proximate active-site residues (Ser-186, Ser-222, Glu-152, Asn-227 and Lys-228).[54] The carbon backbone of the inhibitor lies parallel to the β-indole ring of Trp-212,[54] its negatively charged phosphonate group and hydroxymate group adopt a linear conformation and the inhibitor interacts with the metal through bi-dentate chelation involving the hydroxamate group. [52,53,55]

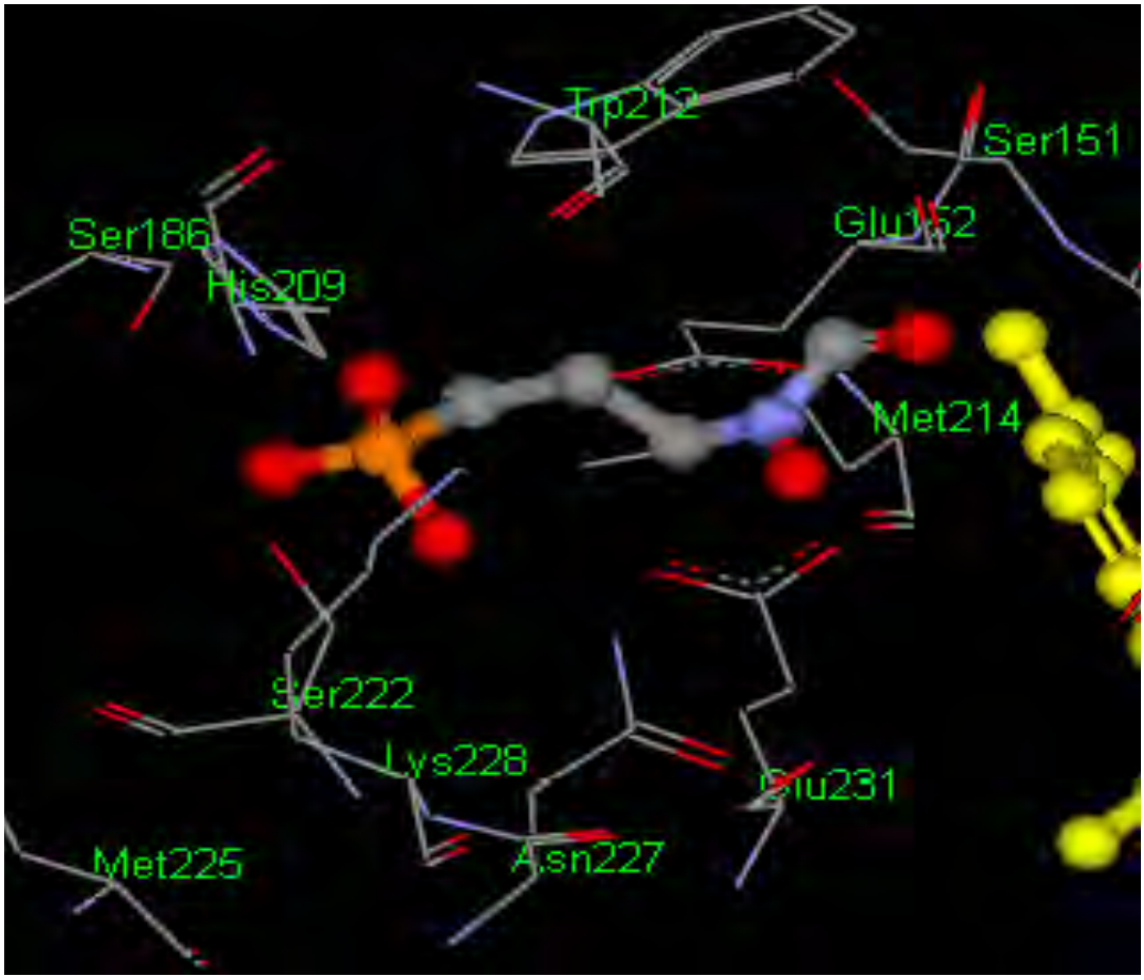

Figure 9. The *Ec*DXR active site with fosmidomycin shown in ball and stick models interacting with active-site residues, and NADPH (yellow) generated using Discovery Studio Visualizer 4.0.[51]

The co-factor metal ions needed for the substrate binding are Mn^{2+}, Mg^{2+} or Co^{2+}, but Mg^{2+} is preferred due to its maximum activity compared to the other co-factors.[48] Reports made on the interactions between the divalent metal cation and DOXP **22** in *Ec*DXR or *Mt*DXR by Steinbacher *et al.*,[55] Yajima *et al.*,[53] and Mac Sweeney *et al.*[54] reveal the formation of an octahedral complex with water molecules and residues Glu-231, Asp-150 and Glu-152. Fosmidomycin **31**, shows interactions with similar residues involved in the complex formation with those for DOXP **22** (Figure 10).[52] The formation of a quaternary complex with the co-factor divalent metal ion (Mg^{2+}) is essential for the correct positioning of the inhibitor in the active-site.[45,53]

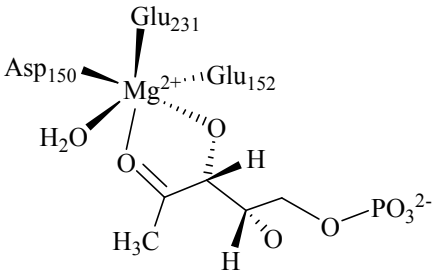

DOXP **22**

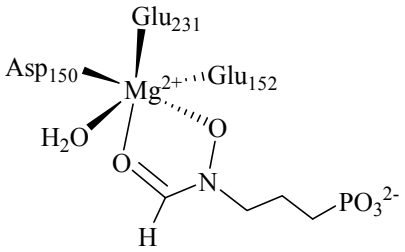

Fosmidomycin **31**

Figure 10. Octahedral complexes formed between residues and water molecules by DOXP and Fosmidomycin.

1.2.3.3. Kinetic Characterization of DXR

The enzymatic features can be described in the correlation between the concentration of substrate and the steady state velocity.[60] The kinetic behaviour of an enzyme can be studied with respect to the *Michaelis* dissociation constant Km, the maximum velocity (V_{max}), the specificity constant (K_{cat}/Km) and second order rate constant.[46,60,61] The *Michaelis* constant Km is the substrate concentration at which the reaction rate is at half-maximum, and is an inverse measure of the substrate's affinity for the enzyme. A decrease in Km indicates high affinity for the enzyme reflecting a tight and effective interaction between the substrate and the enzyme;[46] Km is dependent on the enzyme, substrate, temperature and pH.[46]

The specificity constant (K_{cat}/Km) [46,60] or kinetic efficiency can be defined as the efficiency of an enzyme. This factor is an essential kinetic value that relates to the substrate specificity of an enzyme. The catalytic constant K_{cat} or turnover number reflects the maximum rate at which the enzyme binds to the substrate.[46,61] Kinetic values for *M.tuberculosis* DXR enzymes have been reported, showing that Km varies with divalent metal cation; Co^{2+} has a Km = 42 ± 7 μM, Mn^{2+} Km = 4.0 ± 0.3 μM, and Mg^{2+} Km =100 ± 4 μM. The preference for Mg^{2+} was also based on the Km value. However, no values have been reported for *Pf*DXR.[46,60]

1.3. FOSMIDOMYCIN AS A DXR INHIBITOR

Fosmidomycin **31** has been reported for the treatment of uncomplicated malaria in humans.[45,47] In the late 1970s, the antibiotic, fosmidomycin **31** [3-(*N*-formyl-*N*-hydroxy-amino)propylphosphate], was isolated from *Streptomyces lavendulae,*[44,45] and was reported to inhibit the DXR enzyme. The *N*-acetyl-analogue, FR900098 **32**, which also has herbicidal activity, was also found to have DXR inhibitory activity.[45,47] The only difference between this analogue and fosmidomycin is the replacement of the formyl hydrogen of fosmidomycin by a methyl group (Figure 11) but this results in FR900098 being a more potent DXR inhibitor than fosmidomycin *in vitro*.[45,47]

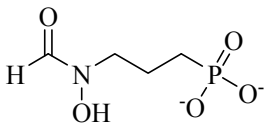

Fosmidomycin **31**

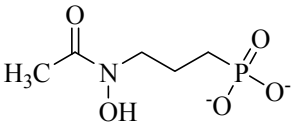

FR900098 **32**

Figure 11. Structure of fosmidomycin **31** and its analogue **32**.

The antibiotic binds in the crevice of the catalytic domain which is differentiated into three regions; each of the regions has a different function necessary for successful binding and its inhibitory effect as an antimalarial.[45] To date, with several DXR inhibitors having been reported, fosmidomycin **31** and its analogue FR900098 **32** have been found to be effective antimalarials on infected mice.[45] However, their potential to become a therapeutic drugs is considered to be poor due to their disadvantages of low absorption, short half-life and low bioavailability.[44,45] Attempts were made to improve the efficiency of fosmidomycin **31** by combining it with clindamycin **11**, but this can only be used to treat uncomplicated malaria, and the combination is also susceptible to malaria resistance.[44,45] In order to inform the design of new drugs and to understand the catalytic mechanism, several crystal structures of DXR complexes with fosmidomycin **31** have been determined. Three apparently essential components for such inhibitors have been proposed; these are illustrated in Figure 12.

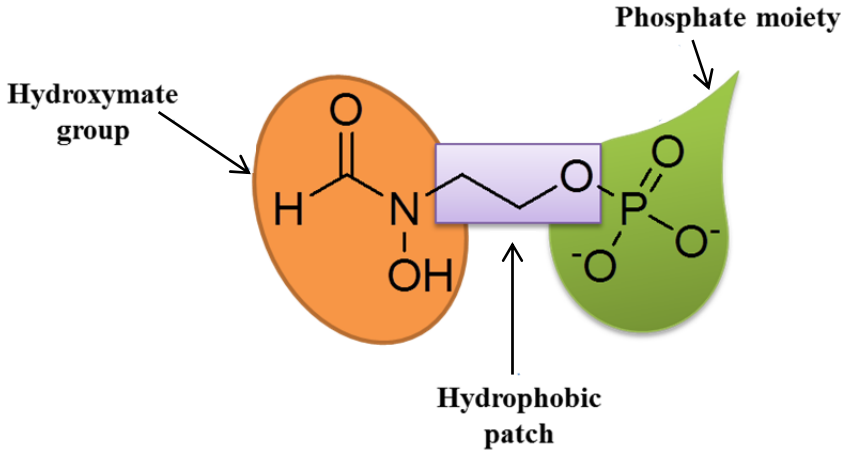

Figure 12. Proposed essential structural components in fosmidomycin **31**.

1.3.1. Modification of fosmidomycin 31 and its analogue 32

The phosphate moiety forms tight hydrogen-bonding with the residues Ser-270, Asn-311, water molecules and His-293 resulting into tightly bound network in the DXR active-site.[28] However, because the O-P bond to phosphates is easily cleaved, it is commonly replaced by the C-P phosphonate bond in inhibitor design.[66] Modifications reported by Umeda *et al.*,[45] include replacement of the phosphonate group with other isosteric groups as in the carboxylic acid **33** and the sulphonic acid **34** (Figure 12a). In *Ec*DXR, these changes result in a drastic decrease in inhibitory activity. In the case of the carboxylic acid analogue **33** the decrease in inhibitory activity is attributed to the fact that the phosphonate moiety has a pyramidal structure while the carboxylate has a planar structure.[45] In the case of the sulfonic acid **34**, the bond-lengths of the C-P and P-O bonds are shorter than the C-S and S-O bonds and this prevents tight binding at the active-site.[45] The diphenyl phosphonate analogue **35** (Figure 12a) was also synthesised, but showed a decrease in DXR inhibitory activity due to the presence of the bulky phenyl rings which cause steric hindrance.[68] The alkyl phosphonate mono-ester **36** (an FR900098 analogue) has shown good inhibitory activity, which increases with the lengthening of the *O*-alkyl chain.[57] Based on the effects of modifications to the phosphate group (Figure 12a), it was concluded that the presence of the negatively charged oxygen is crucial for hydrogen-bonding to the amino acid residues in the active-site.[67]

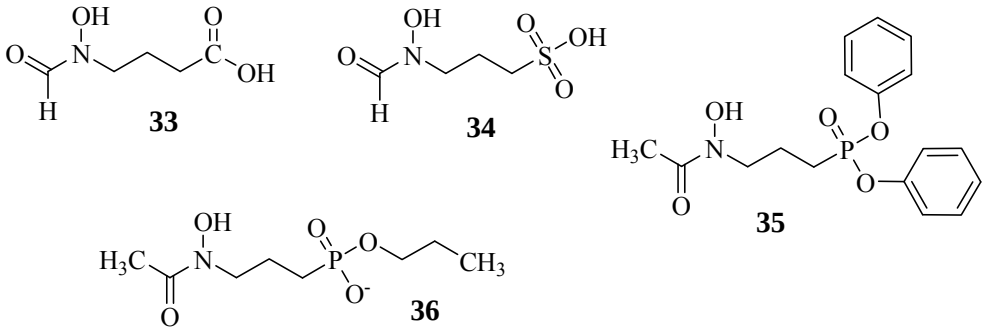

Figure 12a. Modifications on the phosphate moiety.

The hydrophobic patch is the carbon chain between the hydroxamate group and the phosphate moiety. Attempts to shorten the chain to a two-methylene spacer in the "reverse hydroxymate" analogue **40** of fosmidomycin (Figure 12b), results in a drastic decrease in inhibitory activity, while increasing the chain length, as in compound **41**, causes a moderate decrease of the activity.[45] The reason is that the shorter compounds are too short to bind effectively in the active-site, while the longer carbon chain prevents ideal binding.[45] Introduction of an electron-withdrawing group – an ether oxygen in the carbon backbone of compound **42** (Figure 12b), decreases the inhibitory activity, since the electron-withdrawing group prevents interaction with the indole ring of Trp-212 in the active-site, and results in a decrease in the pKa of the phosphonate group.[45] The conformationally-restricted cyclopropyl analogue **43** has two chiral centres, but the stereoisomers exhibited minimal activity.[69] The 3,4-dichlorophenyl substituted analogue **44**, however, has been shown to be an effective DXR inhibitor. The presence of another binding pocket adjacent to the active-site permits additional binding by aromatic or hydrophobic alkyl groups, thus improving the inhibitory activity.[57]

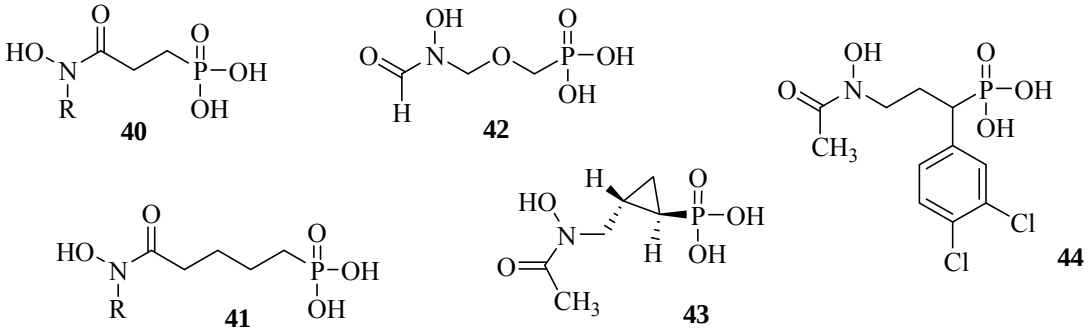

Figure 12b. Modifications on the hydrophobic patch alkyl backbone.

The hydroxamate group is involved in the coordination of the divalent metal ion which acts as a cofactor. The presence of the nitrogen atom has been shown to be crucial in the binding

of inhibitors in the active-site, most likely by changing the conformation of the flexible active-site pocket.[70] If the nitrogen is replaced by a carbon atom, the possibility of stereoisomers arise. Moreover, the presence of the two hydroxamate oxygen atoms in a *syn*-arrangement is responsible for the metal coordination.[45] The reverse arrangement of the hydroxymate group in the fosmidomycin analogue **45**, compared to compounds **40** and **41** does not appear to affect metal coordination ability.[45] Compound **46** (Figure 12c), which contains a cyclic analogue of the hydroxamate moiety, shows good inhibitory activity,[71] but the activity of the hydroxyurea derivative **47** has yet to be demonstrated.[71]

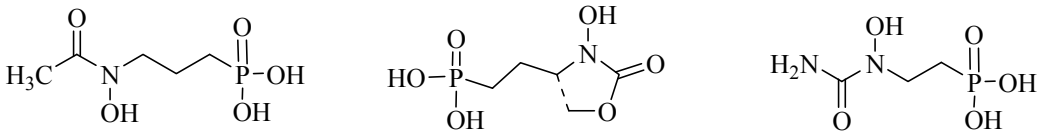

45 **46** **47**

Figure 12c. Modifications on the hydroxamate group.

1.3.2. DOXP and NADPH analogues as potential inhibitors

Attention has also been given to developing analogues of the natural DXR substrate, DOXP, and the co-factor, NADPH. The NADPH analogue **48**, as shown in Figure 13 has exhibited good inhibitory activity against *Ec*DXR, and moderate antimalarial activity, but no evidence of this compound binding to the NADPH binding domain in the active-site has been obtained. Structural analogues of DOXP **22** have also been synthesised; the analogues **49** and **50** lack the C-3 and C-4 hydroxyl groups, respectively, but exhibit *Ec*DXR inhibition at mM concentrations.[72] The DOXP analogue **51** contains a triflourormethyl group (Figure 13) in place of a methyl group; the low inhibitory activity observed for this analogue has been attributed to steric hindrance at the metal binding site.[72,73]

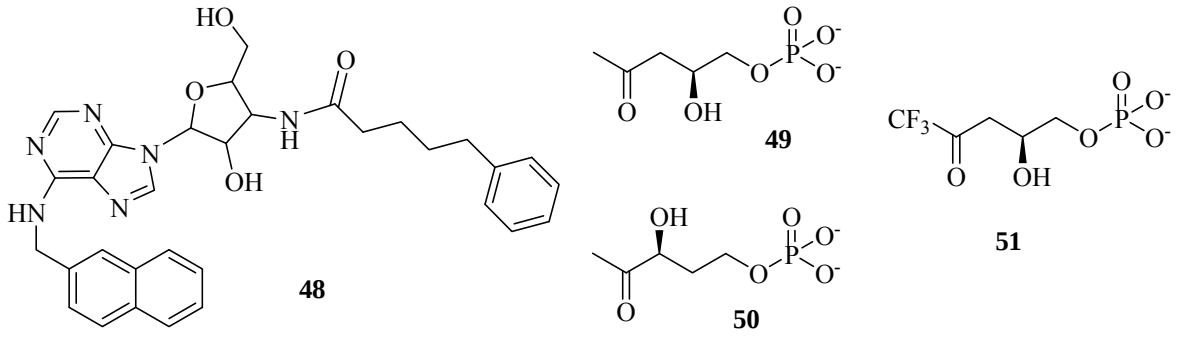

48 **49** **50** **51**

Figure 13. Structural analogues of DOXP and NADPH.

1.4. PREVIOUS WORK IN THE GROUP

The group's specific objective in this area has been to develop novel compounds as potential DXR inhibitors.[74-77] The results of previous studies have provided a platform for this present study.

Conibear synthesised a series of phosphonate esters and their phosphonic acid salts using heterocyclic amino derivatives **52a-e** (2-aminopyridine, furfurylamine, 2-aminothiazole, 3-aminoisothiazole and 5-acetyl-2-amino-4-methylthiazole) as the starting materials. Reaction of these compounds with chloroacetyl chloride or 3-chloropropionyl chloride afforded the corresponding chloroamides **53a-e** and **56a-e** (Scheme 1). *Michaelis-Arbuzov* reactions led to the diethyl phosphonate esters **54a-e** and **57a-e.** Hydrolysis of the esters using bromotrimethylsilane and basification gave the acid salts **55a-e** and **58a-e**. However, these compounds only showed minimal to moderate inhibitory activity.[74,75,78]

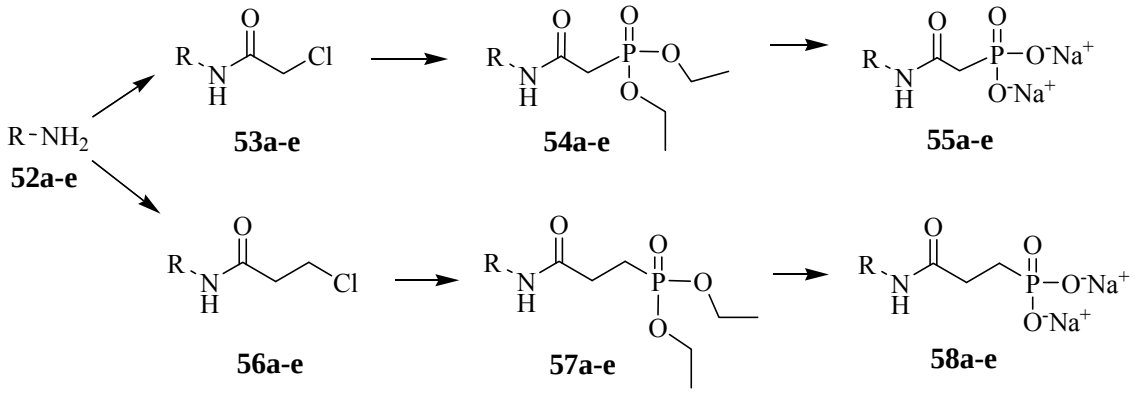

Scheme 1. Synthesis of phosphonate esters (**54a-e** and **57a-e**) and their corresponding acid salts (**55a-e** and **58a-e**) from heterocyclic amines (**52a-e**).

Mutorwa followed the same general route using 3-substituted aniline derivatives to synthesize the phosphonate esters **59a-g**, phosphonic acids **60a-g** and their corresponding monosodium salts **61a-g** (Figure 14). The use of different acid chlorides (chloroacetyl chloride, 3-chloropropionyl chloride, 4-chlorobutanoyl chloride and 5-chloropentanoyl-chloride), provided access to analogues containing 1,2,3, and 4 methylene groups in the hydrophobic patch (Figure 14).[76-77] He also prepared furan-derived phosphate esters and their corresponding phosphoric acids **62a-c** as conformationally-restricted fosmidomycin analogues (Scheme 2). Finally, *N*-benzylated phosphoramidic derivatives **63a-d** were designed following careful *in silico* exploration of the DXR active-site by Conibear.

Representative compounds were obtained by Conibear and Mutorwa in seven steps from the starting material as outlined in Scheme 3.[74-77]

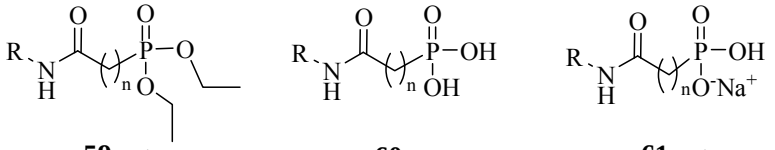

59a-g **60a-g** **61a-g**

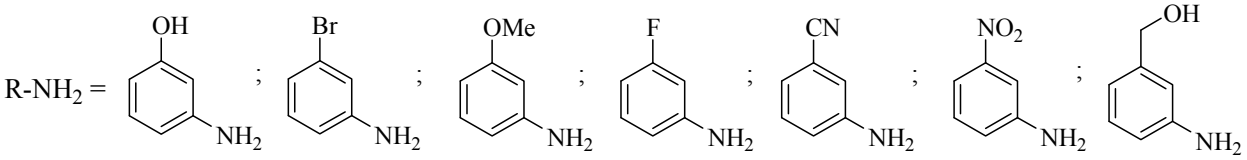

Figure 14. Synthesis of 3-substituted aniline-derived phosphonate esters **59a-g**, phosphonic acids **60a-g** and their corresponding monosodium salts **61a-g**, n= 1-4.

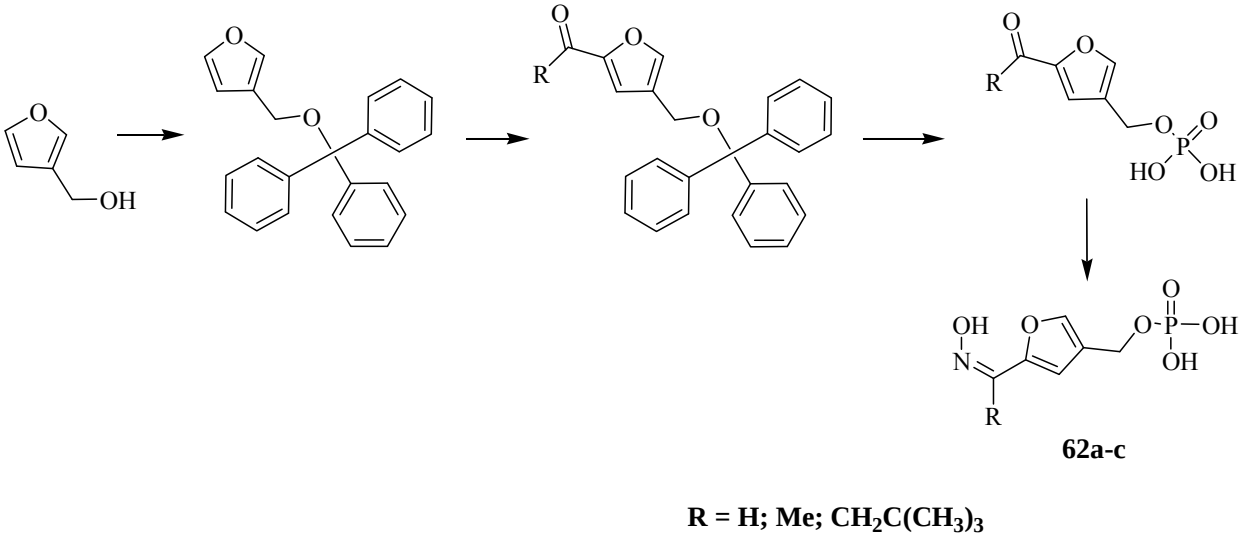

62a-c

R = H; Me; $CH_2C(CH_3)_3$

Scheme 2. Furan-derived phosphate esters and their corresponding phosphoric acids **62a-c** as conformationally-restricted DOXP analogues.

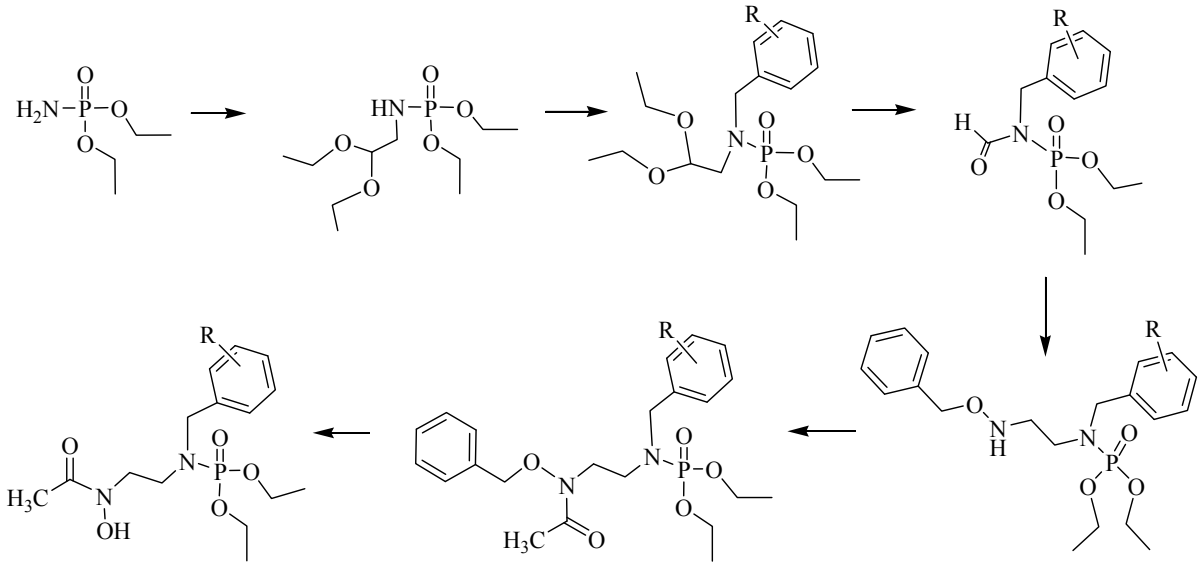

63a-d

R = H; *p*-CH_3; *m*-NH_2; *m*-SH

Scheme 3. Synthesis of rationally designed *N*-benzylated phosphoramidic derivatives.

1.5. AIMS OF THE CURRENT INVESTIGATION

The focus of the present study has been to synthesise novel compounds with the potential to bind in the DXR active-site and serve as DXR inhibitors. More specifically, attention was to be given to the following objectives.

1) Synthesis of a series of *N*- and *C*-benzylated (*N*-phenylcarbamoyl)alkylphosphonate esters.
2) Synthesis of *N*- and *C*-benzylated *N*-heteroarylcarbamoyl analogues.
3) Exploration of bi-functional DXR and HIV-1 reverse transcriptase inhibitor.
4) Evaluation of the binding potential of the synthesised compounds by *in silico* docking studies and their antimalarial potential by *in vitro* bioassays.

2. RESULTS AND DISCUSSION

2.1. SYNTHESIS OF FOSMIDOMYCIN ANALOGUES AS DXR INHIBITORS

As already indicated, a series of phosphonate esters, acids and sodium salts have been prepared by Conibear and Mutorwa,[74-77] some of which have been found to show moderate activity in *Ec*DXR and *Pf*DXR inhibition assays. *In silico* exploration of the *Pf*DXR active-site by Conibear has revealed an adjacent and apparently un-used binding pocket.[75] Consequently, this project has been concerned with the synthesis of a new series of ligands comprising benzylated analogues of some of Conibear's and Mutorwa's compounds that have shown moderate DXR inhibitory activity.

Attention has thus been given to preparing the *C*-benzylated **69** and and *N*-benzylated **77** phosphonate esters as illustrated in Scheme 4 as potential antimalarial pro-drugs. *In vitro* hydrolysis of the ester moiety is expected to release the active phosphonic acids, while it is hoped that occupation of the additional hydrophobic pocket by a benzyl group will enhance binding at the *Pf*DXR active-site. The selected non-benzylated phosphonated compounds initially prepared by Conibear and Mutorwa were identified as substrates for *C*- and *N*-benzylation and their preparation is outlined in Scheme 4.

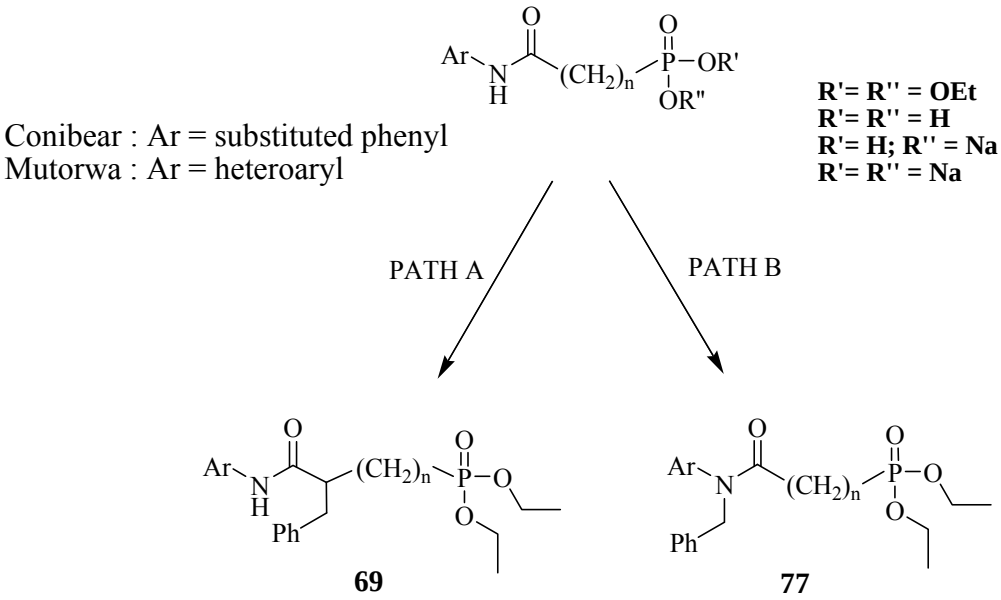

Scheme 4. Proposed *C*- and *N*-benzylated phosphonate esters as potential anti-malarial pro-drugs. n= 1,2.

2.1.1. Preparation of the selected non-benzylated phosphonate esters.

In this study, various primary amines (3-subsituted anilines and heterocyclic amines) **64a-f** were employed as starting materials. The length of the methylene spacer (hydrophobic patch) between the phosphonate moiety and hydroxamate group was varied to explore the enzyme-ligand binding specificity (Scheme 5).

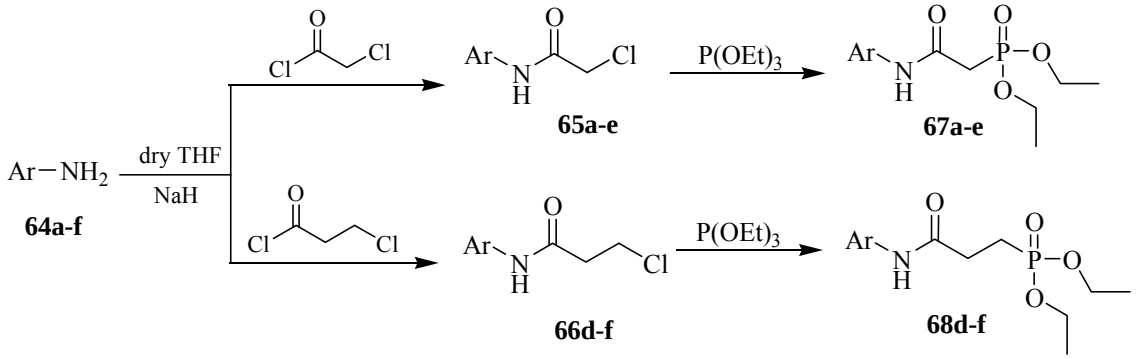

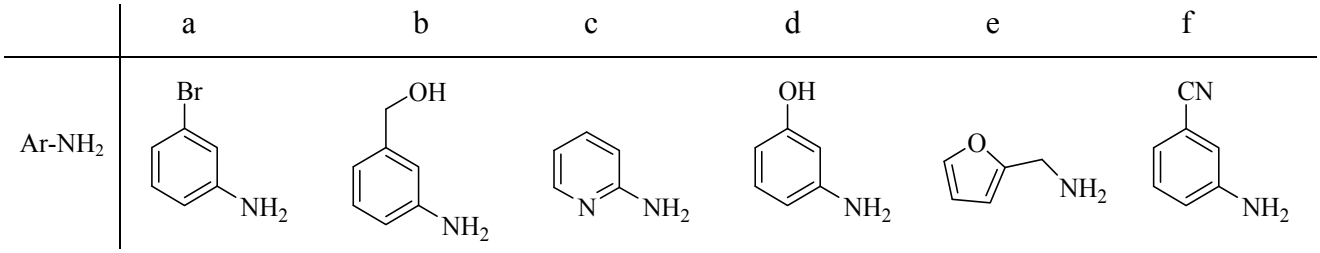

Scheme 5. Synthetic routes towards compounds **67a-e** and **68d-f**.[74-77]

Reagents and conditions:- (i) NaH, dry THF and acid chloride, r.t.; (ii) triethylphosphite, 6h, reflux (160 ^{o}C).

2.1.1.1. Formation of chloroalkanamides.

Reaction between the primary amines **64a-f** and the acid chlorides, chloroacetyl chloride and 3-chloropropionyl chloride, using sodium hydride as a base in dry THF, involves nucleophilic acyl substitution in preference to alkyl substitution (S_N). In the detailed mechanism of this reaction shown in Figure 15, sodium hydride abstracts a proton from the primary amine facilitating nucleophilic attack on the carbonyl carbon of the acid chloride, thereby forming the chloroalkanamide.[74-77]

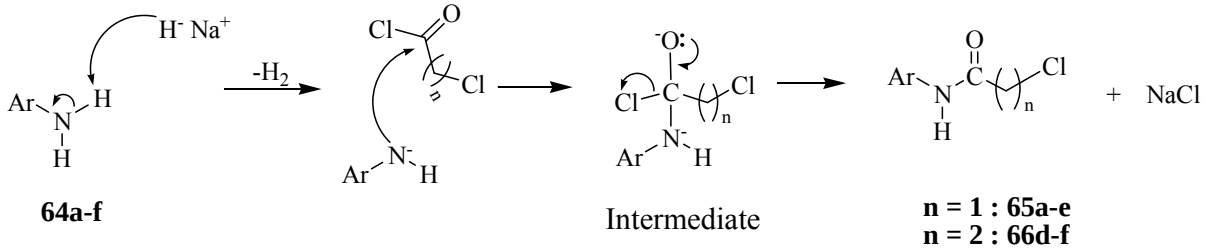

Figure 15. Mechanism of formation of chloroalkanamides.

After stirring under nitrogen for 6 h at room temperature, the reaction mixtures were worked up and the crude *α*-chloroamides **65a-e** were isolated by flash chromatography in reasonable yield (60-70%), as shown in Table 2.1. The chloroamide derivatives were analysed using NMR and IR spectroscopy. The ^{1}H NMR spectrum of 2-chloro-*N*-(pyridin-2-yl)acetamide **65c** (Figure 16a) exhibits a singlet at 4.20 ppm that corresponds to the chloromethylene protons and a broad singlet at 8.88 ppm corresponding to the amide proton. The ^{1}H NMR spectrum of the 3-chloro-*N*-(3-hydroxyphenyl)propanamide analogue **66d** (Figure 17), shows a similar pattern to that of compound **65d**, but exhibits an upfield triplet at 2.79 ppm for the methylene protons next to the carbonyl group and an additional triplet at 3.86 ppm corresponding to chloromethylene protons.[74-77]

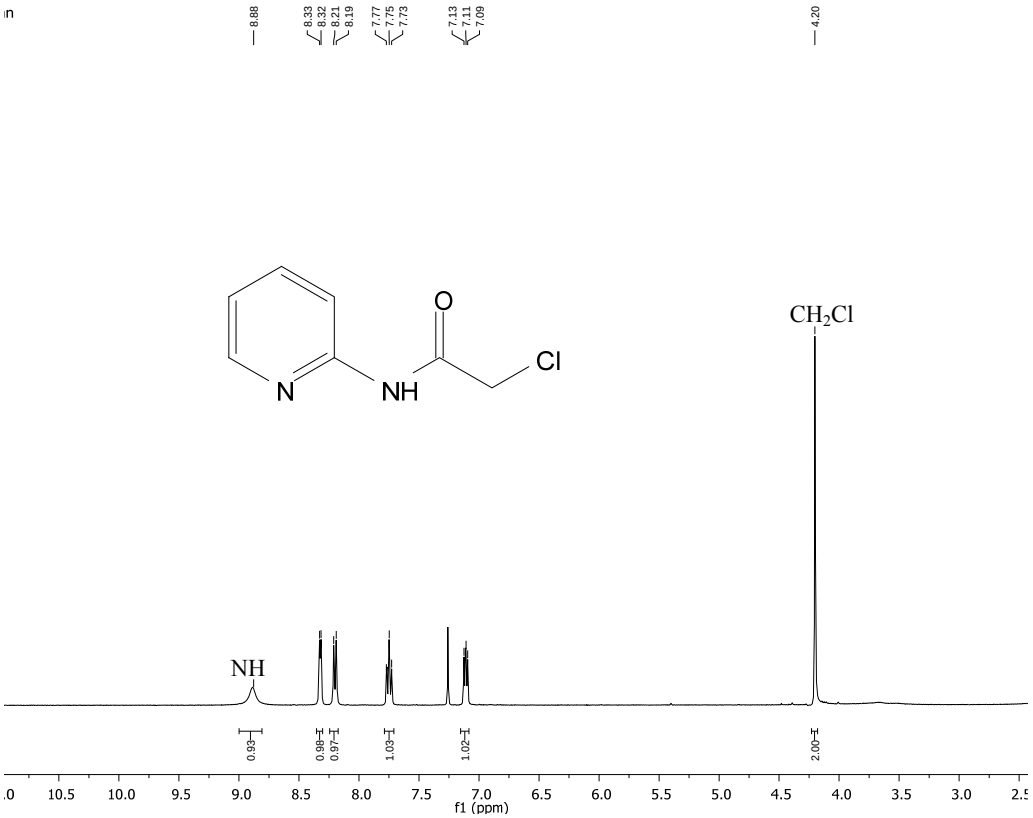

Figure 16a. 400 MHz ^{1}H NMR spectrum of compound **65c** in $CDCl_3$.

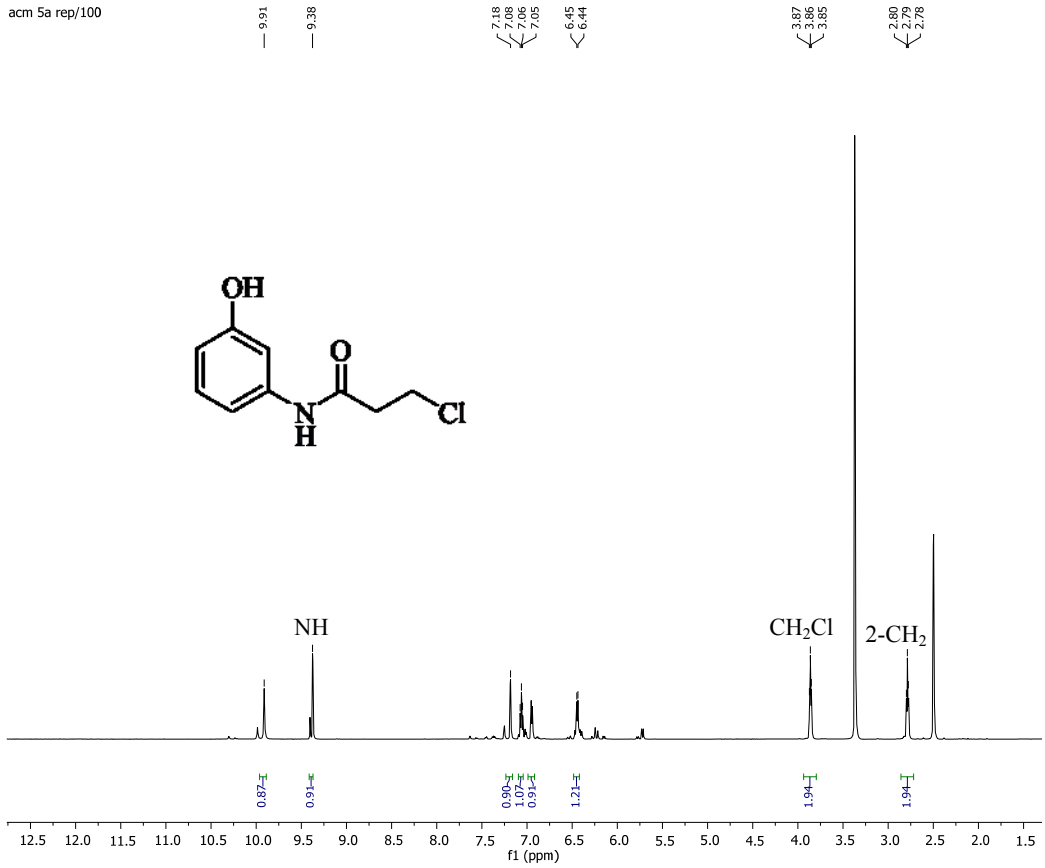

Figure 17. 400 MHz ^{1}H NMR spectrum of compound **66d** in DMSO-d_6.

2.1.1.2. Formation of phosphonate esters via the Michaelis-Arbuzov reaction.[78,79]

The mechanism for the preparation of phosphonate derivatives *via* the *Michaelis-Arbuzov* reaction is illustrated in Scheme 6. This reaction proceeds *via* an S_N mechanism in which the alkyl halide is attacked by the nucleophilic $P(OEt)_3$ permitting the formation of a C-P bond. The chloride ion removes a proton from one of the *O*-ethyl groups of the phosphonium intermediate, and elimination of ethylene results in the formation of the phosphonated derivatives.[78,79]

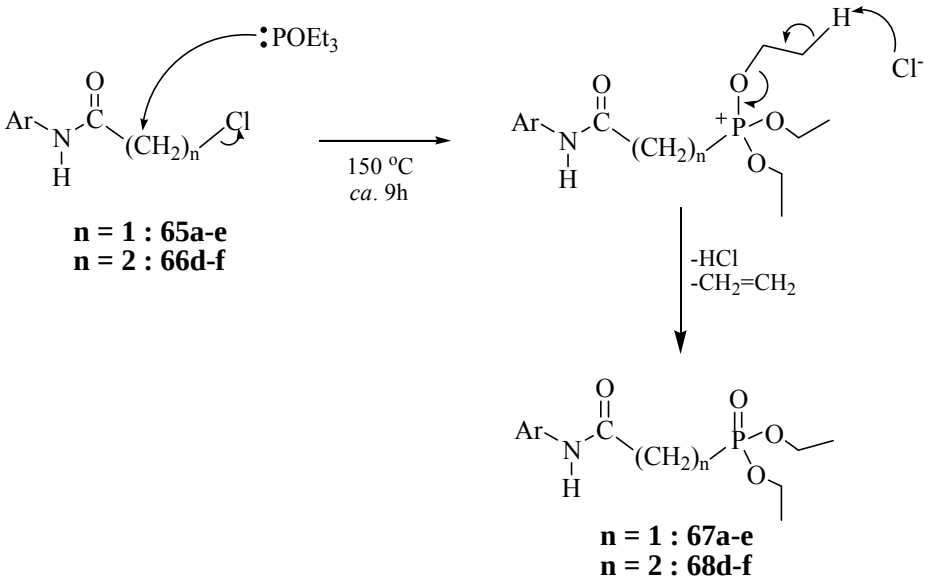

Scheme 6. Formation of phosphonate esters *via* the *Michaelis-Arbuzov* reaction.[78,79]

The chloroamides **65a-e** and **66d-f** were each heated with 2-5 equivalents of triethyl phosphite under solvent free conditions at 150 ^{o}C for *ca* 9 h, under N_2. In each case, the resulting mixture was stirred repeatedly with hexane to remove excess triethyl phosphite, and further purified using flash chromatography to obtain the phosphonate esters **67a-e** and **68d-f** in reasonable yields (60-80%) as shown in Table 2.1. The phosphonate esters were analysed using IR and NMR spectroscopy. The ^{1}H NMR spectrum of diethyl [*N*-(2-pyridyl)-carbamoyl]methylphosphonate **67c** (Figure 18a) reveals a doublet at 3.08 ppm, corresponding to the methylene group attached to phosphorus, with a large coupling constant ($J_{P,H}$ = 21.3 Hz); this splitting is typical of these compounds due to the coupling with phosphorus-31. The triplet at *ca* 1.32 ppm corresponds to the two methyl groups, while the multiplet at 4.19 ppm corresponds to the methyleneoxy protons of the phosphonate moiety. The DEPT 135 NMR spectrum of compound **67c** (Figure 18b) confirms the presence of the two different methylene types; the methylene carbon attached directly to phosphorus resonates as a doublet at *ca* 37 ppm and exhibits a large coupling constant (J = 130.9 Hz) whereas the magnetically equivalent methyleneoxy carbons resonate as a doublet with a much smaller coupling constant (J = 6.4 Hz) since they are further away from the phosphorus-31 nucleus. The ^{1}H NMR spectrum (Figure 19) of the bis-methylene analogue, diethyl [*N*-(3-hydroxy-phenyl)carbamoyl]ethylphosphonate **68d** clearly confirms the presence of the additional methylene group which is responsible for the triplet at 2.72 ppm, with the *P*-methylene protons resonating as a multiplet at 2.17 ppm. The upfield shift of the latter signal reflects the

fact that the P-methylene protons are no longer adjacent to the deshielding amide carbonyl group.

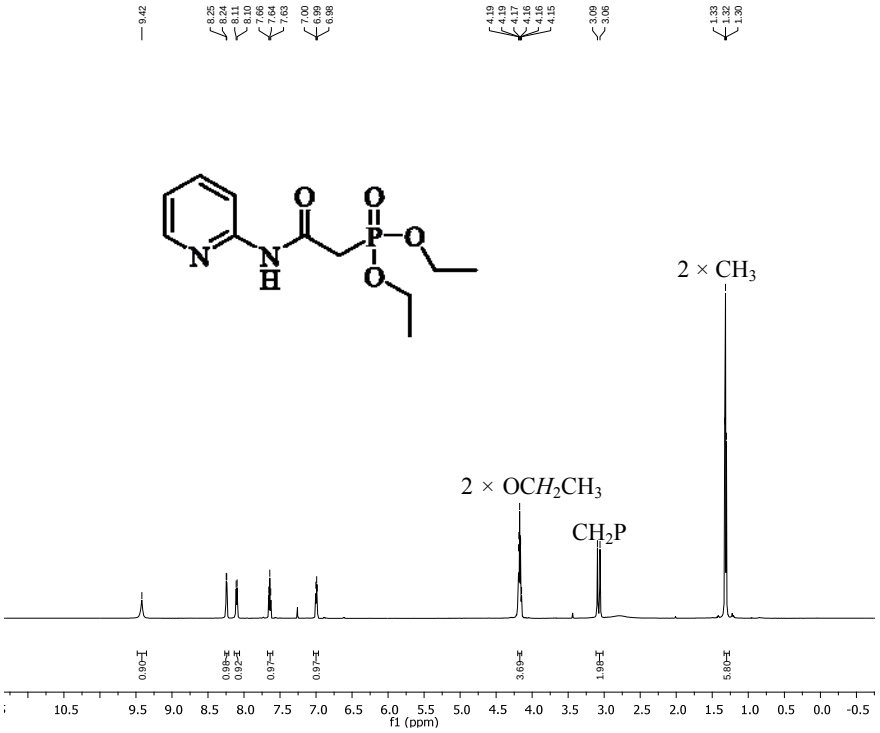

Figure 18a. 400 MHz ^{1}H NMR spectrum of compound **67c** in $CDCl_3$.

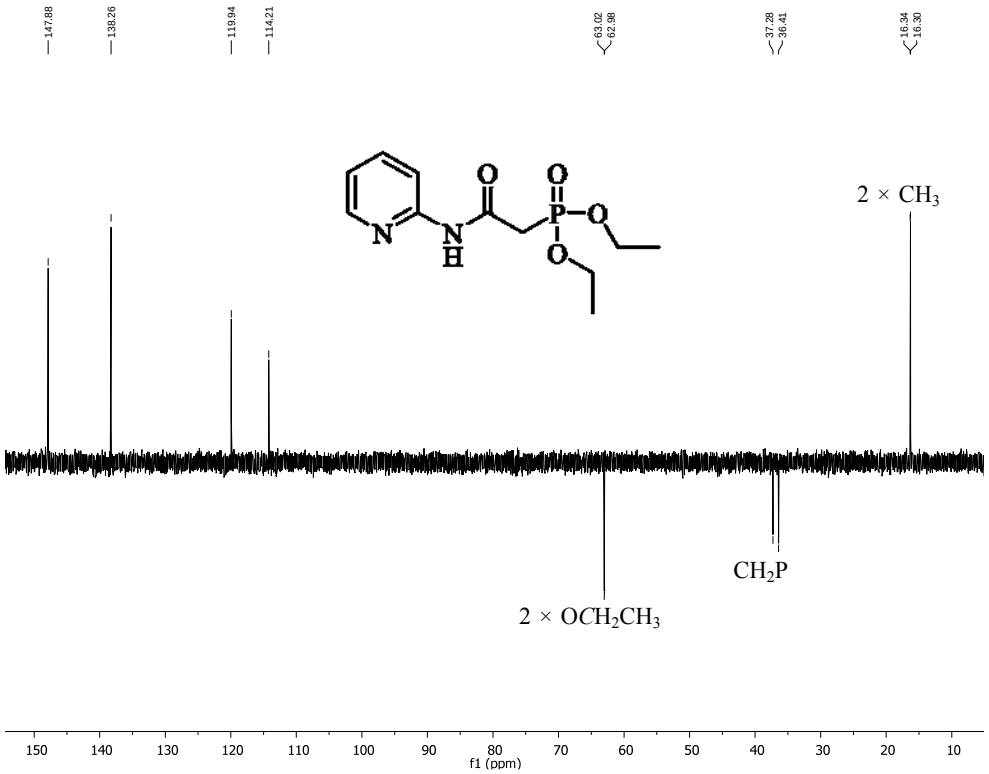

Figure 18b. DEPT 135 NMR spectrum of compound **67d** in $CDCl_3$.

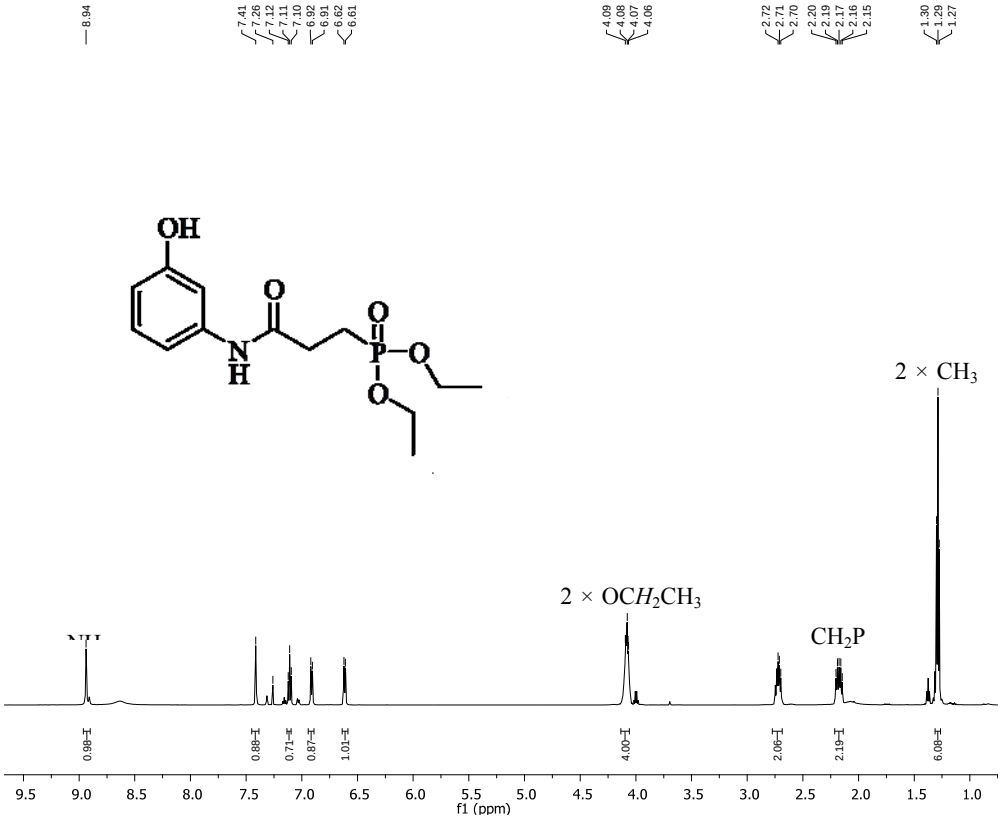

Figure 19. 400 MHz ^{1}H NMR spectrum of compound **68d** in $CDCl_3$.

Table 2.1: Percentage yields obtained for the synthesis of chloroalkanamide products **65-66** and phosphonated products **67-68** in the synthetic route **A**.

Ar-NH$_2$	**n**	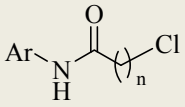	**Yield/%**	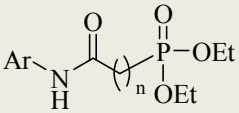	**Yield/%**
3-Bromophenyl	1	**65a**	68	**67a**	60
3-(Hydroxylmethyl)phenyl	1	**65b**	60	**67b**	62
2-Pyridyl	1	**65c**	65	**67c**	72
3-Hydroxyphenyl	1	**65d**	68	**67d**	66
Furfuryl	1	**65e**	62	**67e**	80
3-Hydroxyphenyl	2	**66d**	74	**68d**	65
Furfuryl	2	**66e**	60	**68e**	70
3-Cyanophenyl	2	**66f**	71	**68f**	65

2.1.1.3. Protection of the phenolic group in the phosphonate ester **67d**.

In the case of compound **67d** it was envisaged that there was a need to protect the phenolic-group, in order to prevent *O*-benzylation and formation of a benzyl ether during the *C*- or *N*-benzylation reactions. As shown in Scheme 7, diethyl [*N*-(3-hydroxyphenyl)carbamoyl]-methylphosphonate **67d** and imidazole were dissolved in dichloromethane (DCM) at 0 ^{o}C in an ice bath, *tert*-butyldimethylsilyl chloride was added in portions and the resulting mixture was stirred at room temperature for 2 h. Work-up and chromatography afforded the *tert*-butyldimethylsilyl ether-protected phosphonate ester **71** in 88% yield.[80]

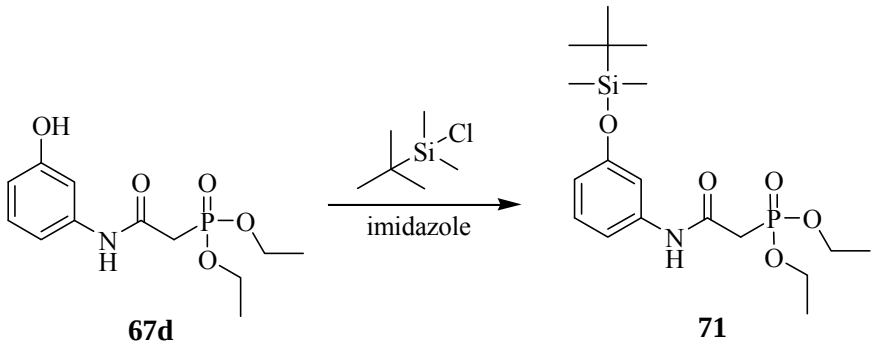

67d **71**

Scheme 7. Protection of the phenolic-group in compound **67d**.

The structure of the protected phosphonate ester **71** was confirmed by NMR spectroscopy and high resolution mass spectrometry. The ^{1}H NMR spectrum of compound **71** (Figure 20a) reveals a 6-proton singlet at 0.20 ppm for the two methyl groups attached to silicon and a 9-proton singlet at 0.97 ppm corresponding to the *tert*-butyl protons. The characteristic signals for the phosphonate ester moiety are also evident: the 6-proton methyl triplet at 1.35 ppm, the doublet at *ca*. 3.00 ppm of the methylene group directly attached to phosphorus and the multiplet at 4.17 ppm corresponding to the *O*-methylene protons. The ^{13}C NMR spectrum of compound **71** (Figure 20b) clearly illustrates the signal for the *Si*-methyl groups at -4.3 ppm, and the *tert*-butyl methyl group signal at 25.8 ppm. The HSQC spectrum (Figure 20c) confirms these signal assignments and shows that the carbons which resonate between 110 and 129 ppm correlates with the aromatic proton signals between 6.65 and 7.16 ppm, while the carbon signals at 129.7, 156.3 and 162.2 ppm correspond to the quaternary aromatic and carbonyl carbons, respectively. The IR spectrum of compound **71** in Figure 20d shows the absence of the broad OH absorption band at 3365cm^{-1} of the phenolic precursor **67d**, and the presence of the amide carbonyl group band at 1673cm^{-1}.

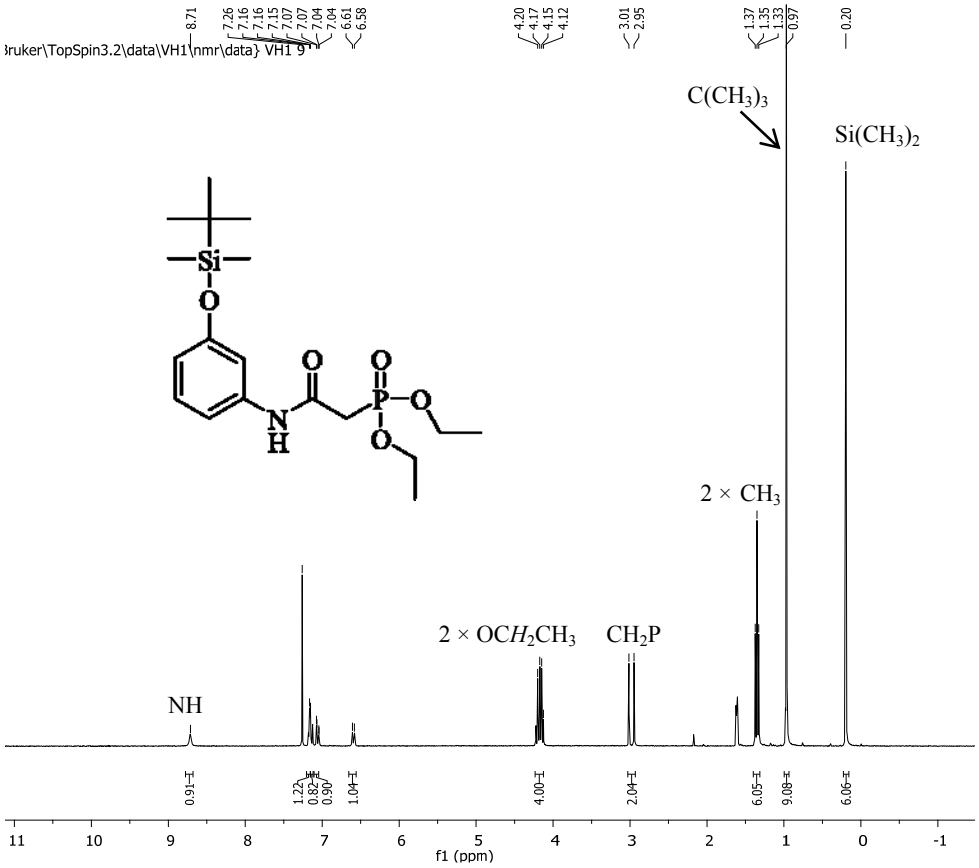

Figure 20a. 400 MHz ^{1}H NMR spectrum of compound **71** in $CDCl_3$.

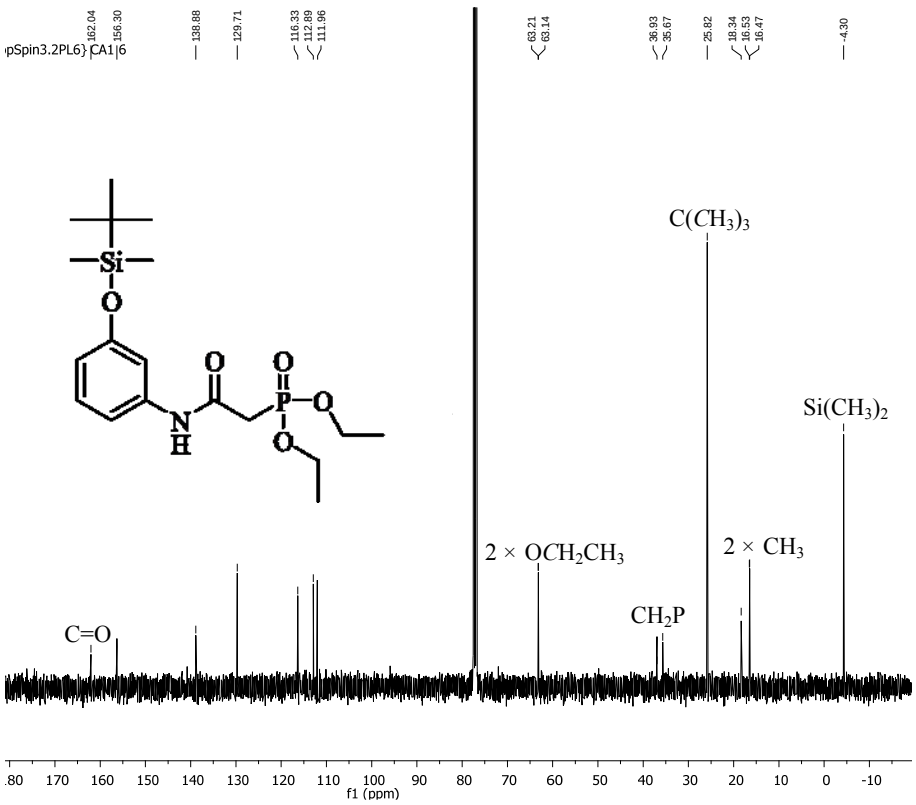

Figure 20b. 100 MHz ^{13}C NMR spectrum of compound **71** in $CDCl_3$.

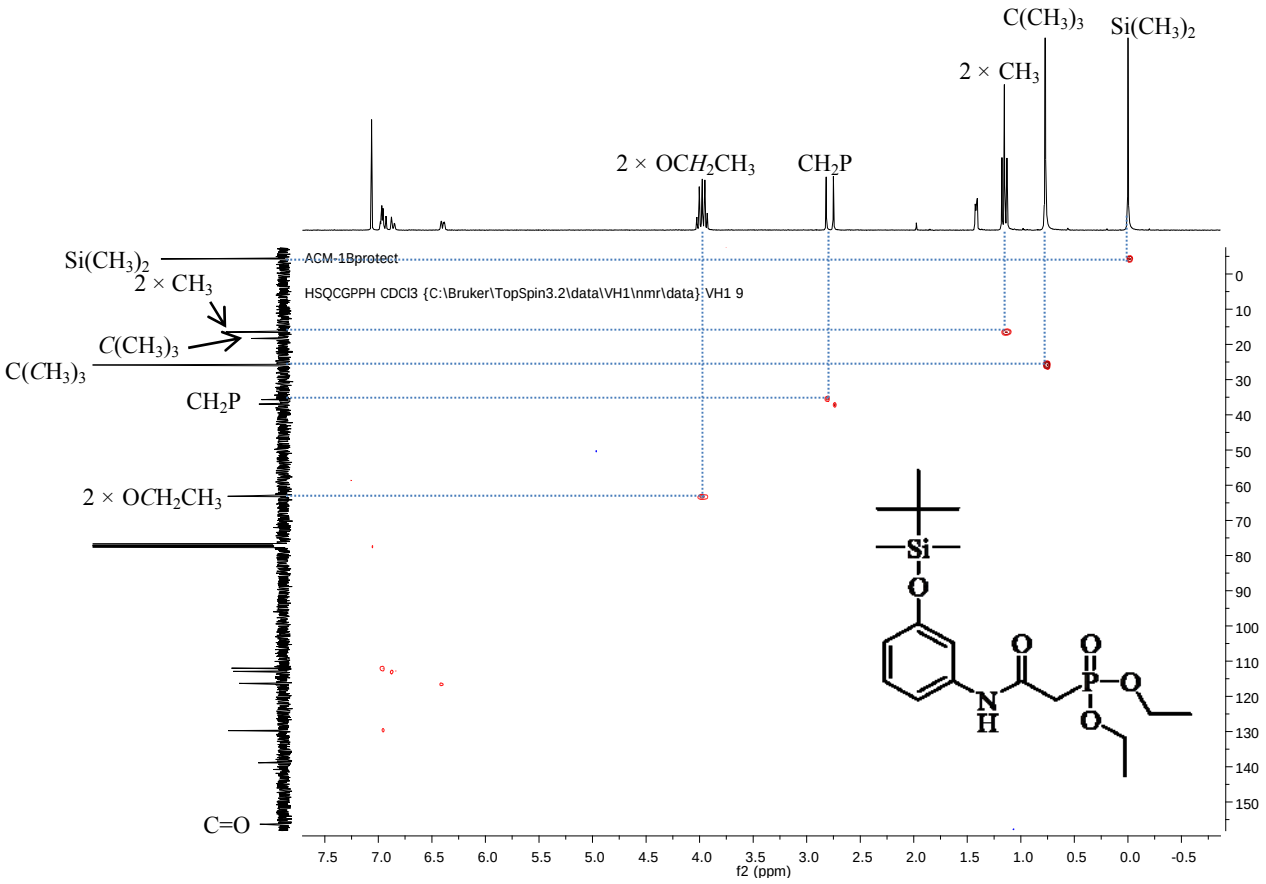

Figure 20c. HSQC NMR spectrum of compound **71** in $CDCl_3$.

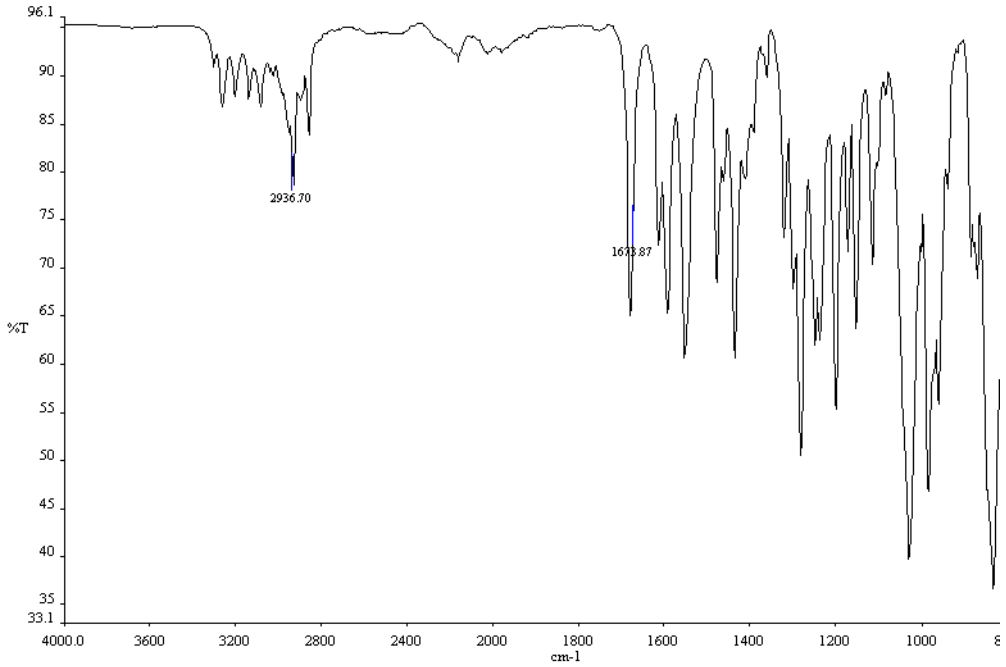

Figure 20d. IR spectrum of compound **71**.

2.1.2. *C*-Benzylation studies

2.1.2.1. Approaches to C*-benzylation of phosphonate esters*.

There are various established methods for the α-benzylation of amides.[81,82] In the current study, the phosphonate ester **67e** was dissolved in dry THF under N_2; the organic base, pyridine, was added, followed by benzyl bromide. The mixture was stirred at r.t. for 7 days and, when no product was observed, the reaction mixture was boiled under reflux for 2 h (Scheme 8), but only starting material was obtained. Use of triethylamine as the base was similarly unsuccessful (Scheme 8). An alternate approach involved refluxing the phosphonate ester **67e** and benzyl bromide in 10% aqueous NaOH for *ca* 2 h; some product formation was, in fact, observed by TLC, but chromatography of the crude mixture afforded the starting material and impurities. Use of finely powdered KOH in dry THF finally afforded the desired *C*-benzylated phosphonated ester **69e**, but only in 10% yield.

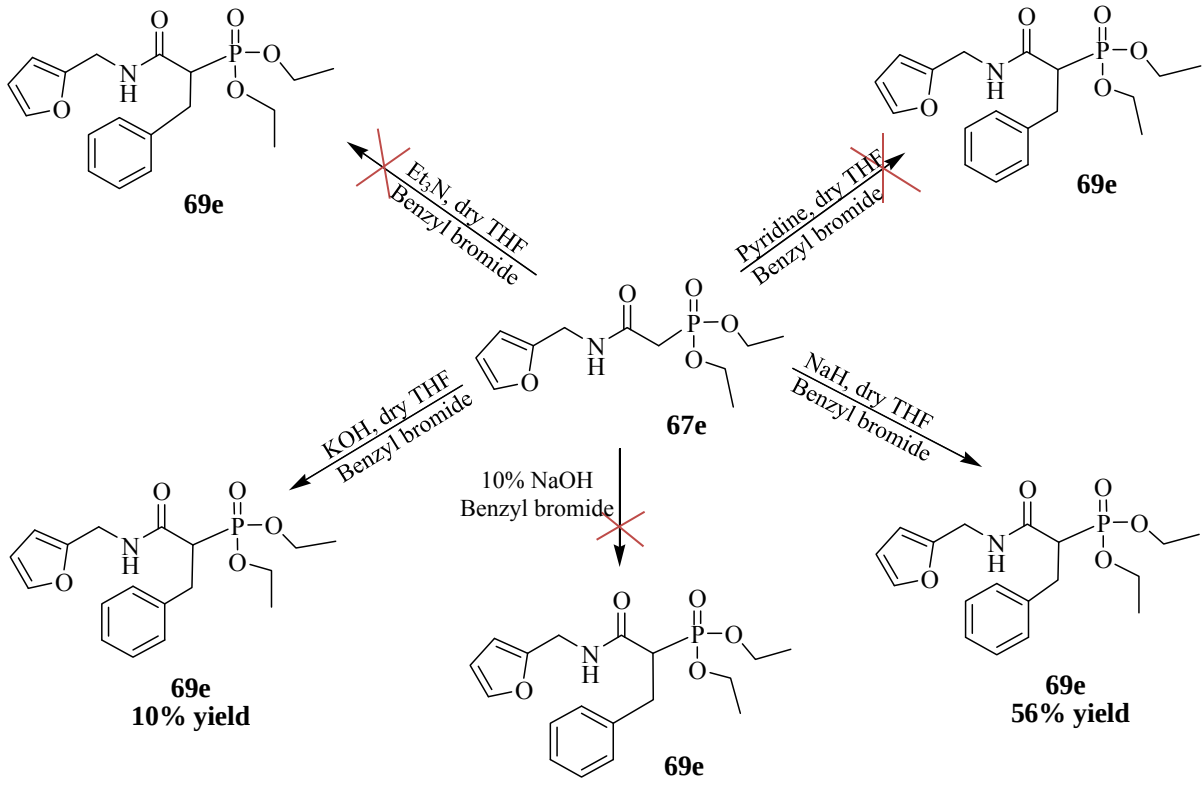

Scheme 8. Attempted *C*-benzylation of the phosphonate ester **67e**.

Attention was finally turned to an approach reported by Uladzimir *et al*., who obtained *N*-benzylated products when the amide was reacted with benzyl bromide in dry THF in the presence of NaH as base.[82] Consequently, the phosphonate ester **67e** was heated under reflux for *ca* 6 h in dry THF, with sodium hydride as base and 2.4 equivalents of benzyl bromide (added in two portions) under an inert atmosphere. The reaction was quenched with 10 mL of water, the solvent was evaporated *in vacuo* and the residue was first filtered to remove excess sodium hydride, and then chromatographed (PLC) to afford the desired *C*-benzylated phosphonate ester **69e** in 56% yield and not the *N*-benzylated analogue (Scheme 8). It was presumed that the pKa of the methylene protons, located between the phosphonate and amide carbonyl groups, is lower than that of the amide proton (pka = 25.1),[83] permitting preferential formation of a resonance stabilised carbanion leading to the desired *C*-benzylated product **69e**.

The ^{1}H NMR spectrum of diethyl 1-(*N*-furfurylcarbamoyl)-2-phenylethylphosphonate **69e** (Figure 21a) shows that the diethyl phosphonate triplet and quartet at 1.30 ppm and 4.09 ppm, respectively, are still present and, importantly, that the broad signal at 6.67 ppm, which corresponds to the amide proton, confirms that the benzyl bromide had not reacted with the amide group. *C*-Benzylation is clearly supported by the benzylic proton signal at 3.03 ppm and the *P*-methine proton signal at 3.32 ppm which is split due to coupling to phosphorus-31 and to the vicinal benzylic protons. The ^{13}C NMR spectrum of compound **69e** (Figure 21b) reveals the benzylic carbon signal at 36.9 ppm, the *P*-methine carbon signal as a doublet at 32.7 ppm and the carbonyl carbon signal at 166.6 ppm. The DEPT 135 NMR spectrum (Figure 21c) clearly confirms the critical assignments of the *P*-methine and benzylic methylene signals. The HSQC spectrum (Figure 21d) shows the correlation between protons and carbons, while the quaternary and carbonyl carbon signals at 138.9, 151.1 and 166.6 ppm respectively show no correlation to any proton.

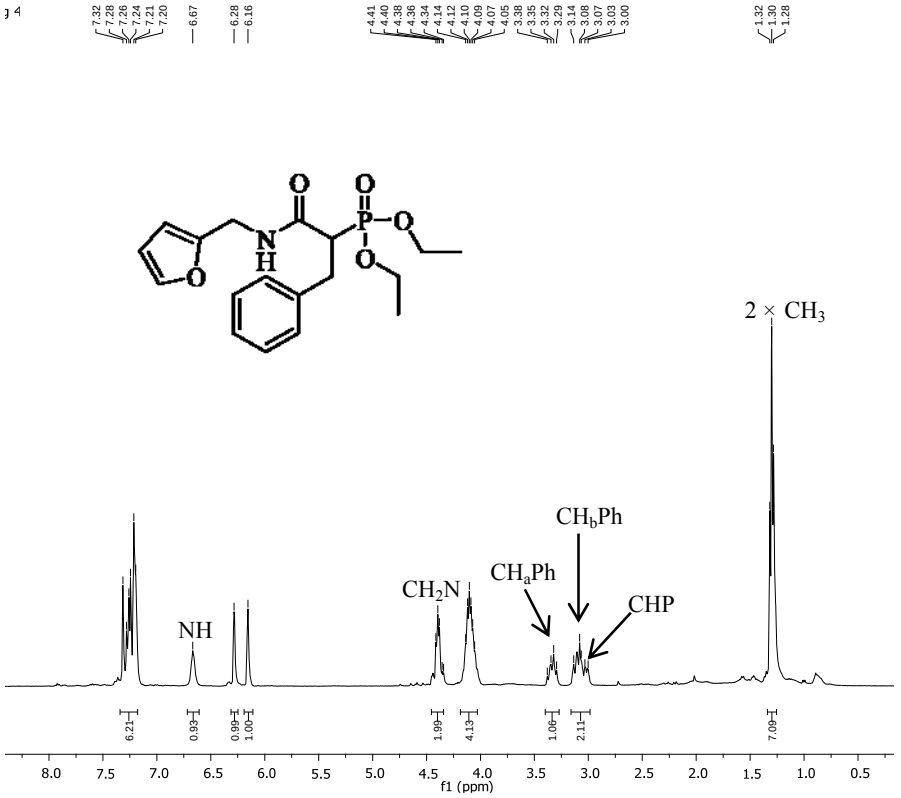

Figure 21a. 300 MHz ^{1}H NMR spectrum of compound **69e** in $CDCl_3$.

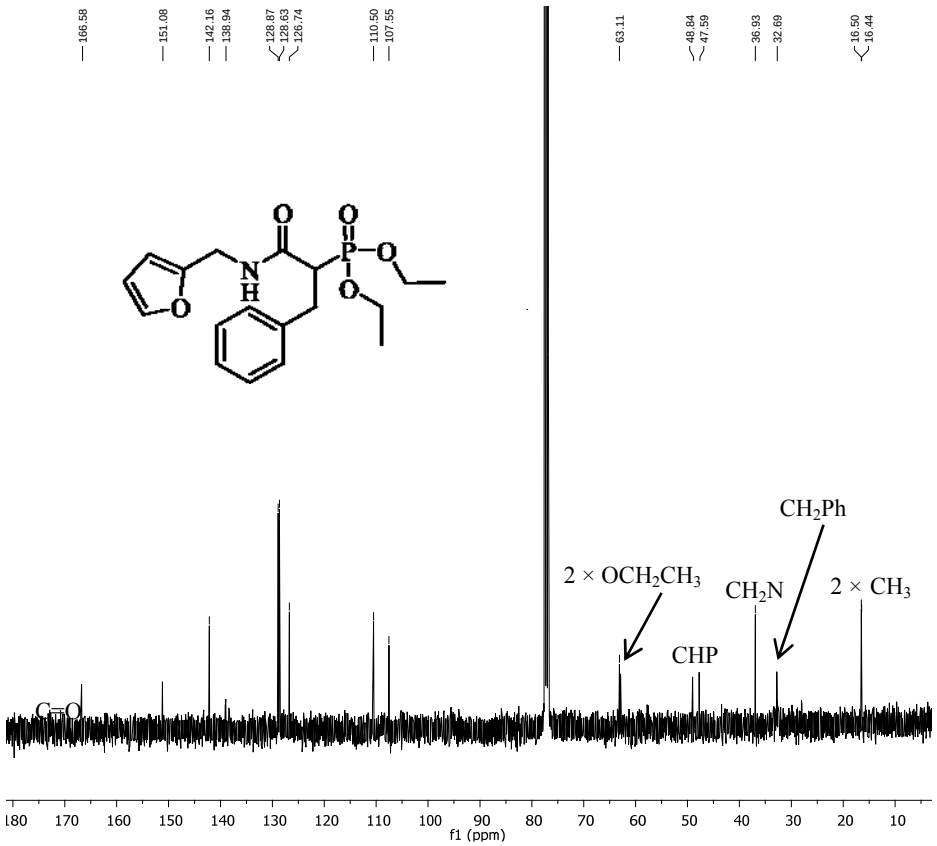

Figure 21b. 75 MHz ^{13}C NMR spectrum of compound **69e** in $CDCl_3$.

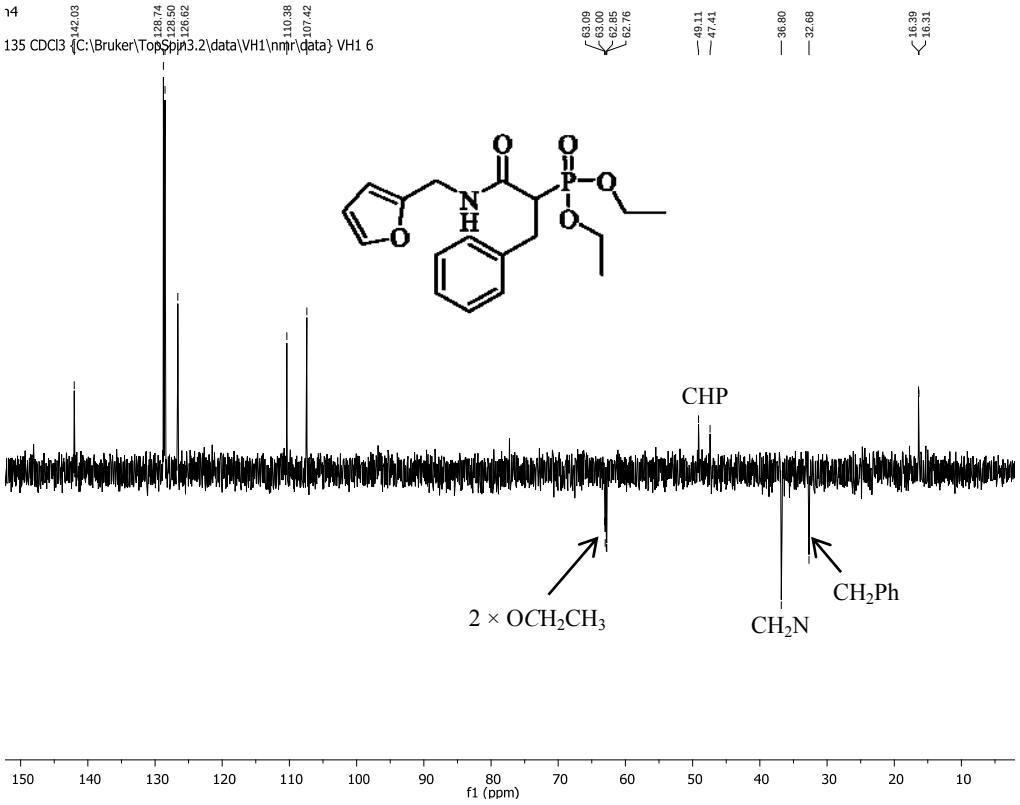

Figure 21c. DEPT 135 NMR spectrum of compound **69e** in $CDCl_3$.

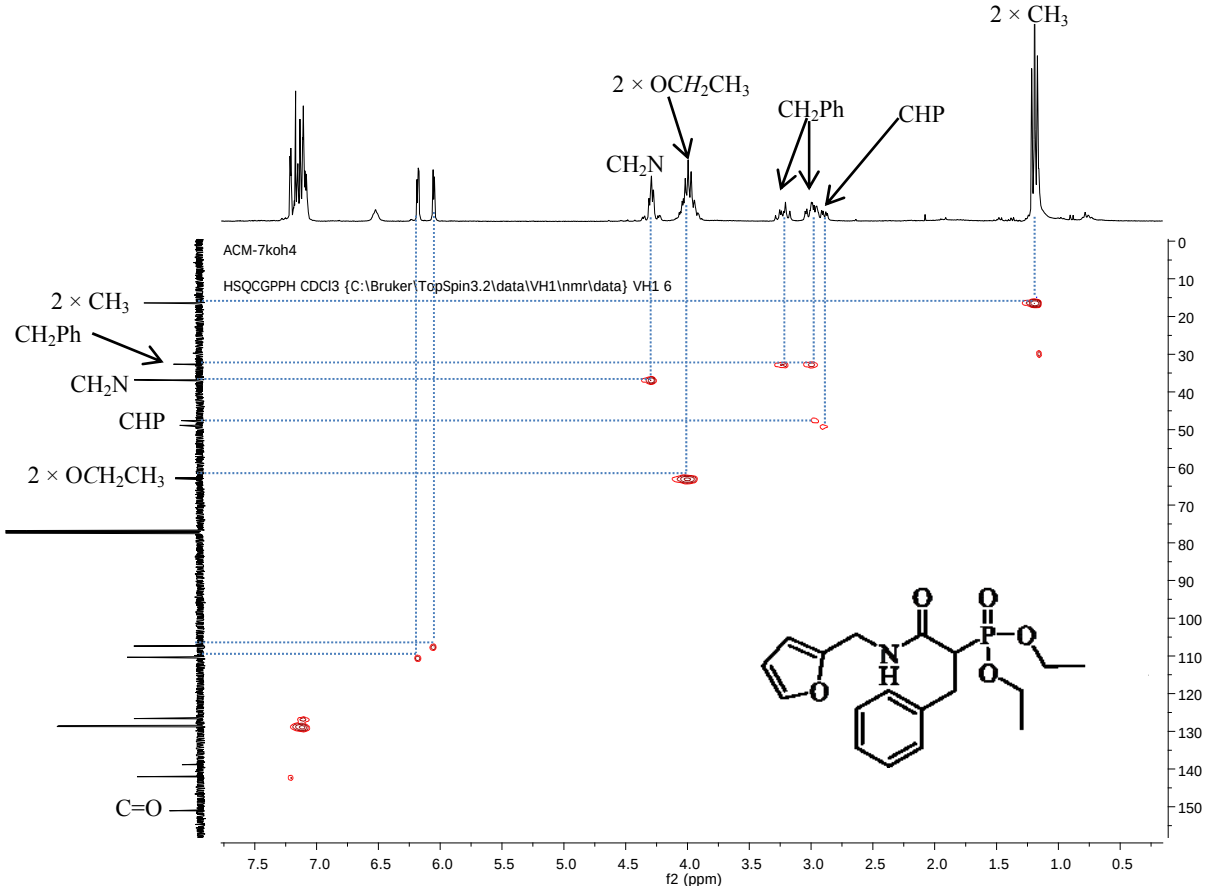

Figure 21d. HSQC NMR spectrum of compound **69e** in $CDCl_3$.

C-Benzylation of the successfully protected phosphonate ester **71** was then attempted, following the method used to obtain the *C*-benzylated product **69e** in 56% yield. NMR analysis of the product, however, revealed the loss of the characteristic protecting group *Si*-methyl and the *tert*-butyl methyl signals, as well as those of the phosphonate ester moiety. It was therefore concluded that the *C*-benzylation of the protected phosphonate ester **71** was unsuccessful.

This reaction was repeated on the methyl phosphonate esters (n=1) **67a-d** using the same method, but the ^{1}H NMR spectra of the purified compounds also show the disappearance of the phosphonate moiety (Scheme 9), a phenomenon typical of this series of reactions. Careful analysis of the experimental data for these compounds (including HRMS, 1- and 2-D NMR) revealed that a totally unexpected transformation had taken place to form compounds **72a-d**. This was attributed to the presence of 2,3-dihydrofuran in the solvent, THF. A tentative mechanism for this transformation is detailed in Figure 22.

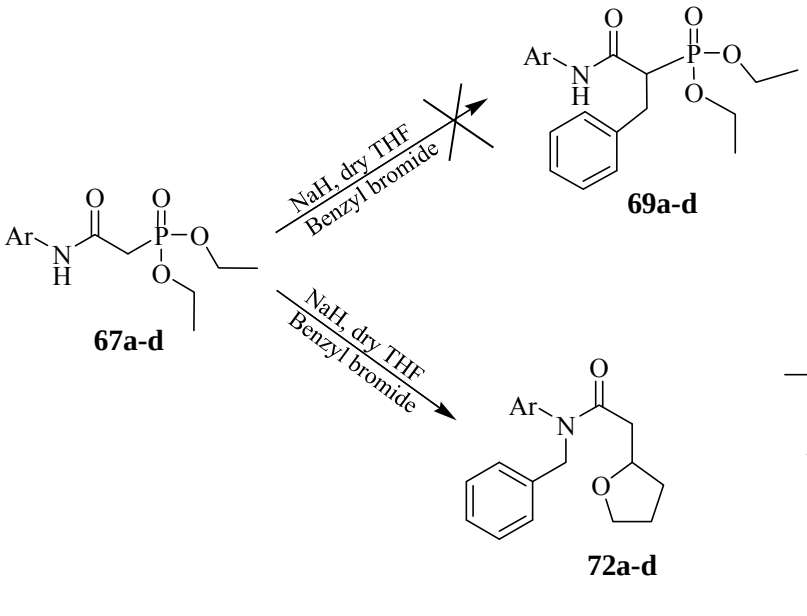

	Ar
a	3-Bromophenyl
b	3-(Hydroxymethyl)phenyl
c	2-Pyridyl
d	3-Hydroxyphenyl

Scheme 9. Formation of compounds **72a-d**.

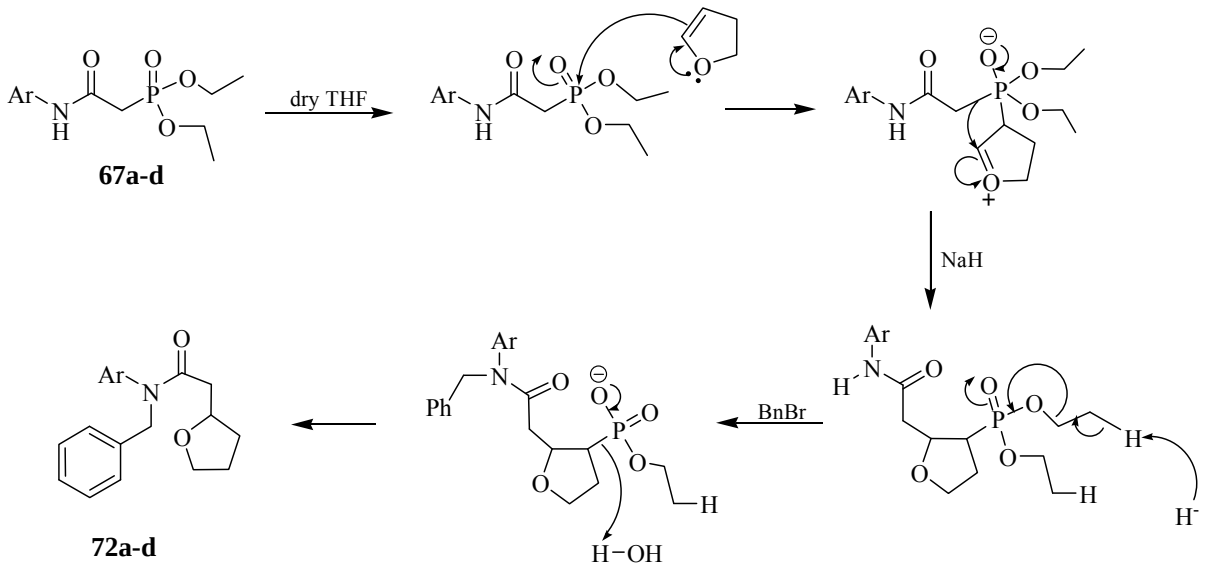

Figure 23. Tentative mechanism for the formation of compounds **72a-d**.

The ^{1}H NMR spectrum of compound **72a** (Figure 23a) shows the *O*-methine proton signal at 4.32 ppm, integrating for 1-proton, as multiplet and a signal at 4.89 ppm corresponding to the benzylic protons. Splitting of the benzylic proton signals arises from the fact that they are diastereotopic since the product is chiral. The additional 5-protons resonating in the aromatic region confirm the presence of a benzyl group. The ^{13}C NMR spectrum (Figure 23b) confirms benzylation, revealing ten-aromatic carbon signals between 122.9 and 143.7 ppm. The DEPT 135 NMR spectrum (Figure 23c) reveals the 3-methine carbon signal at 76.1 ppm and five different methylene carbons. The COSY NMR spectrum (Figure 23d) shows the correlations of the tetrahydrofuran ring protons; however, no correlation was observed with the benzylic protons, which confirms that the products were *N*-benzylated not *C*-benzylated. Confirmation of the assignments of the carbon signals was provided by the HSQC NMR spectrum (Figure 23e). Further support for the structural assignments was provided by the HRMS data for compound **72a** [*m/z* calculated for $C_{19}H_{20}NO_2Br$ (MH^+) 374.0756. Found 374.0749].

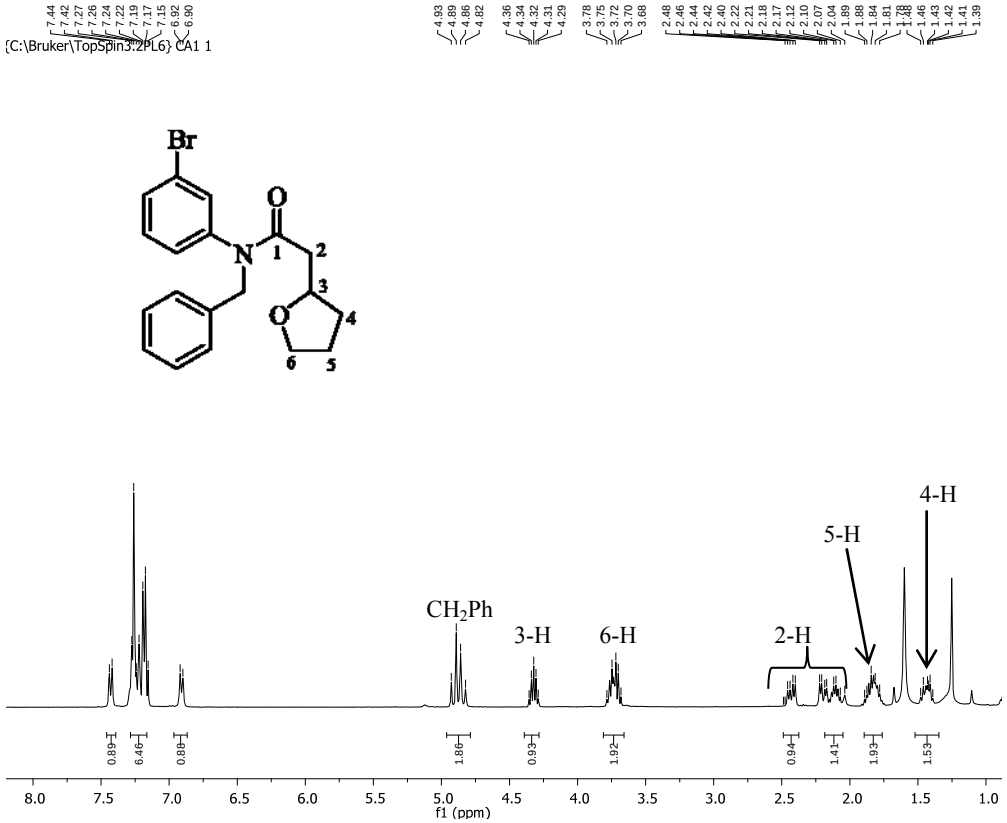

Figure 23a. 400MHz ^{1}H NMR spectrum of compound **72a** in $CDCl_3$.

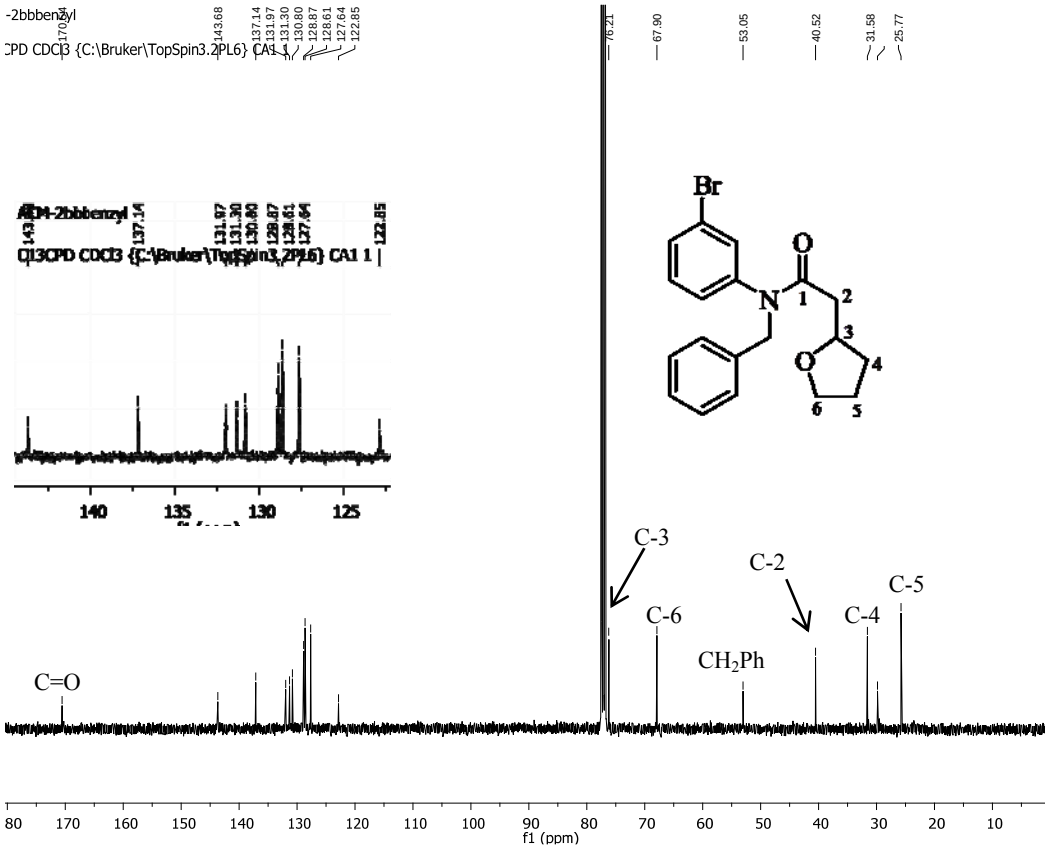

Figure 23b. 100MHz ^{13}C NMR spectrum of compound **72a** in $CDCl_3$.

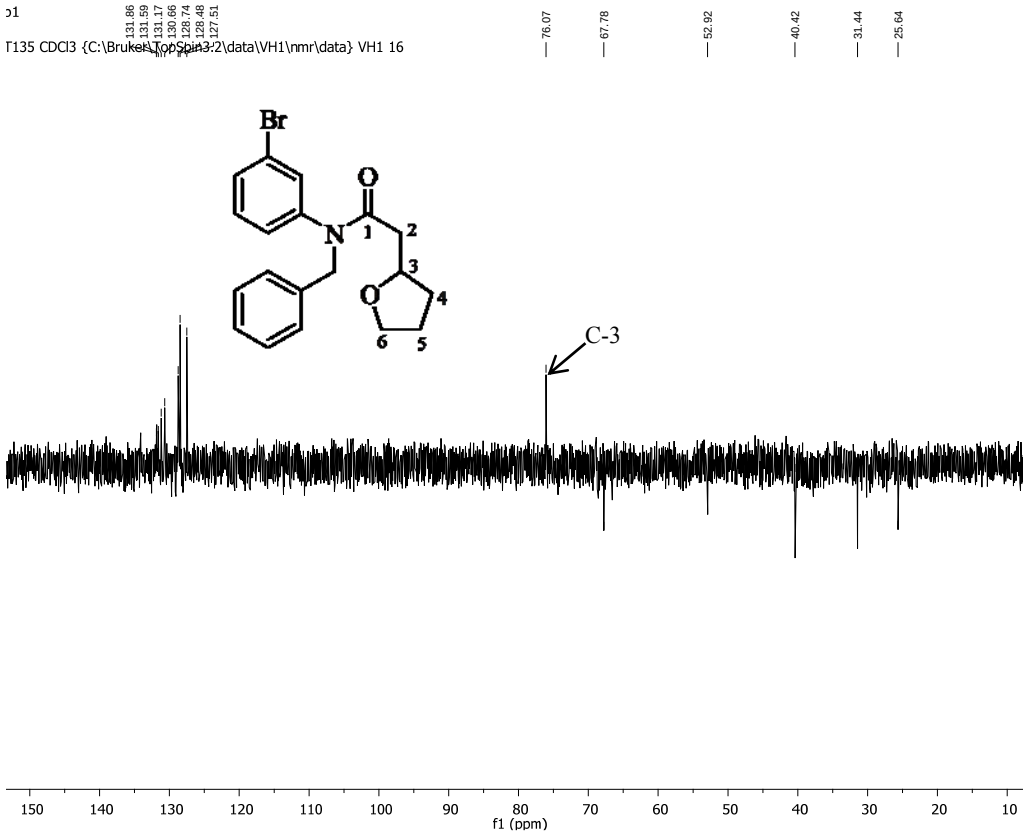

Figure 23c. DEPT 135 NMR spectrum of compound **72a** in $CDCl_3$.

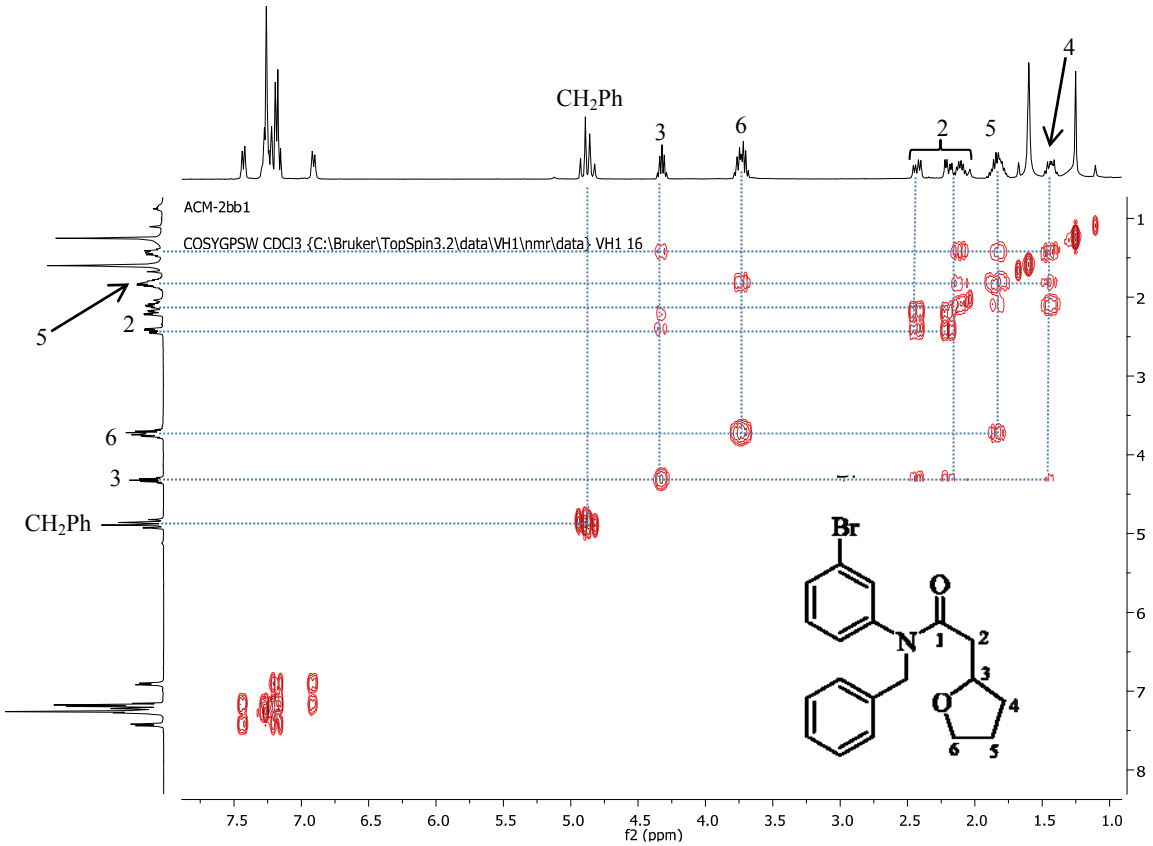

Figure 23d. COSY NMR spectrum of compound **72a** in $CDCl_3$.

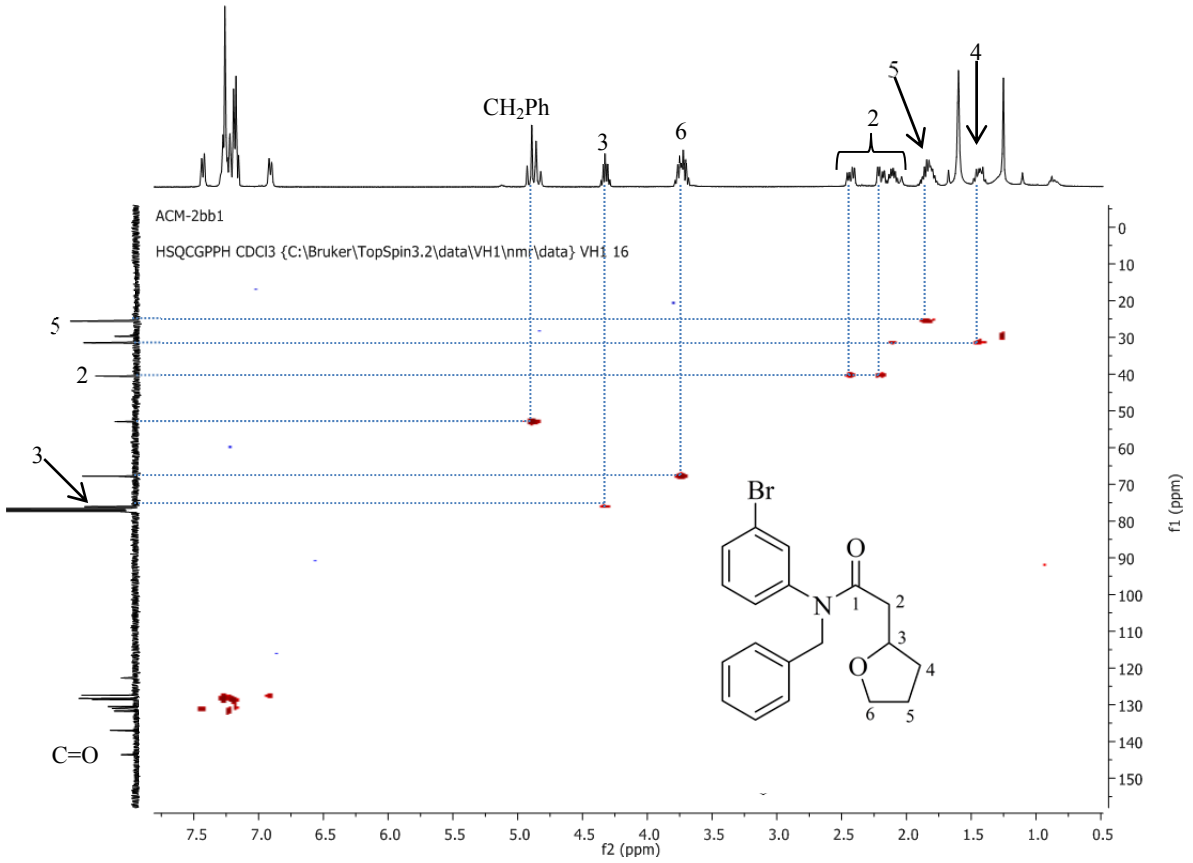

Figure 23e. HSQC NMR spectrum of compound **72a** in $CDCl_3$.

When the ethylphosphonate ester (n=2) **68d** was used as substrates for the *C*-benzylation reaction, it became evident that *N*-benzylation was favoured rather than *C*-benzylation. For example, when diethyl [*N*-(3-hydroxyphenyl)carbamoyl]ethylphosphonate **68d** was reacted with sodium hydride and benzyl bromide in THF, work-up afforded the *N*,*O*-dibenzylated product **70d** and, as a minor product, the mono-benzylated product **73**. The ^{1}H NMR spectrum of compound **70d** (Figure 24a) reveals that the methylene group directly attached to phosphorus is still present, resonating as a multiplet at 2.01 ppm which integrates for two protons; moreover, the two proton multiplet at 2.26 ppm corresponds to the presence of the methylene group adjacent to the carbonyl group. The two singlets at 4.74 and 4.84 ppm integrating for 2 protons each, coupled with the presence of 13 aromatic protons, clearly indicates the presence of two benzyl groups attached to the amide nitrogen and oxygen atoms. The DEPT 135 NMR spectrum (Figure 24b) confirms the presence of the methylene group directly attached to phosphorus and resonating as a doublet at 21.6 ppm. However, the ^{1}H NMR spectrum of the minor product **73**, as shown in Figure 25 reveals the broad singlet at 9.07 ppm corresponding to the amide proton, and a singlet at 5.05 ppm which corresponds to the *O*-benzylic protons.

The evidence provided by the NMR data for compounds **70d** and **73** in Figures 24a,b and 25 confirms the failure of the *C*-benzylation reaction. This failure is attributed to the presence of the additional methylene group in the carbon spacer between the amide nitrogen and the phosphonate ester, making the amide proton more acidic than the methylene protons adjacent to the carbonyl group. The base (sodium hydride) thus, abstracts the phenolic amide protons preferencially over the protons *alpha* to the carbonyl group.

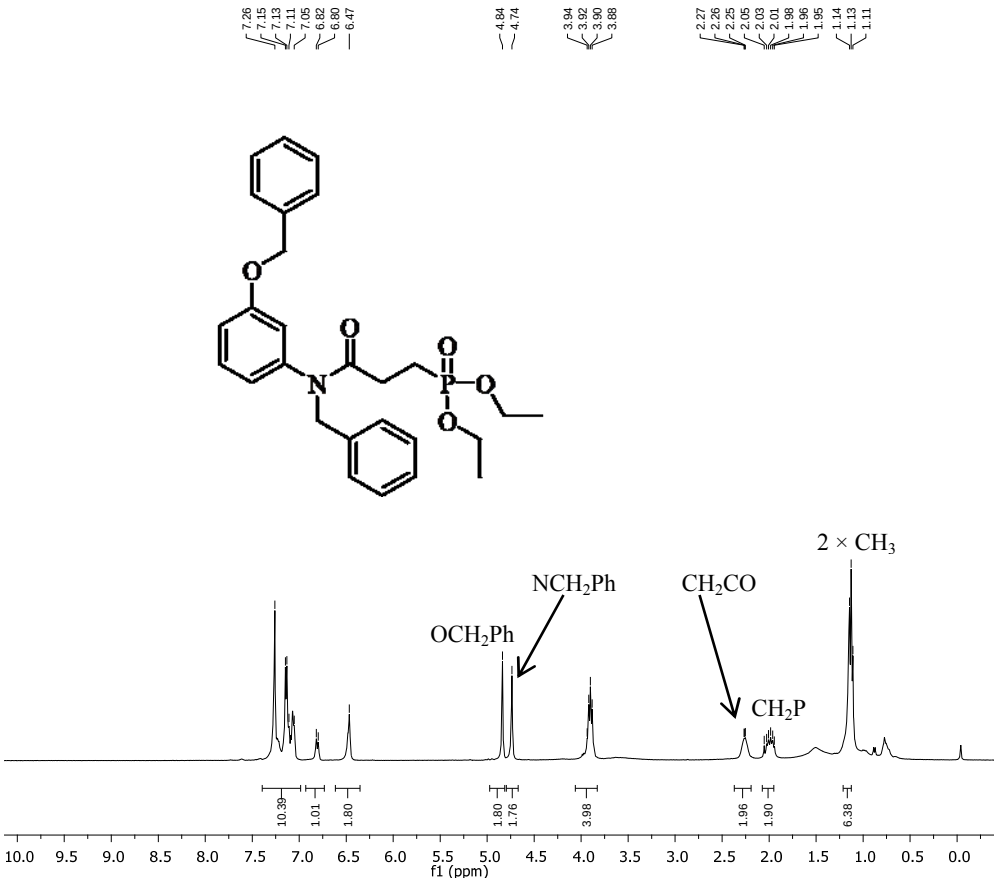

Figure 24a. 300 MHz ^{1}H NMR spectrum for compound **70d** in $CDCl_3$.

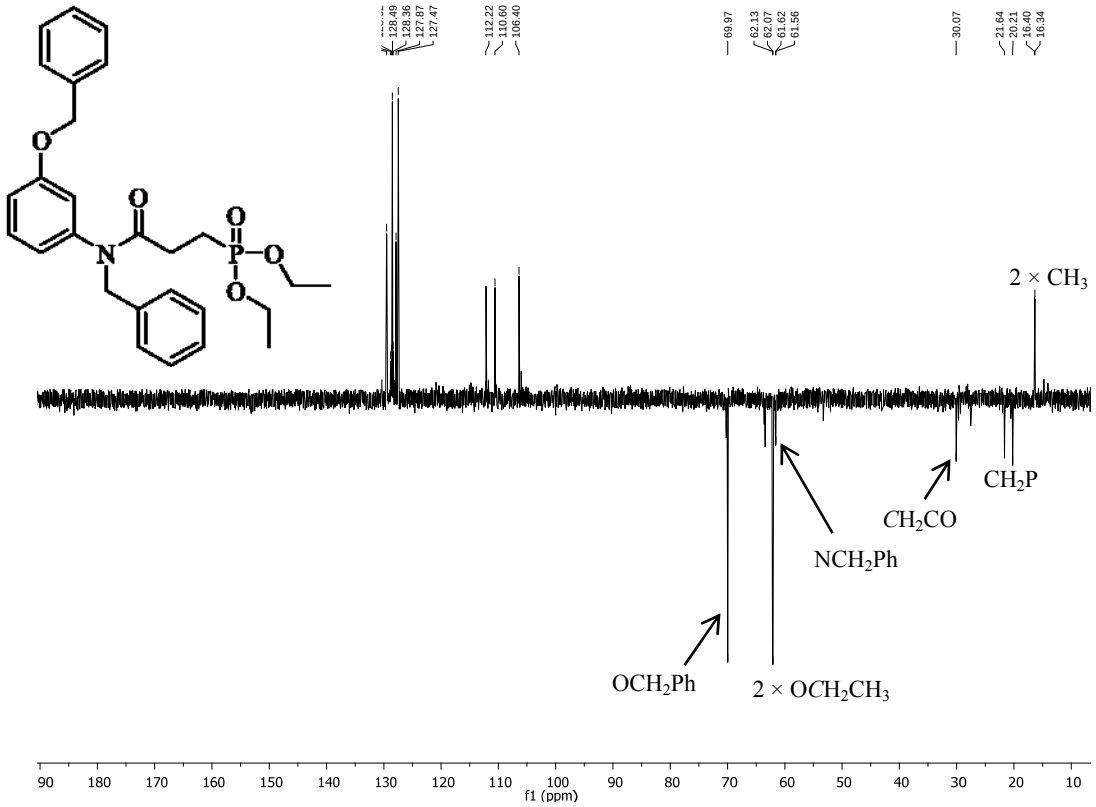

Figure 24b. DEPT 135 NMR spectrum of compound **70d** in $CDCl_3$.

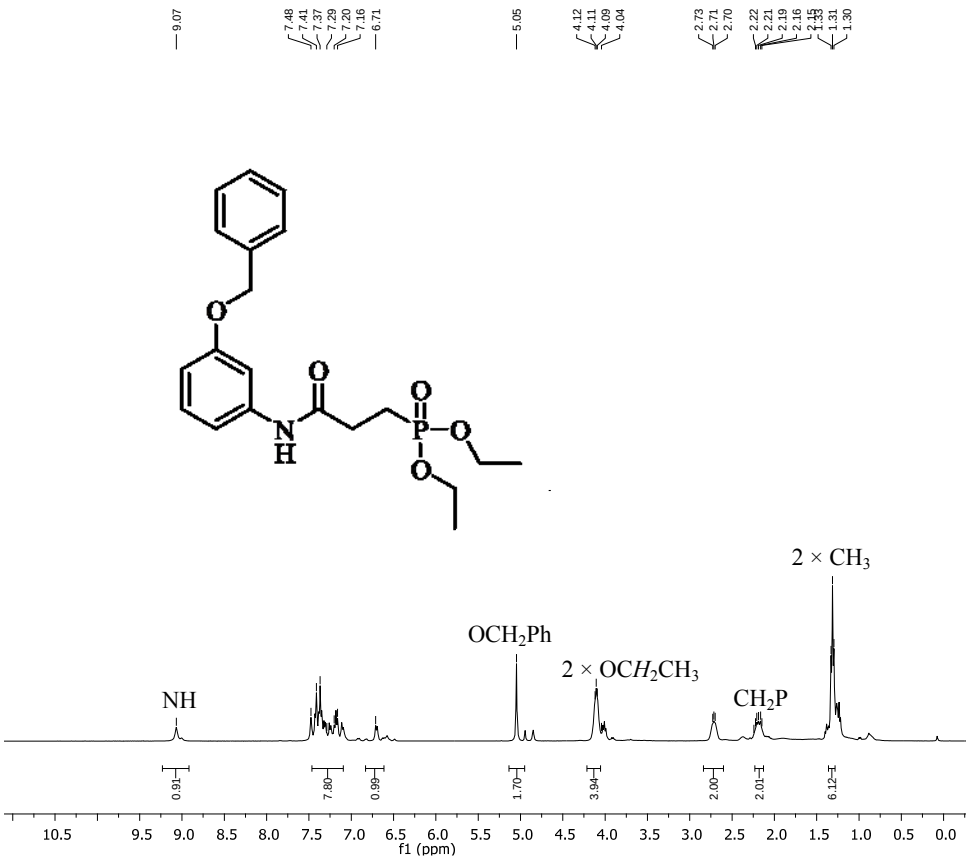

Figure 25. 300 MHz NMR spectrum of compound **73** in $CDCl_3$.

2.1.3. Preparation of *N*-benzylated phosphonate esters.

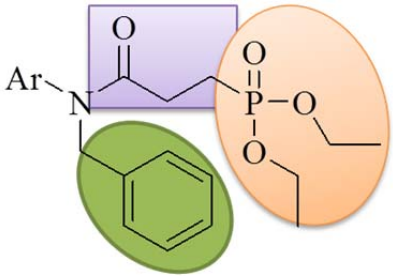

Compounds 77

In the design and synthesis of the *N*-benzylated phosphonate esters **77**, the intention was to react the ethylphosphonate esters **68** with benzyl bromide using NaH as base (Scheme 8) but, due to the problems encountered earlier, this approach was abandoned.

N-Benzylation of the phosphonate ester **77** (Scheme 10) was then attempted by stirring the chloropropanamide derivative **66d** with benzyl bromide in dry THF at room temperature for 5 days using powdered $NaHCO_3$ as base, with the intention of forming the *N*-benzylated chloropropanamide **76d** and, hence, the phosphonated ester *via* an *Arbuzov* reaction. However, when this reaction was monitored by TLC, no product was observed and only the starting materials were recovered (Scheme 10).

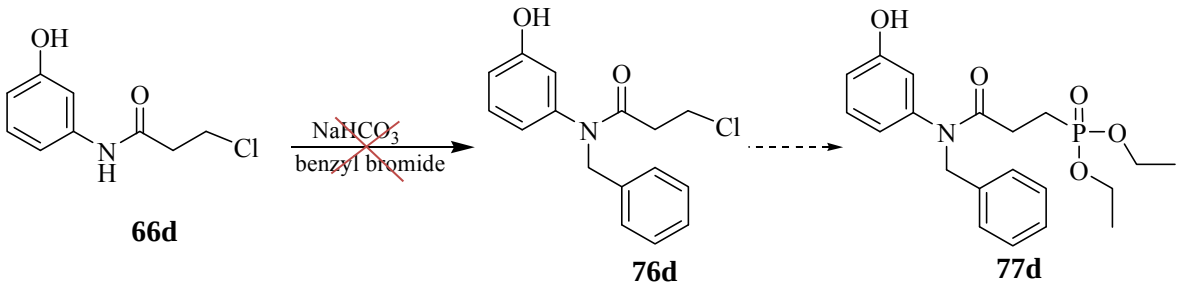

Scheme 10. Attempted synthesis of compound **77d**.

Retrosynthetic analysis of the target molecules **77**,[84] as shown in Figure 26, solved the problem and led to the reaction sequence, commencing from the amine Ar-NH_2, as outlined in Scheme 11.

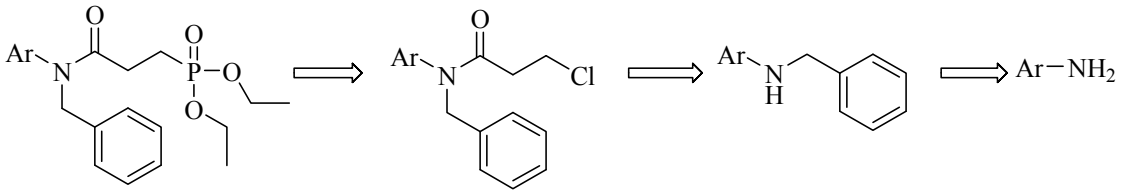

Figure 26. Retrosynthetic analysis for compounds **77**.[84]

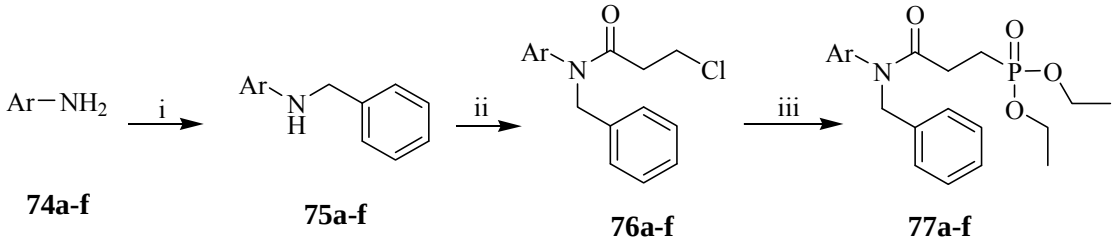

	a	b	c	d	e	f
Ar-NH_2	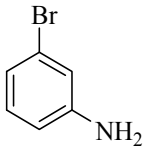	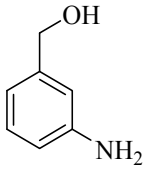	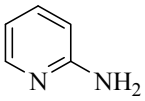	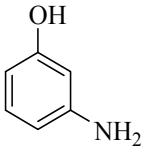	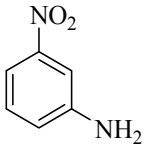	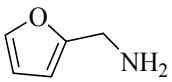

Scheme 11. Synthetic route towards *N*-benzylated phosphonate esters.

Reagents and conditions:- (i) $NaHCO_3$, benzyl bromide, dry THF, overnight, r.t.; (ii) 3-chloropropionyl chloride; and (iii) triethyl phosphite, 6 h, reflux (150 ^{o}C).

2.1.3.1. Synthesis of N-*benzylated amine derivatives*.

There are a number of established methods for the synthesis of secondary amines.[85,86,87] The reaction of a benzyl halide with a primary amine was the approach used for the preparation of the secondary amines in this study. The nucleophilic amine attacks the benzyl halide leading to the formation of a secondary amine; the reaction is effected by simply stirring the primary amine with benzyl bromide in a suitable solvent. The primary amines **74a-f** were reacted with one equivalent of benzyl bromide using dry THF as the solvent (step i, Scheme 11). The mixtures were stirred overnight at room temperature under an inert atmosphere in the presence of a mild base, *viz*., sodium hydrogen carbonate ($NaHCO_3$), in the same molar ratio as that of the primary amine and the benzyl bromide. The reaction was quenched by the addition of water, and the resulting products extracted by sequential washing with DCM. Chromatography afforded the *N*-benzylated derivatives **75a-f**. The products were obtained in yields of up to 76% (Table 2.2.). The ^{1}H NMR spectrum of *N*-benzyl-3-(hydroxymethyl)-aniline **75b** (Figure 27a) shows a broad signal at 2.87 ppm corresponding to the amino proton while the benzylic protons resonate as singlet at 4.21 ppm, confirming the formation of product. The ^{13}C NMR spectrum (Figure 27b) reveals the benzylic carbon signal at 48.3 ppm and the aromatic carbon signals between 111.4-148.5 ppm including the quaternary carbon signals. Analysis of the DEPT 135 NMR spectrum (Figure 27c) clearly shows the benzylic methylene signal at 48.2 ppm and the aromatic methane signals.

In addition to the major product **75b**, the *N*,*O*-bis-benzylated product, *N*-benzyl-3-[(benzyloxy)methyl]aniline **78** was also obtained in 19% yield as the minor product (Scheme 12). The ^{1}H NMR spectrum of the *bis*-benzylated product **78** (Figure 28) shows the signal at 4.57 ppm corresponding to the benzylic protons (NCH_2Ph) and the four *O*-benzylic protons resonating as a singlet at 4.66 ppm.

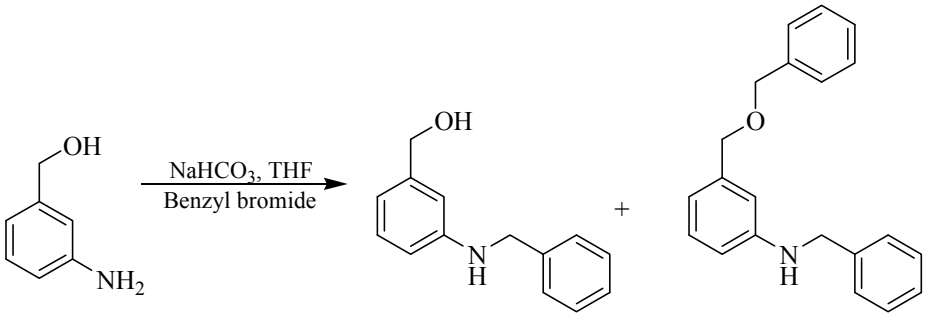

74b **75b** **63% yield** **78** **19% yield**

Scheme 12. Formation of the compound **75b** and the minor product **78**.

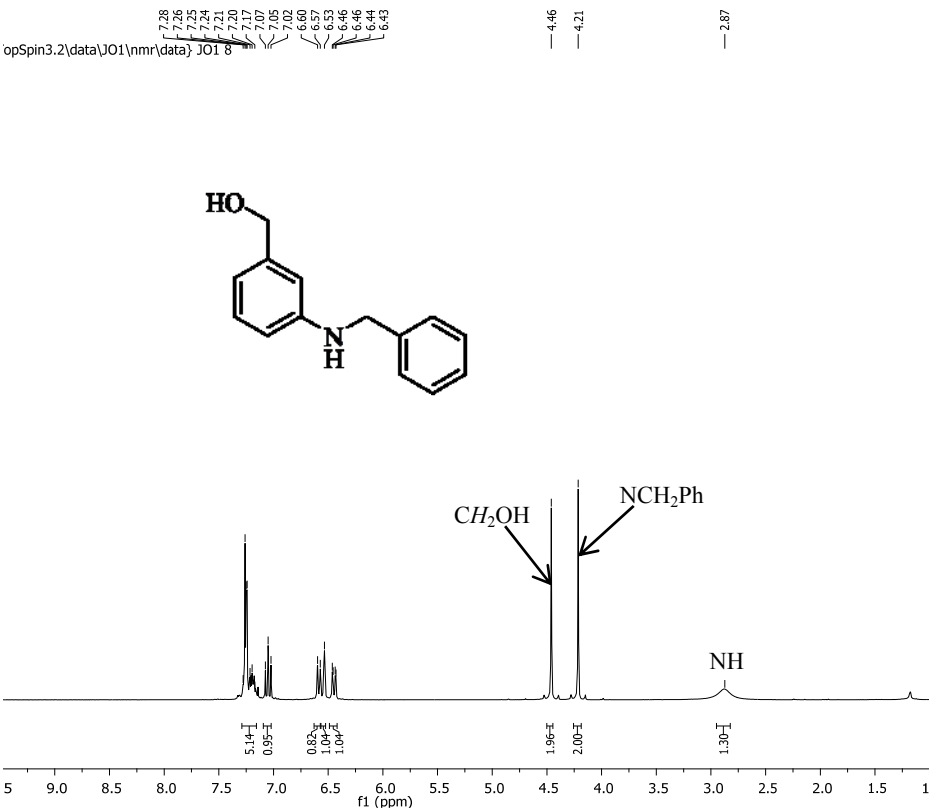

Figure 27a. 400MHz ^{1}H NMR spectrum of compound **75b** in $CDCl_3$.

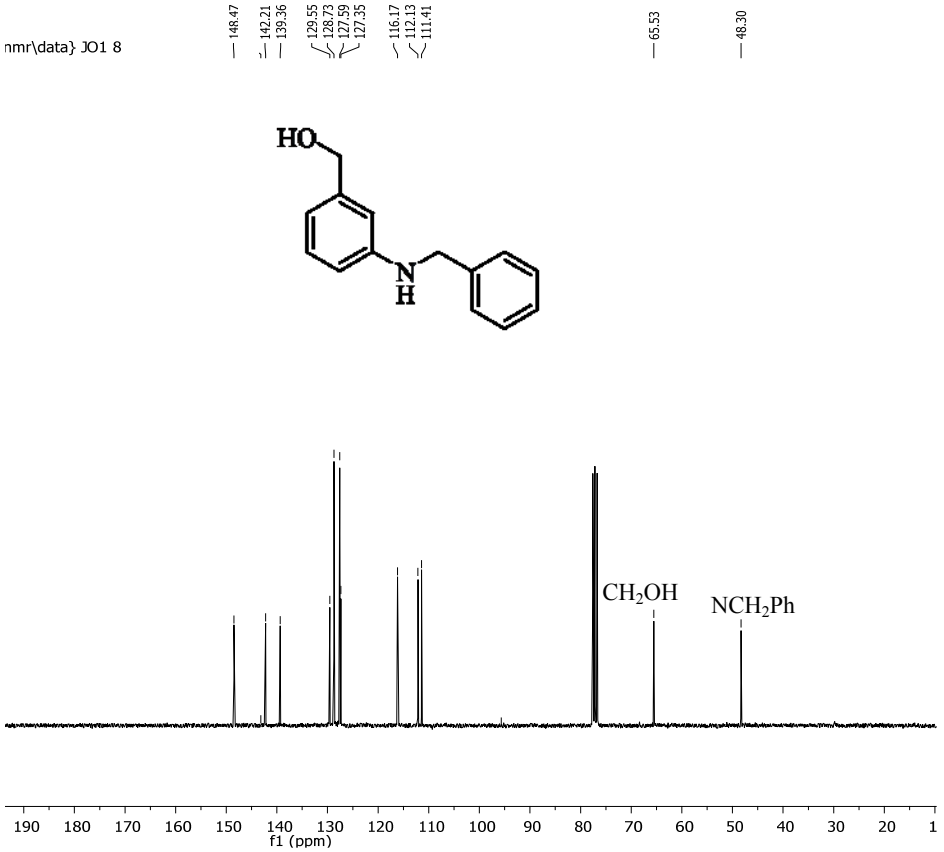

Figure 27b. 100 MHz ^{13}C NMR spectrum of compound **75b** in $CDCl_3$.

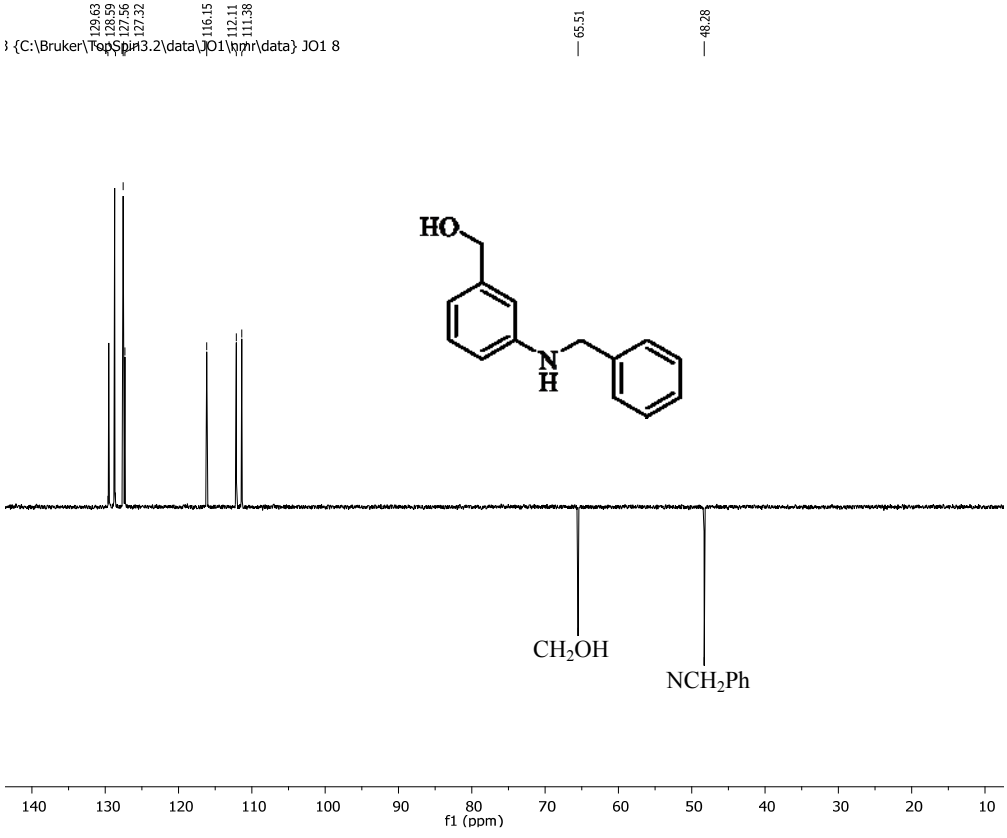

Figure 27c. DEPT 135 NMR spectrum of compound **75b** in $CDCl_3$.

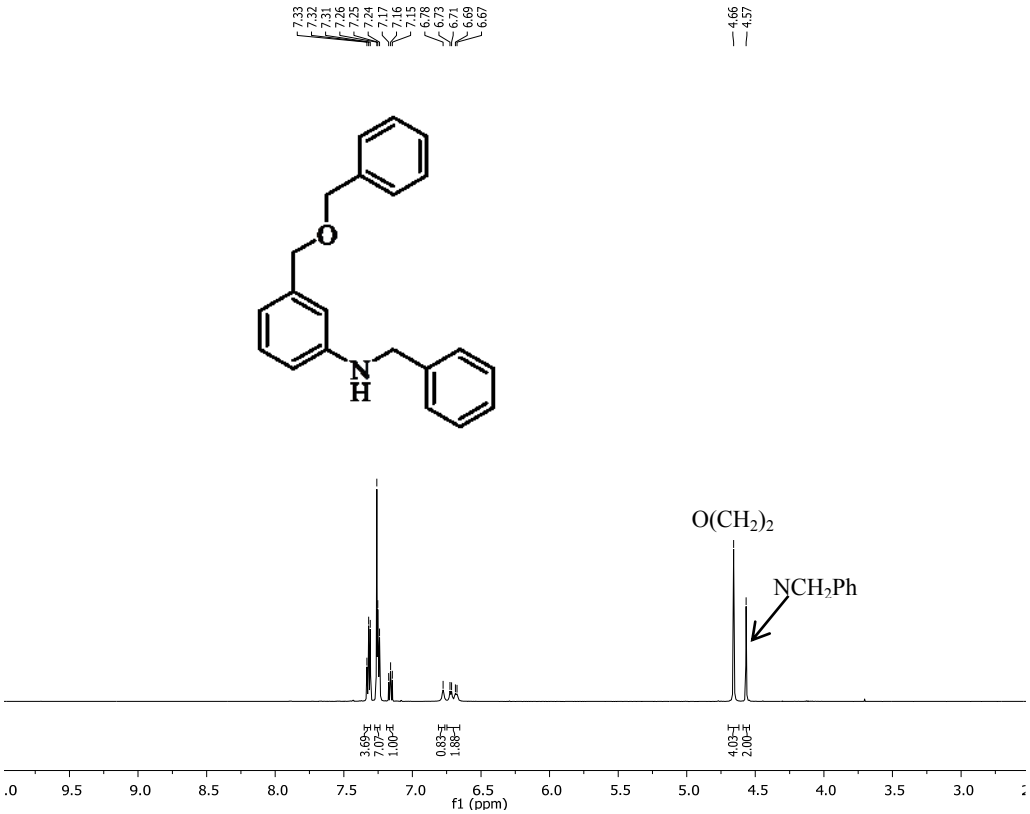

Figure 28. 400 MHz ^{1}H NMR spectrum of *N,O*-bis-benzylated compound **78** in $CDCl_3$.

Table 2.2. Percentage yields obtained for the *N*-benzylated derivatives **75a-f**.

Ar-NH$_2$	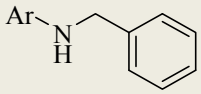	**Yield/%**
3-Bromophenyl	**75a**	65
3-(Hydroxylmethyl)phenyl	**75b**	63
2-Pyridyl	**75c**	56
3-Hydroxyphenyl	**75d**	62
3-Nitrophenyl	**75e**	72
Furfuryl	**75f**	76

2.1.3.2. Synthesis of N-*benzylated 3-chloropropanamides* 76a-f.

Given the success in obtaining the *N*-benzyl-3-aniline derivatives **75a-f**, the next stage involved the introduction of the acid chloride *via* the acylation reaction to form an amide. The *N*-benzyl-3-aniline and furfurylamine derivatives **75a-f** were reacted with 3-chloropropionyl chloride using THF as solvent (Scheme 13). The mixtures were stirred at r.t. under N_2 overnight using sodium hydride as base. The isolated products were washed sequencially with a saturated aqeous solution of $NaHCO_3$, water and brine. Chromatography afforded the amide derivatives **76a-f** in yields of up to 52% (Table 2.3).

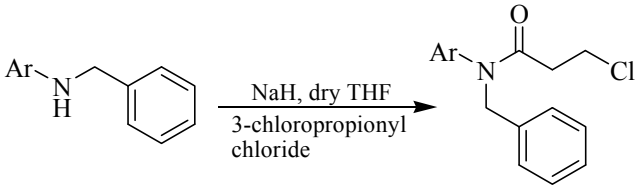

75a-f **76a-f**

Scheme 13. Synthesis of *N*-benzylated 3-chloropropanamides **76a-f**.

These compounds are new and were fully characterised using HRMS, NMR and IR spectroscopic analysis. The ^{1}H NMR spectrum of *N*-benzyl-3-chloro-*N*-(3-nitrophenyl)-propanamide **76e** (Figure 29a) exhibits a pair of triplets at 2.47 ppm and 3.76 ppm integrating for two protons each and corresponding to the CH_2CO and chloromethylene protons, respectively. The DEPT 135 NMR spectrum of compound **76e** (Figure 29b) indicates the CH_2 signals of the two methylene groups at 37.2 and 40.0 ppm and allowed identification of the quaternary carbon signals and the carbonyl carbon signal at 169.1 ppm in the ^{13}C NMR spectrum (Figure 29c). Analysis of the HSQC spectrum of compound **76e** (Figure 29d) confirmed the assignment of the aromatic carbon and proton signals, with the carbonyl and quaternary carbons showing no correlation to any proton signals. The IR spectrum of compound **76e** clearly reveals the absorption band of the carbonyl group (C=O) at 1659 cm^{-1} (Figure 29e). In the preparation of compound **76d**, a by-product was also obtained; this was identified as the di-acylated analogue **79**.

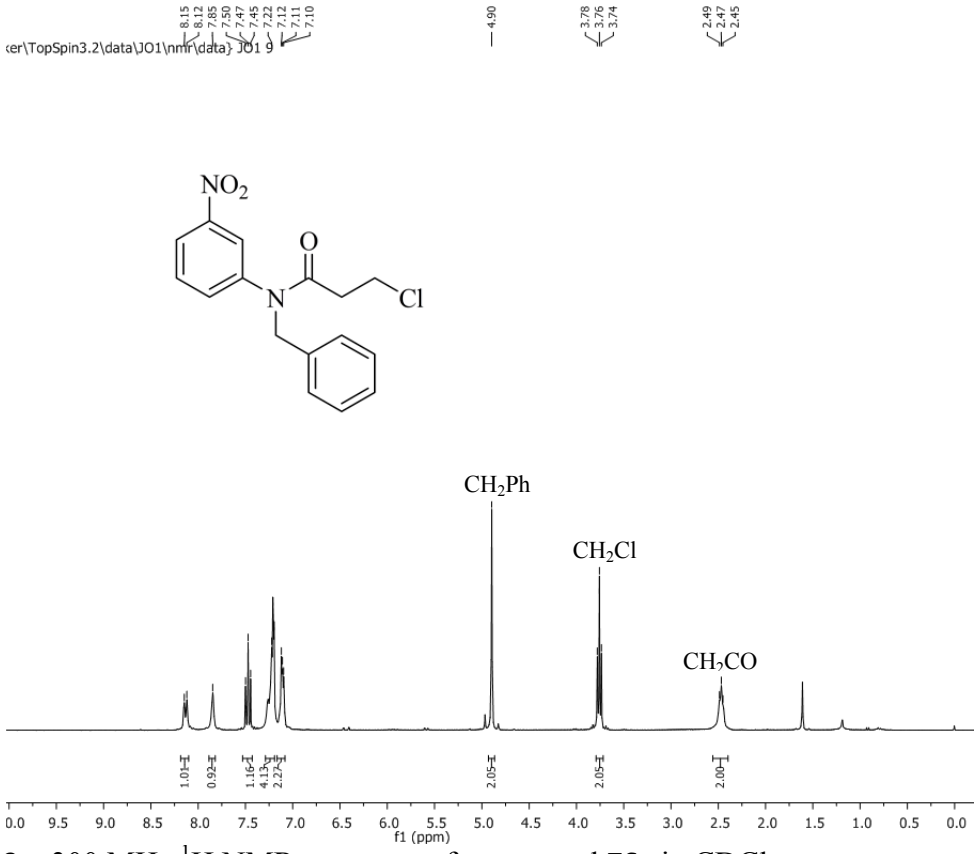

Figure 29a. 300 MHz ^{1}H NMR spectrum of compound **76e** in $CDCl_3$.

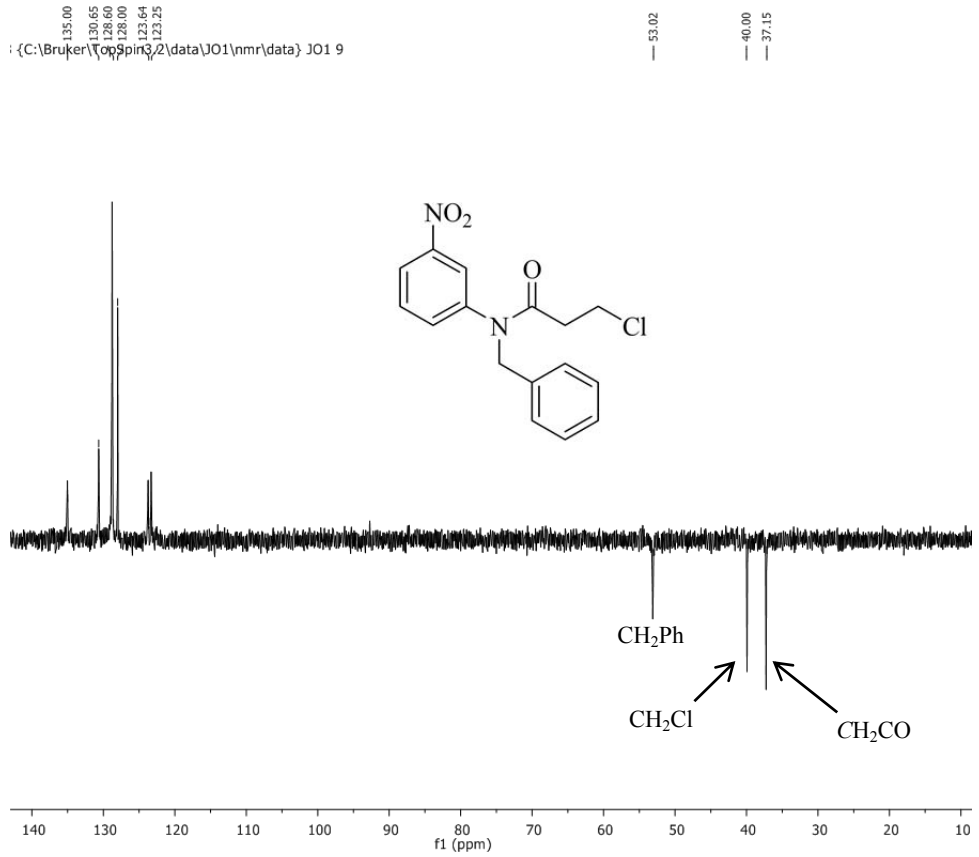

Figure 29b. DEPT 135 NMR spectrum of compound **76e** in $CDCl_3$.

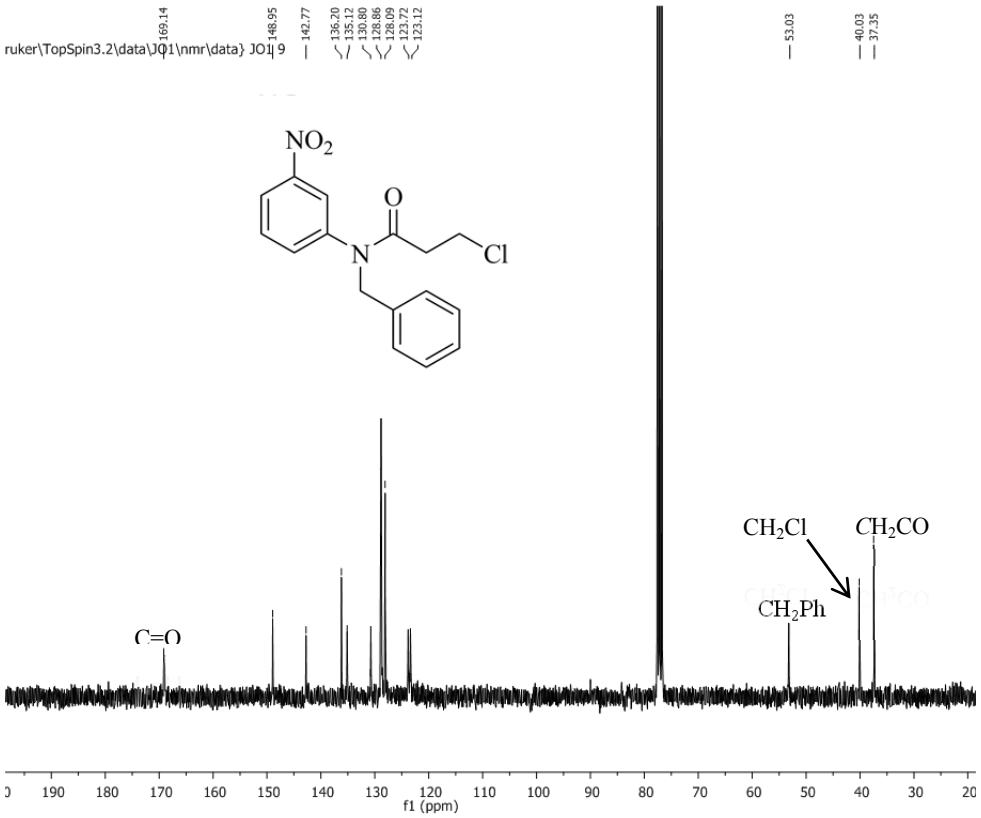

Figure 29c. 75 MHz ^{13}C NMR spectrum of compound **76e** in $CDCl_3$.

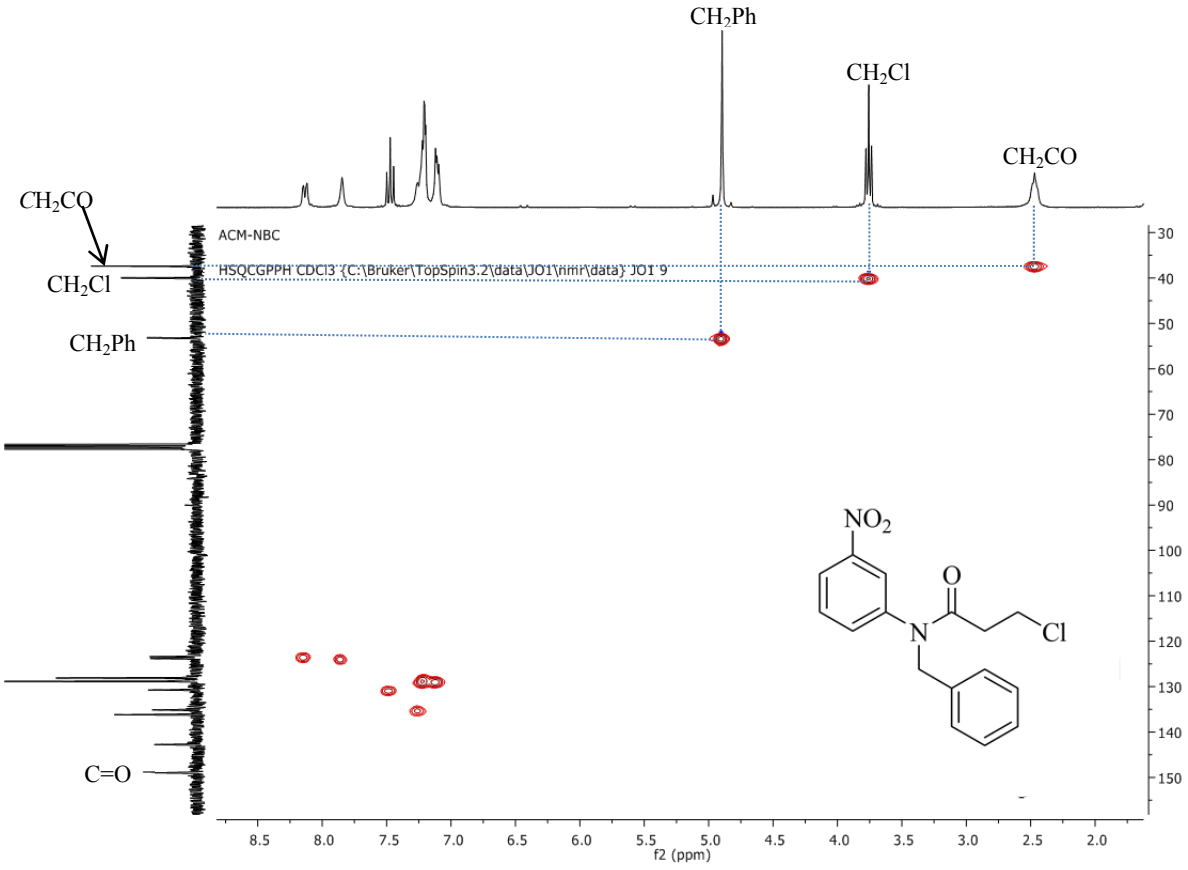

Figure 29d. HSQC NMR spectrum of compound **76e** in $CDCl_3$.

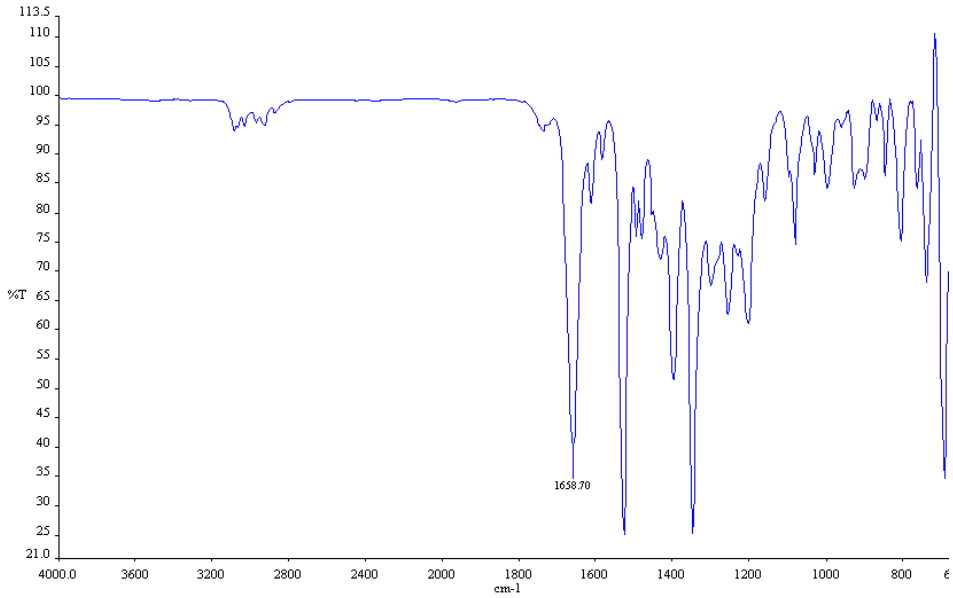

Figure 29e. IR spectrum of compound **76e**.

Table 2.3. Percentage yields obtained for the *N*-benzylated 3-chloropropanamides **76a-f**.

Ar-NH$_2$	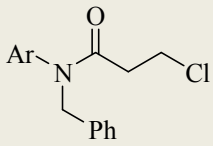	**Yield/%**
3-Bromophenyl	**76a**	50
3-(Hydroxylmethyl)phenyl	**76b**	36
2-Pyridyl	**76c**	33
3-Hydroxyphenyl	**76d**	39
3-Nitrophenyl	**76e**	52
Furfuryl	**76f**	9

2.1.3.3. Synthesis of N-*benzylated phosphonate esters* 77a-e

The 3-chloropropanamide derivatives **76a-e** were reacted with 2 equivalents of triethyl phosphite in *Michaelis-Arbuzov* reactions[78,79] (Scheme 14). The mixtures were refluxed under N_2 at 120-150 ^oC. In an attempt to remove excess triethyl phosphite, the crude products were observed to dissolve in hexane; therefore they were not stirred with hexane. Instead, flash chromatography and evaporation of the residual solvent under vacuum for several hours afforded the phosphonated derivatives **77a-e** in yields of up to 59% (Table 2.4). The *N*-benzylated amines **75a-f** incorporate an ethylene spacer between the amide and the phosphonate ester moieties – a feature which is considered to be important in DXR inhibition.

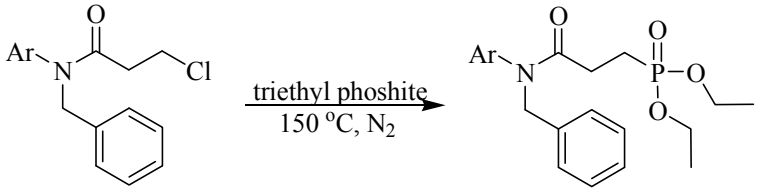

76a-e **77a-e**

Scheme 14. Synthesis of *N*-benzylated phosphonate esters **77a-e**.

These compounds are all new, and were fully characterised using NMR and IR spectroscopic and HRMS techniques. The ^1H NMR spectrum for diethyl 2-[*N*-benzyl-*N*-(3-bromophenyl)-carbamoyl]ethylphosphonate **77a** (Figure 30a) shows the absence of the characteristic chloroethylene triplets observed at 2.46 ppm and 3.72 ppm in the ^1H spectrum of its precursor **76a**, and the presence of a new methylene multiplet and triplet at 2.03 ppm and 2.27 ppm, respectively, the latter reflecting coupling to the ^{31}P nucleus. Moreover, the triplet at 1.18 ppm and the quartet at 3.96 ppm, confirm the formation of the diethyl phosphonate ester. ^{31}P Coupling was also observed in the DEPT 135 NMR spectrum of compound **77a** (Figure 30b), which shows split signals at 16.4 and 61.7 ppm corresponding to the ethyl phosphonate ester carbons and at *ca*. 21 ppm corresponding to the *P*-methylene carbon. The HSQC and COSY spectra of compound **77a** confirm the correlations of the protons to the assigned carbon signals and critical proton-proton couplings, respectively (Figures 30c,d).

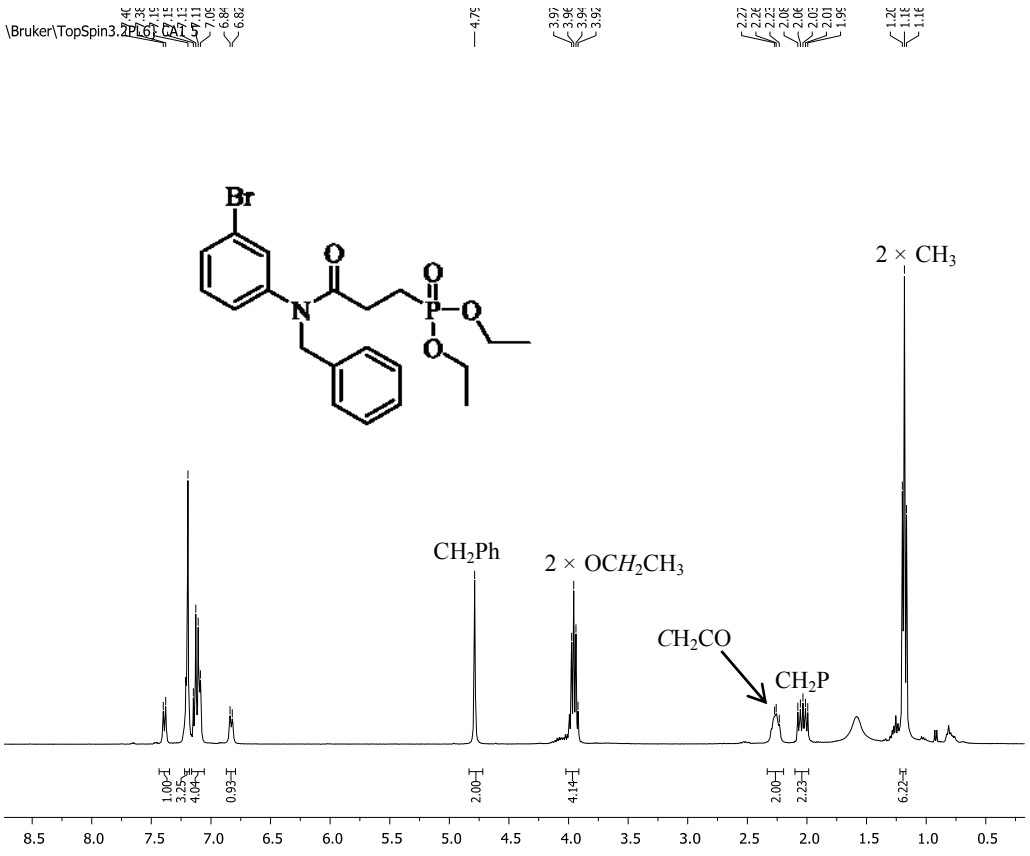

Figure 30a. 300 MHz ^{1}H NMR spectrum of compound **77a** in $CDCl_3$.

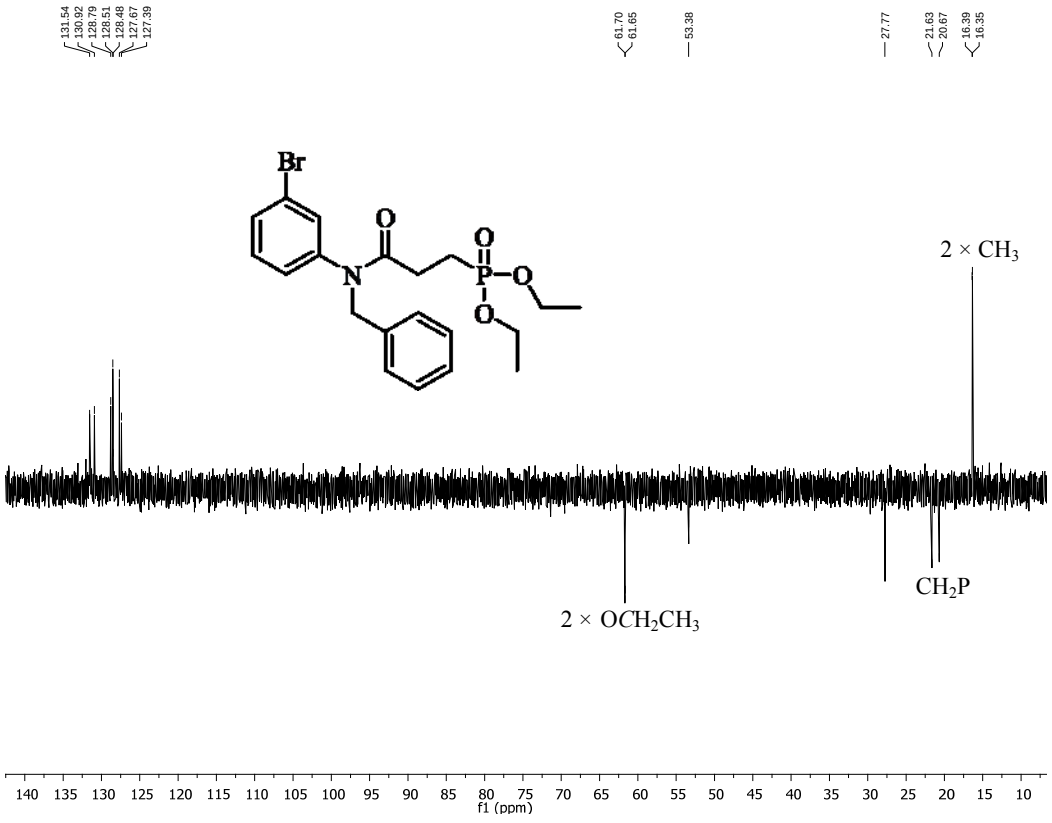

Figure 30b. DEPT 135 NMR spectrum of compound **77a** in $CDCl_3$.

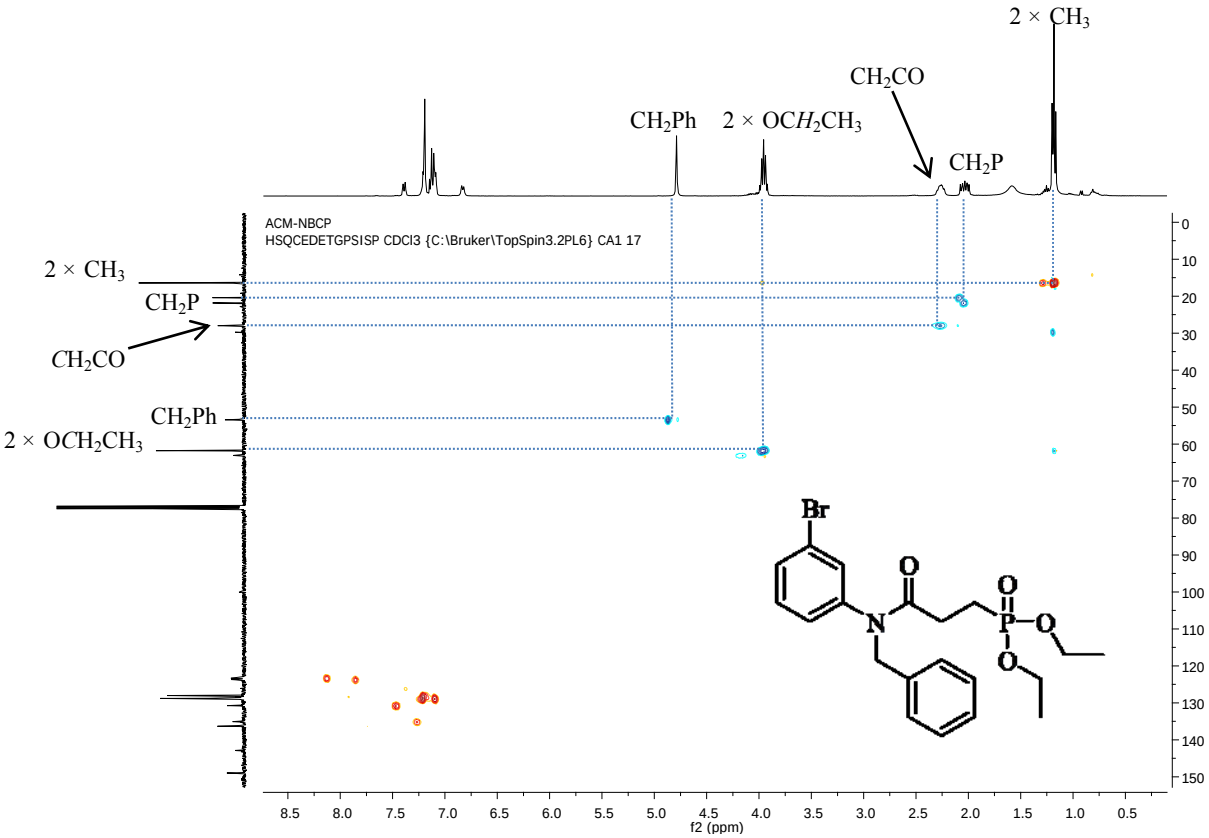

Figure 30c. HSQC NMR spectrum of compound **77a** in $CDCl_3$.

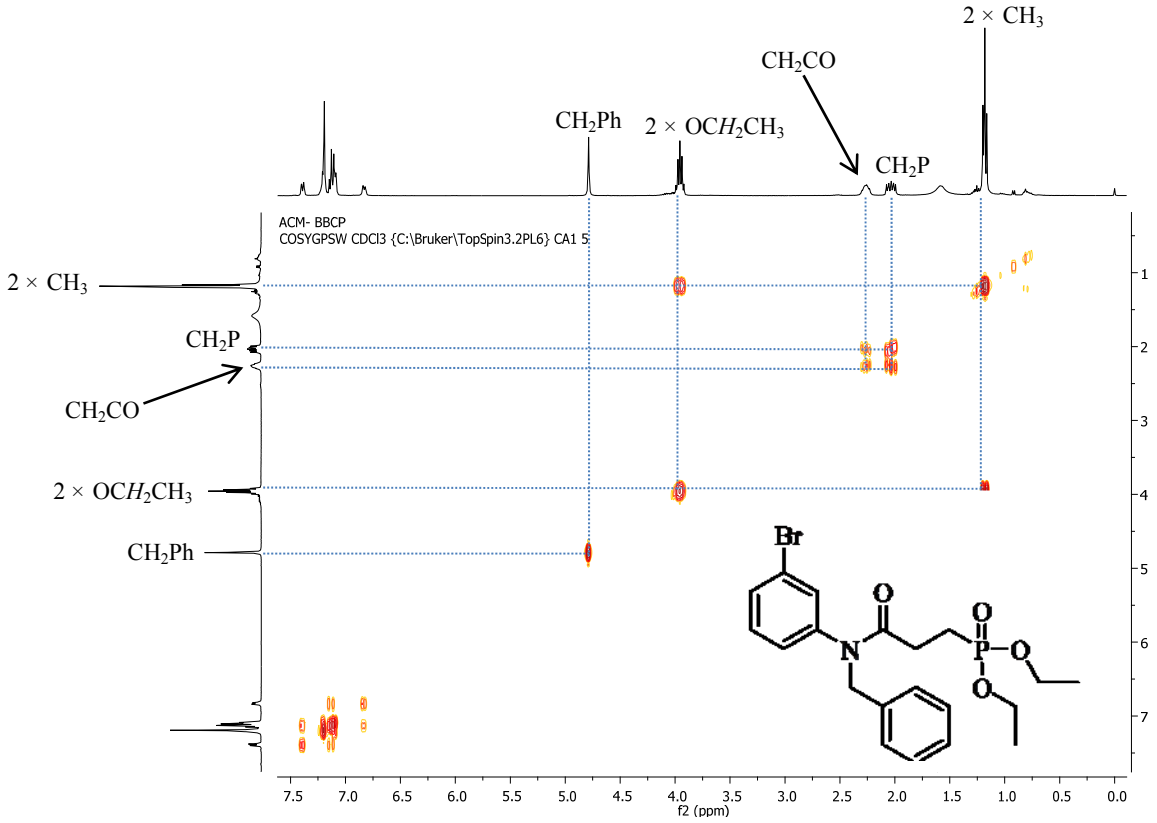

Figure 30d. COSY NMR spectrum of compound **77a** in $CDCl_3$.

Table 2.4. Percentage yields obtained for the *N*-benzylated phosphonate esters **77a-e**.

Ar-NH$_2$	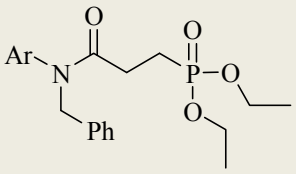	**Yield/%**
3-Bromophenyl	**77a**	51
3-(Hydroxylmethyl)phenyl	**77b**	47
2-Pyridyl	**77c**	49
3-Hydroxyphenyl	**77d**	51
3-Nitrophenyl	**77e**	59

2.2. EXPLORATORY STUDIES TOWARDS THE SYNTHESIS OF POTENTIAL DUAL-ACTION *Pf*DXR AND HIV-1 RT INHIBITORS.

AZT **80**, the first anti-retroviral drug to be approved by the Food and Drug Administration (FDA) as an HIV drug in 1987,[88] is actually a pro-drug which is triphosphorylated *in vivo*.[90]

One of the aims of our research programme is to develop synthetic access to potential dual-action HIV-1 RT / *Pf*DXR inhibitors.[89] In the present study, attention has been given to the construction of conjugates comprising a phosphonated fosmidomycin analogue as a potential *Pf*DXR inhibitor and monophosphorylated AZT as a potential HIV-1 RT inhibitor. The proposed routes to these conjugates are outlined in Scheme 15.

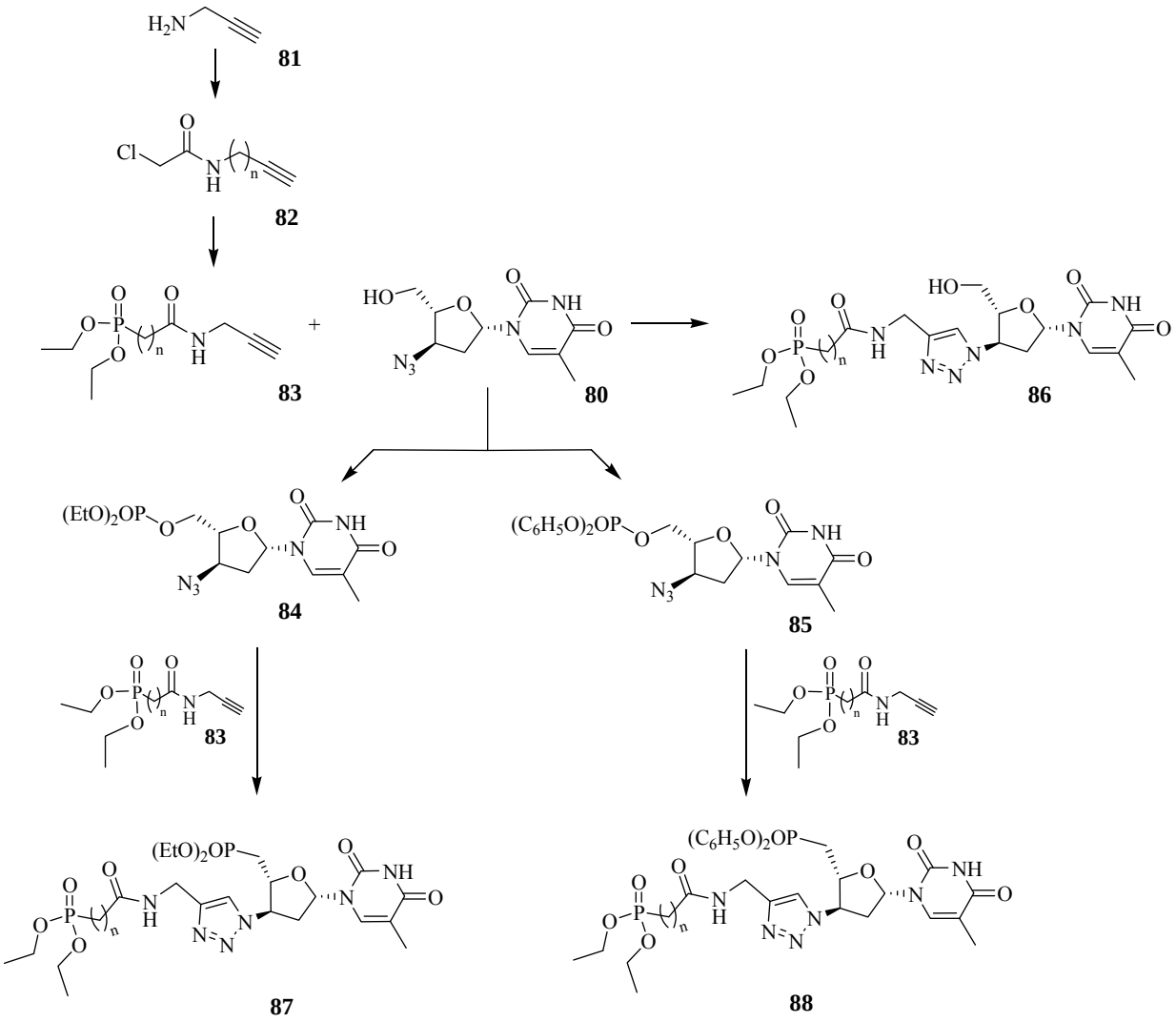

Scheme 15. Proposed synthetic routes to potential dual-action of HIV-1 RT / *Pf*DXR inhibitors, n=1,2.

2.2.1. Synthesis of propagylamine derivatives.

2.2.1.1. Synthesis of N-*propargyl chloroalkanamides*.

It was decided to start the synthesis by the introduction of a propargyl group to facilitate the linkage to the AZT moiety *via* a "Click" reaction. Chloroacetyl chloride or 3-chloropropionyl chloride was reacted with an ice-cooled solution of propargylamine **81** and triethylamine using dry THF as the solvent (Scheme 16). After reacting at r.t. under N_2, the crude product, in each case, was washed with 2% HCl to remove the excess triethylamine, and compounds **82a** and **82b** were obtained in 95% and 92% yield respectively without the need for purification.[90]

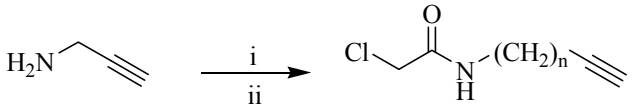

81 **n = 1; 82a**
n = 2; 82b

Scheme 16. Synthesis of *N*-propargyl chloroalkanamides.

Reagents and conditions:- (i) triethylamine, dry THF, 0 ^{o}C; and (ii) chloroacetyl chloride or 3-chloropropionyl chloride.

Compounds **82a** and **82b** are new and were fully characterised using both 1- and 2D-NMR, and IR spectroscopc and HRMS techniques. The ^{1}H NMR spectrum of 2-chloro-*N*-(2-propynyl)acetamide **82a**, for example, reveals the acetylenic proton signal at 2.28 ppm, as shown in Figure 31a; the chloromethylene protons resonate as a singlet at 4.07 ppm, the amino methylene protons as a doublet of doublets at 4.11 ppm, and the amino proton as a broad singlet at 6.79 ppm. Interestingly, the DEPT 135 NMR spectrum (Figure 31b) shows the appearance of two signals in the alkyne carbon region at *ca* 75 ppm, suggesting that the quaternary acetylenic carbon bears a proton. This apparent anomaly was resolved by running a proton-undecoupled ^{13}C NMR spectrum (Figure 31c), which revealed both the terminal and quaternary alkyne carbon signals resonating as doublets of triplets. This splitting arises from: (i) coupling of the terminal alkyne with its attached proton (J = 251.95 Hz) and a small, long-range coupling to the amino methylene protons; and (ii) coupling of the quaternary alkyne carbon with the aminomethylene protons and the terminal alkyne proton ($J_{C,H}$ = 49.69 Hz). The HSQC spectrum in Figure 31d confirms this explanation. This pattern is also evident in the ^{13}C NMR spectra of all the propargyl derivatives prepared in this study. The ^{1}H NMR spectrum of 3-chloro-*N*-(2-propynyl)propanamide **82b** (Figure 32) confirms the presence of

the ethylene spacer with the CH_2Cl and CH_2CO protons, coupling with each other and resonating as triplets.

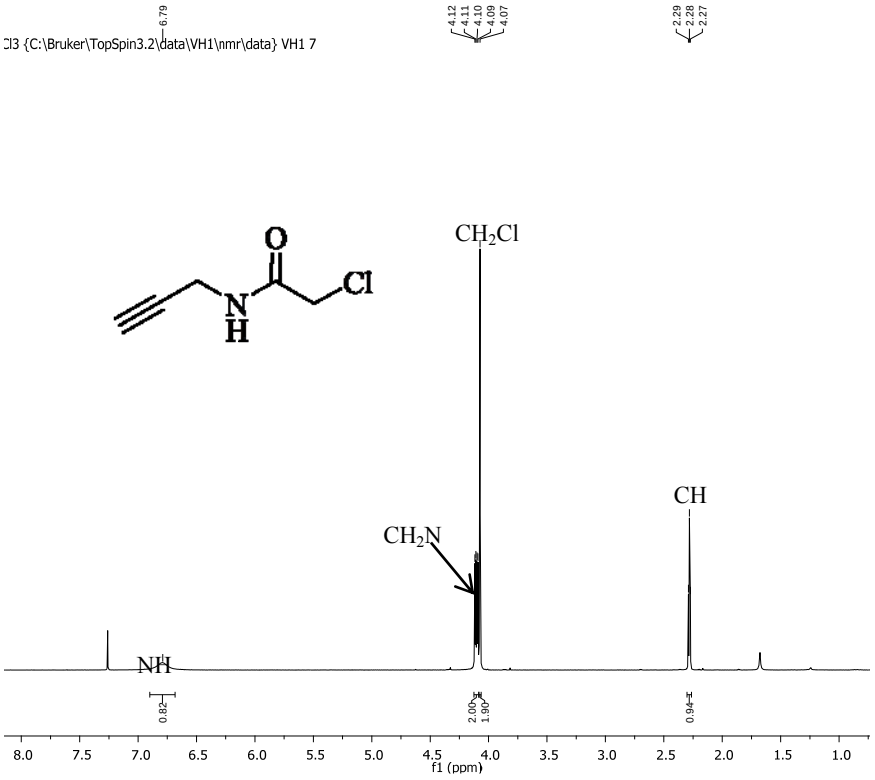

Figure 31a. 400 MHz ^1H NMR spectrum of compound **82a** in $CDCl_3$.

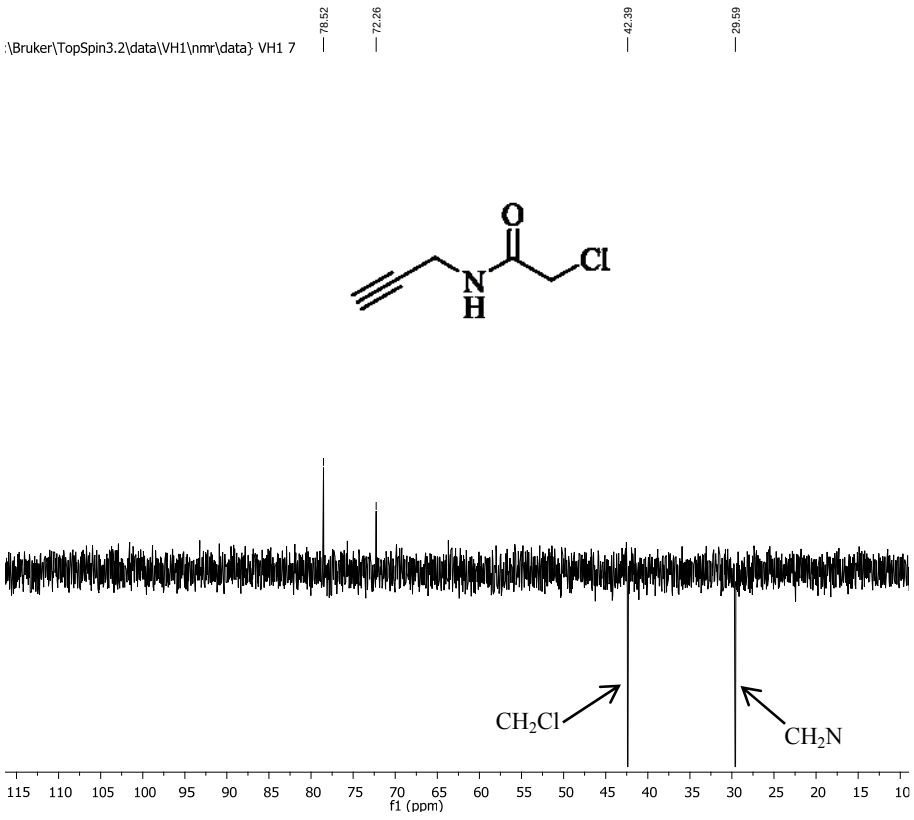

Figure 31b. DEPT 135 NMR spectrum of compound **82a** in $CDCl_3$.

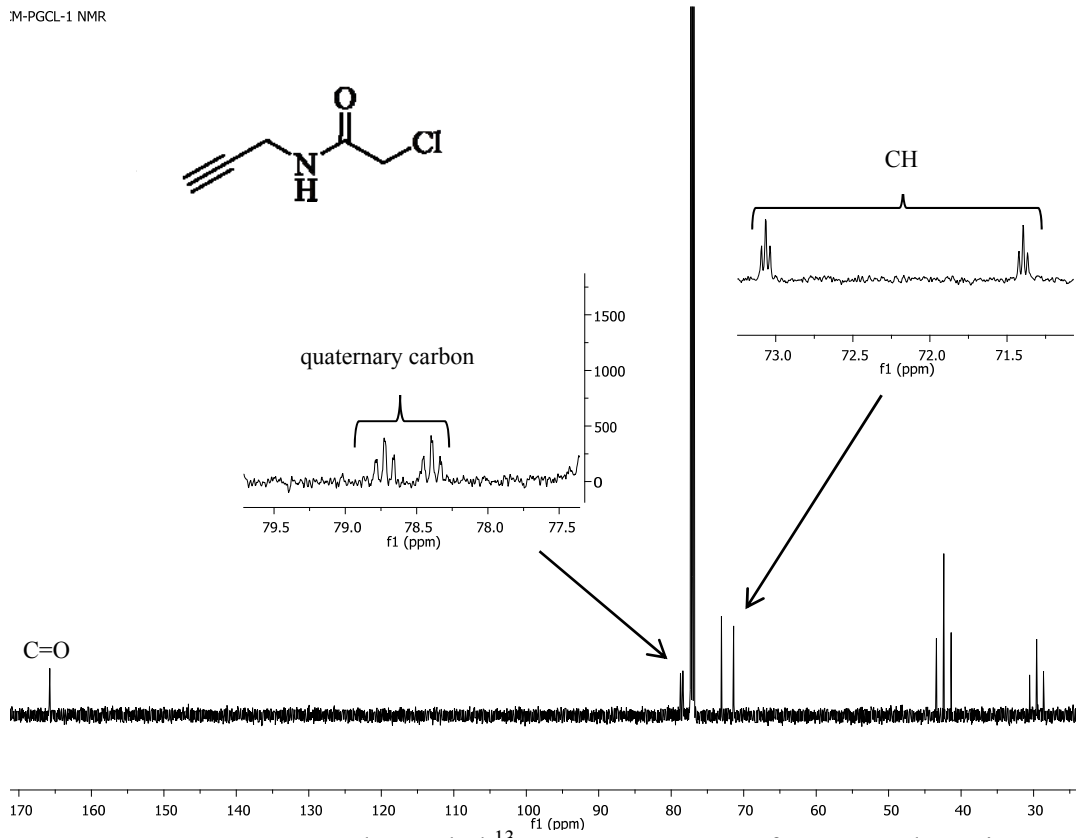

Figure 31c. 150 MHz proton-undecoupled ^{13}C NMR spectrum of compound **82a** in $CDCl_3$.

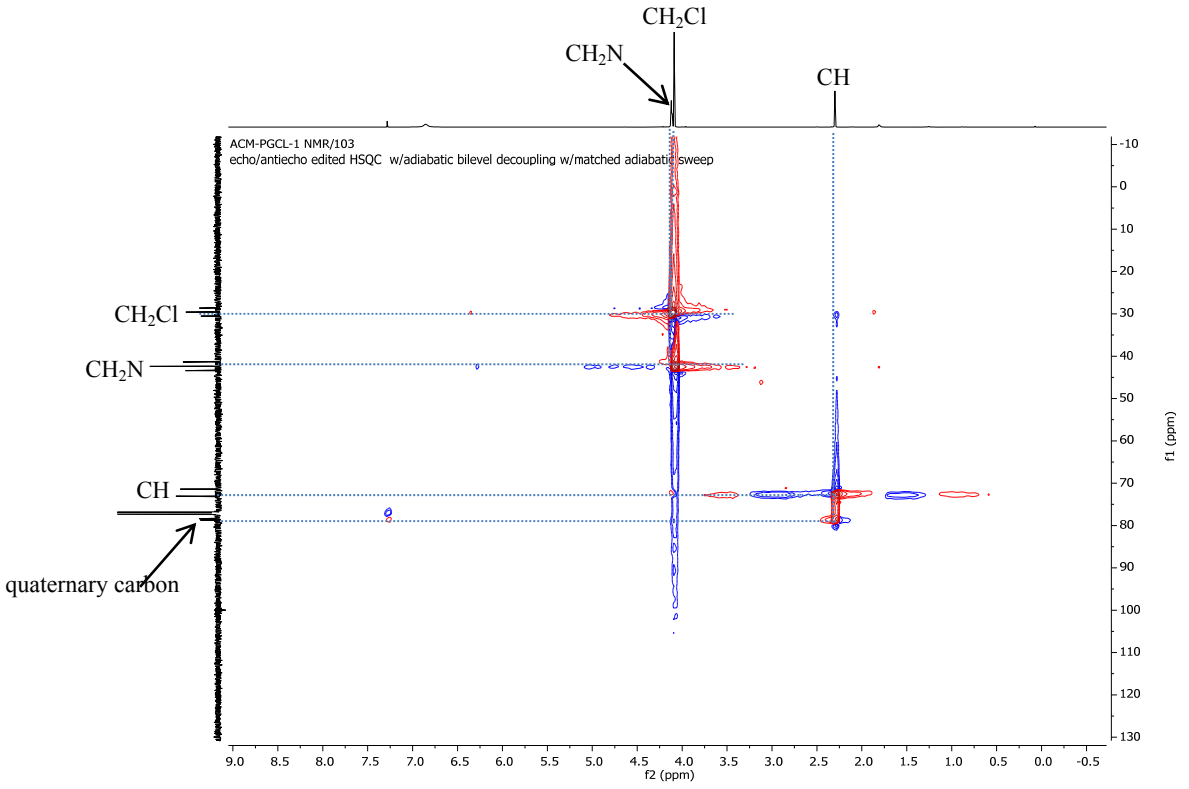

Figure 31d. HSQC NMR spectrum of compound **82a** in $CDCl_3$, using the proton-undecoupled ^{13}C spectrum.

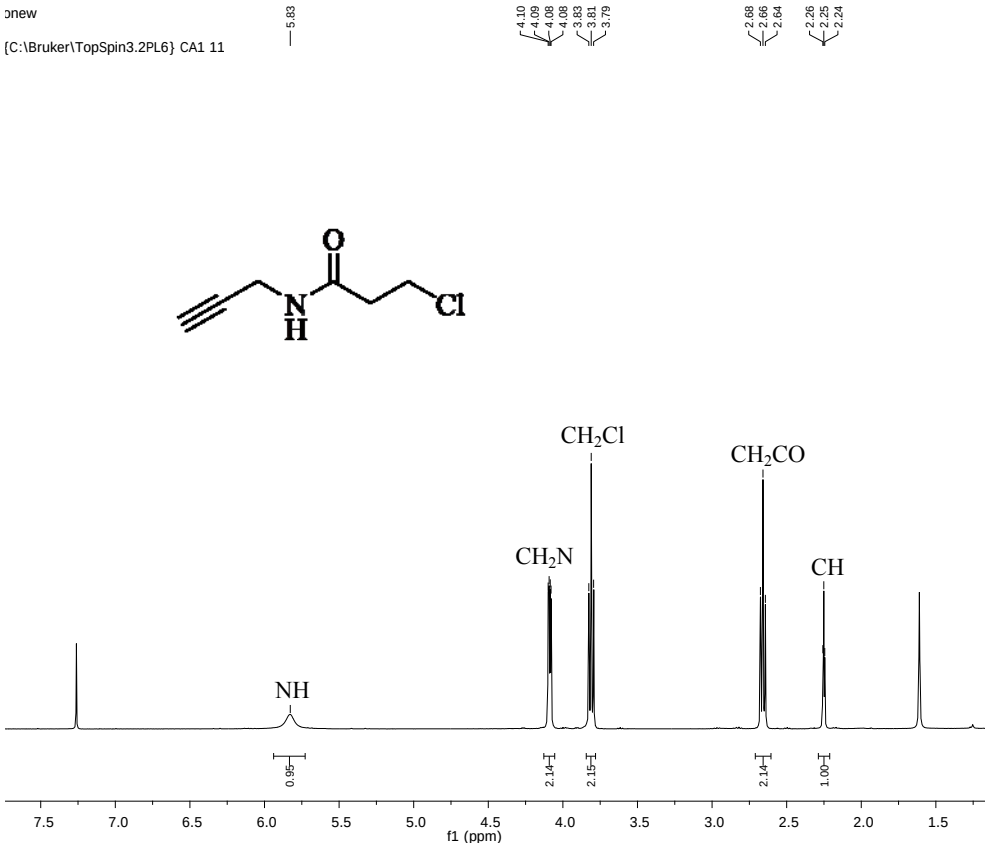

Figure 32. 400 MHz ^{1}H NMR spectrum of compound **82b** in $CDCl_3$.

2.2.1.2. Synthesis of the phosphonated propargylamine derivatives via *the* Arbuzov *reaction*.

Compound **82** was phosphonated using the *Arbuzov* reaction. The chloroacetamide **82a** and 3-chloropropanamide **82b** derivatives were reacted with triethyl phosphite under an inert atmosphere (Scheme 17).[78,79] The crude products were stirred with hexane to remove excess triethyl phosphite, and then purified using flash chromatography to afford the new compounds **83a** and **83b** in up to 68% and 65% yield respectively.

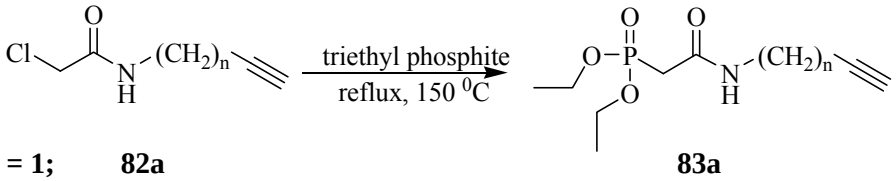

n = 1; 82a **83a**
n = 2; 82b **83b**

Scheme 17. Synthesis of propargyl phophonate esters **83a** and **83b**.

The ^{1}H NMR spectrum of compound **83a** (Figure 33a) shows the characteristic splitting of the methylene protons directly attached to phosphorus – an observation which clearly confirms the formation of the phosphonate product. The ethoxymethylene protons resonating

at 4.12 ppm also reflect coupling to ^{31}P as well as to the adjacent methyl protons. The ^{13}C NMR spectrum of compound **83a** (Figure 33b) reveals the splitting of the methylene carbon signal at 35.0 ppm with large coupling constant ($J_{P,C}$ = 130.9 Hz). The COSY NMR spectrum (Figure 33c) shows the correlation of the proton signals. In the ^{1}H NMR spectrum of compound **83b**, shown in Figure 34a for comparative purposes, reveals the signals for the methylene protons directly attached to phosphorus as a multiplet at 2.07 ppm, reflecting the coupling which is also clearly evident in the DEPT 135 NMR spectrum (Figure 34b).

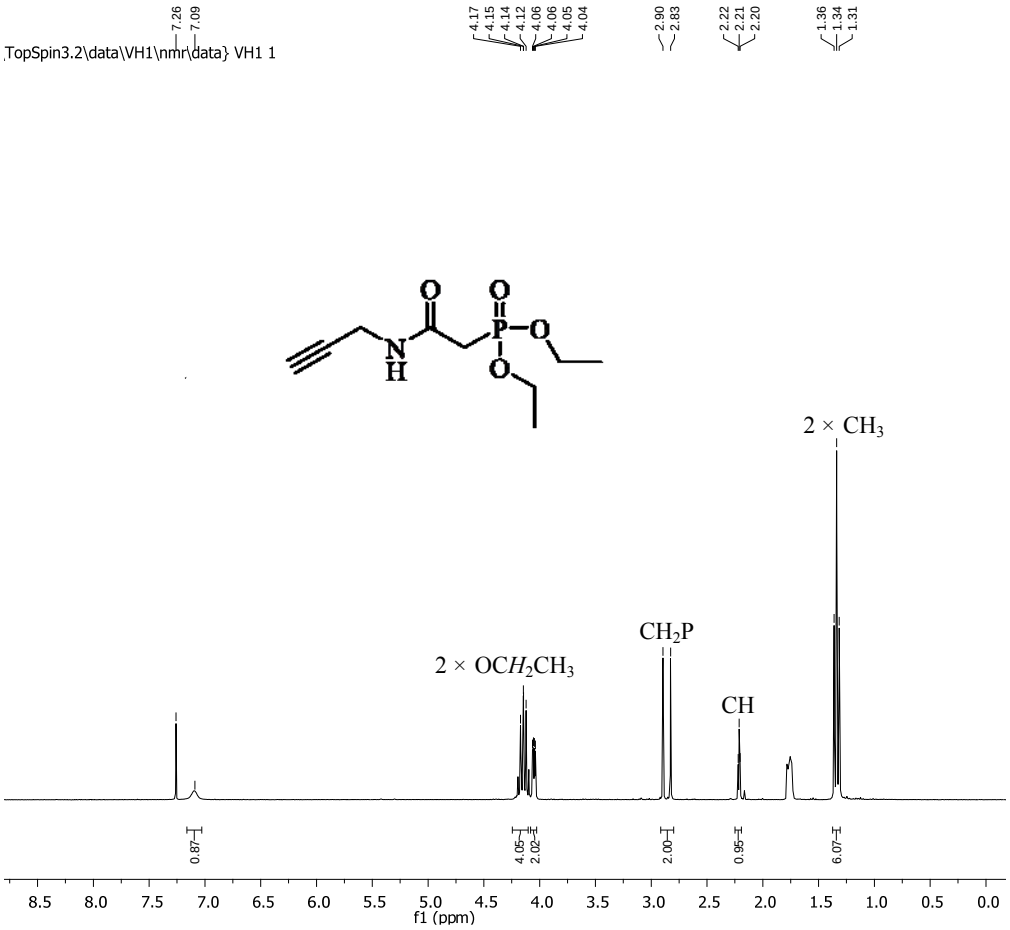

Figure 33a. 400 MHz ^{1}H NMR spectrum of compound **83a** in $CDCl_3$.

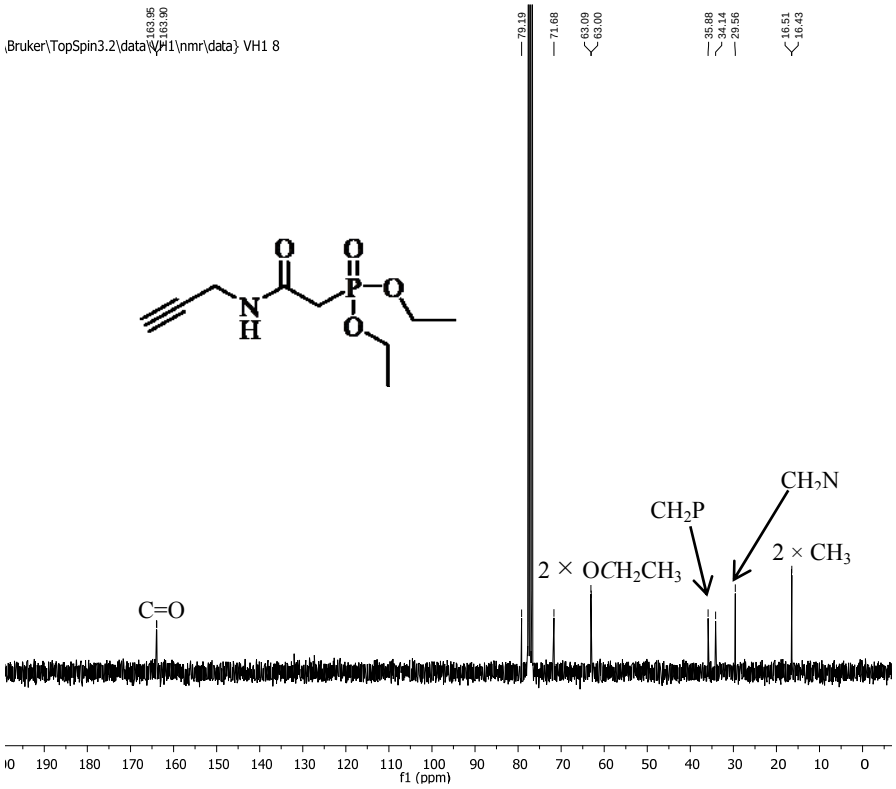

Figure 33b. 100 MHz ^{13}C NMR spectrum of compound **83a** in $CDCl_3$.

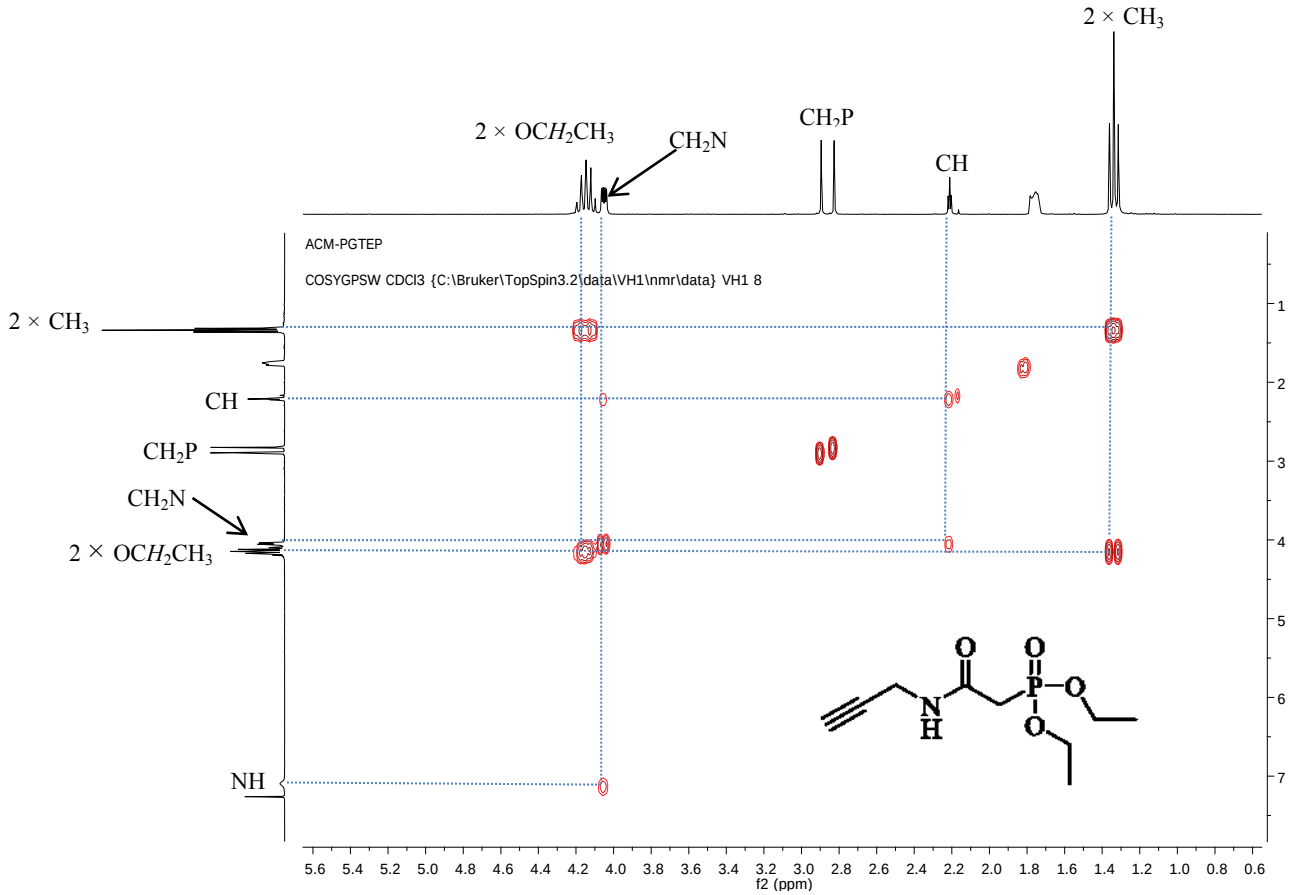

Figure 33c. COSY NMR spectrum of compound **83a** in $CDCl_3$.

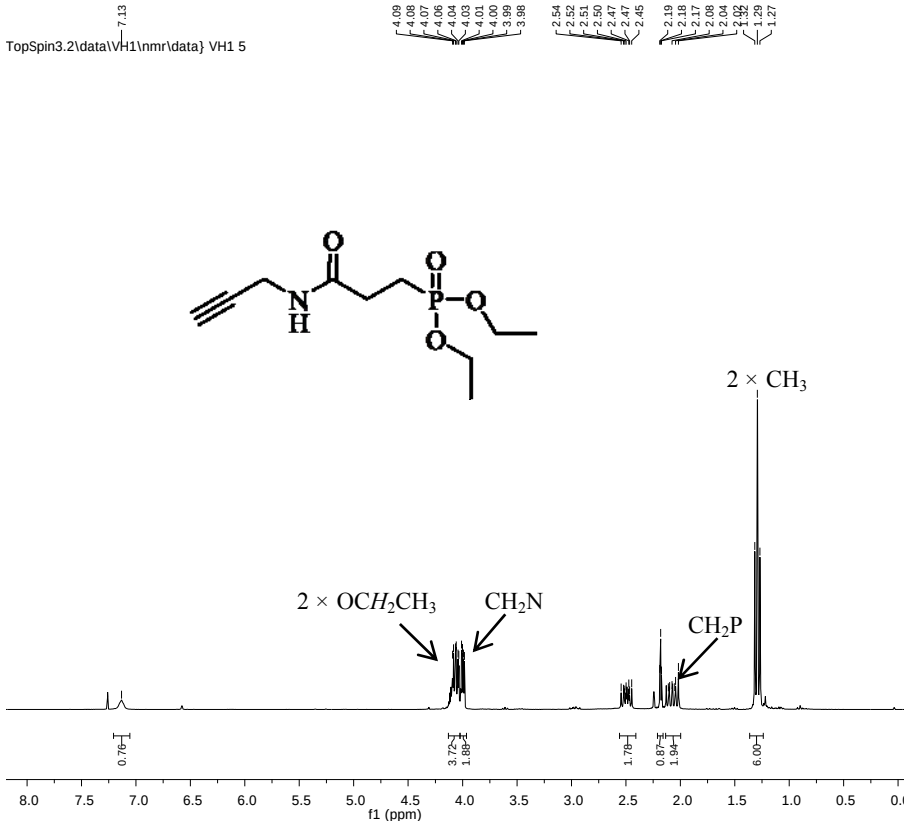

Figure 34a. 400 MHz ^{1}H NMR spectrum of compound **83b** in $CDCl_3$.

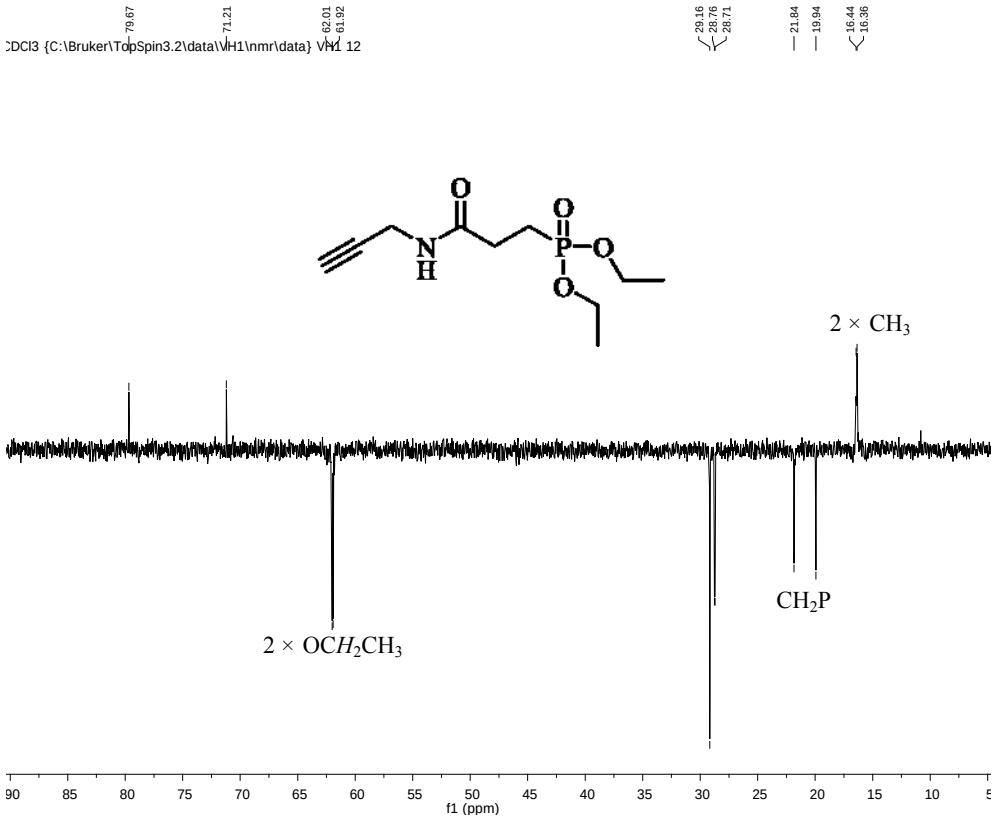

Figure 34b. DEPT 135 NMR spectrum of compound **83b** in $CDCl_3$.

2.2.2. Phosphorylation of azidothymidine (AZT)

Monophosphorylation of AZT **80** has been reported to facilitate the enzymatic phosphorylation to the triphosphate – the form in which it binds to the HIV-1 RT active-site.[89] In this study, monophosphorylation of AZT **80** was effected using both diethyl chlorophosphate and diphenyl chlorophosphate.[91] For this purpose, AZT **80** was dissolved in dry THF and butyllithium was added to the solution at 0 ^{o}C under argon, before adding diethyl chlorophosphate or diphenyl chlorophosphate. Flash chromatography afforded the phosphorylated AZT derivatives **84** and **85** in 73% and 74% yield respectively (Scheme 18).

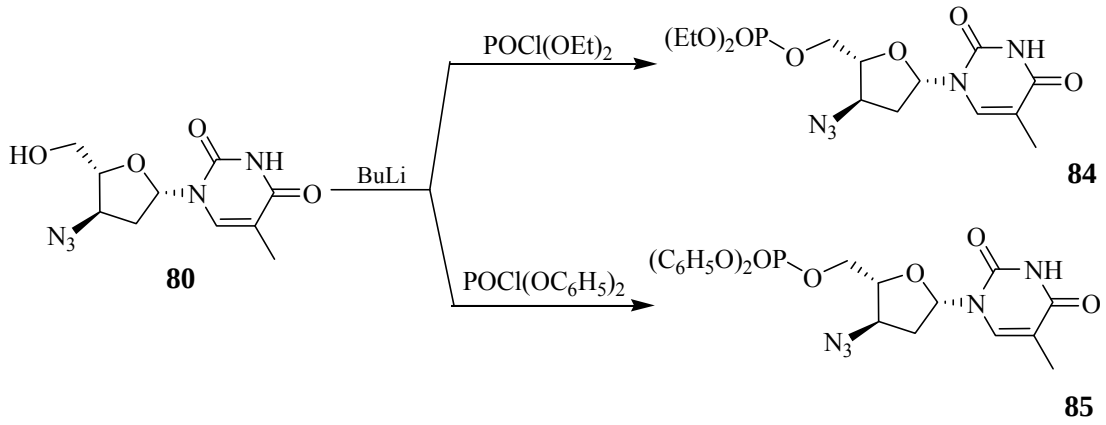

Scheme 18. Monophosphorylation of AZT **80**.[91]

^{1}H NMR analysis of compound **84** (Figure 35a) revealed the methyl protons resonating as a doublet of doublets at 1.35 ppm and the ethoxymethylene protons as a multiplet at 4.16 ppm. The ^{13}C NMR spectrum of compound **84** (Figure 35b) reveals the signals at 16.2 and 64.5 ppm of the diethyl phosphate moiety. The diphenyl ester analogue **85** is a novel compound and its ^{1}H NMR spectrum (Figure 36a) shows the presence of the additional aromatic signals. The ^{13}C NMR spectrum (Figure 36b), clearly reveals the additional aromatic carbon signals and the DEPT 135 NMR spectrum reveals the two expected methylene carbon signals at 12.3 and 67.5 ppm and the aromatic methine signals between 119.9 and 135.0 ppm (Figure 36c). HRMS analysis confirms the expected molecular formula (Figure 36d).

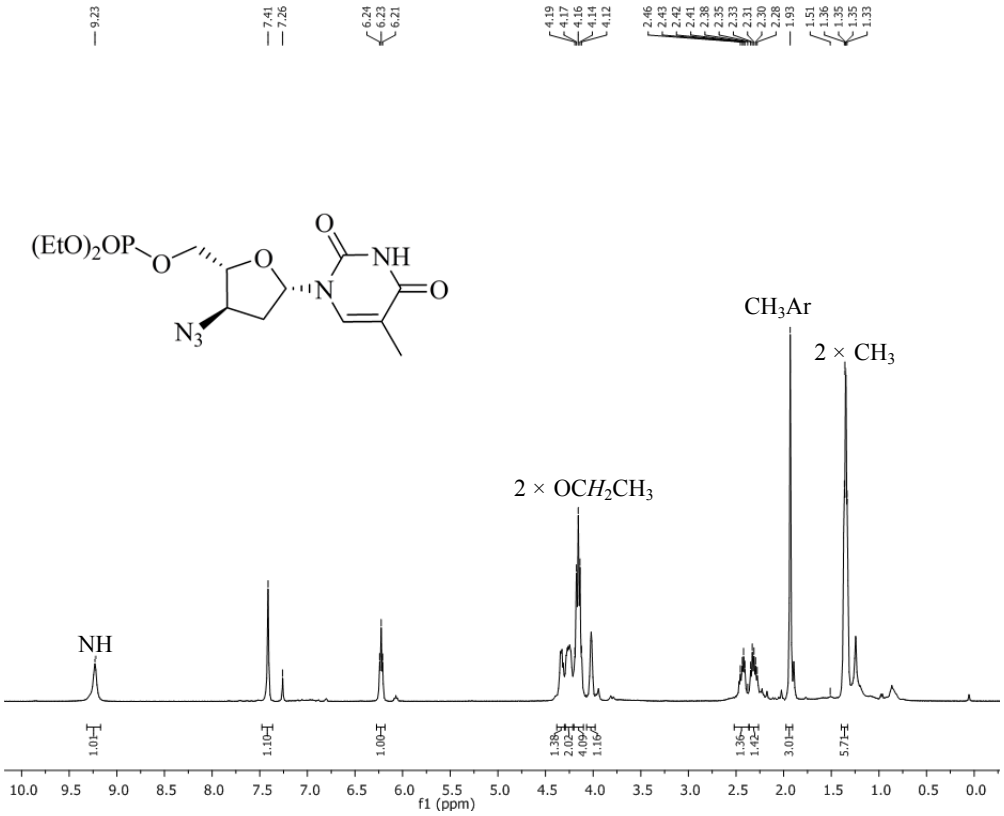

Figure 35a. 400 MHz ^{1}H NMR spectrum of compound **84** in $CDCl_3$.

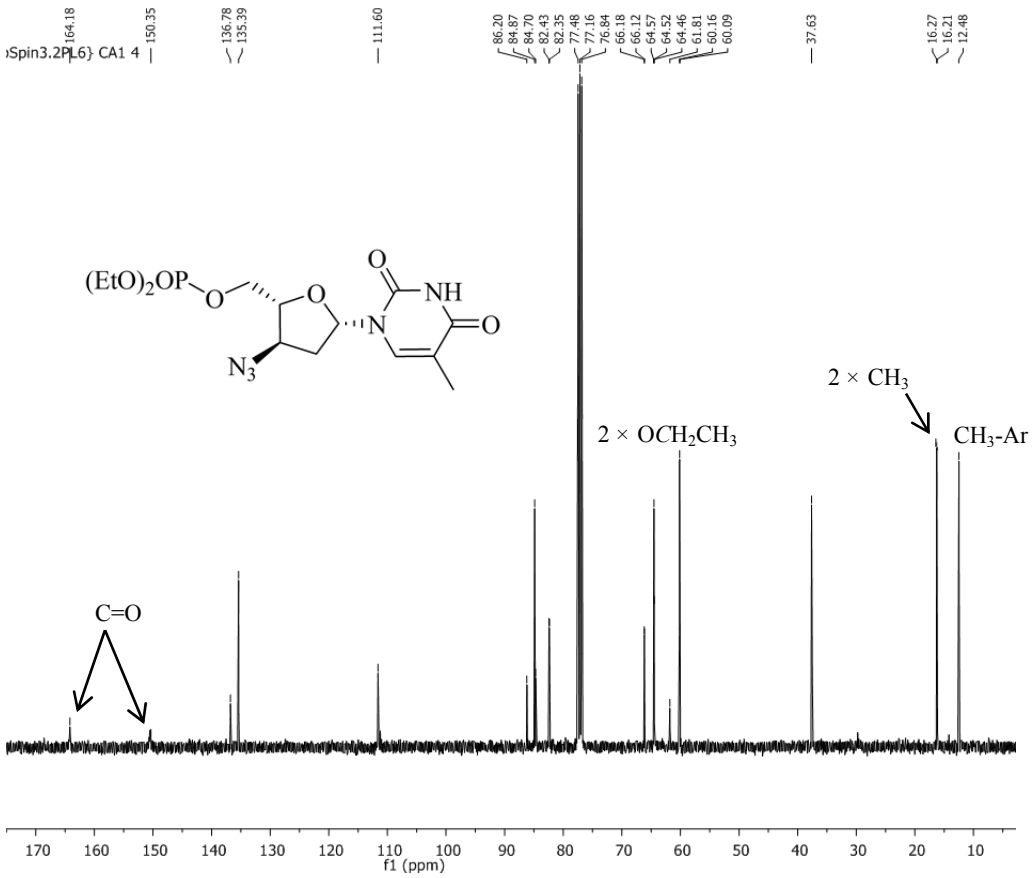

Figure 35b. 100 MHz ^{13}C NMR spectrum of compound **84** in $CDCl_3$.

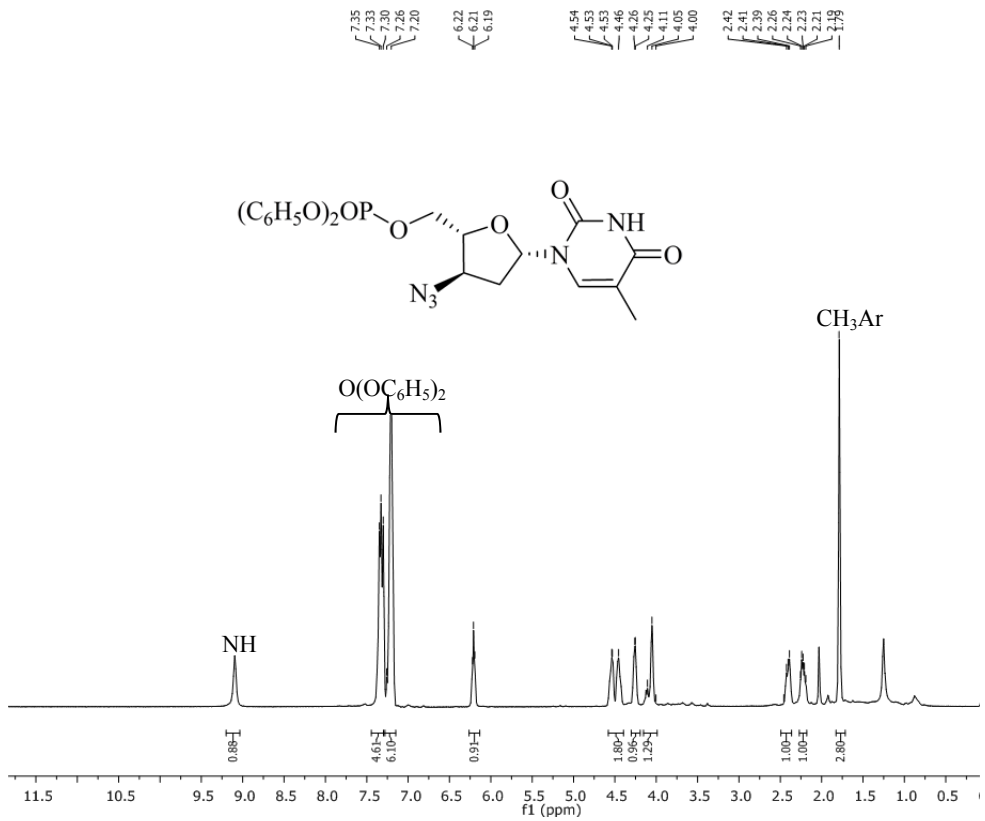

Figure 36a. 400 MHz ^{1}H NMR spectrum of compound **85** in $CDCl_3$.

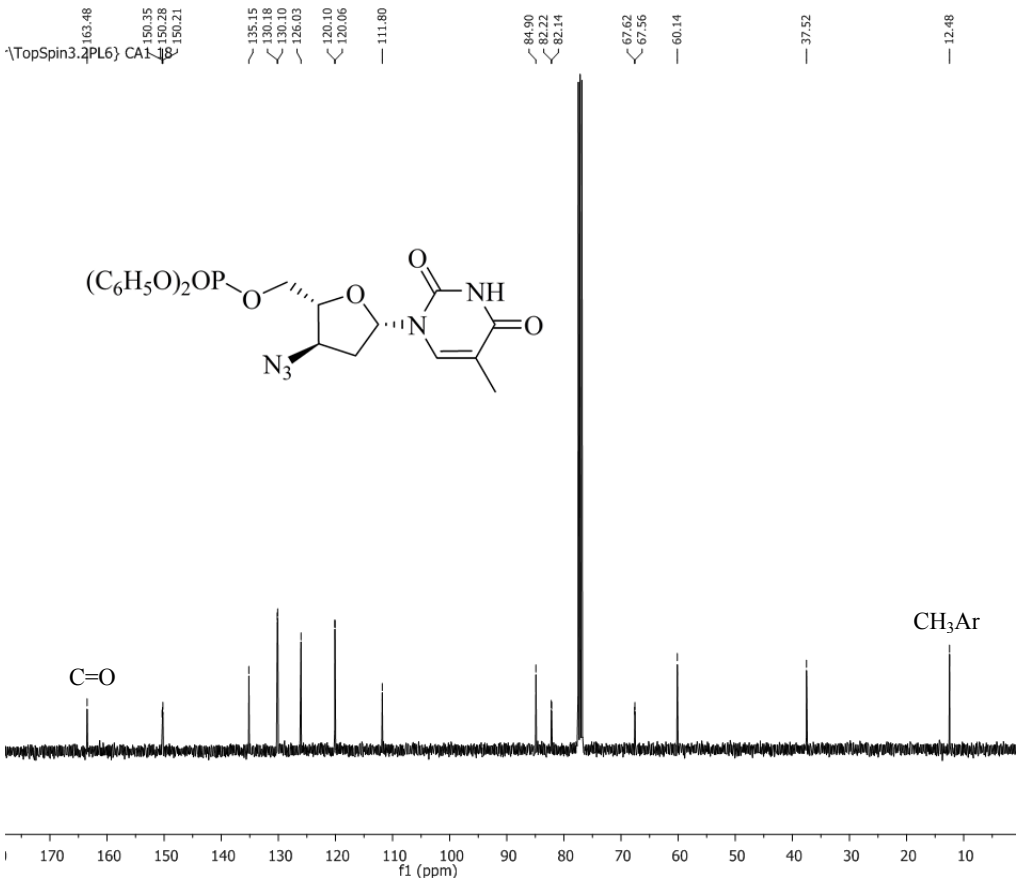

Figure 36b. 100 MHz ^{13}C NMR spectrum of compound **85** in $CDCl_3$.

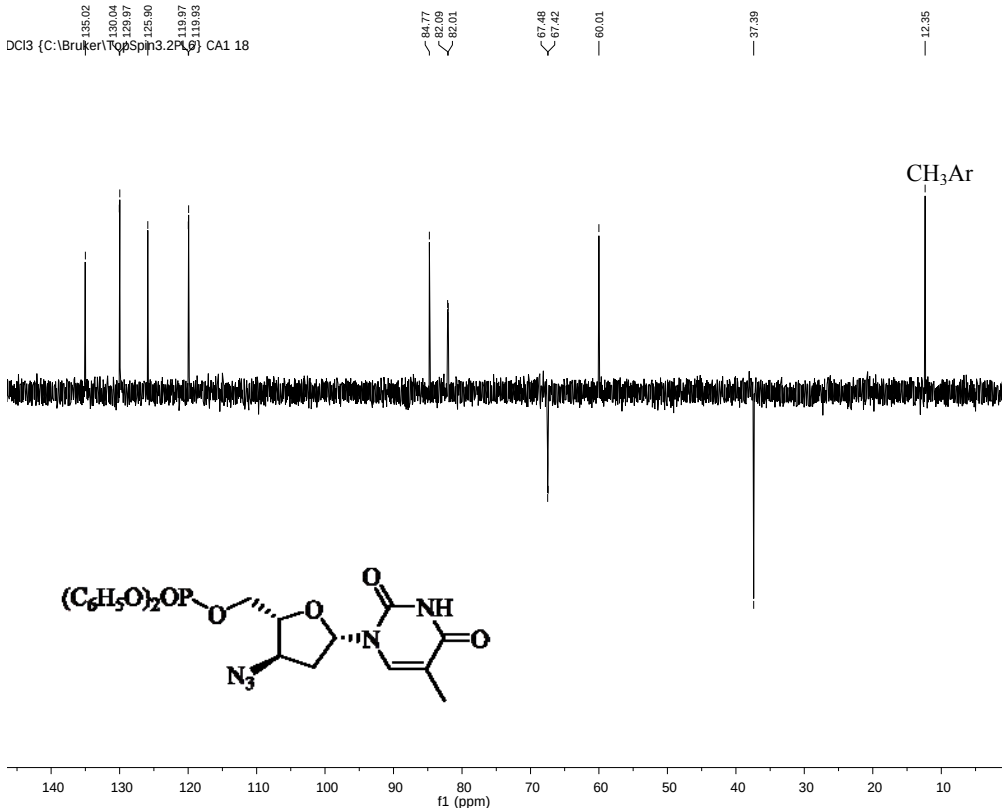

Figure 36c. DEPT 135 NMR spectrum of compound **85** in $CDCl_3$.

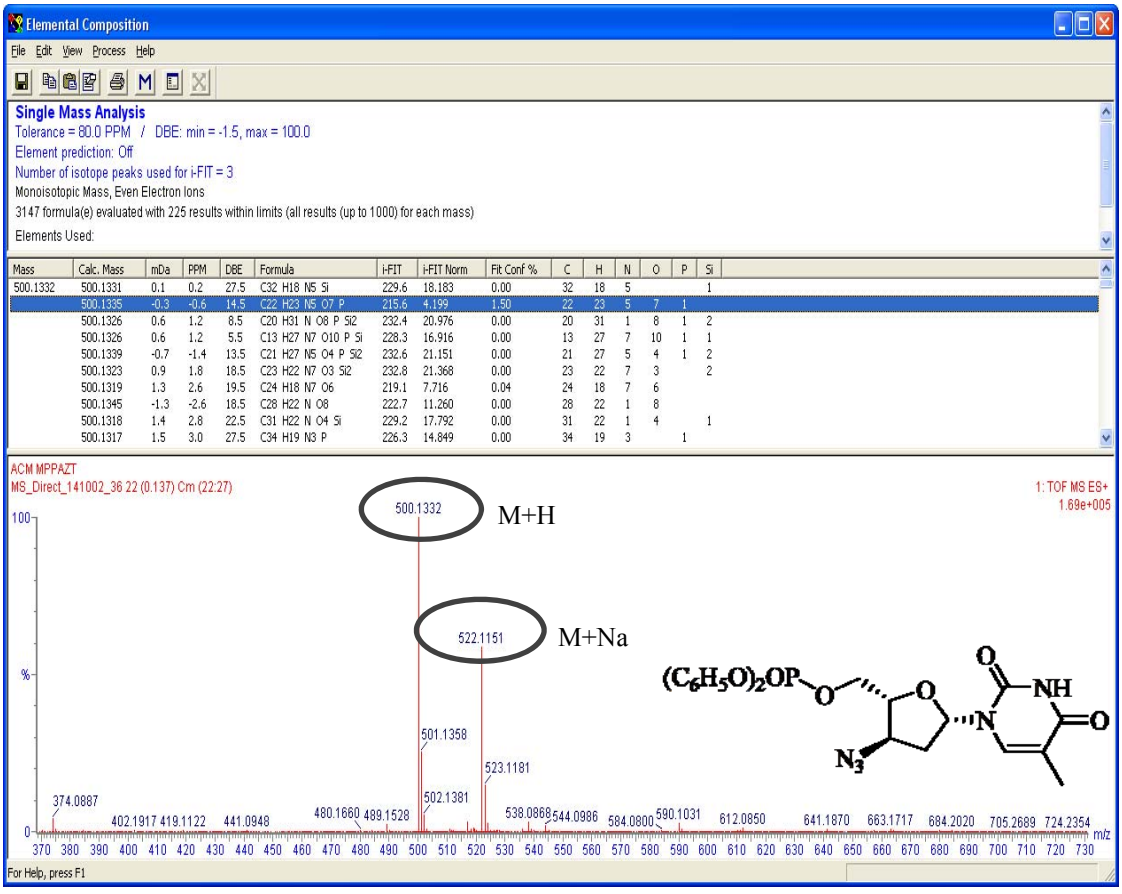

Figure 36d. HRMS spectrum of compound **85**.

2.2.3. Attempted Click reactions.

"Click Chemistry" was introduced by K.B. Sharpless in 2001,[92] as a term used to describe the joining of small molecules in a fast, stereospecific and high yielding reaction, with wide application scope. An example of a click reaction is the Huisgen 1,3-dipolar cycloaddition reaction,[94] which occurs between a terminal alkyne **89** and an azide **90**, under thermal conditions, to yield 1,4- and 1,5-disubstituted triazoles in equimolar quantities (Scheme 19).[95] When Cu(I) was used as a catalyst, the 1,4-susbtituted triazole **91** was afforded in high yield; alternatively the unstable copper (I) salts can be replaced by stable copper (II) salts, for example $CuSO_4.5H_2O$ which can be reduced to Cu(I) *in situ* using sodium ascorbate.[92-93] A ruthenium catalyst, on the other hand, gives the 1,5-disubstituted triazole **92**, raising the possibility of changing the regioselectivity of the reaction.[96]

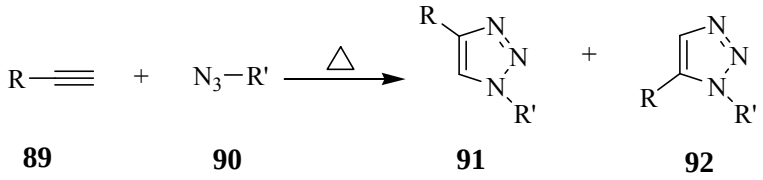

89 **90** **91** **92**

Scheme 19. Thermal Huisgen 1,3-dipolar cycloaddition reaction.[95]

Olomola and Kaye[91] have reported the coupling of the cinnamate ester **93** with phosphorylated AZT **84** in aqueous THF with a Cu(I) catalyst (Scheme 20) to give the potential dual-action HIV-1 IN / RT inhibitor **94**.

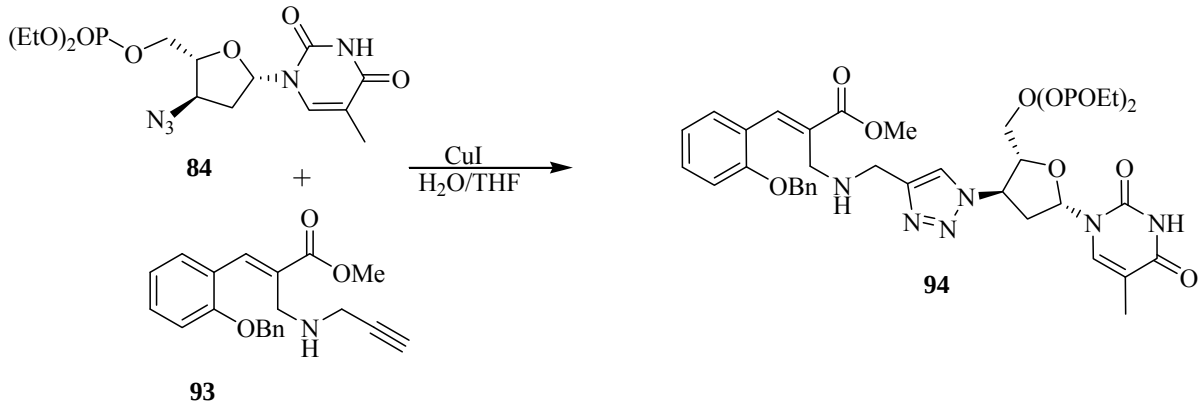

Scheme 20. Click reaction of phosphorylated AZT and cinnamate ester.[91]

In the present study, the use of the click reaction was expected to afford the propargyl ester-AZT conjugate **87** which might serve as a dual-action ligand with the ability to bind at both the HIV-1 RT and *Pf*DXR active-sites. In exploratory studies, the propargylated phosphonate ester **83** was reacted with monophosphorylated AZT **84** in THF / H_2O (1:1) using

$CuSO_4.5H_2O$ and sodium ascorbate in one reaction and CuI in another (Scheme 21). In both cases, the starting materials were isolated; further attempts were also unsuccessful, and unfortunately, time constraints precluded access to these target molecules at this stage. We have, however, successfully achieved the synthesis of the required starting materials, and on-going research will focus on establishing suitable reaction conditions to link them and thus access the desired dual-action ligands.

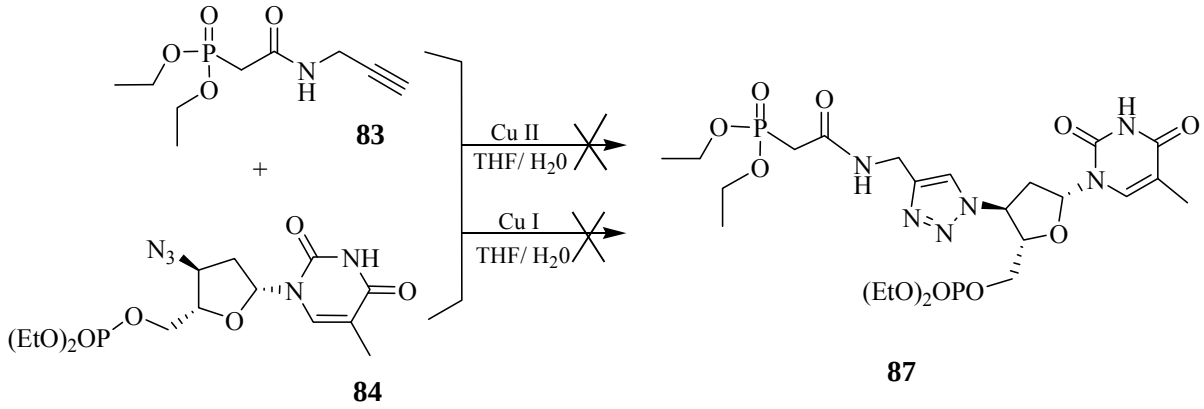

Scheme 21. Attempted synthesis of conjugated propargyl derivative.

2.3. ENZYME INHIBITION ASSAYS

Bioassay, as it is commonly called, is conducted to measure the effect of compounds on living organisms. This is essential for the development of new drugs. The phosphonate esters prepared in this study were thus subjected to malaria parasite inhibition and cytotoxicity screening for the author at Rhodes University.[98]

Cytotoxicity (using Hela cells) and malaria parasite lactate dehydrogenase (PLDH) assays were first conducted using 20mM solutions of the synthesised compounds in triplicate[98,99] (Figure 37). The cytotoxicity of all the phopshonate esters appears to be minimal since, in most cases, 100% cell viability was observed. The *tert*-butyldimethylsilyl ether-protected phosphonate ester **71** and the non-benzylated furan derivative **67e** showed comparable (>50%) malarial and HeLa cell viability and toxicity values.

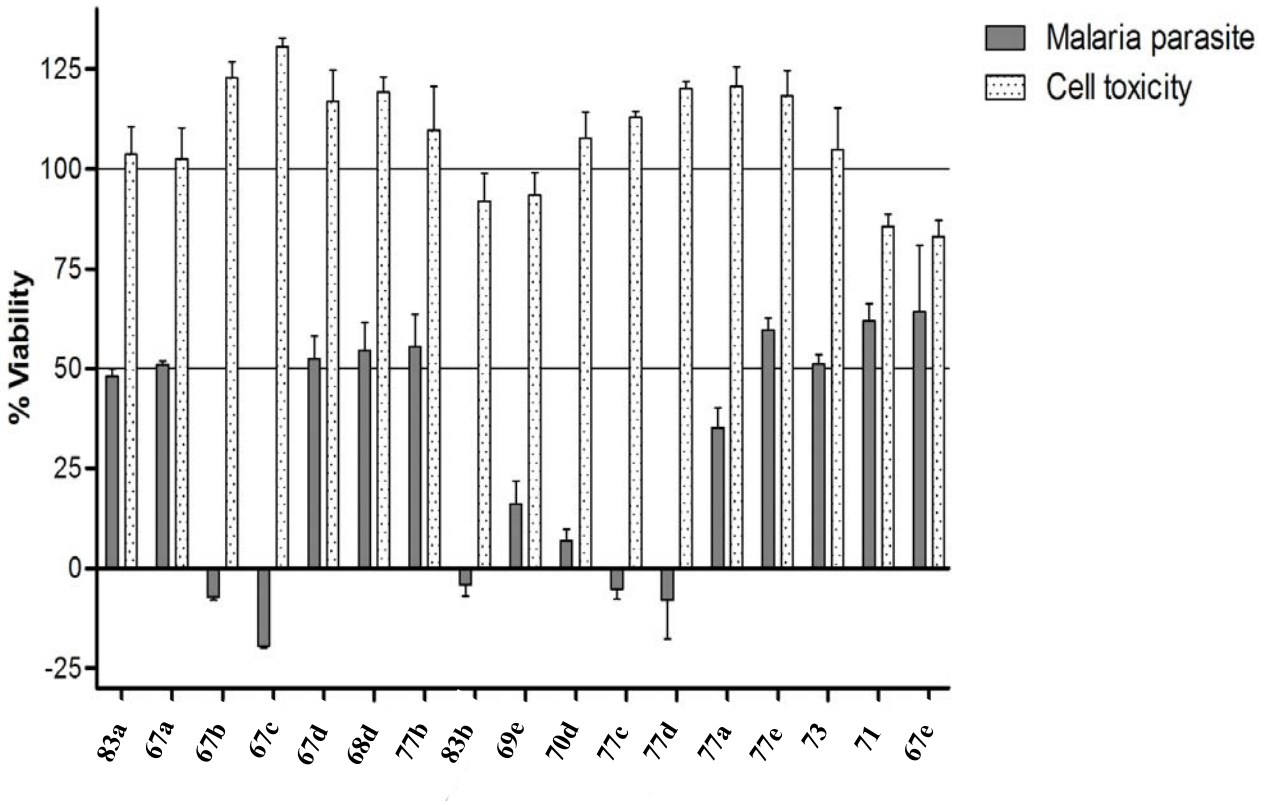

Figure 37. Cell toxicity screening and malaria assay of the synthesised phosphonate esters (20mM).

IC_{50} values were then determined for compounds **67b**, **67c**, **83b**, **69e**, **70d**, **77c** and **77d** (all of which inhibited the parasite completely at a ligand concentration of 20 mM) and for compounds **69e** and **70d** (both of which exhibited < 20% malaria parasite viability). The percentage parasite cell viability was plotted against the logarithm of the ligand concentration (Figure 38) and, with the use of the trend-line, IC_{50} values were determined. Surprisingly, the non-benzylated compound **67b**, which was not toxic in the HeLa cell assay, also has the lowest IC_{50} value at 10.1 μM. Under the same conditions, chloroquine exhibited an IC_{50} value of 0.06 μM. The remaining ligands also gave encouraging IC_{50} values in the low μM range (**67c**: 23.1; **83b**: 20.1; **69e**: 15.1; **70d**: 16.4; **77c**: 22.3; **77d**: 15.9).

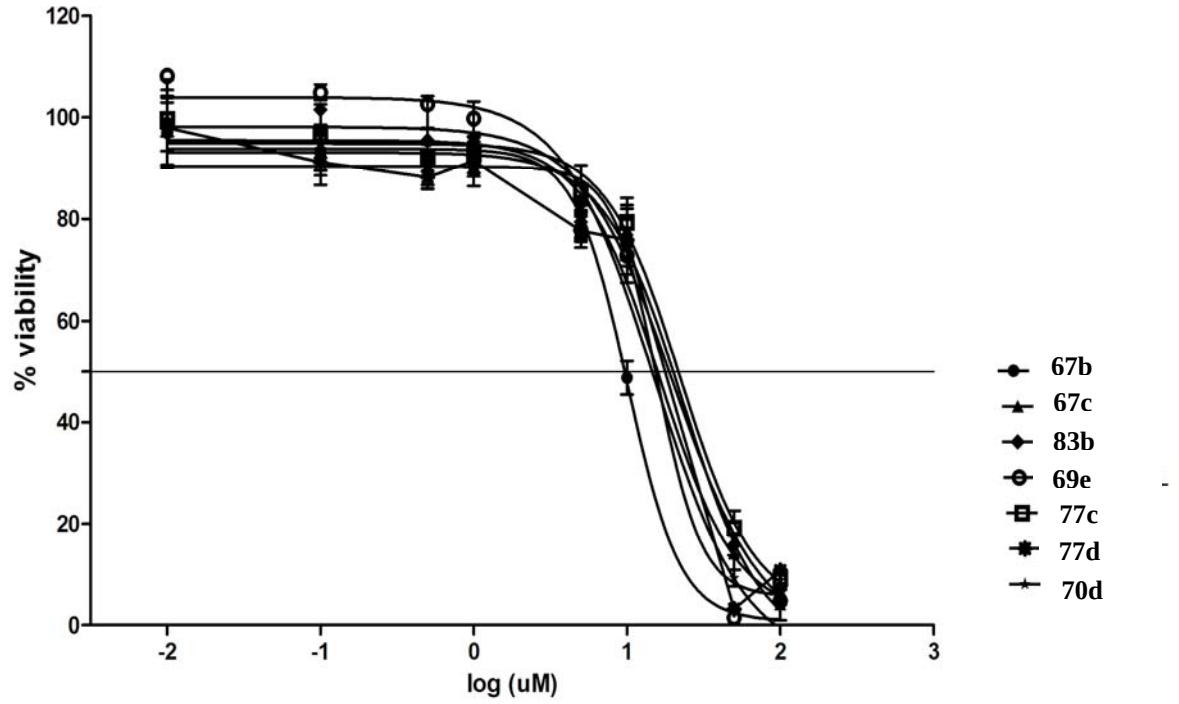

Figure 38. The inhibitory effect of selected compounds, showing percentage viability of *Pf*DXR at various concentrations.

These results reveal that the introduction of the benzyl group which was originally aimed at making the class of novel compounds better *Pf*DXR inhibitors generally appears to have increased inhibitory activity. For example, the benzylated furan derivative **69e**, shows better inhibitory activity when compared (Figure 37) with its non-benzylated analogue **67e**, while the *N*,*O*-dibenzylated product **70d** has better inhibitory activity than the non-benzylated analogue **68d**. Variation of the carbon chain length between the amide and phosphonate ester moieties can clearly be important with compounds containing an ethyl spacer (**77d** and **83b**) having much greater inhibitory effects than the corresponding compounds (**83a** and **67d**, respectively) which each have a methylene spacer.

2.4. PRELIMINARY COMPUTER MODELLING STUDIES.

Computer modelling can play a vital role in the rational design of drugs, by elucidating the interactions between the proposed ligands and the active-site. The different types of interactions that occur between the ligand and the active-site, can be explored and exploited to improve binding. The *Pf*DXR crystal structure[51] used in these modelling studies was accessed from the Research Collaboratory for Structural Bioinformatics (RCSB) protein data bank, using Discovery Studio Visualizer 4.0.[51] Modelling studies of selected ligands (Figure 39) were carried out by the author in order to establish an understanding of the molecular interactions between the phosphonated derivatives (benzylated and non-benzylated) and the *Pf*DXR receptor. In each case, the ligand was docked, using Autodock tools Version 4.2, into the DXR active-site after removing the bound fosmidomycin and water molecules present in the *Pf*DXR X-ray structure; non-polar hydrogens were added and merged.

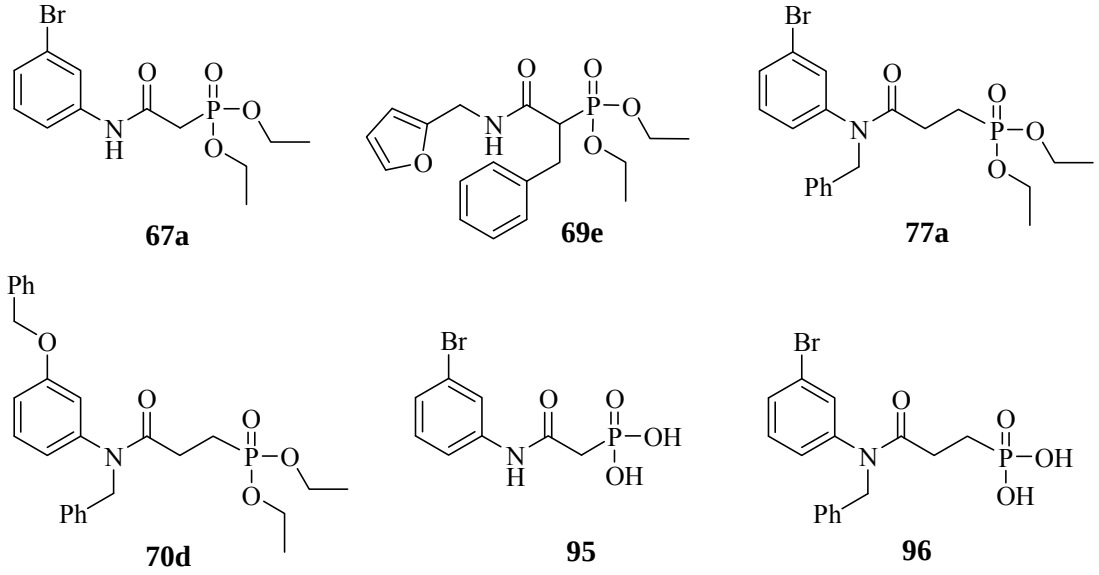

Figure 39. Representative compounds selected for docking in the *Pf*DXR active-site.

The structures of the ligands and the protein were prepared using Discovery Studio Visualizer,[51] and their docking into the *Pf*DXR receptor cavity was explored, using the Autodock 4.2 programme. For these preliminary studies, a rigid docking approach was used. Gasteiger partial charges were used and each atom was assigned appropriate AD4 types (AutoDock tools 4.2); a charge of zero was assigned to the magnesium ion of the protein as a default charge atom type in AD4 parameter file. The result obtained when a zero charge is assigned to Mg has been proven to be the same as when a +2 charge is assigned.[53] The AutoGrid 4.2 algorithm was used to map the interactions between the active-site and the selected ligands and a generic algorithm was applied for conformational search purposes.

The synthesised phosphonate esters may be expected to act as pro-drugs, with the ester groups being hydrolysed *in vivo* by cellular esterases.[62,97] In this study, the docked conformation of phosphonate ester **67a** was compared with that of the corresponding phosphonic acid **95**. In spite of the phophonate ester ethoxy groups, the docking simulation of compound **67a** (Figure 40) revealed that the ligand could be accommodated in the active-site and exhibited potential hydrogen-bonding interactions between the protein residues (Met-309, Met-360 and Gly-272). Additional hydrogen-bonding interactions are indicated between the phosphate group with Ser-232 and between the amide carbonyl oxygen atom and the indole ring Trp-296 in common with the phosphonic acid analogue **95** (see Figures 40 and 41). The latter, phosphonic acid ligand also exhibits a hydrogen-bonding interactions with Glu-233 through one of the phosphonic acid protons. The similarities between the docking of the phosphonate ester **67a** and phosphonic acid **95** are illustrated in Figure 42.

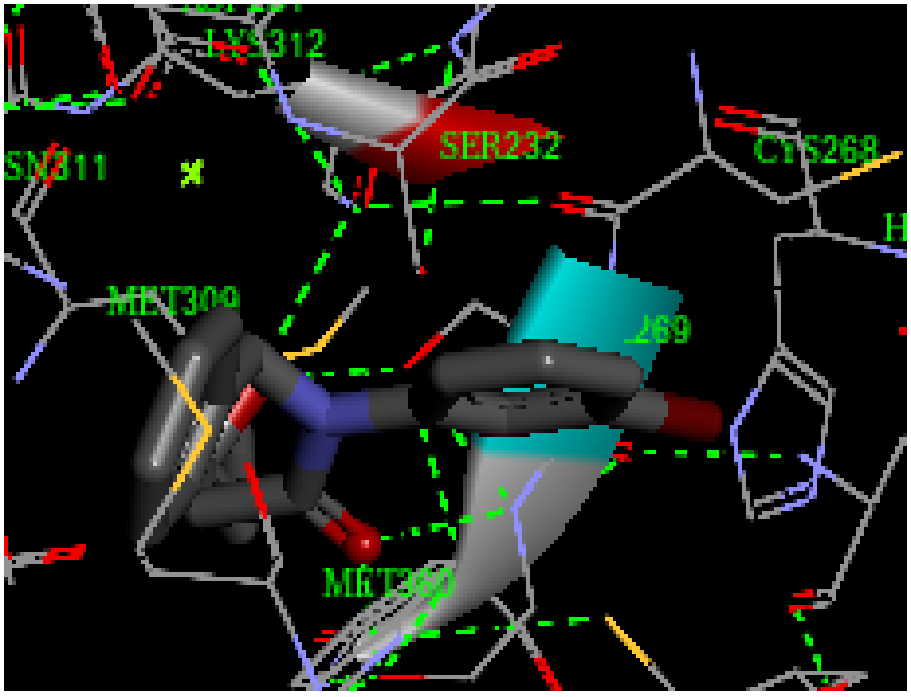

Figure 40. Docked conformation of phosphonate ester **67a** in the *Pf*DXR active-site (3AU9).[51] Protein active-site residues are shown in wire frame and the synthesised ligand in stick model, all coloured by atom type. Hydrogen–bonding interactions are shown as green dashed lines.

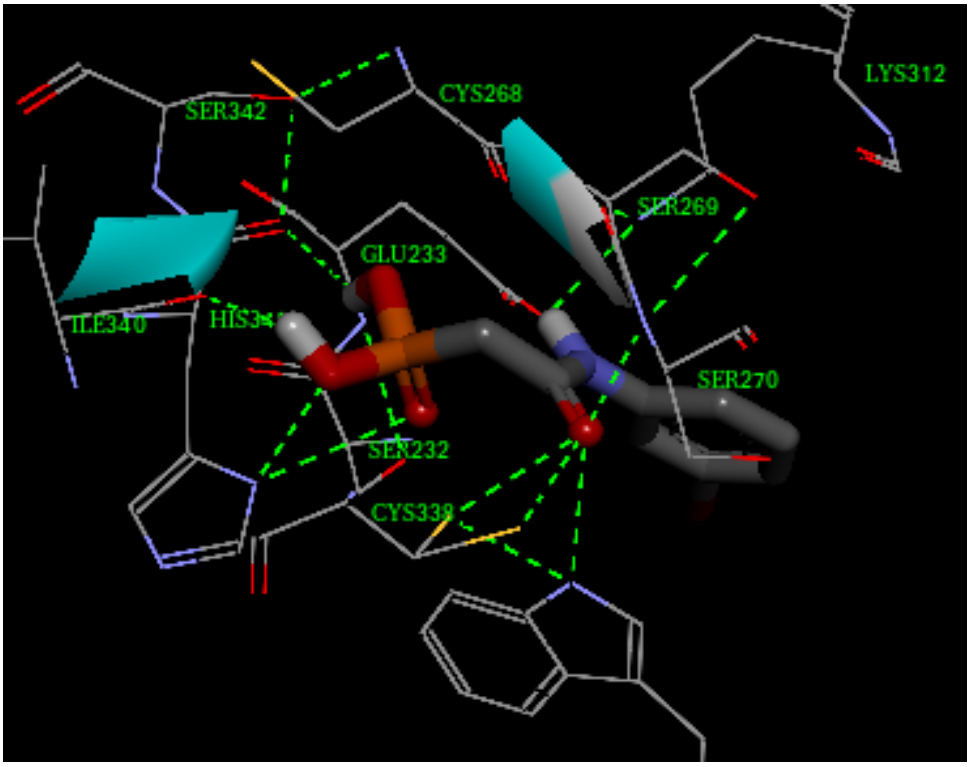

Figure 41. Docked conformation of phosphonic acid **95** in the *Pf*DXR active-site (3AU9).[51] Protein active-site residues are shown in wire frame and the synthesised ligand in stick model, all coloured by atom type. Hydrogen–bonding interactions are shown as green dashed lines.

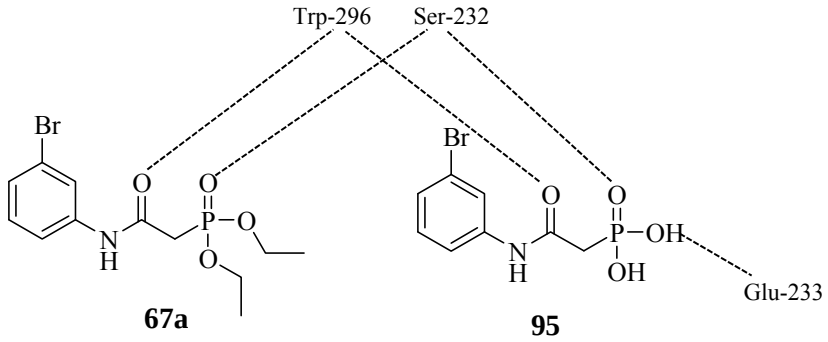

Figure 42. A simplified schematic diagram showing similar and different hydrogen-bonding interactions between the ligand **67a** and **93** in the *Pf*DXR active-site.

Docking of the *N*-benzylated phosphonate ester **77a** (Figure 43) reveals interactions with a number of protein residues (Lys-132, Asn-311, Glu-315, Met-360 and Met-309) and, in common with its phosphonic acid analogue **96** (Figure 44), interactions with Lys-312 and Asp-311. The phosphonic acid **96** also shows an interaction between the acid group and Glu-271 (see Figure 44). The similarities between the docking of the phosphonate ester **77a** and phosphonic acid **95** are illustrated in Figure 45.

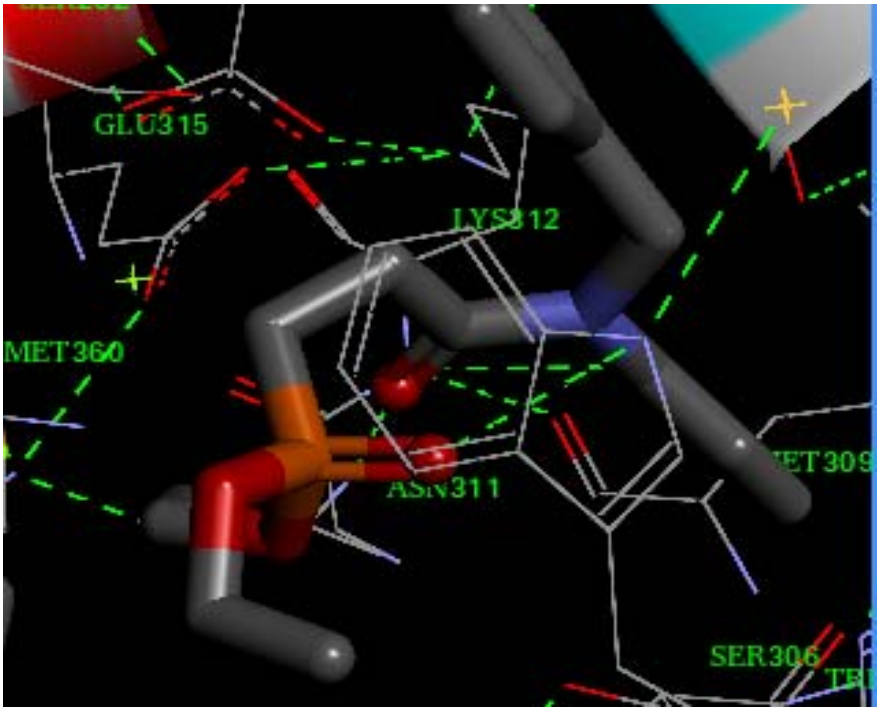

Figure 43. Docked conformation of phosphonate ester **77a** in the *Pf*DXR active-site (3AU9).[51] Protein active-site residues are shown in wire frame and the synthesised ligand in stick model, all coloured by atom type. Hydrogen–bonding interactions are shown as green dashed lines.

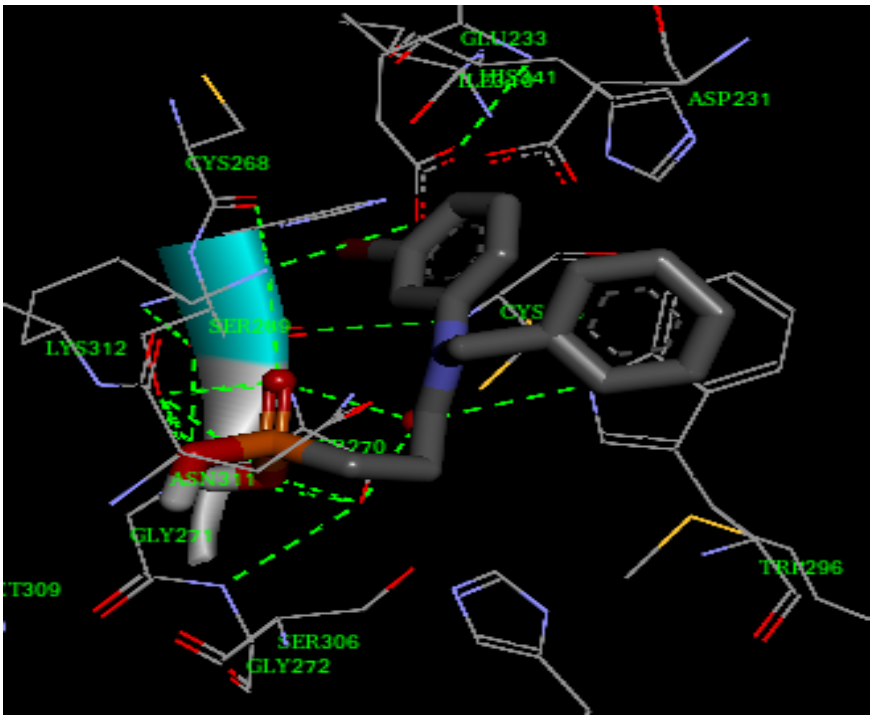

Figure 44. Docked conformation of phosphonic acid **96** in the *Pf*DXR active-site (3AU9).[51] Protein active-site residues are shown in wire frame and the synthesised ligand in stick model, all coloured by atom type. Hydrogen–bonding interactions are shown as green dashed lines.

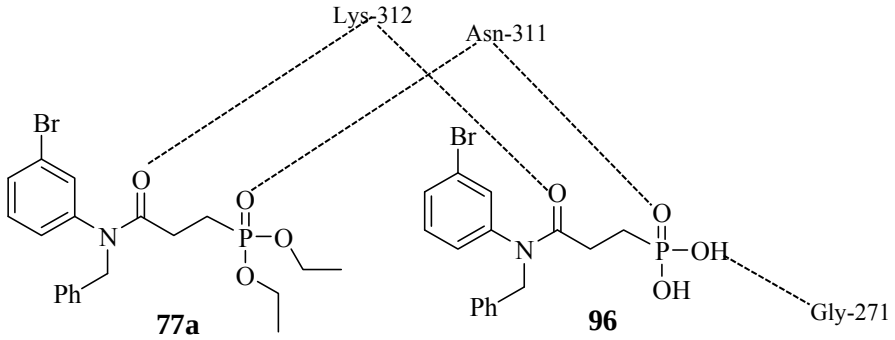

Figure 45. A simplified schematic diagram showing similar and different hydrogen-bonding interactions between the ligand **77a** and **96** in the *Pf*DXR active-site.

The furan derivative **69e** was also docked, as shown in Figure 45, revealing several hydrogen-bonding interactions with the proximal active-site protein residues Asn-311, Lys-312, Ser-306, Trp-296 and Met-360. Interestingly ligand **70d**, the *N*,*O*-dibenzylated phosphonate ester (Figure 46) reveals interaction of the hydrophobic patch (between the phosphonate and amide groups) with the protein residue Trp-296; interactions are also evident between Asn-311, Met-298, Ile-302 and the phosphonate ester moiety. The *O*-benzyl group also shows hydrogen bonding interactions with the proximate protein residues (Asp-359, Met-360 and Ser-232).

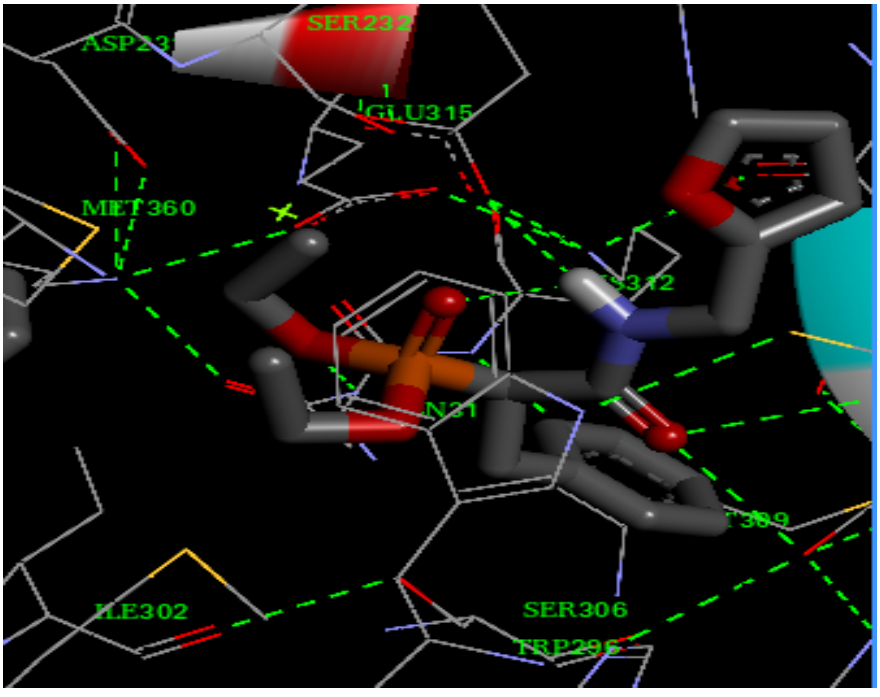

Figure 45. Docked conformation of phosphonate ester **69e** in the *Pf*DXR active-site (3AU9).[51] Protein active-site residues are shown in wire frame and the synthesised ligand in stick model, all coloured by atom type. Hydrogen–bonding interactions are shown as green dashed lines.

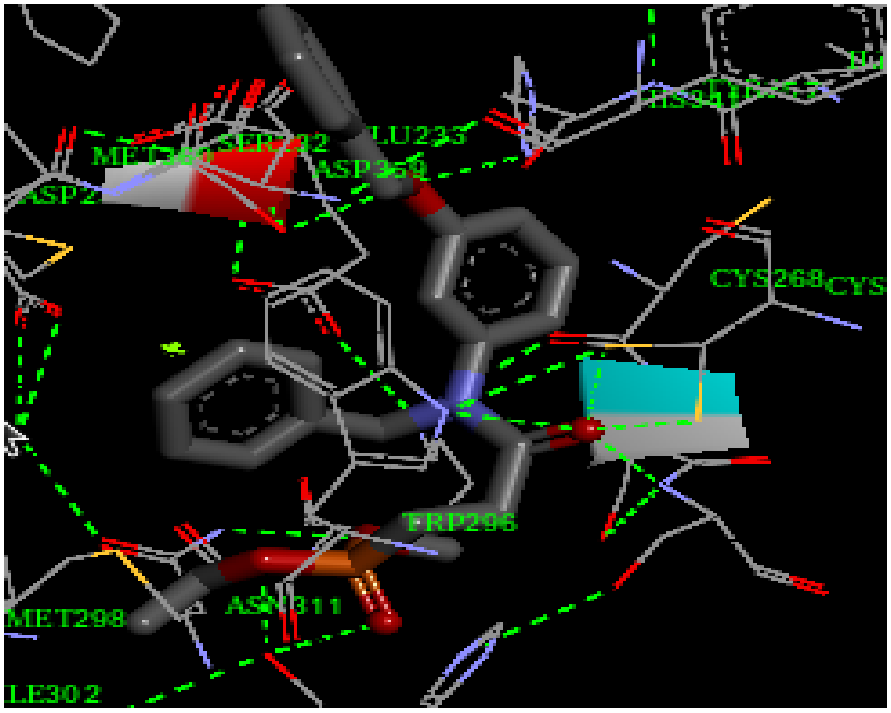

Figure 46. Docked conformation of phosphonate ester **70d** in the *Pf*DXR active-site (3AU9).[51] Protein active-site residues are shown in wire frame and the synthesised ligand in stick model, all coloured by atom type. Hydrogen–bonding interactions are shown as green dashed lines.

The results of the dockings were analysed using the clustering results and the best conformation obtained in each case appeared to correlate well with the active-site cavity of the *Pf*DXR crystal structure.

Table 2.5. The selected ligands, and the ligand interactions with the some of the amino-acid residues at the *Pf*DXR active-site.

Ligands	Amino-acid residues
67a	Ser-232, Met-360, Lys-312
73a	Lys-312, Asn-311, Met-360
69e	Ser-306, Asn-311, Lys-312
69f	Trp-296, Met-298, Met-360
93	Lys-312, Ser-232, Glu-233
94	Asn-311, Trp-296, Gly-271

2.5. CONCLUSIONS

In this study, novel compounds with the potential to bind to the *Pf*DXR active-site and serve as DXR inhibitors were targeted. A series of novel *N*-benzylated (*N*-phenylcarbomoyl)-alkylphosphonate esters were successfully synthesised, but attempts to synthesise *C*-benzylated (*N*-arylcarbamoyl)alkylphosphonate ester analogues, using a variety of synthetic approaches, proved unsuccessful. The novel *N*,*O*-dibenzylated phosphonate ester **70d**, was isolated as well as a series of unexpected tetrahydrofuran derivatives **72a-d**. *N*-Benzylated *N*-heteroarylcarbamoyl analogues were also prepared, while the *C*-benzylated *N*-heteroarylcarbamoyl analogue **69e** was obtained using the phosphonate ester **67e** as the starting material. While the final step in the preparation of bi-functional *Pf*DXR and HIV-1 reverse transcriptase inhibitors using click chemistry was unsuccessful, the starting materials, the propargylated phosphonate esters **83a** and **83b** and monophosphorylated AZT derivatives **84** and **85** were successfully prepared in good yields.

Evaluation of the binding potential of the synthesised compounds using *in silico* docking methods revealed potential hydrogen-bonding interactions with the *Pf*DXR active-site aminoacid residues, while bioassays showed that a number of the synthesised compounds have low toxicity, and very encouraging anti-parasitic activity. These results clearly vindicate the investigation of these compounds in the search for novel fosmidomycin analogues as potential antimalarials.

The aims and objectives of the present study have been largely achieved, and future work based on the research results is expected to include the following.

1. Further exploration of methods for assessing *C*-benzylated (*N*-arylcarbamoyl)-alkylphosphonate esters.
2. Exploitation of click chemistry in connecting both the propargyl phosphonate esters and the mono-phophorylated AZT to afford potential bi-functional *Pf*DXR and HIV-1 RT inhibitors.
3. Further structural elaboration of the phosphonate ester scaffolds to enhance binding to the DXR active-site.
4. QSAR methods to correlate structural changes and calculated molecular properties with the bioassay data obtained for the synthetic compounds.

3. EXPERIMENTAL

3.1. GENERAL

Reagents used were supplied by Sigma Aldrich or Fluka, and used without further purification. When considered necessary, solvents were purified by drying and re-distillation under Nitrogen, following the procedures described by Perrin and Armarego.[101] THF was distilled from Na wire in the presence of benzophenone as an indicator. Ethyl acetate and hexane were also distilled before use.

Thin layer chromatography was performed on Merck TLC silica gel F_{254} plates, and viewed under UV light (254 / 365 nm) or developed with iodine vapour. Flash chromatography was carried out using Merck silica gel 60 [230-400 mesh (particle size 0.040-0.063 mm)], and preparative layer chromatography (PLC) was carried out using Merck silica gel 60 F_{254} as the stationary phase.

Percentage yields of chromatographed products are based on the mass of crude material obtained prior to chromatographic separation. NMR spectra were recorded on Bruker 300 MHz, Bruker 400 MHz, or Bruker biospin 600 MHz spectrometers and were calibrated relative to the solvent signals ($CDCl_3$: δ_H = 7.26 ppm and δ_C = 77.00 ppm; for DMSO-d_6: δ_H = 2.50 ppm; δ_C = 39.40 ppm). IR spectra were recorded on a Perkin-Elmer Spectrum 100 FT-IR spectrometer, analysing the compounds neat on a diamond window. Melting points were determined using a hot stage apparatus and are uncorrected. High-resolution mass spectra (HRMS) were recorded on a Waters API Q-TOF Ultima spectrometer at the University of Stellenbosch, and elemental analysis was done on a Vario MICRO VI.6.2 elemental analyser system GmbH.

3.2. SYNTHESIS OF PHOSPHONATE ESTERS

3.2.1. Reaction of primary amines with acid chlorides.[74-77]

N-*(3-Bromophenyl)-2-chloroacetamide* 65a

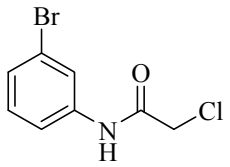

3-Bromoaniline **64a** (0.70 mL, 6.5 mmol) was dissolved in dry THF (15 mL) and NaH (60% dispersion in mineral oil; 0.31 g, 7.8 mmol) was added in small portions (controlling the evolution of H_2) and the mixture was stirred for 30 min. Chloroacetyl chloride (0.51 mL, 6.5 mmol) was then added slowly through a septum to the resulting mixture. After stirring at r.t. for *ca*. 6 h under N_2, the solvent was evaporated *in vacuo* and the residue dissolved in EtOAc (2 × 50 mL). The combined organic extracts were washed with saturated aqueous $NaHCO_3$ (2 × 100 mL), water (2 × 100 mL) and brine (2 × 100 mL). The aqueous washings were extracted with EtOAc and the combined organic solutions was dried with anhydrous $MgSO_4$, filtered and concentrated *in vacuo* to afford *N*-(3-bromophenyl)-2-chloroacetamide **65a** as a brown solid (1.09 g, 68%), m.p. 104-106 ^oC (Lit.[77] 100-102 °C); ν_{max}/cm^{-1} 1680 (C=O); δ_H/ppm (400 MHz; $CDCl_3$) 4.15 (2H, s, CH_2Cl), 7.15 (1H, t, *J* = 7.98 Hz, Ar-H), 7.25 (1H, d, *J* = 7.93 Hz, Ar-H), 7.43 (1H, d, *J* = 8.02 Hz, Ar-H), 7.75 (1H, s, Ar-H) and 8.25 (1H, br s, NH); δ_C/ppm (100 MHz; $CDCl_3$) 43.4 (CH_2Cl), 118.8, 122.3, 122.9, 127.9, 130.4 and 137.7 (Ar-C) and 162.8 (C=O).

***2-Chloro*-N-*[3-(hydroxymethyl)phenyl]acetamide* 65b**

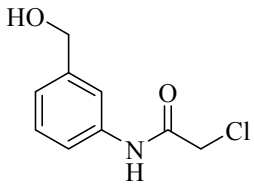

The general procedure for the synthesis of *N*-(3-bromophenyl)-2-chloroacetamide **65a** was employed, using 3-aminobenzyl alcohol **64b** (1.02 g, 8.28 mmol), NaH (0.52 g, 13 mmol) and chloroacetyl chloride (0.67 mL, 8.4 mmol) in dry THF (15 mL). Work-up, chromatography [on silica gel; elution with hexane-EtOAc (1:4)] and subsequent evaporation of the solvent *in vacuo* afforded 2-chloro-*N*-[3-(hydroxymethyl)phenyl]acetamide **65b** as a

yellow solid (1.65 g, 60%), m.p. 95-97 °C (Lit.[77] 91-93 °C); ν_{max}/cm^{-1} 3348 (OH) and 1682 (C=O); δ_H/ppm (400 MHz; $CDCl_3$) 4.31 (2H, s, CH_2Cl), 4.40 (1H, s, OH), 4.55 (2H, s, CH_2OH), 7.15 (1H, d, *J* = 7.63 Hz, Ar-H), 7.28 (1H, t, *J* = 7.60 Hz, Ar-H), 7.50 (1H, d, *J* = 8.02 Hz, Ar-H), 7.59 (1H, s, Ar-H) and 9.89 (1H, br s, NH); δ_C (100 MHz; $CDCl_3$) 43.7 (CH_2Cl), 62.0 (CH_2OH), 117.1, 117.6, 121.4, 128.6, 138.2 and 143.3 (Ar-C) and 163.8 (C=O).

***2-Chloro*-N-*(pyridin-2-yl)acetamide* 65c**

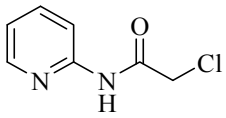

The general procedure for the synthesis of *N*-(3-bromophenyl)-2-chloroacetamide **65a** was employed, using 2-aminopyridine **64c** (1.32 g, 28 mmol), NaH (0.60 g, 15 mmol) and chloroacetyl chloride (1.10 mL, 28 mmol) in dry THF (15 mL). The crude product was isolated as a brown oil (1.49 g), purified by column chromatography [on silica gel; elution with hexane-EtOAc (1:1)] to afford 2-chloro-*N*-(pyridin-2-yl)acetamide **65c** as grey crystals (1.52 g, 65%), m.p. 85-87 °C (Lit.[74] 82-86 °C); ν_{max}/cm^{-1} 1685 (C=O); δ_H/ppm (400 MHz; $CDCl_3$) 4.20 (2H, s, CH_2Cl), 7.11 (1H, t, *J* = 8.56 Hz, Ar-H), 7.75 (1H, t, *J* = 8.73 Hz, Ar-H), 8.20 (1H, d, *J* = 8.30 Hz, Ar-H), 8.32 (1H, d, *J* = 4.80 Hz, Ar-H) and 8.88 (1H, br s, NH); δ_C/ppm (100 MHz; $CDCl_3$) 42.8 (CH_2Cl), 113.7, 120.6, 138.7, 147.8 and 150.2 (Ar-C) and 164.6 (C=O).

***2-Chloro*-N-*(3-hydroxyphenyl)acetamide* 65d**

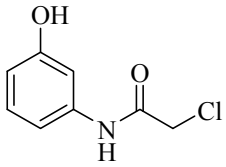

The general procedure for the synthesis of *N*-(3-bromophenyl)-2-chloroacetamide **65a** was employed, using 3-aminophenol **64d** (1.50 g, 27.0 mmol), NaH (0.60 g, 15 mmol) and chloroacetyl chloride (1.10 mL, 28.0 mmol) in dry THF (15 mL). 2-Chloro-*N*-(3-hydroxyphenyl)acetamide **65d** was isolated as a cream solid (3.13 g, 68 %), m.p. 136-138 °C (Lit.[77] 132-134 °C); ν_{max}/cm^{-1} 3367 (OH) and 1648 (C=O); δ_H/ppm (400 MHz; DMSO-d_6) 4.21 (2H, s, CH_2Cl), 6.48 (1H, d, *J* = 8.02 Hz, Ar-H), 6.95 (1H, d, *J* = 7.95 Hz, Ar-H), 7.10 (1H, t, *J* = 7.91 Hz, Ar-H), 7.17 (1H, s, Ar-H), 9.45 (1H, s, NH) and 10.15 (1H, s, OH);

δ_C/ppm (100 MHz; DMSO-d_6) 44.10 (CH_2Cl), 106.9, 110.5, 111.4, 129.9, 139.4 and 157.6 (Ar-C) and 165.0 (C=O).

***2-Chloro*-N-*furfurylacetamide* 65e**

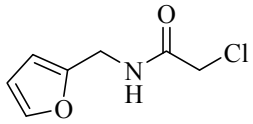

The general procedure for the synthesis of *N*-(3-bromophenyl)-2-chloroacetamide **65a** was employed, using furfurylamine **64e** (1.3 mL, 28 mmol), NaH (0.60 g, 15 mmol) and chloroacetyl chloride (1.10 mL, 28.0 mmol) in dry THF (15 mL). Column chromatography [on silica gel; elution with hexane-EtOAc (2:3)] afforded 2-chloro-*N*-furfurylacetamide **65e** as a pale yellow solid (1.54 g, 62%), m.p. 63-65 °C (Lit.[74] 58-60 °C); ν_{max}/cm^{-1} 1648 (C=O); δ_H/ppm (400 MHz; $CDCl_3$) 4.07 (2H, s, CH_2Cl), 4.49 (2H, d, *J* = 5.47 Hz, CH_2N), 6.26 (1H, d, *J* = 3.08 Hz, Ar-H), 6.33 (1H, d, *J* = 1.69 Hz, Ar-H), 6.88 (1H, br s, NH) and 7.37 (1H, s, Ar-H); δ_C/ppm (100 MHz; $CDCl_3$) 36.7 (CH_2N), 42.6 (CH_2Cl), 108.0, 110.7, 142.6 and 143.1 (Ar-C) and 150.5 (C=O).

***3-Chloro*-N-*(3-hydroxyphenyl)propanamide* 66d**

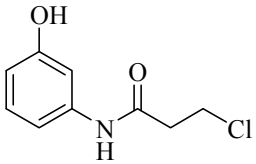

The general procedure for the synthesis of *N*-(3-bromophenyl)-2-chloroacetamide **65a** was employed, using 3-aminophenol **64d** (1.50 g, 14.0 mmol), NaH (0.60 g, 15 mmol), 3-chloropropionyl chloride (1.31 mL, 14.0 mmol) in dry THF (15 mL), to afford 3-chloro-*N*-(3-hydroxyphenyl)propanamide **66d** as an off-white solid (2.04 g, 74%), m.p. 123-125 ^oC (Lit.[77] 119-121 °C); γ_{max}/cm^{-1} 3350 (OH) and 1683 (C=O); δ_H/ppm (400 MHz; DMSO-d_6) 2.79 (2H, t, *J* = 6.23 Hz, 2-CH_2), 3.86 (2H, t, *J* = 6.6 Hz, CH_2Cl), 6.46 (1H, t, *J* = 8.09 Hz, Ar-H), 6.95 (1H, dd, *J* = 1.40 and 8.90 Hz, Ar-H), 7.06 (1H, t, *J* = 8.10 Hz, Ar-H), 7.18 (1H, s, Ar-H), 9.38 (1H, s, NH) and 9.91 (1H, s, OH); δ_C/ppm (100 MHz; DMSO-d_6) 39.7 (2-CH_2), 41.3 (CH_2Cl), 106.7, 110.3, 110.9, 129.8, 139.9 and 158.3 (Ar-C) and 164.3 (C=O).

***3-Chloro*-N-*furfurylpropanamide* 66e**

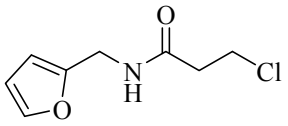

The general procedure for the synthesis of *N*-(3-bromophenyl)-2-chloroacetamide **65a** was employed, using furfurylamine **64e** (1.3 mL, 28mmol), NaH (0.60 g, 15 mmol) and 3-chloropropionyl chloride (1.35 mL, 28 mmol) in dry THF (15 mL). The crude product was isolated as a brown oil (1.37 g) and purified using column chromatography [on silica gel; elution with hexane-EtOAc (1:3)] to afford 3-chloro-*N*-furfurylpropanamide **66e** as a cream solid (1.58 g, 60%), m.p. 74-76 °C (Lit.[74] 70-72 °C); ν_{max}/cm^{-1} 1648 (C=O); δ_H/ppm (400 MHz; $CDCl_3$) 2.66 (2H, t, *J* = 6.8 Hz, 2-CH_2), 3.81 (2H, t, *J* = 6.8 Hz, CH_2Cl), 4.47 (2H, d, *J* = 5.2 Hz, CH_2N), 6.25 (1H, d, *J* = 3.4 Hz, Ar-H), 6.32 (1H, dd, *J* = 2.0 and 3.3 Hz, Ar-H), 6.67 (1H, br s, NH) and 7.35 (1H, d, *J* = 1.9 Hz, Ar-H); δ_C/ppm (100 MHz; $CDCl_3$) 36.6 (2-CH_2), 39.6 (CH_2N), 40.1 (CH_2Cl), 107.7, 110.7, 142.5 and 150.9 (Ar-C) and 169.9 (C=O).

***3-chloro*-N-*(3-cyanophenyl)propanamide* 66f**

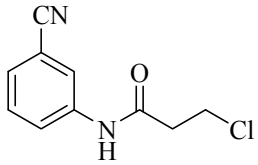

The general procedure for the synthesis of *N*-(3-bromophenyl)-2-chloroacetamide **65a** was employed, using 3-aminobenzonitrile **64f** (0.60 g, 10 mmol), NaH (0.27 g, 6.8 mmol) and chloropropionyl chloride (0.47 mL, 10 mmol) in dry THF (15 mL). The crude product was isolated as a brown oil (1.37 g) and purified using column chromatography [on silica gel; elution with hexane-EtOAc (1:1)] to afford 3-chloro-*N*-(3-cyanophenyl)-propanamide **66f** as a cream solid (0.71 g, 71%), m.p. 112-114 °C (Lit.[77] 108-110 °C); ν_{max}/cm^{-1} 2235 (C≡N) and 1659 (C=O); δ_H/ppm (300 MHz; $CDCl_3$) 2.87 (2H, t, *J* = 6.1 Hz, 2-CH_2), 3.87 (2H, t, *J* = 6.1 Hz, CH_2Cl), 7.43 (2H, m, Ar-H), 7.75 (1H, s, Ar-H), 7.96 (1H, t, *J* = 2.0 Hz, Ar-H) and 8.02 (1H, s, NH); δ_C/ppm (75 MHz; $CDCl_3$) 34.4 (2-CH_2), 44.3 (CH_2Cl), 119.0 (C≡N), 113.2, 122.8, 124.5, 129.9, 131.0 and 138.9 (Ar-C) and 168.9 (C=O).

3.2.2. Synthesis of phosphonate esters using *Michaelis-Arbuzov* methodology.

***Diethyl [N-(3-bromophenyl)carbamoyl]methylphosphonate* 67a**

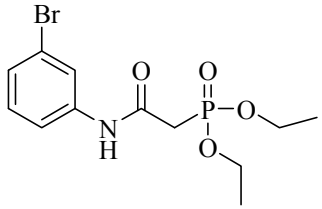

To 2-chloro-*N*-(3-bromophenyl)acetamide **65a** (0.67 g, 2.7 mmol) was added triethyl phosphite (0.92 mL, 5.4 mmol) and the mixture was boiled under reflux at 150 ^{o}C for *ca* 9 h. Upon completion of the reaction, as monitored by TLC, hexane (20 mL) was added (to remove excess triethyl phosphite) and the mixture stirred for *ca.* 20 min, followed by the decantation of the hexane layer; stirring and decanting was repeated 3 times, and the crude product was then purified by flash column chromatography [on silica gel; elution with EtOAc (1:1)] to afford diethyl [*N*-(3-bromophenyl)carbamoyl]methylphosphonate **67a** as a brown solid (0.23 g, 60%), m.p. 77-79 °C (Lit.[77] 73-75 °C); ν_{max}/cm^{-1} 1648 (C=O) and 1240 (P=O); δ_H/ppm (300 MHz; $CDCl_3$) 1.36 (6H, t, J = 6.83 Hz, 2 × CH_3), 3.05 (2H, d, $J_{P\text{-}H}$ = 21.2 Hz, CH_2P), 4.11 (4H, m, 2 × O*C*H_2CH_3), 7.05 (1H, t, J = 8.02 Hz, Ar-H), 7.10 (1H, t, J = 8.04 Hz, Ar-H), 7.29 (1H, d, J = 8.02 Hz, Ar-H) 7.67 (1H, s, Ar-H) and 7.98 (1H, s, NH); δ_C/ppm (75 MHz; $CDCl_3$) 16.5 (d, J = 6.0 Hz, 2 × CH_3), 35.9 (d, $J_{P\text{-}C}$ = 129.5 Hz, CH_2P), 63.5 (d, J = 6.66 Hz, 2 × O*C*H_2CH_3), 112.6, 117.6, 112.5, 126.5, 129.8 and 139.2 (Ar-C) and 162.5 (C=O).

***Diethyl [N-(3-hydroxymethyl)phenylcarbamoyl]methylphosphonate* 67b**

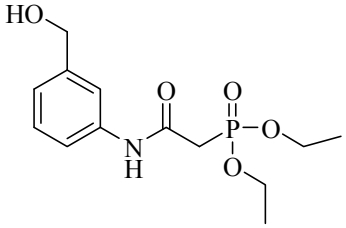

The procedure described for the synthesis of diethyl [*N*-(3-bromophenyl)carbamoyl]-methylphosphonate **67a** was employed, using 2-chloro-*N*-[3-(hydroxymethyl)phenyl]-acetamide **65b** (0.30 g, 1.5 mmol) and triethyl phosphite (0.51 mL, 3.0 mmol). The crude product was purified by flash chromatography [on silica gel; elution with hexane-EtOAc

(9:1)] to afford diethyl [*N*-(3-hydroxymethyl)phenylcarbamoyl]methylphosphonate **67b** as a yellow oil, (0.29 g, 62%); ν_{max}/cm^{-1} 3365 (OH) and 1648 (C=O); δ_H/ppm (400 MHz; $CDCl_3$) 1.35 (6H, t, *J* = 6.9 Hz, 2 × CH_3), 3.01 (2H, d, J_{P-H} = 21.4 Hz, CH_2P), 4.19 (4H, m, 2 × OCH_2CH_3), 4.46 (2H, s, CH_2OH), 7.05 (1H, d, *J* = 7.7 Hz, Ar-H), 7.28 (1H, t, *J* = 8.04 Hz, Ar-H), 7.44 (1H, s, Ar-H), 7.48 (1H, d, *J* = 8.02 Hz, Ar-H) and 8.87 (1H, s, NH); δ_C/ppm (100 MHz; $CDCl_3$) 16.5 (d, *J* = 6.04 Hz, 2 × CH_3), 35.8 (d, J_{P-C} = 128.7 Hz, CH_2P), 63.3 (d, *J* = 7.4 Hz, 2 × OCH_2CH_3), 66.7 (CH_2OH), 116.7, 119.7, 123.9, 129.0, 137.9 and 139.8 (Ar-C) and 162.1 (C=O).

***Diethyl [N-(2-pyridyl)carbamoyl]methylphosphonate* 67c**

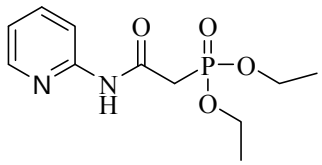

The procedure described for the synthesis of diethyl [*N*-(3-bromophenyl)carbamoyl]-methylphosphonate **67a** was employed, using 2-chloro-*N*-(pyridin-2-yl)acetamide **65c** (0.39 g, 2.3 mmol) and triethyl phosphite (1.73 mL, 2.0 mmol). The crude product was purified by flash chromatography [on silica gel; elution with hexane-EtOAc (9:1)], and subsequent evaporation of the solvent *in vacuo* afforded diethyl [*N*-(2-pyridyl)-carbamoyl]methyl-phosphonate **67c** as a yellow oil (0.49 g, 72%); ν_{max}/cm^{-1} 1648 (C=O); δ_H/ppm (400 MHz; $CDCl_3$) 1.32 (6H, t, *J* = 7.10 Hz, 2 × CH_3), 3.08 (2H, d, J_{P-H} = 21.3 Hz, CH_2P), 4.19 (4H, m, 2 × OCH_2CH_3), 6.99 (1H, dd, *J* = 5.11 and 6.72 Hz, Ar-H), 7.64 (1H, t, *J* = 7.08 Hz, Ar-H), 8.10 (1H, d, *J* = 8.28, Ar-H), 8.24 (1H, d, *J* = 4.11 Hz, Ar-H) and 9.42 (1H, s, NH); δ_C/ppm (100 MHz; $CDCl_3$) 16.4 (d, *J* = 6.02 Hz, 2 × CH_3), 36.9 (d, J_{P-C} = 130.9 Hz, CH_2P), 63.1 (d, *J* = 6.4 Hz, 2 × OCH_2CH_3), 114.3, 120.2, 138.3, 148.0 and 151.3 (Ar-C) and 163.1 (C=O).

***Diethyl [N-(3-hydroxyphenyl)carbamoyl]methylphosphonate* 67d**

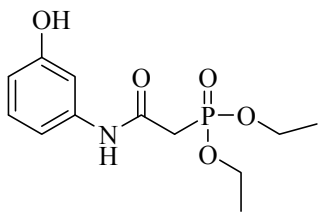

The procedure described for the synthesis of diethyl [*N*-(3-bromophenyl)carbamoyl]-methylphosphonate **67a** was employed, using 2-chloro-*N*-(3-hydroxyphenyl)acetamide **65d**

(0.51 g, 3.0 mmol) and triethyl phosphite (0.71 mL, 4.1 mmol). The crude product was purified by flash chromatography [on silica gel; elution with hexane-EtOAc (3:7)], and subsequent evaporation of the solvent *in vacuo* afforded diethyl [*N*-(3-hydroxyphenyl)-carbamoyl]methylphosphonate **67d** as a grey solid, (0.58 g, 66%); m.p. 120-122 °C (Lit.[77] 116-118 °C); ν_{max}/cm^{-1} 3365 (OH) and 1644 (C=O); δ_H/ppm (300 MHz; $CDCl_3$) 1.29 (6H, t, J = 6.87 Hz, 2 × CH_3), 3.07 (2H, d, J_{P-H} = 21.1 Hz, CH_2P), 4.14 (4H, m, 2 × OCH_2CH_3), 6.59 (1H, d, J = 6.87 Hz, Ar-H), 6.82 (1H, d, 7.2 Hz, Ar-H), 7.04 (1H, t, J = 8.10 Hz, Ar-H), 7.39 (1H, s, Ar-H), 8.45 (1H, br s, OH) and 9.11 (1H, s, NH); δ_C/ppm (75 MHz; $CDCl_3$) 16.3 (d, J = 5.9 Hz, 2 × CH_3), 36.9 (d, J_{P-C} = 131.3 Hz, CH_2P), 63.3 (d, J = 6.3 Hz, 2 × OCH_2CH_3), 107.3, 111.1, 112.1, 129.8, 138.8 and 157.5 (Ar-C) and 162.9 (C=O).

***Diethyl (*N*-furfurylcarbamoyl)methylphosphonate* 67e**

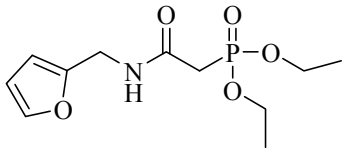

The procedure described for the synthesis of diethyl [*N*-(3-bromophenyl)carbamoyl]-methylphosphonate **67a** was employed, using 2-chloro-*N*-furfurylacetamide **65e** (0.52 g, 3.0 mmol) and triethyl phosphite (2.6 mL, 15 mmol) to afforded diethyl (*N*-furfurylcarbamoyl)-methylphosphonate **67e** as an orange oil, (0.66 g, 80%); ν_{max}/cm^{-1} 1648 (C=O); δ_H/ppm (400 MHz; $CDCl_3$) 1.31 (6H, t, J = 6.99 Hz, 2 × CH_3), 2.87 (2H, d, J_{P-H} = 20.55 Hz, CH_2P), 4.10 (4H, m, 2 × OCH_2CH_3), 4.45 (2H, d, J = 5.25 Hz, CH_2N), 6.24 (1H, s, Ar-H), 6.30 (1H, s, Ar-H), 7.11 (1H, br s, NH) and 7.33 (1H, s, Ar-H); δ_C/ppm (100 MHz; $CDCl_3$) 16.4 (d, J = 6.14 Hz, 2 × CH_3), 35.1 (d, J_{P-C} = 130.7 Hz, CH_2P), 36.9 (CH_2N), 62.9 (d, J = 6.44 Hz, 2 × OCH_2CH_3), 107.6, 110.5, 142.3 and 151.1 (Ar-C) and 164.1 (C=O).

***Diethyl [*N*-(3-hydroxyphenyl)carbamoyl]ethylphosphonate* 68d**

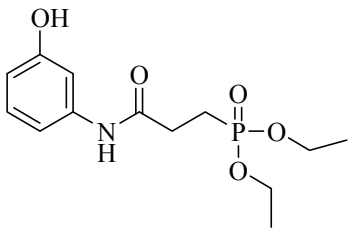

The procedure described for the synthesis of diethyl [*N*-(3-bromophenyl)carbamoyl]-methylphosphonate **67a** was employed, using 3-chloro-*N*-(3-hydroxyphenyl)propanamide

66d (0.50 g, 2.5 mmol) and triethyl phosphite (0.86 mL, 5.0 mmol). Flash chromatography [on silica gel; elution with hexane-EtOAc (3:7)] and subsequent evaporation of the solvent *in vacuo* afforded diethyl [*N*-(3-hydroxyphenyl)carbamoyl]ethylphosphonate **68d** as a pale yellow oil (0.49 g, 65%); ν_{max}/cm^{-1} 3367 (OH) and 1642 (C=O); δ_H/ppm (400 MHz; $CDCl_3$) 1.29 (6H, t, J = 6.87 Hz, 2 × CH_3), 2.17 (2H, m, CH_2P), 2.71 (2H, m, 2-CH_2), 4.08 (4H, m, 2 × OCH_2CH_3), 6.62 (1H, d, J = 8.07 Hz, Ar-H), 6.91 (1H, d, J = 7.96 Hz, Ar-H), 7.11 (1H, t, J = 8.05 Hz, Ar-H), 7.41 (1H, s, Ar-H), 8.94 (1H, s, NH); δ_C/ppm (100 MHz; $CDCl_3$) 16.5 (d, J = 6.00 Hz, 2 × CH_3), 21.2 (d, J_{P-C} = 143.0 Hz, CH_2P), 29.1 (d, J = 3.8 Hz, 2-CH_2), 62.5 (d, J = 6.67 Hz, 2 × OCH_2CH_3), 107.4, 111.3, 111.9, 129.9, 139.2 and 159.6 (Ar-C), and 170.1 (C=O).

***Diethyl (*N*-furfurylcarbamoyl)ethylphosphonate* 68e**

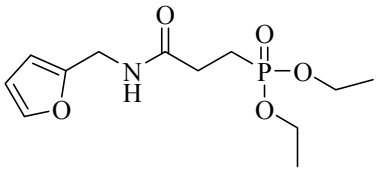

The procedure described for the synthesis of diethyl [*N*-(3-bromophenyl)carbamoyl]-methylphosphonate **67a** was employed, using 3-chloro-*N*-furfurylpropanamide **66e** (0.45 g, 2.3 mmol) and triethyl phosphite (1.95 mL, 11.3 mmol). Flash chromatography [on silica gel; elution with hexane-EtOAc (3:7)] and subsequent evaporation of the solvent *in vacuo* afforded diethyl (*N*-furfurylcarbamoyl)ethylphosphonate **68e** as a yellow oil (0.49 g, 70%); ν_{max}/cm^{-1} 1646 (C=O); δ_H/ppm (400 MHz; $CDCl_3$) 1.30 (6H, t, J = 7.0 Hz, 2 × CH_3), 2.10 (2H, m, CH_2P), 2.47 (2H, m, 2-CH_2), 4.09 (4H, m, 2 × OCH_2CH_3), 4.43 (2H, d, J = 5.6 Hz, CH_2N), 6.25 (lH, d, J = 3.2 Hz, Ar-H), 6.31 (lH, d, J = 2.0 Hz, Ar-H), 6.67 (lH, br s, NH) and 7.33 (lH, dd, J = 0.6 and 1.9 Hz, Ar-H); δ_C/ppm (100 MHz; $CDCl_3$) 16.4 (d, J = 6.89 Hz, 2 × CH_3), 21.0 (d, J_{P-C} = 142.5 Hz, CH_2P), 29.2 (2-CH_2), 36.6 (CH_2N), 61.8 (2 × OCH_2CH_3), 107.6, 110.7, 142.5 and 151.3 (Ar-C) and 170.8 (C=O).

***Diethyl [*N*-(3-cyanophenyl)carbamoyl]ethylphosphonate* 68f**

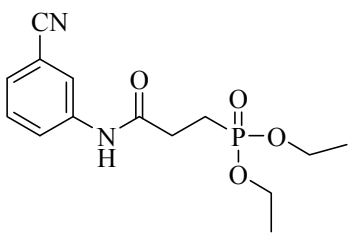

The procedure described for the synthesis of diethyl [*N*-(3-bromophenyl)carbamoyl]methyl-phosphonate **67a** was employed, using 3-chloro-*N*-(3-cyanophenyl)propanamide **66f** (0.50 g, 2.5 mmol) and triethyl phosphite (0.51 mL, 3.0 mmol). Flash chromatography [on silica gel; elution with hexane-EtOAc (3:7)] and subsequent evaporation of the solvent *in vacuo* afforded diethyl [*N*-(3-cyanophenyl)carbamoyl]ethylphosphonate **68f** as a brown oil (0.48 g, 65%); ν_{max}/cm^{-1} 1648 (C=O); δ_H/ppm (400 MHz; $CDCl_3$) 1.34 (6H, t, *J* = 7.3 Hz, 2 × CH_3), 2.18 (2H, m, CH_2P), 2.70 (2H, m, 2-CH_2), 4.13 (4H, m, 2 × O*C*H_2CH_3), 7.35 (2H, m, Ar-H), 7.86 (lH, t, *J* = 8.01 Hz, Ar-H), 7.98 (lH, s, Ar-H) and 9.63 (lH, s, NH); δ_C/ppm (100 MHz; $CDCl_3$) 16.4 (d, *J* = 6.12, 2 × CH_3), 20.8 (d, J_{P-C} = 142.7 Hz, CH_2P), 29.6 (2-CH_2), 62.7 (d, *J* = 6.65 Hz, 2 × O*C*H_2CH_3), 118.7 (C≡N), 112.6, 122.7, 123.5, 127.3, 129.7 and 139.7 (Ar-C) and 170.2 (C=O).

3.2.3. Phenolic protection of the phosphonate ester 67d.

Tert-*butyldimethylsilyl ether-protected phosphonate ester* 71

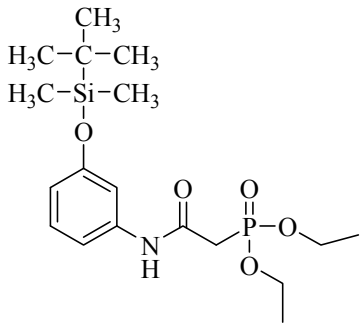

To a solution of diethyl [*N*-(3-hydroxyphenyl)carbamoyl]methylphosphonate **67d** (0.50 g, 1.7 mmol) and imidazole (0.15 g, 2.3 mmol) in dichloromethane (DCM) (20 mL) at 0 ^oC (ice bath) was added *tert*-butyldimethylsilyl chloride (0.29 g, 1.9 mmol) in portions and the mixture was stirred at r.t. for 2 h. The mixture was diluted with DCM (10 mL) and washed with water (2 × 20 mL) and brine (2 × 20 mL). The organic layer was then dried over $MgSO_4$, filtered and concentrated *in vacuo*. The crude product was purified by column chromatography [on silica gel; elution with hexane-EtOAc (9:1)] to afford the *tert*-butyl-dimethylsilyl ether-protected phosphonate ester **71** as a white soild (0.62 g, 88%); m.p. 70-72 ^oC; [HRMS: *m/z* calculated for $C_{18}H_{33}NO_5PSi$ (MH^+) 402.1866. Found 402.1861]; ν_{max}/cm^{-1}: 1673 (C=O); δ_H (400 MHz; $CDCl_3$) 0.20 [6H, s, $Si(CH_3)_2$], 0.97 [9H, s, $C(CH_3)_3$], 1.35 (6H, t, *J* = 7.07 Hz, 2 × CH_3), 2.98 (2H, d, J_{P-H} = 21.0 Hz, CH_2P), 4.17 (4H, m, 2 × O*C*H_2CH_3), 6.60 (lH, dd, *J* =1.32 and 7.96 Hz, Ar-H), 7.06 (lH, dd, *J* = 1.50 and 6.58 Hz, Ar-H), 7.16 (2H, m,

Ar-H) and 8.71 (lH, s, NH); δ_C/ppm (100 MHz; $CDCl_3$) -4.3 [$Si(CH_3)_2$], 16.5 (d, J = 6.03 Hz, 2 × CH_3), 18.34 [$C(CH_3)_3$], 25.8 [$C(CH_3)_3$], 36.3 (d, J_{P-C} = 129.4 Hz, CH_2P), 63.2 (d, J = 6.44 Hz, 2 × OCH_2CH_3), 112.0, 112.9, 116.3, 129.7, 138.9 and 156.3 (Ar-C) and 162.2 (C=O).

3.3. APPROACHES TO THE SYNTHESIS OF *C*-BENZYLATED PHOSPHONATE ESTERS.

***Diethyl 1-(*N*-furfurylcarbamoyl)-2-phenylethylphosphonate* 69e**

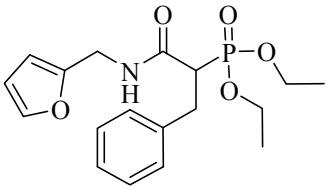

To a stirred suspension of NaH (0.034 g, 1.4 mmol) in dry THF (10 mL) under N_2, a solution of diethyl *N*-(furfurylcarbamoyl)methylphosphonate **67e** (0.35 g, 1.3 mmol) in THF (10 mL) was added drop-wise within 10 min. The reaction mixture was stirred until the mixture became clear (30 min; hydrogen gas evolved), and a solution of benzyl bromide (0.19 mL, 1.7 mmol) in THF (5 mL) was added drop-wise within 10 min. The resulting solution was refluxed for 4 h and then filtered to remove excess NaH and 10 mL of water was added to quench the reaction. THF was removed by concentrating *in vacuo*. The crude product was chromatographed [PLC on silica gel; elution with hexane-EtOAc (7:3)] to afford diethyl 1-(*N*-furfurylcarbamoyl)-2-phenylethylphosphonate **69e** as an orange oil (0.26 g, 56%), [HRMS: *m/z* calculated for $C_{18}H_{25}NO_5P$ (MH^+) 366.1470. Found 366.1466]; ν_{max}/cm^{-1}: 1675 (C=O); δ_H/ppm (300 MHz; $CDCl_3$) 1.30 (6H, t, J = 6.86 Hz, 2 × CH_3), 3.03 (1H, m, CHP), 3.08 (1H, m, CH_aPh), 3.32 (1H, m, CH_bPh), 4.09 (4H, m, 2 × OCH_2CH_3), 4.38 (2H, m, CH_2N), 6.16 (lH, s, Ar-H), 6.28 (1H, s, Ar-H), 6.67 (lH, br s, NH) and 7.20-7.32 (6H, overlapping m, ArH); δ_C/ppm (75 MHz; $CDCl_3$) 16.5 (d, J = 5.99 Hz, 2 × CH_3), 32.7 (CH_2Ph), 36.9 (CHN), 48.6 (d, J_{P-C} = 128.3 Hz, CHP), 63.1 (dd, J = 6.67 and 23.82 Hz, 2 × OCH_2CH_3), 107.6, 110.5, 126.7, 128.6, 128.9, 138.9, 142.2 and 151.1 (Ar-C) and 166.6 (C=O).

***Diethyl* N-*benzyl-[3-(benzyloxy)phenyl]-carbamoylethylphosphonate* 70d**

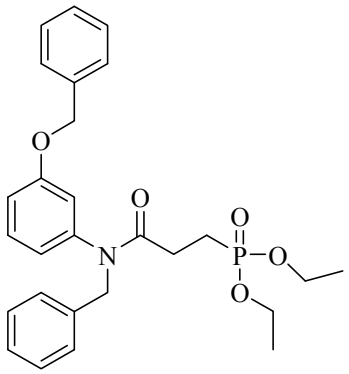

***Diethyl 2-[3-(benzyloxy)phenyl-carbamoyl]ethylphosphonate* 73**

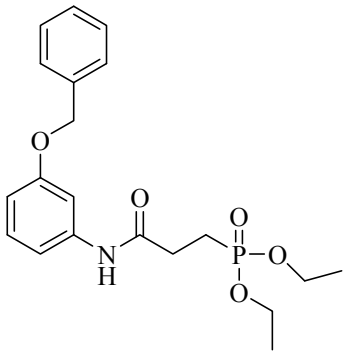

The procedure described for the synthesis of diethyl 1-(*N*-furfurylcarbamoyl)-2-phenylethyl-phosphonate **69e** was followed, using diethyl [*N*-(3-hydroxyphenyl)carbamoyl]ethyl-phosphonate **68d** (0.35 g, 1.2 mmol), NaH (0.030 g, 1.3 mmol) and benzyl bromide (0.19 mL, 1.5 mmol) in dry THF (10 mL). The mixture was refluxed for 4 h., and the crude product was flash chromatographed [on silica gel; elution with hexane-EtOAc (3:2)] to afford two fractions.

Fraction 1: *Diethyl* N-*benzyl-[3-(benzyloxy)phenyl]carbamoylethylphosphonate* **70d** as a yellow oil (0.27 g, 46%) [HRMS: *m/z* calculated for $C_{27}H_{33}NO_5P$ (MH^+) 482.2096. Found 482.2094]; ν_{max}/cm^{-1}: 1645 (C=O); δ_H/ppm (300 MHz; $CDCl_3$) 1.13 (6H, t, J = 6.37 Hz, 2 × CH_3), 2.01 (2H, m, CH_2P), 2.26 (1H, m, CH_2CO), 3.92 (4H, m, 2 × OCH_2CH_3), 4.74 (2H, s, CH_2Ph), 4.84 (2H, s, OCH_2Ph), 6.47 (2H, s, Ar-H), 6.82 (1H, d, J = 8.57 Hz, Ar-H) and 7.05-7.26 (11H, overlapping m, Ar-H); δ_C/ppm (75 MHz; $CDCl_3$) 16.4 (d, J = 6.01 Hz, 2 × CH_3), 21.6 (d, J_{P-C} = 142.7 Hz, CH_2P), 30.1 (CH_2CO), 53.5 (NCH_2Ph), 62.1 (d, J = 6.36 Hz, 2 × OCH_2CH_3), 70.0 (OCH_2Ph), 106.4, 110.6, 112.1, 125.8, 127.5, 127.8, 128.4, 128.6, 128.8, 129.5, 130.5, 136.5, 137.5 and 143.1 (Ar-C) and 159.8 (C=O).

Fraction 2: *Diethyl 2-[3-(benzyloxy)phenylcarbamoyl]ethylphosphonate* **73** as a yellow oil (0.077 g, 16%). [HRMS: *m/z* calculated for $C_{20}H_{27}NO_5P$ (MH^+) 329.1627. Found 392.1616]; ν_{max}/cm^{-1}: 1647 (C=O); δ_H/ppm (300 MHz; $CDCl_3$) 1.31 (6H, t, J = 1.31 Hz, 2 × CH_3), 2.18 (2H, m, CH_2P), 2.71 (2H, d, J = 6.19 Hz, CH_2CO), 4.10 (4H, m, 2 × OCH_2CH_3), 5.05 (2H, s, OCH_2Ph), 6.71 (1H, d, J = 7.35 Hz, Ar-H), 7.16-7.48 (8H, overlapping m, Ar-H) and 9.07 (1H, s, NH); δ_C/ppm (75 MHz; $CDCl_3$) 16.5 (d, J = 5.73 Hz, 2 × CH_3), 21.1 (d, J_{P-C} = 143.7 Hz, CH_2P), 30.2 (CH_2CO), 62.3 (d, J =6. 32 Hz, 2 × OCH_2CH_3), 70.1 (OCH_2Ph), 106.5, 110.8, 112.3, 127.6, 128.0, 128.6, 129.7, 137.2, 140.0 and 159.5 (Ar-C) and 169.7 (C=O).

N-*Benzyl*-N-*(3-bromophenyl)-2-(tetrahydrofuran-2-yl)acetamide* 72a

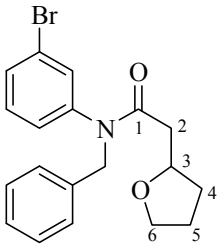

The procedure described for the synthesis of diethyl 1-(*N*-furfurylcarbamoyl)-2-phenylethylphosphonate **69e** was followed, using diethyl [*N*-(3-bromophenyl)carbamoyl]-methylphosphonate **67a** (0.10 g, 0.29 mmol), NaH (0.007 g, 0.3 mmol) and benzyl bromide (0.042 mL, 0.35 mmol) in dry THF (10 mL). Chromatography [PLC on silica gel; elution with hexane-EtOAc (1:2)] afforded *N*-benzyl-*N*-(3-bromophenyl)-2-(tetrahydrofuran-2-yl)acetamide **72a** as an orange oil (0.034, 32%) [HRMS: *m/z* calculated for $C_{19}H_{20}NO_2Br$ (MH^+) 374.0756. Found 374.0749]; ν_{max}/cm^{-1}: 1671 (C=O); δ_H/ppm (400 MHz; $CDCl_3$) 1.44 (2H, m, 4-CH_2), 1.84 (2H, m, 5-CH_2), 2.15 (1H, m, 2-CH_a), 2.45 (1H, m, 2-CH_b), 3.73 (2H, m, 6-CH_2), 4.32 (1H, m, 3-CH), 4.88 (2H, m, CH_2Ph), 6.91 (lH, d, J = 7.79 Hz, Ar-H), 7.15-7.22 (7H, overlapping m, ArH) and 7.43 (1H, d, J = 7.97 Hz, Ar-H); δ_C/ppm (100 MHz; $CDCl_3$) 25.8 (C-5), 31.6 (C-6), 40.5 (C-2), 53.1 (CH_2Ph), 67.9 (C-4), 76.2 (C-3), 122.8, 127.6, 128.6, 128.9, 128.9, 130.8, 131.3, 132.0, 137.1 and 143.7 (Ar-C) and 170.5 (C=O).

N-*Benzyl*-N-*[3-(hydroxymethyl)phenyl]-2-(tetrahydrofuran-2-yl)acetamide* 72b

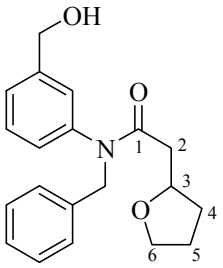

The procedure described for the synthesis of *N*-benzyl-*N*-(3-bromophenyl)-2-(tetrahydrofuran-2-yl)acetamide **72a** was followed, using diethyl [*N*-(3-hydroxymethyl)-phenylcarbamoyl]methylphosphonate **67b** (0.15 g, 0.5 mmol), NaH (0.013 g, 0.55 mmol) and benzyl bromide (0.077 mL, 6.5 mmol) in dry THF (10 mL). Chromatography [PLC on silica gel; elution with hexane-EtOAc (1:3)] afforded *N*-benzyl-*N*-[3-(hydroxymethyl)-phenyl]-2-(tetrahydrofuran-2-yl)acetamide **72b** as a yellow oil (0.032 g, 20%); ν_{max}/cm^{-1}: 3365 (OH) and 1674 (C=O); δ_H/ppm (400 MHz; $CDCl_3$) 1.35 (2H, m, 4-CH_2), 1.81 (2H, m, 5-CH_2), 2.07

(1H, m, 2-CH_a), 2.16 (1H, m, 2-CH_b), 3.68 (2H, m, 6-CH_2), 4.44 (1H, m, 3-CH), 4.47 (2H, m, CH_2Ph), 4.89 (2H, s, C*H*$_2$OH), 7.05 (lH, d, *J* = 7.79 Hz, Ar-H), 7.00 (lH, d, *J* = 7.79 Hz, Ar-H) and 7.20-7.39 (7H, overlapping m, ArH); δ_C/ppm (100 MHz; $CDCl_3$) 27.0 (C-5), 31.9 (C-6), 41.6 (C-2), 53.1 (CH_2Ph), 65.1 (CH_2OH), 66.8 (C-4), 75.3 (C-3), 124.1, 126.5, 129.4, 129.9, 130.1, 130.8, 131.5, 133.5, 137.6 and 143.5 (Ar-C) and 169.5 (C=O).

N-*Benzyl*-N-*(2-pyridyl)-2-(tetrahydrofuran-2-yl)acetamide* 72c

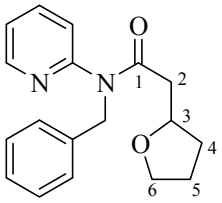

The procedure described for the synthesis of diethyl 1-(*N*-furfurylcarbamoyl)-2-phenyl-ethylphosphonate **69e** was followed, using diethyl [*N*-(2-pyridyl)carbamoyl]methyl-phosphonate **67c** (0.12 g, 0.44 mmol), NaH (0.012 g, 0.48 mmol) and benzyl bromide (0.068 mL, 0.57 mmol) in dry THF (10 mL). Chromatography [PLC on silica gel; elution with hexane-EtOAc (2:1)] afforded *N*-benzyl-*N*-(2-pyridyl)-2-(tetrahydrofuran-2-yl)-acetamide **72c** as a brown oil (0.023 g, 18%); ν_{max}/cm^{-1}: 1680 (C=O); δ_H/ppm (400 MHz; $CDCl_3$) 1.50 (2H, m, 4-CH_2), 1.73 (2H, m, 5-CH_2), 2.10 (1H, m, 2-CH_a), 2.24 (1H, m, 2-CH_b), 3.83 (2H, m, 6-CH_2), 4.23 (1H, m, 3-CH), 4.75 (2H, m, CH_2Ph), 6.94 (lH, d, *J* = 7.79 Hz, Ar-H), 7.25-7.32 (7H, overlapping m, ArH) and 7.47 (1H, d, *J* = 7.97 Hz, Ar-H); δ_C/ppm (100 MHz; $CDCl_3$) 24.8 (C-5), 32.6 (C-6), 46.5 (C-2), 52.1 (CH_2Ph), 68.9 (C-4), 78.2 (C-3), 127.8, 126.9, 127.6, 128.1, 128.9, 130.1, 130.8, 135.2 and 139.9 (Ar-C) and 167.0 (C=O).

N-*Benzyl*-N-*(3-hydroxyphenyl)-2-(tetrahydrofuran-2-yl)acetamide* 72d

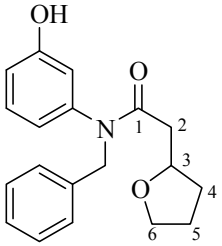

The procedure described for the synthesis of diethyl 1-(*N*-furfurylcarbamoyl)-2-phenyl-ethylphosphonate **69e** was followed, using diethyl [*N*-(3-hydroxyphenyl)carbamoyl]-methylphosphonate **67d** (0.16 g, 0.56 mmol), NaH (0.015 g, 0.61 mmol) and benzyl bromide (0.086 mL, 0.73 mmol) in dry THF (10 mL). Chromatography [PLC on silica gel; elution

with hexane-EtOAc (2:1)] afforded *N*-Benzyl-*N*-(3-hydroxyphenyl)-2-(tetrahydrofuran-2-yl)acetamide **72d** as a yellow oil (0.45 g, 26%); ν_{max}/cm^{-1}: 3376 (OH) and 1675 (C=O); δ_H/ppm (300 MHz; $CDCl_3$) 1.39 (2H, m, 4-CH_2), 1.79 (2H, m, 5-CH_2), 2.04 (1H, m, 2-CH_a), 2.17 (1H, m, 2-CH_b), 3.73 (2H, m, 6-CH_2), 4.29 (1H, m, 3-CH), 4.89 (2H, m, CH_2Ph), 6.60 (lH, d, *J* = 7.79 Hz, Ar-H), 6.91 (lH, d, *J* = 7.79 Hz, Ar-H) and 7.19-7.37 (7H,overlapping m, ArH); δ_C/ppm (75 MHz; $CDCl_3$) 25.6 (C-5), 31.4 (C-6), 40.2 (C-2), 52.8 (CH_2Ph), 67.7 (C-4), 75.4 (C-3), 122.2, 127.9, 127.3, 127.5, 128.1, 128.3, 128.6, 128.8, 130.2, and 142.8 (Ar-C) and 170.2 (C=O).

***Attempted synthesis of the* C-*benzylated phosphonate ester* 69e**

1. A solution of diethyl *N*-(furfurylcarbamoyl)methylphosphonate **67e** (0.28 g, 0.1 mmol) in dry THF (10 mL) was stirred under N_2 for 30 min. Pyridine (0.02 mL, 0.2 mmol) was added and the mixture allowed to stir for 20 min; benzyl bromide (0.132 mL, 1.1 mmol) was then added and the resulting mixture was stirred at r.t for 7 days. The mixture was later refluxed for 2 h. The resulting solution was concentrated *in vacuo*, and the residue was dissolved in DCM (30 mL), washed with 2% HCl (20 mL) and brine (20 mL), dried with $MgSO_4$, filtered, and then evaporated *in vacuo*. NMR spectroscopy analysis of the crude product showed only starting material.
2. To a solution of diethyl *N*-(furfurylcarbamoyl)methylphosphonate **67e** (0.14 g, 0.05 mmol) in dry THF (10 mL) under N_2, triethylamine (0.08 mL, 0.05 mmol) was added. After stirring for 30 min, benzyl bromide (0.07 mL, 0.55 mmol) was added and the resulting mixture was stirred at r.t. for 7 days. The residue was dissolved in DCM (30 mL), and washed sequentially with 10% HCl (10 mL) and water (10 mL), dried with $MgSO_4$, filtered, and concentrated *in vacuo* to afford starting material and impurities.
3. The diethyl *N*-(furfurylcarbamoyl)methylphosphonate **67e** (1 eq.) was dissolved in 10% aq. NaOH (1.1 eq.); benzyl bromide (1.3 eq.) was then added to the solution and the mixture was refluxed for 2 h. After cooling, water (10 mL) was added and the solvent was removed *in vacuo* to give the crude product. Flash column chromatography [on silica gel; elution with hexane-EtOAc (9:1)] afforded an intractable mixture, NMR spectroscopic analysis of which showed the presence of impurities and the starting material.

4. To a solution of diethyl *N*-(furfurylcarbamoyl)methylphosphonate **67e** (0.35 g, 1.3 mmol) in dry THF (10 mL) was added finely powdered KOH (0.08 g, 1.4 mmol) and the resulting mixture was stirred for 30 min. Benzyl bromide (0.19 mL, 1.6 mmol) was added to the solution and the mixture which was then stirred at r.t. for 48 h. The mixture was concentrated *in vacuo*, and the residue purified using PLC [on silica gel; elution with hexane-EtOAc (7:3)], to afford diethyl 1-(*N*-furfurylcarbamoyl)-2-phenylethylphosphonate **69e** as an orange oil (0.05 g, 10%)

3.4. SYNTHESIS OF *N*-BENZYLATED PHOSPHONATE ESTERS.

3.4.1. Reaction of primary amines with benzyl bromide.

(Some of these compounds has already been reported,[85,86,87] but a new synthetic approach was used in this work)

N-*Benzyl-3-bromoaniline* 75a

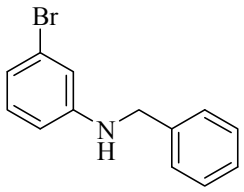

Benzyl bromide (1.28 mL, 10.9 mmol) was added to a mixture of 3-bromoaniline **74a** (1.20 mL, 11 mmol) and $NaHCO_3$ (0.92 g, 11 mmol) in dry THF (10 mL). The mixture was stirred at r.t. overnight under nitrogen. Water (20 mL) was then added and the organic aqueous layer extracted with $CHCl_3$ (2 × 50 mL). The combined organic extracts were then washed with brine (2 × 30 mL), dried with anhydrous $MgSO_4$, filtered and concentrated *in vacuo* to give a dark brown oil. Chromatography [PLC on silica gel; elution with hexane-EtOAc (4:1)] afforded *N*-benzyl-3-bromoaniline **75a** as a yellow oil (1.65 g, 65%); ν_{max}/cm^{-1} 3380 (NH); δ_H/ppm (400 MHz; $CDCl_3$) 4.31 (2H, s, NCH_2Ph), 4.10 (1H, br s, NH), 6.54 (1H, d, J = 8.07 Hz, Ar-H), 6.80 (1H, s, Ar-H), 6.84 (1H, d, J = 7.76 Hz, Ar-H), 7.02 (1H, t, J = 8.0 Hz, Ar-H) and 7.30-7.36 (5H, overlapping m, Ar-H); δ_C/ppm (100 MHz; $CDCl_3$) 48.1 (NCH_2Ph), 111.6, 115.5, 120.4, 123.2, 126.6, 127.5, 128.8, 130.6, 135.7 and 149.4 (Ar-C).

N-*Benzyl-3-(hydroxymethyl)aniline* 75b

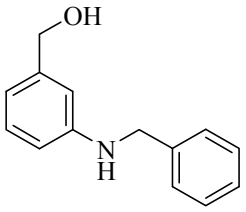

N-*Benzyl-3-[(benzyloxy)methyl]aniline* 78

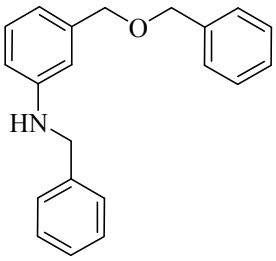

The procedure described for the synthesis of the *N*-benzyl-3-bromoaniline **75a** was followed, using 3-aminobenzyl alcohol **74b** (2.0 g, 16 mmol), $NaHCO_3$ (1.36 g, 16 mmol) and benzyl bromide (1.90 mL, 16 mmol) in dry THF (10 mL). Work-up and chromatography [PLC on silica gel; elution with hexane-EtOAc (5:1)] gave two fractions.

Fraction 1: N-*Benzyl-3-(hydroxymethyl)aniline* **75b** as a brown oil (2.17 g, 63%); ν_{max}/cm^{-1} 3385 (NH) and 3340 (OH); δ_H/ppm (400 MHz; $CDCl_3$) 2.87 (1H, s, NH), 4.21 (2H, s, NCH_2Ph), 4.46 (2H, s, CH_2OH), 6.45 (1H, d, J = 8.1 Hz, Ar-H), 6.52 (1H, s, Ar-H), 6.59 (1H, d, J = 7.51 Hz, Ar-H), 7.76 (1H, t, J = 7.76 Hz, Ar-H) and 7.16-7.28 (5H, overlapping m, ArH); δ_C/ppm (100 MHz; $CDCl_3$) 48.3 (NCH_2Ph), 65.5 (CH_2OH), 111.4, 112.1, 116.2, 127.4, 127.6, 128.7, 129.6, 139.4, 142.2 and 148.5 (Ar-C).

Fraction 2: N-Benzyl-3-[(benzyloxy)methyl]aniline **78** as white crystals (1.08 g, 19%), m.p. 88-90 ^oC; [HRMS: *m/z* calculated for $C_{21}H_{22}NO$ (MH^+) 304.1701. Found 304.1698]; ν_{max}/cm^{-1} 3384 (NH), δ_H/ppm (400 MHz; $CDCl_3$) 4.57 (2H, s, NCH_2Ph), 4.66 [4H, s, $O(CH_2)_2$], 6.68 (1H, d, J = 7.41 Hz , Ar-H), 6.71 (1H, m, Ar-H), 6.78 (1H, br, s, NH), 7.16 (1H, m, Ar-H), 7.24-7.26 (7H, overlapping m, Ar-H), 7.30-7.33 (4H, overlapping m, Ar-H); δ_C/ppm (100 MHz; $CDCl_3$) 46.3 (NCH_2Ph), 75.1 [4H, s, $O(CH_2)_2$] 111.7, 112.5, 115.9, 126.7, 127.0, 127.5, 128.2, 128.9, 129.1, 129.7, 136.2, 140.3, 141.5 and 146.8 (Ar-C).

***2-(Benzylamino)pyridine* 75c**

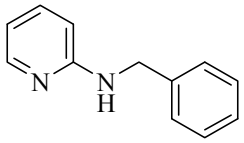

The procedure described for the synthesis of *N*-benzyl-3-bromoaniline **75a** was followed, using 2-aminopyridine **74c** (1.5 g, 16 mmol), $NaHCO_3$ (1.3 g, 16 mmol) and benzyl bromide (1.9 mL, 16 mmol) in dry THF (10 mL). Work-up and flash chromatography [on silica gel; elution with hexane-EtOAc (1:1)] afforded 2-(benzylamino)pyridine **75c** as white crystals

(1.62 g, 56%), m.p. 80-82 ^{o}C (Lit.[102] 80 °C); ν_{max}/cm^{-1} 3385 (NH); δ_H/ppm (400 MHz; $CDCl_3$) 4.51 (2H, d, *J* = 5.38 Hz, NCH_2Ph), 4.87 (1H, s, NH), 6.37 (1H, d, *J* = 8.24 Hz, Ar-H), 6.59 (1H, t, *J* = 7.51 Hz, Ar-H), 7.27 (2H, d , *J* = 4.01 Hz, Ar-H), 7.31-7.41 (5H, overlapping m, Ar-H) and 8.11 (1H, d, *J* = 4.01 Hz, Ar-H); δ_C/ppm (100 MHz; $CDCl_3$) 46.20 (NCH_2Ph), 106.7, 113.1, 127.3, 127.4, 128.7, 137.6, 139.3, 147.8 and 148.4 (Ar-C).

N-*Benzyl-3-(hydroxylphenyl)aniline* 75d

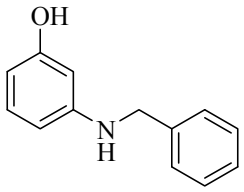

The procedure described for the synthesis of *N*-benzyl-3-bromoaniline **75a** was followed, using 3-aminophenol **74d** (2.0 g, 18 mmol), $NaHCO_3$ (1.54 g, 18.0 mmol) and benzyl bromide (2.18 mL, 18.0 mmol) in dry THF (10 mL). Work-up and flash chromatography [on silica gel; elution with hexane-EtOAc (4:1)] afforded *N*-benzyl-3-(hydroxylphenyl)-aniline **75d** as a yellow oil (2.30 g, 62%); ν_{max}/cm^{-1} 3379 (NH) and 3340 (OH); δ_H/ppm (400 MHz; $CDCl_3$) 4.31 (2H, s, NCH_2Ph), 6.13 (1H, t, *J* = 2.19 Hz, Ar-H), 6.19 (1H, dd, *J* = 1.88 and 7.93 Hz, Ar-H), 6.24 (1H, dd, *J* = 1.77 and 8.02 Hz, Ar-H), 7.02 (1H, t, *J* = 8.08 Hz, Ar-H) and 7.27-7.34 (5H, overlapping m, Ar-H); δ_C/ppm (100 MHz; $CDCl_3$) 48.5 (NCH_2Ph), 100.2, 105.0, 106.3, 127.5, 127.8, 128.9, 130.5, 139.4, 149.9 and 156.9 (Ar-C).

N-*Benzyl-3-nitroaniline* 75e

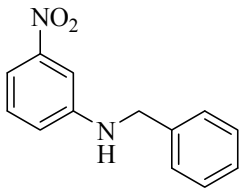

The procedure described for the synthesis of *N*-benzyl-3-bromoaniline **75a** was followed, using 3-nitroaniline **74e** (1.5 g, 11 mmol), $NaHCO_3$ (0.91 g, 11 mmol) and benzyl bromide (1.28 mL, 11.0 mmol) in dry THF (10 mL). Work-up and chromatography [PLC on silica gel; elution with hexane-EtOAc (2:1)] afforded *N*-benzyl-3-nitroaniline **75e** as yellow solid (1.78 g, 72%), m.p. 92-94 ^{o}C (Lit.[103] m.p. not cited); ν_{max}/cm^{-1} 3387 (NH); δ_H/ppm (400 MHz; $CDCl_3$) 4.39 (2H, s, NCH_2Ph), 6.88 (1H, ddd, *J* = 0.58, 2.38 and 8.12 Hz, Ar-H), 7.28 (2H, m, Ar-H), 7.36-7.37 (4H, overlapping m, Ar-H), 7.44 (1H, t, *J* = 2.28 Hz, Ar-H) and 7.53

(1H, ddd, J = 0.67, 2.10 and 8.07 Hz, Ar-H); δ_C/ppm (100 MHz; $CDCl_3$) 48.2 (NCH_2Ph), 106.7, 112.2, 118.8, 127.6, 127.8, 128.9, 129.9, 138.1, 148.9 and 149.5 (Ar-C).

N-*Benzylfurfurylamine* 75f

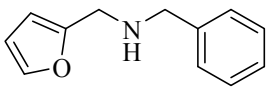

The procedure described for the synthesis of *N*-benzyl-3-bromoaniline **75a** was followed, using furfuylamine **74f** (0.65 g, 6.5 mmol), $NaHCO_3$ (0.56 g, 6.5 mmol) and benzyl bromide (0.77 mL, 6.5 mmol) in dry THF (10 mL). Work-up and flash chromatography [on silica gel; elution with hexane-EtOAc (9:1)] afforded *N*-benzyl-furfurylamine **75f** as a yellow oil (0.96 g, 76%); ν_{max}/cm^{-1} 3384 (NH); δ_H/ppm (400 MHz; $CDCl_3$) 3.62 (2H, s, CH_2N), 3.63 (2H, s, NCH_2Ph), 6.20 (1H, d, J = 2.60 Hz, Ar-H), 6.34 (1H, d, J = 1.93 Hz, Ar-H), 7.25 (1H, m, Ar-H), 7.27 (1H, s, NH), 7.33 (2H, t, J = 7.35 Hz, Ar-H) and 7.42 (3H, d, J = 7.73 Hz, Ar-H); δ_C/ppm (100 MHz; $CDCl_3$) 49.3 (NCH_2Ph), 57.6 (CH_2N), 108.7, 110.2, 127.0, 128.4, 129.0, 139.6, 142.0 and 152.9 (Ar-C).

3.4.2. Chloroacetylation of *N*-benzylanilines.

N-*Benzyl*-N-*(3-bromophenyl)-3-chloropropanamide* 76a

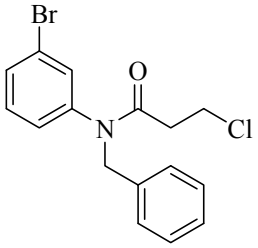

N-Benzyl-3-bromoaniline **75a** (0.68 g, 2.2 mmol) was dissolved in dry THF (20 mL) and NaH (0.10 g, 4.2 mmol) was added in portions. The mixture was stirred for 30 min and 3-chloropropionyl chloride (0.22 mL, 2.2 mmol) was then added slowly to control evolution of hydrogen. After stirring overnight at r.t. under N_2, the solvent was removed *in vacuo*, and the crude product was dissolved in EtOAc (2 × 50 mL). The resulting solution was washed sequentially with satd. aq. $NaHCO_3$ (2 × 30 mL), distilled water (2 × 30 mL) and brine (2 × 30 mL), dried ($MgSO_4$), filtered and the solvent removed *in vacuo*. Chromatography [PLC on silica gel; elution with hexane-EtOAc (7:3)] to afford *N*-benzyl-*N*-(3-Bromophenyl)-3-chloropropanamide **76a** as a yellow oil (0.45 g, 50%) [HRMS: *m/z* calculated for $C_{16}H_{16}NOClBr$ (MH^+) 352.0104. Found 352.0103]; ν_{max}/cm^{-1}: 1649 (C=O); δ_H/ppm (400

MHz; $CDCl_3$) 2.46 (2H, t, *J* = 6.53 Hz, CH_2CO), 3.72 (2H, t, *J* = 6.64 Hz CH_2Cl), 4.81 (2H, s, NCH_2Ph), 6.83 (1H, d, *J* = 7.66 Hz, Ar-H), 7.09-7.12 (4H, overlapping m, Ar-H), 7.18 (3H, overlapping m, Ar-H), and 7.39 (1H, d, *J* = 8.06 Hz, Ar-H); δ_C/ppm (100 MHz; $CDCl_3$) 37.3 (CH_2CO), 40.1 (CH_2Cl) and 53.2 (NCH_2Ph), 123.1, 127.6, 127.8, 128.7, 128.9, 131.0, 131.7, 131.7, 136.8 and 143.1 (Ar-C) and 169.3 (C=O).

N-*Benzyl-3-chloro*-N-*[3-(hydroxymethyl)phenyl]propanamide* 76b

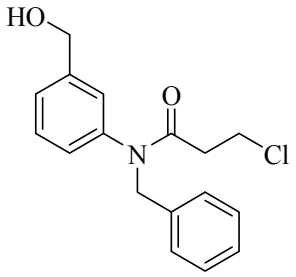

The procedure described for the synthesis of *N*-benzyl-*N*-(3-bromophenyl)-3-chloro-propanamide **76a** was followed, using *N*-benzyl-3-(hydroxymethyl)aniline **75b** (0.53 g, 2.5 mmol), NaH (0.15 g, 6.4 mmol) and 3-chloropropionyl chloride (0.24 mL, 2.5 mmol) in dry THF (20 mL). Work-up and chromatography [PLC on silica gel; elution with hexane-EtOAc (7:3)] afforded *N*-benzyl-3-chloro-*N*-[3-(hydroxymethyl)phenyl]propanamide **76b** as a pale yellow oil (0.27 g, 36%) [HRMS: *m/z* calculated for $C_{16}H_{16}NOClBr$ (MH^+) 304.1104. Found 304.1107]; ν_{max}/cm^{-1}: 3346 (OH) and 1649 (C=O); δ_H/ppm (300 MHz; $CDCl_3$) 2.47 (2H, t, *J* = 6.72 Hz, CH_2CO), 3.71 (2H, t, *J* = 6.73 Hz, CH_2Cl), 4.59 (2H, s, NCH_2Ph), 4.83 (2H, s, CH_2OH), 6.81 (1H, td, *J* = 2.14 and 4.57 Hz, Ar-H), 6.95 (1H, s, Ar-H), 7.12-7.19 (5H, overlapping m, Ar-H) and 7.24 (2H, m, Ar-H); δ_C/ppm (75 MHz; $CDCl_3$) 37.3 (CH_2CO), 40.3 (CH_2Cl), 53.3 (NCH_2Ph) and 64.5 (CH_2OH), 126.7, 127.5, 127.6, 127.7, 128.6, 128.9, 128.9, 137.2, 142.0 and 143.11, (Ar-C) and 169.6 (C=O).

N-*Benzyl-3-chloro*-N-*(2-pyridyl)propanamide* 76c

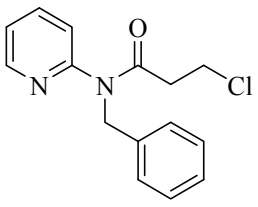

The procedure described for the synthesis of *N*-benzyl-*N*-(3-bromophenyl)-3-chloro-propanamide **76a** was followed, using 2-(benzylamino)pyridine **75c** (0.57 g, 3.0 mmol), NaH (0.080 g, 3.0 mmol) and 3-chloropropionyl chloride (0.3 mL, 3.0 mmol) in dry THF (20 mL).

Work-up and chromatography [PLC on silica gel; elution with hexane-EtOAc (3:2)] afforded *N*-benzyl-3-chloro-*N*-(2-pyridyl)-propanamide **76c** as a yellow oil (0.28 g, 33%) [HRMS: *m/z* calculated for $C_{15}H_{15}ClN_2O$ (MH^+) 274.2738. Found 274.2735]; ν_{max}/cm^{-1}: 1661 (C=O); δ_H/ppm (400 MHz; $CDCl_3$) 2.80 (2H, t, *J* = 6.94 Hz, CH_2CO), 3.80 (2H, t, *J* = 6.94 Hz, CH_2Cl), 4.49 (2H, s, NCH_2Ph), 6.46 (1H, d, *J* = 8.74 Hz, Ar-H), 6.61 (1H, t, *J* = 6.33 Hz, Ar-H), 7.31-7.36 (5H, overlapping m, Ar-H), 7.52 (1H, ddd, *J* = 1.70, 7.19 and 8.79 Hz, Ar-H) and 7.91 (1H, d, *J* = 4.95 Hz, Ar-H); δ_C/ppm (100 MHz; $CDCl_3$) 39.3 (CH_2CO), 40.3 (CH_2Cl) and 46.1 (NCH_2Ph), 107.8, 111.9, 126.9, 127.6, 128.8, 140.7, 141.7, 142.2 and 144.2 (Ar-C) and 174.4 (C=O).

N-*Benzyl-3-chloro*-N-*(3-hydroxyphenyl)-propanamide* 76d

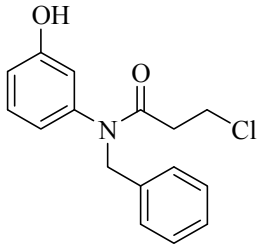

***3-(*N-*Benzyl-3-chloropropanamido)phenyl 3-chloropropanoate* 79**

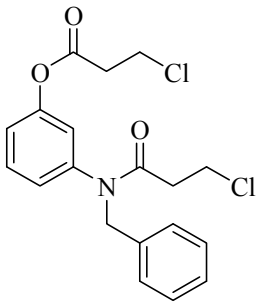

The procedure described for the synthesis of *N*-benzyl-*N*-(3-bromophenyl)-3-chloro-propanamide **76a** was followed, using *N*-benzyl-3-(hydroxylphenyl)aniline **75d** (0.6 g, 3.0 mmol), NaH (0.12 g, 5.1 mmol) and 3-chloropropionyl chloride (0.29 mL, 3.0 mmol) in dry THF (20 mL). Work-up and chromatography [PLC on silica gel; elution with hexane-EtOAc (3:2)] gave two fractions.

Fraction 1: N-*Benzyl-3-chloro*-N-*(3-hydroxyphenyl)propanamide* **76d** as a brown oil (0.33 g, 39%) [HRMS: *m/z* calculated for $C_{16}H_{17}NO_2Cl$ (MH^+) 290.0948. Found 290.0941]; ν_{max}/cm^{-1} : 3345 (OH) and 1668 (C=O); δ_H/ppm (400 MHz; $CDCl_3$) 2.58 (2H, t, *J* = 6.56 Hz, CH_2CO), 3.77 (2H, t, *J* = 6.62 Hz, CH_2Cl), 4.87 (2H, s, NCH_2Ph), 6.52 (2H, m, Ar-H), 6.56 (1H, s, OH), 6.84 (1H, dd, *J* = 1.47 and 8.15 Hz, Ar-H) and 7.18-7.25 (6H, overlapping m, Ar-H); δ_C/ppm (100 MHz; $CDCl_3$) 37.2 (CH_2CO), 40.3 (CH_2Cl), 53.27 (NCH_2Ph), 115.5, 115.7, 120.6, 127.7, 128.6, 128.9, 130.8, 137.1, 142.9 and 157.0 (Ar-C) and 169.9 (C=O).

Fraction 2: *3-(*N-*Benzyl-3-chloropropanamido)phenyl 3-chloropropanoate* **79** as a brown oil (0.16 g, 14%) [HRMS: *m/z* calculated for $C_{19}H_{19}NO_3Cl_2$ (MH^+) 380.0820. Found 380.0823]; ν_{max}/cm^{-1}: 1727 (O-C=O) and 1668 (N-C=O); δ_H/ppm (400 MHz; $CDCl_3$) 2.58-2.66 (4H, m, 2

× C*H*$_2$CO), 3.77 (4H, m, 2 × CH_2Cl), 4.66 (2H, s, NCH_2Ph), 6.68 (2H, m, Ar-H), 7.03-7.15 (6H, overlapping m, Ar-H) and 7.29 (1H, t, *J* = 8.15 Hz, Ar-H); δ_C/ppm (100 Hz; $CDCl_3$) 36.5 and 37.4 (2 × *C*H_2CO), 40.5 and 42.1 (2 × CH_2Cl) and 49.9 (NCH_2Ph), 113.4, 116.2, 118.2, 127.7, 128.6, 129.9, 130.8, 137.1, 142.9 and 153.6 (Ar-C) 170.9 and 172.0 (2 × C=O).

N-*Benzyl-3-chloro*-N-*(3-nitrophenyl)propanamide* 76e

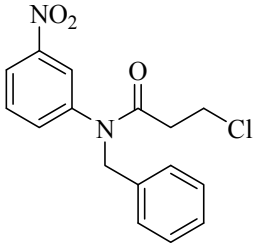

The procedure described for the synthesis of *N*-benzyl-*N*-(3-bromophenyl)-3-chloro-propanamide **76a** was followed, using *N*-benzyl-3-nitroaniline **75e** (0.68 g, 3.0 mmol), NaH (0.13 g, 5.3 mmol) and 3-chloropropionyl chloride (0.28 mL, 3.0 mmol) in dry THF (20 mL). Work-up and chromatography [PLC on silica gel; elution with hexane-EtOAc (7:3)] afforded *N*-benzyl-3-chloro-*N*-(3-nitrophenyl)propanamide **76e** as a pale yellow oil (0.48 g, 52%) [HRMS: *m/z* calculated for $C_{16}H_{16}N_2O_3Cl$ (MH^+) 319.0849. Found 319.0842]; ν_{max}/cm^{-1} : 1659 (C=O); δ_H/ppm (300 MHz; $CDCl_3$) 2.47 (2H, t, *J* = 6.43 Hz, CH_2CO), 3.76 (2H, t, *J* = 6.53 Hz, CH_2Cl), 4.40 (2H, s, NCH_2Ph), 7.10-7.12 (2H, overlapping m, Ar-H), 7.21-7.24 (4H, overlapping m, Ar-H), 7.47 (1H, t, *J* = 8.09 Hz, Ar-H), 7.85 (1H, s, Ar-H) and 8.13 (1H, d, *J* = 8.05 Hz, Ar-H); δ_C/ppm (75 MHz; $CDCl_3$) 37.2 (*C*H_2CO), 40.0 (CH_2Cl) and 53.0 (NCH_2Ph), 123.1, 123.7, 128.1, 128.5, 128.9, 130.8, 135.1, 136.2, 142.8 and 148.9 (Ar-C) and 169.1 (C=O).

N-*Benzyl-3-chloro*-N-*furfurylpropanamide* 76f

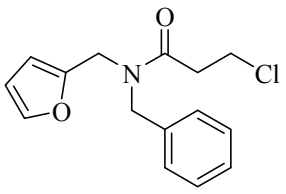

The procedure described for the synthesis of *N*-benzyl-*N*-(3-bromophenyl)-3-chloro-propanamide **76a** was followed, using *N*-benzylfurfurylamine **75f** (0.60 g, 3 mmol), NaH (0.085 g, 3.5 mmol) and 3-chloropropionyl chloride (0.29 mL, 3 mmol) in dry THF (20 mL). Work-up and chromatography [PLC on silica gel; elution with hexane-EtOAc (1:1)] afforded *N*-benzyl-3-chloro-*N*-[(furan-2-yl)methyl]propanamide **76f** as a yellow oil (0.03 g, 9%)

[HRMS: *m/z* calculated for $C_{17}H_{18}NO_2Cl$ (MH^+) 288.1155. Found 288.1147]; ν_{max}/cm^{-1}: 1664 (C=O); δ_H/ppm (300 MHz; $CDCl_3$) 2.80 (2H, t, *J* = 6.81 Hz, CH_2CO), 3.82 (2H, t, *J* = 6.80 Hz, CH_2Cl), 4.38 (2H, s, NCH_2Ph), 4.55 (2H, s, CH_2N), 7.07 (1H, d, *J* = 7.33 Hz, Ar-H), 7.14 (1H, d, *J* = 6.78 Hz, Ar-H), 7.10-7.13 (2H, overlapping m, Ar-H) and 7.23-7.29 (4H, overlapping m, Ar-H); δ_C/ppm (75 MHz; $CDCl_3$) 36.3 (CH_2CO), 40.3 (CH_2Cl), 48.6 (CH_2N), 49.9 (NCH_2Ph), 126.5, 127.7, 127.9, 128.4, 128.8, 129.2, 131.1 and 137.1 (Ar-C) and 170.5 (C=O).

3.4.3. Arbuzov reactions of *N*-benzyl-3-chloropropanamide products.

***Diethyl 2-[N-benzyl-N-(3-bromophenyl)carbamoyl]ethylphosphonate* 77a**

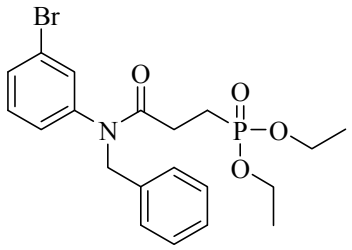

To *N*-benzyl-*N*-(3-bromophenyl)-3-chloropropanamide **76a** (0.25 g, 0.72 mmol) was added triethyl phosphite (0.25 mL, 1.44 mmol) and the mixture was heated under reflux at 120-150 ^oC for 6 h under N_2. The reaction was monitored by TLC and, upon completion of the reaction, the crude product was separated by preparative layer chromatography [on silica gel; elution with EtOAc] to afford diethyl 2-[*N*-benzyl-*N*-(3-bromophenyl)carbamoyl]ethyl-phosphonate **77a** as a yellow oil (0.16 g, 51%) [HRMS: *m/z* calculated for $C_{20}H_{26}NO_4BrP$ (MH^+) 454.0763. Found 454.0777]; ν_{max}/cm^{-1}: 1240 (P=O) and 1654 (C=O); δ_H/ppm (300 MHz; $CDCl_3$) 1.16 (6H, t, *J* = 7.06 Hz, 2 × CH_3), 2.03 (2H, m, CH_2P), 2.27 (2H, m, CH_2CO), 3.96 (4H, m, 2 × OCH_2CH_3), 4.79 (2H, s, NCH_2Ph), 6.82 (1H, d, *J* = 7.53 Hz, Ar-H), 7.09-7.13 (4H, overlapping m, Ar-H), 7.19 (3H, overlapping m, Ar-H) and 7.40 (1H, d, *J* = 7.93 Hz, Ar-H); δ_C/ppm (75 MHz; $CDCl_3$) 16.4 (d, *J* = 6.02 Hz, 2 × CH_3), 21.5 (d, J_{P-C} = 143.67 Hz, CH_2P), 27.6 (CH_2CO), 53.4 (NCH_2Ph), 61.8 (d, *J* = 6.44 Hz, 2 × OCH_2CH_3), 122.9, 127.4, 127.6, 128.5, 128.8, 130.1, 131.5, 135.0, 136.8 and 143.1 (Ar-C) and 169.1 (C=O).

***Diethyl 2-{*N*-*benzyl*-N-*[3-(hydroxymethyl)phenyl]carbamoyl}ethylphosphonate* 77b**

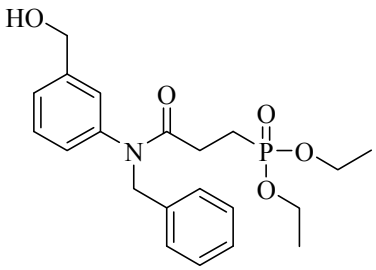

The procedure described in the experimental procedure for the synthesis of diethyl 2-[*N*-benzyl-*N*-(3-bromophenyl)carbamoyl]ethylphosphonate **77a** was followed using afforded *N*-benzyl-3-chloro-*N*-[3-(hydroxymethyl)phenyl]propanamide **76b** (0.24 g, 0.8 mmol) and triethyl phosphite (0.34 mL, 1.6 mmol). Flash chromatography [on silica gel; elution with EtOAc] afforded diethyl 2-{*N*-benzyl-*N*-[3-(hydroxymethyl)-phenyl]carbamoyl}ethyl-phosphonate **77b** as a yellow oil (0.15 g, 47%) [HRMS: *m/z* calculated for $C_{21}H_{27}NO_5P$ (MH^+) 404.1625. Found 404.1627]; ν_{max}/cm^{-1}: 3345 (OH), 1664 (C=O) and 1245 (P=O); δ_H/ppm (400 MHz; $CDCl_3$) 1.25 (6H, t, J = 6.98 Hz, 2 × CH_3), 2.12 (2H, m, CH_2P), 2.34 (2H, m, CH_2CO), 4.01 (4H, m, 2 × OCH_2CH_3), 4.65 (2H, s, NCH_2Ph), 4.85 (2H, s, CH_2OH), 6.89 (1H, d, J = 7.45 Hz, Ar-H), 7.07 (1H, s, Ar-H), 7.19 (2H, d, J = 7.08 Hz, Ar-H), 7.24-7.27 (4H, overlapping m, Ar-H) and 7.07 (1H, d, J = 7.60 Hz, Ar-H); δ_C/ppm (100 MHz; $CDCl_3$) 16.5 (d, J = 6.02 Hz, 2 × CH_3), 21.7 (d, J_{P-C} = 143.22 Hz, CH_2P), 29.8 (CH_2CO), 53.4 (NCH_2Ph), 61.9 (d, J = 6.44 Hz, 2 × OCH_2CH_3), 64.6 (CH_2OH), 122.7, 126.7, 126.9, 127.6, 128.6, 128.9, 131.4, 131.6, 134.8 and 135.4 (Ar-C) and 169.5 (C=O).

***Diethyl 2-[*N*-*benzyl*-N-*(2-pyridyl)carbamoyl]ethylphosphonate* 77c**

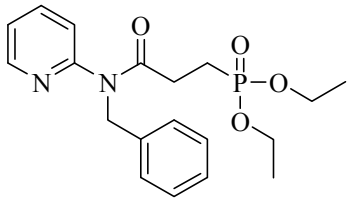

The procedure described in the experimental procedure for the synthesis of diethyl 2-(*N*-benzyl-*N*-(3-bromophenyl)carbamoyl)ethylphosphonate **77a** was followed using *N*-benzyl-3-chloro-*N*-(2-pyridyl)propanamide **76c** (0.20 g, 0.75 mmol) and triethyl phosphite (0.50 mL, 2.9 mmol). Chromatography [PLC on silica gel; elution with EtOAc] afforded diethyl 2-[*N*-benzyl-*N*-(2-pyridyl)carbamoyl]ethylphosphonate **77c** as a yellow oil (0.14 g, 49%) [HRMS: *m/z* calculated for $C_{19}H_{26}NO_4P$ (MH^+) 377.1630. Found 377.1627]; ν_{max}/cm^{-1}: 1670 (C=O)

and 1248 (P=O); δ_H/ppm (400 MHz; $CDCl_3$) 1.25 (6H, t, J = 6.45 Hz, 2 × CH_3), 2.14 (2H, m, CH_2P), 2.56 (2H, m, CH_2CO), 4.02 (4H, m, 2 × OCH_2CH_3), 5.07 (2H, s, NCH_2Ph), 7.18-7.25 (7H, overlapping m, Ar-H), 7.67 (1H, td, J = 1.92 and 7.77 Hz, Ar-H) and 8.50 (1H, d, J = 3.66 Hz, Ar-H); δ_C/ppm (100 MHz; $CDCl_3$) 16.2 (d, J = 6.06 Hz, 2 × CH_3), 21.7 (d, J_{P-C} = 143.57 Hz, CH_2P), 28.0 (CH_2CO), 51.4 (NCH_2Ph), 61.4 (2 × OCH_2CH_3), 120.4, 121.6, 122.3, 127.1, 127.7, 128.3, 137.1, 138.2 and 149.2 (Ar-C) and 154.45 (C=O).

***Diethyl 2-[N-benzyl-N-(3-hydroxyphenyl)carbamoyl]ethylphosphonate* 77d**

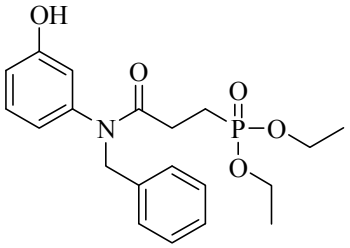

The procedure described in the experimental procedure for the synthesis of diethyl 2-[*N*-benzyl-*N*-(3-bromophenyl)carbamoyl]ethylphosphonate **77a** was followed using *N*-benzyl-3-chloro-*N*-(3-hydroxyphenyl)propanamide **76d** (0.30 g, 1.1 mmol) and triethyl phosphite (0.36 mL, 2.1 mmol). Chromatography [PLC on silica gel; elution with EtOAc] afforded diethyl 2-[*N*-benzyl-*N*-(3-hydroxyphenyl)carbamoyl]ethylphosphonate **77d** as a yellow oil (0.21 g, 51%) [HRMS: *m/z* calculated for $C_{20}H_{27}NO_5P$ (MH^+) 392.1627. Found 392.1623]; ν_{max}/cm^{-1}: 3340 (OH), 1667 (C=O) and 1242 (P=O); δ_H/ppm (400 MHz; $CDCl_3$) 1.25 (6H, t, J = 6.98 Hz, 2 × CH_3), 2.11 (2H, m, CH_2P), 2.40 (2H, m, CH_2CO), 4.01 (4H, m, 2 × OCH_2CH_3), 4.84 (2H, s, NCH_2Ph), 6.43 (1H, d, J = 7.74 Hz, Ar-H), 6.52 (1H, s, Ar-H), 6.75 (1H, dd, J = 1.68 and 8.17 Hz, Ar-H), 7.08 (1H, t, J = 8.01 Hz, Ar-H) and 7.13-7.22 (5H, overlapping m, Ar-H); δ_C (100 MHz; $CDCl_3$) 16.4 (d, J = 6.20 Hz, 2 × CH_3), 21.9 (d, J_{P-C} = 143.44 Hz, CH_2P), 27.3 (CH_2CO), 53.4 (NCH_2Ph), 62.2 (2 × OCH_2CH_3), 115.5, 115.8, 119.3, 127.5, 128.5, 128.9, 130.4, 138.3, 142.8 and 158.2 (Ar-C) and 170.2 (C=O).

***Diethyl 2-[N-benzyl-N-(3-nitrophenyl)carbamoyl]ethylphosphonate* 77e**

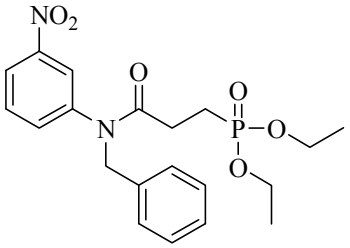

The procedure described in the experimental procedure for the synthesis of diethyl 2-(*N*-benzyl-*N*-(3-bromophenyl)carbamoyl)ethylphosphonate **77a** was followed using *N*-benzyl-3-chloro-*N*-(3-nitrophenyl)propanamide **76e** (0.46 g, 1.4 mmol) and triethyl phosphite (0.51 mL, 2.9 mmol). Chromatography [PLC on silica gel; elution with EtOAc] afforded diethyl 2-[*N*-benzyl-*N*-(3-nitrophenyl)carbamoyl]ethylphosphonate **77e** as a yellow oil (0.35 g, 59%) [HRMS: *m/z* calculated for $C_{20}H_{26}N_2O_6P$ (MH^+) 421.1526. Found 421.1522]; ν_{max}/cm^{-1}: 1661 (C=O) and 1243 (P=O) and; δ_H/ppm (400 MHz; $CDCl_3$) 1.18 (6H, t, J = 6.98 Hz, 2 × CH_3), 2.06 (2H, m, CH_2P), 2.25 (2H, m, CH_2CO), 3.96 (4H, m, 2 × OCH_2CH_3), 4.86 (2H, s, NCH_2Ph), 7.11-7.21 (6H, overlapping m, Ar-H), 7.46 (1H, t, J = 8.04 Hz, Ar-H), 7.84 (1H, s, Ar-H) and 8.12 (1H, d, J = 7.46 Hz, Ar-H); δ_C/ppm (100 MHz; $CDCl_3$) 16.4 (d, J = 6.20 Hz, 2 × CH_3), 21.8 (d, J_{P-C} = 143.8 Hz, CH_2P), 28.0 (CH_2CO), 53.4 (NCH_2Ph), 61.8 (d, J = 6.42 Hz, 2 × OCH_2CH_3), 123.3, 123.7, 128.0, 128.4, 128.8, 130.7, 135.1, 136.3, 142.9 and 148.9 (Ar-C) and 170.5 (C=O).

3.5. PROPARGYLATION REACTION.

3.5.1. Acylation of propargylamine.

***2-Chloro*-N-*(2-propynyl)acetamide* 82a**

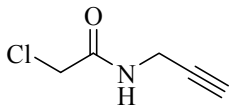

A solution of propargylamine **81** (0.58 mL, 9.0 mmol) and triethylamine (1.3 mL, 9.0 mmol) in dry THF (20 mL) was cooled to 0 ^oC (ice-bath) under N_2. Chloroacetyl chloride (0.72 mL, 9.0 mmol) was then added slowly through a septum to the solution which was kept at 0 ^oC for 45 min and then stirred for 2 h at r.t. The solvent was removed *in vacuo* and the residue was dissolved in DCM (2 × 50 mL). The resulting solution was washed sequentially with 10% dil HCl (50 mL) (to remove excess triethylamine) and water (50 mL); the aqueous layers were then re-extracted with DCM (100 mL). The organic layers were combined, dried with anhydrous $MgSO_4$ and evaporated *in vacuo* to afford 2-chloro-*N*-(2-propynyl)acetamide **80a** an off-white solid (1.13 g, 95%), m.p. 68-70 °C [HRMS: *m/z* calculated for C_5H_6NOCl (MH^+) 131.0142. Found 131.0132]; ν_{max}/cm^{-1}: 3387 (NH) and 1661 (C=O); δ_H/ppm (400 MHz; $CDCl_3$) 2.28 (1H, t, J = 2.57 Hz, CH), 4.07 (2H, s, CH_2Cl), 4.11 (2H, dd, J = 2.57 and

5.39 Hz, NCH_2) and 6.79 (1H, s, NH); δ_C/ppm (100 MHz; $CDCl_3$) 29.6 (CH_2N), 42.4 (CH_2Cl), 72.3 (C≡*C*H), 78.6 (*C*≡CH) and 165.8 (C=O).

***Synthesis of 3-chloro*-N-*(2-propynyl)propanamide* 82b**

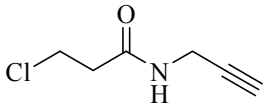

The procedure described for the synthesis of 2-chloro-*N*-(2-propynyl)acetamide **82a** was followed, using propargylamine **81** (0.58 mL, 9.0 mmol), 3-chloropropionyl chloride (0.87 mL, 9.0 mmol) and triethylamine (1.3 mL, 9.0 mmol) in dry THF (20 mL). Work-up afforded 3-chloro-*N*-(2-propynyl)propanamide **82b** as a white solid (1.21 g, 92%), m.p. 72-74 °C [HRMS: *m/z* calculated for C_6H_8NOCl (MH^+) 146.0367. Found 146.0373]; ν_{max}/cm^{-1}: 3377 (NH) and 1653 (C=O); δ_H/ppm (400 MHz; $CDCl_3$) 2.25 (1H, t, *J* = 2.55 Hz, CH), 2.66 (2H, t, *J* = 6.49 Hz, CH_2CO), 3.81 (2H, t, *J* = 6.49 Hz, CH_2Cl), 4.09 (2H, dd, *J* = 2.55 and 5.22 Hz, NCH_2) and 5.83 (1H, s, NH); δ_C/ppm (100 MHz; $CDCl_3$) 29.5 (CH_2N), 39.4 (*C*H_2CO), 39.9 (CH_2Cl), 72.1 (C≡*C*H), 79.2 (*C*≡CH) and 169.2 (C=O) .

3.5.2. Phosphonation of propargylamine derivatives *via* the Arbuzov reaction.

***Diethyl [*N*-*(2-propynyl)carbamoyl]methylphosphonate* 83a**

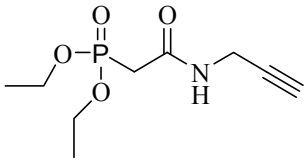

Triethyl phosphite (2.3 mL, 14 mmol) was added through a septum to 2-chloro-*N*-(2-propynyl)acetamide **82a** (0.9 g, 7 mmol) under N_2 in an oven-dried round-bottomed flask and the resulting mixture was refluxed for 4 h. The cooled mixture was stirred with hexane (5 × 25 mL) decanting the hexane layer each time to remove excess triethyl phosphite. Flash chromatography [on silica gel; elution with hexane-EtOAc (1:4)] and evaporation of the solvent *in vacuo* afforded diethyl [*N*-(2-propynyl)carbamoyl]methylphosphonate **83a** as a brown oil (1.08 g, 68%) [HRMS: *m/z* calculated for $C_9H_{16}NO_4P$ (MH^+) 234.0895. Found 234.0892]; ν_{max}/cm^{-1}: 3340 (NH), 1734 (C=O) and 1245 (P=O); δ_H/ppm (400 MHz; $CDCl_3$) 1.34 (6H, t, *J* = 7.07 Hz, 2 × CH_3), 2.21 (1H, t, *J* = 2.25 Hz, CH), 2.86 (2H, d, $J_{P\text{-}H}$ = 20.58 Hz, CH_2P), 4.05 (2H, dd, *J* = 2.54 and 5.34, CH_2N), 4.16 (4H, m, 2 × O*C*H_2CH_3) and 7.09

(1H, s, NH); δ_C/ppm (100 MHz; $CDCl_3$) 16.5 (d, *J* = 6.11 Hz, 2 × CH_3), 29.6 (CH_2N), 35.0 (d, J_{P-C}= 130.9 Hz, CH_2P), 63.1 (d, *J* = 6.50 Hz, 2 × O*C*H_2CH_3), 71.7(C≡*C*H), 79.2 (*C*≡CH) and 163.9 (C=O).

***Synthesis of diethyl [*N*-(2-propynyl)carbamoyl]ethylphosphonate* 83b**

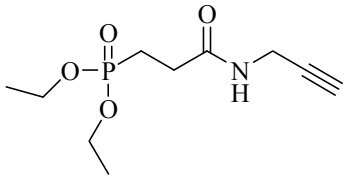

The procedure described for the synthesis of diethyl [*N*-(2-propynyl)carbamoyl]methyl-phosphonate **83a** was followed, using 3-chloro-*N*-(2-propynyl)propanamide **82b** (1.0 g, 6.8 mmol) and triethyl phosphite (2.3 mL, 14 mmol). Flash chromatography [on silica gel; elution with EtOAc] afforded diethyl [*N*-(2-propynyl)carbamoyl]ethylphosphonate **83b** as a dark brown oil (1.11 g, 65%) [HRMS: *m/z* calculated for $C_{10}H_{18}NO_4Cl$ (MH^+) 248.1052. Found 248.1051]; ν_{max}/cm^{-1}: 3340 (NH), 1738 (C=O) and 1247 (P=O); δ_H/ppm (400 MHz; $CDCl_3$) 1.29 (6H, t, *J* = 7.07 Hz, 2 × CH_3), 2.07 (2H, m, CH_2P), 2.18 (1H, t, *J* = 2.56 Hz, CH), 2.49 (2H, m, CH_2CO), 4.01 (2H, ddd, *J* = 2.47, 4.14 and 7.88 Hz, CH_2N), 4.07 (4H, m, 2 × O*C*H_2CH_3) and 7.13 (1H, s, NH); δ_C/ppm (100 MHz; $CDCl_3$) 16.5 (d, *J* = 6.06 Hz, 2 × CH_3), 21.0 (d, J_{P-C} = 143.7 Hz, CH_2P), 28.8 (*C*H_2CO), 29.3 (CH_2N), 61.6 (d, *J* = 6.57 Hz, 2 × O*C*H_2CH_3), 70.8 (C≡*C*H), 79.3 (*C*≡CH) and 170.9 (C=O).

3.5.3. Phosphorylation of AZT.

3'-*Azido*-3'-*deoxythymidine diethyl phosphate* 84

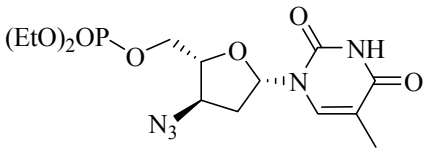

BuLi (2.5 M in hexane, 1.5 mL) was added to a solution of *3′*-azido-*3′*-deoxythymidine **80** (0.83 g, 3.1 mmol) in dry THF (20 mL) and kept at 0 °C under Ar. After stirring for 40 min, diethyl chlorophosphate (1.8 mL, 3.9 mmol) was added and the mixture was allowed to stir for 3 h at 0 °C and then overnight at r.t. The reaction was quenched by adding saturated aq. NH_4Cl (30 mL), and the crude product was extracted with DCM (3 × 30 mL). The combined organic extracts were washed with brine (50 mL), dried over anhydrous $MgSO_4$, filtered and

concentrated *in vacuo*. Flash chromatography [on silica gel; elution with hexane-EtOAc (3:7)] afforded *3*'-azido-*3′*-deoxythymidine diethyl phosphate **84** as a yellow oil (0.92 g, 73%); ν_{max}/cm^{-1} 2106 (N≡N) and 1685 (C=O); δ_H/ppm (400 MHz; $CDCl_3$) 1.35 (6H, dd, *J* = 4.49 and 6.48 Hz, 2 × CH_3), 1.93 (3H, s, CH_3Ar), 2.31 and 2.44 (2H, m, C*H*$_2$CHN), 4.02 (1H, m, OCHC*H*N), 4.16 (4H, m, 2 × OC*H*$_2$CH$_3$), 4.26 (2H, m, CH_2OP), 4.33 (1H, m, OC*H*CH_2OP), 6.23 (1H, t, *J* = 6.28 Hz, OCHN), 7.41 (1H, s, Ar-H) and 9.23 (1H, br s, NH); δ_C/ppm (100 MHz; $CDCl_3$) 12.5 (CH_3Ar), 16.2 (d, J_{P-C} = 6.5 Hz, 2 × CH_3), 37.6 (CH_2CHN), 60.1 (CHN), 64.5 (d, *J* = 5.3 Hz, 2 × O*C*H_2CH_3), 66.2 (d, $J_{P,C}$ = 5.5 Hz, CH_2OP), 82.4 (d, *J* = 7.93 Hz, PO*C*H_2CHO), 84.7 (NCHO), 111.6, 135.4, 136.8 and 150.6 (Ar-C) and 164.2 (C=O).

3'-*Azido*-3'-*deoxythymidine diphenyl phosphate* 85

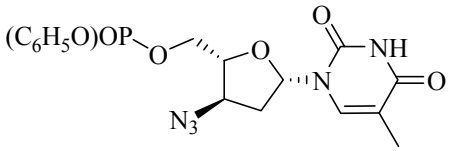

The procedure described for the synthesis of *3′*-azido-*3′*-deoxythymidine diethyl phosphate **84** was followed, using *3′*-azido-*3*'-deoxythymidine **80** (0.83 g, 3.1 mmol), BuLi (2.5 M in hexane, 1.5 mL) and diphenyl chlorophosphate (0.81 mL, 3.9 mmol) in dry THF (20 mL). Work up and chromatography [on silica gel; elution with hexane-EtOAc (9:1)] afforded *3′*-azido-*3′*-deoxythymidine diphenyl phosphate **85** as a pale yellow oil (1.15 g, 74%) [HRMS: *m/z* calculated for $C_{22}H_{23}N_5O_7P$ (MH^+) 500.1335. Found 500.1332]; ν_{max}/cm^{-1} 2101 (N≡N) and 1681 (C=O); δ_H (400 MHz; $CDCl_3$) 1.69 (3H, s, CH_3Ar), 2.11 and 2.32 (2H, m, C*H*$_2$CHN), 3.97 (1H, d, *J* = 7.20 and 9.96 Hz, OCHC*H*N), 4.17 (1H, m, CH_aOP), 4.35 (1H, m, CH_bOP), 4.46 (1H, ddd, *J* = 2.72, 6.01 and 11.16 Hz, OC*H*CH_2OP), 6.12 (1H, t, *J* = 6.55 Hz, OCHN) and 7.13-7.18 (11H, overlapping m, Ar-H); δ_C (100 MHz; $CDCl_3$) 12.5 (CH_3Ar), 37.5 (CH_2CHN), 60.1 (CHN), 67.6 (d, *J* = 6.12 Hz, CH_2OP), 82.2 (d, *J* = 7.58 Hz, PO*C*H_2CHO), 84.9 (NCHO), 111.8, 120.1, 126.0, 130.1, 135.2 and 150.3 (Ar-C) and 163.5 (C=O).

3.6. BIOASSAY PROCEDURE

The assays were conducted for the author by Ms Michelle Isaacs (Chemistry Department, Rhodes University).[98] 20 mM solutions of the phosphonated esters in DMSO were kept in the freezer. The assays were done for each of the compounds in triplicate.[99]

Cell toxicity screening. Using a sterile working area, the HeLa cells (6.7×10^5 cells; 150 μL) were loaded on the 96 well plate were allowed to grow for 24 h in the incubator; 50 μL of the phosphonate ester solution and 20 μL of resazurin dye were then added to each well, and the plate was returned to the incubator for 2 h. The plates were placed in the gyratory shaker to equilize distribution, and the samples were analysed flurorometrically at wavelength of 560 nm and 590 nm.

PLDH assay. Using chloroquine as a reference standard, the assays were carried out by further dilution of the 20 mM ligand solutions to 20 μM in DMSO; 100 μL of the diluted solution of each compound was transferred to the 96 well plate in triplicate, and 100 μL of 2% of haematocrit and 100 μL of 2% parasitemia was added to each well. After incubation under CO_2 for 48 h, 20 μL from each well was transferred to a fresh well plate, and mixed with 125 μL of Malstat and NBT/PES. The mixtures were kept in a dark cupboard and read at 620 nm after 30 min.

3.7. COMPUTER MODELLING STUDIES

The structures of the selected compounds were drawn using Discovery Studio Visualizer[51], the docking studies were carried out using the X-ray crystal structure of *Pf*DXR taken from RCSB Protein Data Base (PDB entry code 3AU9)[45]; water molecules were removed from the protein, hydrogen atoms were added, and each atom was assigned an Autodock Type using AutoDock Tools (ADT). For docking, the Autodock 4.2 programme was used to explore the binding and the interactions of the selected ligands with the proximate active-site amino acid residues. Non-polar hydrogens were merged and Gasteiger partial charges were assigned to the ligands. The AutoGrid 4.0 algorithm was employed to locate the *Pf*DXR active-site with agrid box of dimensions $40 \times 40 \times 40$ units along the x-, y- and z-directions. The Mg atom was assigned a charge of +2 prior to docking using the AD4 parameter file value. A Larmarckian genetic algorithm was used to conduct the *in silico* docking of each of the ligands with the following parameters: runs of 150; population size of 1500; maximum of 27 000 generations and 2.5×10^6 energy evaluations; mutation rate of 0.02 and a cross over rate

of 0.8. For each docking run conformations were generated, analysed using the clustering histogram, and the best docked conformer was selected for each of the ligands, and visualized using the Discovery Studio Visualizer.[51]

4. REFERENCES

1. Centre for diseases control and prevention. *http//www.cdc.gov/malaria/about/history /index.html.*
2. Webb, J.L.A. An introduction to Malaria in Human History. In *Humanity's Burden, A Global History of Malaria*, Cambridge University Press, New York, **2009**, Pp. 1-17.
3. World Health Organization Report, **2012**. *http://www.who.int/gho/malaria/en/*
4. Jeffrey, S. and Pia, M. Nature, **2002**, *415*, 680-685.
5. National Institute of Allergy and Infectious Diseases. http://www.niaid.nih.gov/; *Life cycle of the Malaria Parasite*. **2012**.
6. Phillips, R.S. *Clin. Microbiol*. Rev., **2001**, *14*, 208-226.
7. Greenwood, B.M., Fidock D.A., Kyle D.E., Kappe S.H.I., Alonso P.L., Collins F.H. and Duffy P.E. *J. Clin. Invest*., **2008**, *118*(4), 1266-1276
8. Chitnis, C.E. and Blackman, M.J. *Parasitol. Today*, **2000**, *16*, 411-415.
9. Rosenthal, P.J. Overview of Parasitic Infections. In *Comprehensive Medicinal Chemistry II*, Elsevier, New York, **2008**, *7*, 749-755.
10. Barnwell, J.W. and Galinski, M.R. Invasion of Vertebrate Cells: *Erythrocytes.* In *Malaria, Parasite Biology, Pathogenesis, and Protection;* Sherman, I.W., Ed.; American Society for Microbiology, Washington, DC, **1998**, Pp. 93-107.
11. Ghosh, A., Edwards, M.J. and Jacobs-Lorena, M. *Parasitol. Today,* **2000**, *16*, 196-201.
12. Beier, J.C. and Vanderberg J.P. Sporogonic Development in the Mosquito. *In Malaria, Parasite Biology, Pathogenesis, and Protection*; Sherman, I.W., Ed.; American Society for Microbiology, Washington, DC, **1998**, Pp.49-59.
13. Chang, H.H., Falick, A.M., Carlton, P.M., Sedat, J.W., DeRisi, J.L. and Marletta, M.A. *Molecular and Biochemical Parasitology*, **2008**, *160*, 107-115.
14. Ashley, E., McGready, R., Proux S. and Nosten F. *Travel Med and Infect Dis*., **2006**, *4*, 159-173.
15. Clark, I.A. and Cowden, W.B. *Pharmacol Ther.,* **2003**, *99,* 221-260.

16. Silvie, O., Mota, M., Matuschewski, K. and Prudencio, M. *Curr. Opin. Microbiol.,* **2008**, *11*, 352-359.

17. Areqawi, M., Cibulskis, R., Otten, M., Williams, R. and Dye, C. *World Malaria Repor*t; World Health Organization: Geneva, **2008**, Pp. 1-215.

18. Trigg, P.I. and Kondrachine, A.V. The Current Global Malaria Situation. In *Malaria, Parosite Biology, Pathogenesis, and Protection*; Sherman, I.W., Ed.; American Society for Microbiology, Washington, DC, **1998**, Pp. 11-22.

19. Casman, E.A. and Dowlatabadi, H. Introduction. In *The Contextual Determinants of Malaria*; Resources for the Future: Washington, DC, **2002**, Pp. 1-5.

20. Hyde, J.E. *Acta Trop.,* **2005**, *94*, 191-206.

21. Olliaro, P.L. and Yuthavong, Y. *Pharmacol. Ther.,* **1999**, *81*, 91-110.

22. Milhous, W.K. and Kyle D.E. Introduction to the Modes of Action of and Mechanisms of Resistance to Antimalarials. In *Malaria, Parasite Biology, Pathogenesis, and Protection*; Sherman, I.W., Ed.; American Society for Microbiology, Washington, DC, **1998**, Pp. 303-311.

23. McMurry, J. *Organic Chemistry*, 3rd ed., Brooks/Cole, California, **1992**, Pp. 1115-1116.

24. Meshnick, S.R. From Quinine to Qinghaosu: Historical Perspectives. In *Malaria, Parasite Biology, Pathogenesis, and Protection*; Sherman, I.W., Ed.; American Society for Microbiology, Washington, DC, **1998**, Pp. 341-349 .

25. Dewick, P. *Medicinal Natural Products: A Biosynthetic Approach*, John Wiley and Sons, New York, **1998**, Pp. 334-339.

26. Muraleedharan, K.M. and Avery M.A. Advances in the Discovery of New Antimalarials. In *Comprehensive Medicinal Chemistry II*, Elsevier, New York, **2007**, *7*, Pp. 765-813.

27. O'Neill, P.M., Bray P.G., Hawley S.R., Ward S.A. and Park B. K. *Pharmacol. Ther.,* **1998**, *77*, 29-58.

28. Krogstad, D.J. and De, D. Chloroquine: Modes of Action and the Activity of Chloroquine Analogs. In *Malaria, Parasite Biology, Pathogenesis, and Protection*; Sherman, I.W., Ed.; American Society for Microbiology, Washington, DC, **1998**, Pp. 331-337.

29. Ashley, E., McGready, R., Proux, S. and Nosten, F. *Travel Medicine and Infectious Disease,* **2006**, *4*, 159-173.

30. Mital, A. *Curr*. *Med. Chem*., **2007**, *14*, 759-773.

31. Cowman, A.F. The Molecular Basis of Resistance to the Sulfones, Sulfonamides, and Dihydrofolate Reductase Inhibitors. In *Malaria, Parasite Biology, Pathogenesis, and Protection;* Sherman, I.W., Ed.; American Society for Microbiology, Washington, DC, **1998**, Pp. 317-325.

32. Ntsaluba, A. *Guidelines for the Prevention of Malaria in South Africa*; The National Department of Health: Pretoria, **2003**, Pp. 7-41.

33. Bannister, L. and Mitchell, G. *Trends Parasitol*., **2003**, *19*, 209-213.

34. Nosten, F. and White, N.J. *Am. J. Trop. Med. Hyg*., **2007**, *77*, 181-192.

35. Vaidya, A.B. Mitochondrial Physiology as a Target for Atovaquone and Other Antimalarials; *In Malaria, Parasite Biology, Pathogenesis, and Protection;* Sherman, I.W., Ed.; American Society for Microbiology: Washington, DC, **1998**, Pp. 355-370.

36. Rangarajan, P.N., Padmanaban, P. *Opin. Therap. Targets,* **2001**, *5*, 423–441.

37. Jana S. and Paliwal J. *Int. J. Antimicrob. Agents*, **2007**, *30*, 4-10.

38. Rosenthal, P.J. *J. Exp. Biol*., **2003**, *206*, 3735-3744.

39. Singh, N., Chevé, G., Avery, M.A. and McCurdy, C.R. *J. Chem. Inf. Model*, **2006***, 46*, 1360-1370.

40. Köhler, S., Delwiche, C.F., Denny, P.W., Tilney, L.G., Webster, P., Wilson, R.J.M., Palmer, J.D. and Roos, D.S. *Science,* **1997**, *275*, 1485-1488.

41. Ralph, S.A., Van Dooren, G.G., Waller, R.F., Crawford, R.J., Fraunholz, M.J., Foth, B.J., Tonkin, C.J., Roos, D.F. and McFadden, G.I. *Nature Rev*., **2004**, *2*, 203-216

42. Mandal, S., Moudgil M. and Mandal S. K. *Eur. J. Pharamacol*., **2009**, *625*, 90-100.

43. Rohdich, F., Bacher A. and Eisenreich W. *Biochem*. *Soc. Trans*., **2005**, *33*, 785-791.

44. Singh, N., Cheve, G., Avery, M. A. and McCurdy, C. R. *Curr. Pharm. Des*., **2007**, *13*, 1161-1177.

45. Tomonobu, U., Nobutatada, T., Yoshion, K., Masayuki, N., Yukio K. and Kazuo, T.N. Scientific report; *Molecular basis of fosmidomycin,* **2011**, Pp. 1-8.

46. Nelson, D.L. and Cox, M.M. *Lehninger Principles of Biochemistry*, 4th ed., Freeman, New York, **2004**, Pp. 787-832.

47. Wiesner, J. and Jomaa, H. *Curr. Drug Targets*, **2007**, *8*, 3-13.

48. Hoeffler, J.F., Tritsch, D., Grosdemange-Billiard, C. and Rohmer M. *Eur. J. Biochem*., **2002**, *269*, 4446-4457.

49. Argyrou, A., and Blanchard J.S. *Biochemistry*, **2004**, *43*, 4375-4384.

50. Proteau, P.J., Woo Y.H., Williamson, R.T. and Phaosiri C. *Org. Lett*., **1999**, *1*, 921.

51. Discovery Studio Visualizer, Release 4.0; Accelrys Software Inc.: Computer Center IIT Kanpur, **2013**.

52. Reuter, K., Sanderbrand, S., Jomaa H., Wiesner J., Steinbrecher, I., Beck, E., Hintz, M., Klebe, G. and Stubbs, M.T. *J. Biol. Chem*., **2002**, *277*, 5378-5384.

53. Yajima, S., Hara, K., Lino, D., Sasaki, Y., Kuzuyama, T., Ohsawa, K. and Seto H. *Acta. Crystallogr. Sect. F: Struct. Biol. Cryst. Comm*., **2007**, *63*, 466-470.

54. Mac Sweeney, A., Lange R., Fernandes, R.P.M., Schulz, H., Dale, G.E., Douangamath, A., Proteau, P.J. and Oefner, C. *J. Mol. Biol*., **2005**, *345*, 115-127.

55. Steinbacher, S., Kaiser, J., Eisenreich, W., Huber, R., Bacher, A. and Rohdich, F. *J. Biol. Chem.,* **2003**, *278*, 18401-18407

56. Henriksson, L.M., Unge, T., Carlsson, J., Aqvist, J., Mowbray, S.L. and Jones, T.A. *Biol. Chem*., **2007**, *282*, 19905-19916.

57. Perruchon, J., Ortmann, R., Altenkamper, M., Silber K., Wiesner, J., Jomaa, H., Klebe, G. and Schlitzer, M. *ChemMedChem.,* **2008**, *3*, 1232-1241.

58. Bock, C.W., Katz, A.K., Markham, G.D. and Glusker, J.P. *J. Am. Chem. Soc*. **1999**, *121*, 7360-7372.

59. Koppisch, A.T., Fox, D.T., Blagg, B.S.J. and Poulter, C.D. *Biochemistry (N. Y.),* **2002**, *41*, 236-243.

60. Proteau, P. *J. Bioorg. Chem*., **2004**, *32*, 483-493.

61. Voet D. and Voet, J.G. Amino acid metabolism; In *Biochemistry*; John Wiley & Sons Inc: New Jersey, **2004**, Pp. 1023-1024.

62. Lichtenthaler, H.K. *Biochem. Soc. Trans*., **2000**, *28*, 785-789.

63. Okuhara, M., Kuroda, Y. and Goto, T. *Antibiot*., **1980**, *33*, 13-17.

64. Wiesner, J., Borrmann, S. and Jomaa, H. *Parasitol. Res*., **2003**, *90*, S71-S76.

65. Kuzuyama, T., Shimizu, T., Takahashi, S. and Seta, H. *Tetrahedron Lett*., **1998**, *39*, 7913-7916.

66. Meyer, O., Grosdemange-Billiard, C., Tritsch, D. and Rohmer, M. *Org. Biomol. Chem*., **2003**, *1*, 4367- 4372.

67. Giessmann, D., Heidler, P., Haemers, T., Van Calenbergh, S., Reichenberg, A., Jomaa, H., Weidemeyer, C., Sanderbrand, S., Wiesner, J. and Link, A. *Chem. Biodiversity,* **2008**, *5*, 643-656.

68. Reichenberg, A., Wiesner, J., Weidemeyer, C., Dreiseidler, E., Sanderbrand, S., Altincicek, B., Beck, E., Schlitzer, M. and Jomaa, H. *Bioorg. Med. Chem. Lett*., **2001**, *11*, 833-835.

69. Devreux, V., Wiesner, J., Goeman, J., Van D.Eycken, J., Jomaa H. and Van Calenbergh, S.1. *Med. Chem*., **2006**, *49*, 2656-2660.

70. Zubrzycki, I.Z. and Blatch G.L. *J. Mol. Model*, **2001**, *7*, 378-383.

71. Kuntz, L., Tritsch, D., Grosdemange-Billiard, C., Hemmerlin, A., Willem, A., Bach, T.J. and Rohmer, M. *Biochem. J*., **2005**, *386*, 127-135.

72. Fox, D.T. and Poulter, C.D. *J. Org. Chem.,* **2005**, *70*, 1978-1985.

73. Walker, J.R. and Poulter, C.D. *J. Org. Chem.*, **2005**, *70*, 9955-9959.

74. Conibear, A.C. *Synthesis and Evaluation of Novel Inhibitors of 1-Deoxy-D-xylulose-5-phosphate Reductoisomerase as Potential Antimalarials,* MSc. Thesis, Rhodes University, Grahamstown, **2010**.

75. Bodill, T., Conibear, A.C., Blatch, G L., Lobb, K.A. and Kaye, P.T. *Bioorg. Med. Chem*., **2011**, *19*, 1321-1327.

76. Mutorwa, M., Salisu, S., Blatch, G. L., Kenyon, C., Kaye P. T. *Synth. Commun.*, **2009**, *39*, 2723-2736.

77. Mutorwa, M. *Synthesis of Novel Inhibitors of 1-Deoxy-D-xylulose-5-phosphate Reductoisomerase as Potential Anti-malarial Lead Compounds*, Ph.D. Thesis, Rhodes University, Grahamstown, **2011**.

78. Arbuzov, B.A. *Pure Appl. Chem*., **1964**, *9*, 307–353.

79. Fall, Y., Teran, C., Teijeira, M., Satana, L. and Uriarte, E. *Synthesis,* **2000**, 643.

80. Achinto, S., Jorge, B., Eric, S., Linda, B., Jonathan, S. and John, S. *Cancer Prev. Res*., **2014**, *7,* 627-638.

81. Dusan, Z.M., Vida, D.J., and Slobodan, D.P. *J. Serb. Chem. Soc.,* **2004**, *69*(2), 85-92.

82. Uladzimir, L., Alexey, Y.K., Ka Y.L., Jeff, W., Victor, N.N. and Viktor, V.Z. *Angew Chem.*, **2005**, *117*, 7289-7293.

83. Bordwell, F.G. and Ji, G.Z. *J. Am. Chem. Soc.,* **1991**, *113*, 8398.

84. http://en.wikipedia.org/wiki/Retrosynthetic_analysis.

85. Kwong, F.Y., Klapars, A. and Buchwald. S.L. *Organic Lett.,* **2002**, *4*, 581-581.

86. Chun, C.L. and Shiuh. T.L. *Chem. Commun*., **2011**, *47*, 6981-6982.

87. Ablimit, A., Hongming, J., Yinxiang, C. and Chengjian, Z. *Tetrahedron Lett*., **2014**, *30*, 4172.

88. Fung, H.B., Stone, E.A. and Piacenti, F.J. *Clin Ther*., **2002**, *24*, 1515-1548.

89. Furman, P.A., Fyfe, J.A., St Clair, J.A., Weinhold, K., Rideout, J.L., Freeman, G.A., Lehrmann, S.N., Bolognesi, D.P., Broder, S., Mitsuya, H. and Barry, D.W. *Proc. Natl. Acad. Sci. USA,* **1986**, *83*, 8333-8337.

90. Eugen, M. and Thomas, J.J.M. *Chem. Commun*., **2006**, *10*, 4817-4819.

91. Olomola, T.O. *Synthesis and evaluation of novel HIV-1 enzyme inhibitors,* Ph.D. Thesis, Rhodes University, Grahamstown, **2011**.

92. Kolb, H.C., Finn, M.G. and Sharpless, K.B. *Angew. Chem., Int. Ed*., **2001**, *40*, 2004-2021.

93. Moses, J.E. and Moorhouse, A.D. *Chem. Soc. Rev*., **2007**, *36*, 1249-1262

94. Kolb, H.C. and Sharpless, K.B. *Drug Discov. Today,* **2003**, *8*, 1128-1137.

95. Huisgen, R., *Proc. Chem. Soc*., **1961**, 357-369.

96. Zhang, L., Chen, X., Xue, P., Sun, H.H.Y., Williams, I.D., Sharpless, K.B., Fokin, V.V. and Jia. G. *J. Am. Chem. Soc.,* **2005**, *127*, 15998-15999.

97. Kurz, T., Schluter, K., Kaula, U., Bergmann, B., Walter, R.D. and Geffken, D. *Bioorg. Med. Chem*., **2006**, *14*, 5121-5135.

98. Michelle Isaacs, Bioassay Technician, Chemistry Department, Rhodes University, Grahamstown, **2014**.

99. *http://www.sigma-aldrich.com. In vitro* toxicology assay kit.

100. Gasteiger, J. and Marsili, M. *Tetrahedron,* **1980**, *36*, 3219-3228.

101. Perrin, D.D. and Armarego, W.L.F. *Purification of Laboratory Chemicals, 3rd edn.*, Pergamon Press, Oxford, **1988**.

102. Zhang, Z., Mao, J., Zhu, D., Wu, F., Chen, H. and Wan, B. *Tetrahedron Lett.,* **2006**, *62*, 4435-4443.

103. Stilinovic, V. and Portada, T. *Acta Cryst*., **2011**, *67*, 3013.